

**Spectroscopic Investigations of  
Light-Harvesting 2 Complexes  
from *Rps. acidophila***

Fluorescence-Excitation and Emission Spectroscopy  
on Ensembles and Individual Complexes

Von der Universität Bayreuth  
zur Erlangung des Grades eines  
Doktors der Naturwissenschaften (Dr. rer. nat.)  
genehmigte Abhandlung

von

Ralf Erich Kunz

aus

Lauf a. d. Pegnitz

1. Gutachter: Prof. Dr. Jürgen Köhler
2. Gutachter: Prof. Dr. Anna Köhler

Tag der Einreichung: 02. Dezember 2013

Tag des Kolloquiums: 20. Februar 2014



# Abstract

A better understanding of light capturing and energy transfer processes in natural photosynthesis can contribute to the development of a highly efficient, artificial, molecular-based technology that utilizes the sun for mankind's energy supply.

Being a prominent example, the light-harvesting 2 (LH2) antenna complexes located in the photosynthetic apparatus of anoxygenic non-sulfur purple bacteria has already provided a deep insight into how nature has developed a pigment-protein complex with highly efficient light-harvesting and energy transfer characteristics on a confined nanoscale geometry. In order to gain more detailed information about the electronic structure in LH2 complexes from *Rhodospseudomonas (Rps.) acidophila* (strain 10050), the absorbing and emitting states of these antenna complexes have been studied in this thesis by means of ensemble as well as single-molecule fluorescence-excitation and emission spectroscopy at low temperature.

The outcome of this thesis helps to clarify some long-standing problems concerning the discrepancies between the absorption and emission characteristics of ensembles of isolated LH2 complexes from purple bacteria, as well as discrepancies between the spectroscopic results obtained from ensemble and single-molecule studies on these pigment-protein antenna complexes.

It was shown that the optical spectra of the ensemble sample, either dissolved in bulk-buffer solution or, according to the single-molecule preparation method, embedded in a thin polymer film, strongly depend on the sample preparation conditions and temperature.

For the first time, fluorescence-excitation and emission spectra of the same individual LH2 complexes could be recorded at 1.2 K. In these experiments a significant difference between the emission spectra of single complexes concerning the correlation between spectral positions and widths (full width at half maximum, FWHM) was found. This strongly implied the existence of a different electron-phonon coupling strength for each complex, and moreover, led to the conclusion that at least for some of the complexes an exciton self-trapping process is effective.

In a subsequent experiment, series of emission spectra from individual LH2 complexes have been recorded at 1.2 K with a significantly improved spectral and temporal resolution. Drastic fluctuations of the emission profiles were found to occur within individual complexes. In addition, the correlation between the shape and the peak position of the emission spectra provides direct evidence for fluctuations of the electron-phonon coupling strength not only within single LH2 complexes, but also between different ones.

Finally, a direct comparison of fluorescence-excitation and emission spectra that were recorded for the same individual LH2 complexes allowed, by reduction of spectral and temporal inhomogeneities, an unambiguous assignment of the lowest

exciton state for some of the LH2 complexes. This experiment provides evidence that the emission of the lowest exciton state can result in a narrow zero-phonon line and that emission spectroscopy of isolated LH2 complexes is to great extent affected by fluctuations of the electron-phonon coupling strength in the individual complexes. The work has resulted in four publications which can be found in part II of the thesis.

In a first step (**publication P1**), a comprehensive optical characterization of ensembles of isolated LH2 complexes has been performed as a function of sample preparation conditions and temperature by means of steady-state fluorescence-excitation, emission and fluorescence-anisotropy excitation spectroscopy. Spectral parameters (peak position, FWHM of the absorption/emission band, Stokes shift, excitonic bandwidth, etc.) which have been obtained from the optical spectra of LH2 ensembles, either dissolved in a buffer-detergent solution (with/without glycerol) or embedded in a spin-coated thin polymer film, were compared with those from native membranes at ambient and cryogenic temperatures. While buffer-detergent solutions and the polymer film matrix are the environments commonly used in bulk and single-molecule spectroscopic studies, respectively, native membranes served as the reference in which the LH2 complexes are naturally embedded. The most remarkable finding was a significant blue-shift of the B850 excitonic absorption band at 5 K upon transfer of the LH2 complexes from bulk-buffer solution into the spin-coated polymer film. Within the molecular exciton model this shift could be disentangled into three parts, namely to an increase of the local site energies, a contraction of the exciton band, and a decrease of the displacement energy. These results help to facilitate the comparison of results from single-molecule studies with those obtained from ensemble studies.

In the second step (**publication P2**), fluorescence-excitation and emission spectra of the same individual LH2 complexes have been recorded at 1.2 K for the first time. The recorded emission spectra could be related to two classes of complexes with distinctively different types of emission spectra. One class of antenna complexes showed spectra with a relatively narrow spectral profile and a clear signature of a zero-phonon line (ZPL), whereas the other class displayed spectra that consisted of a broad featureless band. Further analysis of the emission spectra revealed clear correlations between the peak position and width (FWHM) of the emission band. This observation clearly indicated that the electron-phonon coupling strength strongly varies from complex to complex, as well as being a function of the spectral peak position. Due to long integration times, however, the influence of fast unresolved spectral diffusion on the width of the broad spectra could not be fully ruled out. Next, emission spectra of single LH2 complexes were recorded at 1.2 K with enhanced spectral resolution and significantly reduced exposure times. This allowed recording of series of emission spectra (100 - 2000) with an unprecedented spectral and temporal resolution for 26 LH2 complexes. Narrow ZPLs as well as broad structureless spectra from the same individual complex could be observed, suggesting a

strong spectral diffusion. A multivariate statistical algorithm (MSA) was applied to the emission spectra to surpass weak signal intensities and strong spectral diffusion, resulting in so-called class-averaged spectra (CAS). From analysis of the CAS in terms of spectral widths (FWHM) and peak positions it followed that for each complex the width of the red-most CAS is always larger than the blue-most CAS, whatever the actual profile of the spectrum looked like. This correlation of the spectral profiles with peak positions can be interpreted as different electron-phonon coupling strengths within each individual LH2 complex. Moreover, this study revealed a much larger variety of the emission profiles than previously observed in **P2** and testifies, for the first time, that the electron-phonon coupling of an individual pigment-protein complex cannot be regarded as static. The measured linewidths of the ZPLs ( $\leq 10 \text{ cm}^{-1}$ ) in the individual spectra, are the narrowest ever observed in emission spectra of LH2 complexes. These results have been published in **publication P3**.

Finally, the fluorescence-excitation and emission spectra that have been recorded from individual LH2 complexes at 1.2 K, both showing strong temporal and spectral fluctuations, were directly compared for each individual complex. This comparison revealed that for 2/3 of the complexes the fluorescence-excitation spectrum could not be fully recorded due to the cut-off of the detection filter characteristics. However, for those complexes with fully recorded fluorescence-excitation spectra, a correlation of the red-most spectral feature of the excitation spectrum with the blue-most spectral feature of the emission spectrum allows an unambiguous assignment of the lowest exciton state. Thus, the combination of fluorescence-excitation and emission spectroscopy on a single-molecule level allowed to surpass the spectral and temporal inhomogeneities such that the presence of the lowest exciton state in the excited state manifold of individual LH2 complexes could be unmasked for the first time. The results of this approach, which are in good agreement with the data obtained from spectral hole-burning studies, have been published in **publication P4**.



## Kurzdarstellung

Ein besseres Verständnis der in der natürlichen Photosynthese auftretenden Licht-einfang- und Energietransferprozesse, kann zur Entwicklung hocheffizienter, künstlicher, auf Moleküle basierender Technologien beitragen, welche die Energie der Sonne zur Energieversorgung der Menschheit nutzbar macht. Als besonders eindrucksvolles Beispiel kann hier der Lichtsammelantennenkomplex 2 (LH2), welcher sich im Photosyntheseapparat der anoxygenen nicht-schwefelhaltigen Purpurbakterien befindet, genannt werden. Aus Pigmenten und Proteinen hat die Natur einen Komplex auf der Nanoskala gebildet, der hocheffiziente Lichtsammel- und Energietransfereigenschaften in sich vereinigt. Um mehr über die elektronische Struktur des LH2 Komplexes der Spezies *Rhodospseudomonas (Rps.) acidophila* (strain 10050) zu erfahren, wurden in der vorliegenden Dissertation die absorbierenden und emittierenden Zustände dieses Antennenkomplexes anhand von Fluoreszenz-Anregungs- und Emissionsspektroskopie im Ensemble und auf der Einzelmolekülebene, bei tiefen Temperaturen, untersucht.

Die Resultate der Dissertation helfen einige, seit langem bestehende Probleme aufzuklären, die einerseits auf Diskrepanzen zwischen den Absorptions- und Emissionscharakteristika isolierter, im Ensemble gemessener LH2 Komplexe von Purpurbakterien beruhen und andererseits auf widersprüchliche Erkenntnisse aus Ensemble- und Einzelmolekülspektroskopiestudien dieser Pigment-Protein-Komplexe zurückzuführen sind.

In der vorliegenden Arbeit wurde gezeigt, dass die optischen Spektren einer Ensembleprobe stark von den Präparationsbedingungen der Probe (in Puffer-Detergenz-Lösung oder eingebettet in einem Polymerfilm) sowie der Temperatur abhängen. Erstmals wurden Fluoreszenz-Anregungs- und Emissionsspektren von den gleichen, einzelnen LH2 Komplexe bei einer Temperatur von 1.2 K gemessen. In diesen Experimenten konnte ein bedeutender Unterschied zwischen den Emissionsspektren der Komplexe bezüglich der Korrelation ihrer spektralen Position und ihrer Breite (Halbwertsbreite, FWHM) festgestellt werden. Dies gab Anlass zu Vermutung, dass innerhalb der Komplexe verschieden starke Elektron-Phonon-Kopplungen vorherrschen. Zudem führte es zu der Schlussfolgerung, dass in einigen der untersuchten Komplexe ein sogenannter Exciton-Self-Trapping Prozess auftritt.

In einem weiteren Experiment wurden Serien von Emissionsspektren einzelner LH2 Komplexen mit einer deutlich verbesserten spektralen und zeitlichen Auflösung bei einer Temperatur von 1.2 K aufgenommen. Hierbei wurden erhebliche Fluktuationen der Emissionsprofile beobachtet. Eine Korrelation zwischen der Form und der Position des Maximums des Spektrums, erbrachte zusätzlich den Nachweis, dass die Elektron-Phonon-Kopplungsstärke nicht nur innerhalb eines einzelnen LH2 Komplexes fluktuiert, sondern auch zwischen den Komplexen unterschiedlich ist.

Der direkte Vergleich der Fluoreszenz-Anregungs- und Emissionsspektren, welche von den gleichen, einzelnen LH2 Komplexen aufgenommen wurden, ermöglichte das Umgehen spektraler und zeitlicher Inhomogenitäten und dadurch für einige LH2 Komplexe eine eindeutige Bestimmung des untersten, anregbaren Exzitonenzustands. Dieses Vorgehen lieferte den Beweis, dass die Emission aus dem untersten Exzitonenzustand eine schmale Null-Phononenlinie aufweisen kann und dass die Emissionsspektroskopie isolierter LH2 Komplexe zu einem großen Anteil von Fluktuationen der Elektron-Phonon-Kopplungsstärke innerhalb der einzelnen Komplexe beeinflusst ist. Die Ergebnisse dieser Arbeit resultierten in vier Publikationen, welche im Teil II der Arbeit zu finden sind.

Im ersten Schritt (**Publikation P1**) erfolgte eine umfassende, optische Charakterisierung von Ensembleproben isolierter LH2 Komplexe als Funktion der Präparationsbedingungen und der Temperatur mithilfe der Fluoreszenz-Anregungs-, Emissions- und Fluoreszenz-Anisotropie-Anregungsspektroskopie. Hierbei wurden spektrale Parameter (Position der Bande, FWHM der Absorptions-/Emissionsbande, Stokes-Verschiebung, exzitonische Bandbreite, etc.) von LH2 Ensembles, welche entweder in einer Puffer-Detergenz-Lösung (mit/ohne Glycerol) oder in einem gespincoateten, dünnen Polymerfilm eingebettet waren, mit denen einer nativen Membran bei Umgebungs- und Tieftemperatur verglichen. Zwischen den Absorptionsspektren der LH2 Komplexe, welche sich in der Puffer-Detergenz-Lösung und im aufgeschleuderten Polymerfilm befinden, wurde bemerkenswerterweise eine erhebliche Blauverschiebung der B850-Exzitonbande, bei einer Temperatur von 5 K, festgestellt. Innerhalb des Exziton-Modells konnten dieser Verschiebung drei Ursachen zugeordnet werden. Erstens einem Anstieg der lokalen Bindungsenergien, zweitens der Kontraktion der Exzitonbande und drittens der Abnahme der sogenannten Displacement-Energie. Diese Erkenntnisse ermöglichen einen besseren Vergleich zwischen den Resultaten aus Ensemblestudien und denen aus Einzelmolekülexperimenten.

Im zweiten Schritt (**Publikation P2**) wurden Fluoreszenz-Anregungs- und Emissionsspektren derselben LH2 Komplexe bei 1.2 K erstmalig aufgenommen. Die gemessenen Emissionsspektren konnten aufgrund ihres Aussehens in zwei Klassen von Komplexen mit sich stark voneinander unterscheidenden Emissionsspektren eingeteilt werden. In eine Klasse wurden diejenigen Antennenkomplexe eingeteilt, welche ein relativ schmales spektrales Profil sowie eine klare Signatur einer Null-Phononenlinie (ZPL) erkennen ließen. Die andere Klasse hingegen, bestand aus den Komplexen, deren Emissionsspektren eine breite, unstrukturierte Bande aufwies. Eine weitere Analyse der Spektren ergab, dass eine klare Korrelation zwischen der spektralen Position der Bande und ihrer FWHM besteht. Diese Beobachtung deutete an, dass die Elektron-Phonon-Kopplungsstärke von Komplex zu Komplex nicht nur stark variiert, sondern auch mit der spektralen Position der Emissionsbande zusammenhängt. Aufgrund der langen Integrationszeiten, konnte der Einfluss schneller spektraler Diffusion auf die Halbwertsbreite der Spektren hier jedoch nicht

vollständig ausgeschlossen werden.

In einem dritten Schritt wurden die Emissionsspektren einzelner LH2 Komplexe bei 1.2 K mit einer wesentlich höheren spektralen Auflösung und reduzierten Auslesezeiten aufgenommen. Für 26 LH2 Komplexe konnten so ganze Serien von Emissionsspektren (100 - 2000) mit bislang unerreichter spektraler und zeitlicher Auflösung aufgezeichnet werden. In diesen wurden sowohl scharfe Null-Phononenlinien als auch breite, strukturlose Spektren von ein- und denselben Komplexen beobachtet, was auf eine starke spektrale Diffusion hindeutete. Die Anwendung eines multivariaten statistischen Algorithmus auf diese Spektren, mit welchem dem Problem kleiner Signalintensität und spektraler Diffusion begegnet werden konnte, resultierte in sogenannten klassengemittelten Spektren (CAS). Eine Analyse der CAS in Bezug auf ihre Halbwertsbreite und der Position ihrer Maxima ergab, dass für jeden Komplex die Breite des CAS, welches das Maximum am weitesten im langwelligen Spektralbereich besitzt, stets größer ist, als dasjenige CAS, dessen Maximum bei der kürzesten Wellenlänge liegt. Dies gilt unabhängig davon, welches tatsächliche Profil die Spektren aufwiesen. Eine solche Korrelation der Emissionsprofile mit ihren spektralen Positionen, kann als unterschiedliche Elektron-Phonon-Kopplung innerhalb eines jeden einzelnen LH2 Komplexes aufgefasst werden. Überdies, konnte hierbei, im Gegensatz zur **Publikation P2**, eine weitaus größere Vielfalt an Emissionsprofilen nachgewiesen werden, was gleichzeitig ein Beleg dafür ist, dass die Elektron-Phonon-Kopplung eines einzelnen LH2 Komplexes nicht als statisch angesehen werden kann. Die gemessenen Linienbreiten der Null-Phononenlinien ( $\leq 10 \text{ cm}^{-1}$ ) sind die schmalsten, die jemals in LH2 Emissionsspektren beobachtet werden konnten. Diese Erkenntnisse wurden in der **Publikation P3** veröffentlicht.

Im letzten Schritt wurden alle, im Rahmen dieser Arbeit bei 1.2 K gemessenen Fluoreszenz-Anregungs- und Emissionsspektren einzelner LH2 Komplexe, welche beide starke zeitliche und spektrale Fluktuationen aufwiesen, für jeden Komplex direkt miteinander verglichen. Aus diesem Vergleich ergab sich, dass, aufgrund der Detektionsfiltercharakteristik, für zwei Drittel aller Komplexe, das Anregungsspektrum nicht vollständig aufgenommen werden konnten. Für diejenigen Komplexe jedoch, deren Anregungsspektren vollständig aufgezeichnet werden konnten, hat die Korrelation der spektralen Eigenschaften am langwelligen Ende des Anregungsspektrums mit den spektralen Eigenschaften im kurzwelligen Wellenlängenbereich des zugehörigen Emissionsspektrums, eine eindeutige Zuweisung des untersten Exzitonenzustands ermöglicht. Damit konnte gezeigt werden, dass sich durch Kombination von Fluoreszenz-Anregungs- und Emissionsspektroskopie auf der Einzelmolekülebene, spektrale und zeitliche Inhomogenitäten umgehen lassen und dadurch eine Bestimmung des untersten, anregbaren Zustands der B850 Exzitonengebände, für einzelne LH2 Komplexe möglich ist. Die Ergebnisse dieser Herangehensweise, welche in der **Publikation P4** veröffentlicht wurden, decken sich weitgehend mit den Daten, die aus spektralen Lochbrennexperimenten gewonnen wurden.



# Contents

Abstract	i
Kurzdarstellung	v
I Introduction	1
1 Motivation	3
2 Photosynthesis of purple bacteria	7
2.1 Photosynthesis in general . . . . .	7
2.2 Photosynthetic unit of purple bacteria . . . . .	7
2.3 Light-harvesting 2 complexes . . . . .	9
3 Spectroscopy on LH2 complexes	13
3.1 Interaction strengths and excitation energy transfer . . . . .	13
3.2 Theory of excitons . . . . .	14
3.3 Disorder, homogeneous and inhomogeneous broadening . . . . .	16
3.4 Homogeneous linewidth of ZPL . . . . .	17
3.5 Linear electron-phonon coupling, PSB and $S$ -factor . . . . .	17
3.6 Stokes shift . . . . .	20
3.7 Ensemble spectroscopy . . . . .	21
3.7.1 Discrepancies of the Frenkel exciton model . . . . .	23
3.7.2 Polaron formation, self-trapping of excitons . . . . .	24
3.8 Spectroscopy on single LH2 complexes . . . . .	27
3.9 Aim of this work . . . . .	32
4 Materials and methods	35
4.1 Sample preparation . . . . .	35
4.2 Experimental setup . . . . .	36
4.2.1 Wide-field imaging . . . . .	37
4.2.2 Fluorescence-excitation spectroscopy . . . . .	38
4.2.3 Fluorescence-emission spectroscopy . . . . .	39
4.2.4 Ensemble spectroscopy . . . . .	41
4.2.5 Fluorescence-anisotropy excitation spectroscopy . . . . .	42
4.3 Data analysis . . . . .	43
4.4 Tables of chemicals, optical filters and detectors . . . . .	45

5	Supplementary information	47
5.1	Shortcomings and comparability of ensemble and single-molecule studies . . . . .	47
5.1.1	Site selective ensemble spectroscopy . . . . .	47
5.1.2	Single-molecule spectroscopy . . . . .	48
5.1.3	Comparability of ensemble and single-molecule studies . . .	59
5.2	Polarization dependence of the B850 ring exciton states . . . . .	59
5.3	Interaction strength calculation . . . . .	60
	Bibliography	65
	Danksagung	85
	Erklärung	87
II	Publications	89
P1.	Fluorescence-Excitation and Emission Spectra from LH2 Antenna Complexes of <i>Rhodospseudomonas acidophila</i> as a Function of the Sample Preparation Condition	91
P2.	Exciton Self Trapping in Photosynthetic Pigment-Protein Complexes Studied by Single-Molecule Spectroscopy	103
P3.	Fluctuations in the Electron-Phonon Coupling of a Single Chromoprotein	112
P4.	Single-Molecule Spectroscopy Unmasks the Lowest Exciton State of the B850 Assembly in LH2 from <i>Rps. acidophila</i>	124

# Part I

## Introduction



So far, human civilization has made use almost exclusively of fossil solar energy. Would it not be advantageous to make better use of radiant energy?

---

*Giacomo Ciamician, Science, 36, 385 (1912)*

## 1 Motivation

At present the rate of global energy consumption by humanity is about 15 TW (1 terrawatt =  $10^{12}$  Watt) per year. From that amount  $\sim 85\%$  comes from burning fossil fuels like oil, gas and coal, whereas the remaining part is provided by nuclear and the so-called renewables, such as hydroelectric, biomass energy, solar, wind, tide and wave [1, 2]. However, the limited resources of the fossil fuels will not be the biggest problem for mankind in the immediate future, but rather the rising carbon dioxide level, due to combustion of the fossil fuels and its direct impact on global climate [2, 3]. In any case, for solving the energy/carbon dioxide problem that the world will certainly face in coming years new ideas are needed, with which people can meet the challenge, to keep the current standard of living in the industrialized countries (at best with an adaption to the developing countries) on the one hand, and to satisfy the ongoing global demand for energy, while avoiding an environmental catastrophe on the other hand. It is generally recognized that only a mix of sustainable technologies can help to solve this problem.

From the sun a total power of about 120,000 TW per year is delivered to earth by radiation, of which probably more than 50 TW could be used by mankind. In human terms, the sun represents an inexhaustible energy source that is completely sustainable, available everywhere, and its use is harmless to the environment and the climate. Hence, it should play a dominating role in the energy concept of the future [2, 4, 5].

One successful attempt of capturing the sunlight for a reliable production of electricity are photovoltaic systems that are based on inorganic materials like silicon. However, due to their low efficiency and/or high costs of production, these systems require further improvement to provide a real alternative to fossil fuels. Another promising strategy for utilizing the energy from the sun is "artificial photosynthesis", i.e. the combination of cheap organic materials with concepts derived from natural photosynthesis [2, 3, 5].

Thus, learning from nature by understanding the highly efficient light-absorption, energy-transfer, charge-separation and energy-storage processes that take place in photosynthesis could contribute to this approach. The study of photosynthesis in purple bacteria, which are the oldest photosynthetic organisms, is advantageous for this purpose, due to their relatively simple supramolecular structure with re-

spect to that of higher plants [3, 6, 7]. Purple bacteria typically live in layers of ponds and lakes where no oxygen is available (so-called anaerobic layers) and where only the part of the solar spectrum is disposable that has been filtered by other photosynthetic organisms prevailing in the higher layers, e.g. algae [8]. Through the competition with the other photosynthetic organisms for the available light, various light climates and an optimization process that is balanced between starvation and photodamage, this type of bacteria has evolved an elegant photosynthetic apparatus with intriguing simplicity and impressing efficiency [9]. The photosynthetic apparatus of most purple bacteria, contains two types of antenna complexes: the peripheral light-harvesting 2 (LH2) complexes and the so-called core or LH1 complexes. While the LH2 complexes are responsible for an enhancement of the absorption cross section as well as the efficient energy transfer towards the LH1 complexes, the latter enclose the reaction center (RC), in which finally the captured sunlight is utilized for the production of chemical energy that keeps the bacterial metabolism running. From high resolution structural studies it is well-known that both complexes are ring-like structures consisting of bacteriochlorophyll (Bchl) *a* and carotenoid pigments, which are embedded in a protein scaffold [10–12]. Comprehensive spectroscopic studies have further shown that the efficient light-harvesting and energy-transferring capabilities in these complexes are mainly based on the highly symmetric arrangement of the constituents within the complexes [13–15].

First attempts that are made to benefit from the intriguing attributes of these complexes are, for example, the patterned assembly of LH2 complexes on artificial surfaces, while the function of the natural complexes is retained [16, 17]. Such a "bio-engineered" approach, which directly exploits the light-harvesting capabilities of LH2, offers a great promise for the design of so-called hybrid solar energy devices consisting of natural as well as artificial components. Furthermore, from the highly symmetric arrangement of the pigments in the LH2 complexes, researchers have even been inspired to mimic the natural systems by developing cyclic porphyrin arrays [18]. Unfortunately, it turned out that only mimicking the ring structure of the LH antennae did not give rise to similar light-harvesting characteristics. Moreover, incorporation of more pigments into perylene bisimide macrocycles - a prototypical artificial ring-like light-harvesting system - which should increase the light-absorption capability, did not lead to a higher efficiency either, as photochemical degradation and structural distortions deteriorate the excitation energy transfer, finally resulting in inefficient light-harvesting ability [19]. Thus, the light-harvesting efficiency of natural LH complexes cannot be based solely on structural principles.

LH2 complexes from purple bacteria, sometimes called the "hydrogen atoms of photosynthesis", are probably the most thoroughly studied photosynthetic antenna complexes within the last decades [20]. Lately, these complexes have even attracted researchers to study quantum coherence effects, which are believed to direct the flow

---

of energy more efficiently [21–25]. The tight and highly symmetric structural arrangement of the Bchl pigments, with inter-pigment distances of less than 1 nm, results in a strong electronic coupling between the pigments. Upon light excitation, the strong electronic coupling leads to a coherent sharing of the excitation (delocalization) among them [8, 14, 15]. So-called molecular excitons are formed, facilitating energy transfer without any movement of charges. These excitons provide an extended spectral coverage of photon collection as well as enable a highly efficient energy transfer within the complexes [26, 27]. However, it is not only the actual assembly and the number of pigments that is of importance for efficient light-harvesting in the LH complexes, but also the interplay of the pigments with the surrounding matrix, i.e. the proteins and lipids in the close proximity [3, 8]. On the one hand, the protein scaffold stabilizes the structure and symmetry of the whole complex and thus provides a remarkable robustness and shielding against various environmental disorders. On the other hand, due to the non-covalent character of the binding between the pigments and the proteins, the dynamics of the proteins as well as the conformational flexibility of the complex is maintained, both being indispensable for the function in a biological membrane.

Hence, a detailed understanding of the pigment-protein interactions in natural LH complexes, which seem to bridge the gap between molecular biology and quantum physics, can contribute to the overall knowledge of the efficiency in photosynthesis and, thereby, provide the possibility of finding new biomimetic principles that could be utilized for bio-inspired technical applications involving solar energy conversion in the future [28].

For that purpose, in this thesis, LH2 complexes from the purple non-sulfur photosynthetic bacterium *Rhodospseudomonas (Rps.) acidophila* (strain 10050) have been investigated, by means of ensemble as well as single-molecule spectroscopy at cryogenic temperatures. Until now, ensemble experiments failed to explain the discrepancies between the absorption and emission spectra of LH2 complexes. However, recording the fluorescence-excitation and emission spectra of exactly the same individual LH2 complex, enables one to compare directly the electronic structure of the absorbing and emitting states within this complex by surpassing ensemble averaging. Furthermore, the analysis of the emission spectra of individual complexes provides valuable information about the dynamic nature of the electron-phonon coupling strength, i.e. the interaction of the electronic excitation with the vibrations of the (protein) lattice that is surrounding the pigments, which is otherwise masked in ensemble studies.

This cumulative thesis has been carried out in an international cooperation between the groups of Prof. Jürgen Köhler at the University of Bayreuth (Germany), Prof. Arvi Freiberg at the University of Tartu (Estonia) and Prof. Richard Cogdell at the University of Glasgow (U.K.). It is organised into two parts, namely the introduction (part I) and the publications (part II). The motivation in part I is followed by chapter 2, in which photosynthesis in general, with the main focus on

the photosynthesis of purple bacteria is shortly discussed. It also includes a section dealing with the structure and function of the LH2 complex. Chapter 3 contains a general description about the parameters and quantities that are important for understanding and performing optical spectroscopy on LH2 complexes. This chapter includes sections about the results from absorption and emission experiments of ensemble and single-molecule studies on LH2 complexes known from literature. A further section outlines the aim of this work. In chapter 4 the materials and methods, which have been used in this work, are described. Finally, in chapter 5 a supplementary information is given, in which noteworthy issues that have not been published in any of the publications are covered. Part I is closed by the bibliography and a list of the publications. In part II all the publications of this work are attached, as published in the journals.

## 2 Photosynthesis of purple bacteria

### 2.1 Photosynthesis in general

In photosynthesis light energy from the sun is converted into a stable form of chemical energy by either bacteria, algae or plants. The chemical energy produced by photosynthesis is used to keep the metabolism of these organisms running. For a classification, one may distinguish between two types of photosynthetic organisms, oxygenic and anoxygenic ones, i.e. if these organisms are either producing molecular oxygen as a byproduct of photosynthesis or not. While cyanobacteria, algae and plants are representatives of the first type, purple bacteria belong to the second class.

In any case, the photosynthetic apparatus consists of an antenna system for the purpose of light-harvesting (LH) and a so-called reaction center (RC), acting as a "transducer". The aim of the LH antenna system is the efficient absorption and ultrafast transfer of excitation energy towards the RC. In the RC an oxidation of a photoactive pigment and the stabilization of a charge-separated state by secondary electron-transfer processes occurs which in turn is utilized for the production of ATP, the energy currency in any organism [7]. During the evolutionary process from anoxygenic towards oxygenic photosynthesis the antenna system (energy-transfer component) underwent significant modifications, whereas the RC (charge-transfer component) stayed rather unchanged. This was due to the fact that the physics of energy transfer is much more tolerant with respect to structural and geometrical changes than the physics of electron transfer is [29].

Studying the complicated processes of photosynthesis in purple bacteria is advantageous with respect to that of algae and higher plants because of its relatively simple supramolecular structure compared to that of the latter ones [30].

### 2.2 Photosynthetic unit of purple bacteria

The habitat of photosynthetic purple bacteria are the anaerobic layers of ponds and lakes where the sunlight has already been filtered by the chlorophyll absorption of algae [31]. Defying the extreme conditions, the lack of oxygen and light, these bacteria have evolved an elegant photosynthetic unit, in which a fast ( $\sim 100$  ps) and

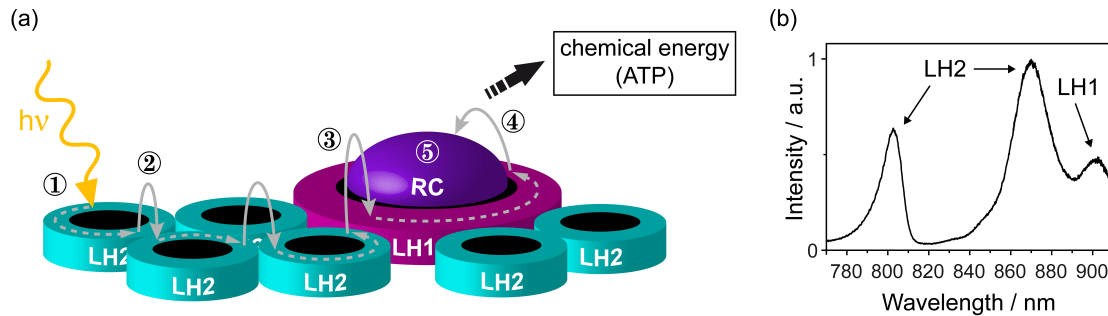


**Figure 2.1:** (a) Schematic representation of the two-dimensional antenna network in the photosynthetic unit from purple bacteria. The light reactions of bacterial photosynthesis are indicated by the numbers: Incoming sunlight is absorbed by the peripheral LH2 complexes, ①, and the excitation energy is transferred within (grey dashed arrows) and between LH2 complexes, ②, via a LH1 complex, ③, towards the RC, ④. The excitation energy transfer is followed immediately by a charge separation process in the RC, ⑤. This is the starting point for further reactions, called dark reactions, which end with the production of chemical energy in the form of ATP. (b) Fluorescence-detected absorption spectrum of chromatophores from *Rps. acidophila* in a buffer solution, recorded at 1.2 K.

highly efficient ( $\sim 95\%$  quantum efficiency) energy conversion takes place [13].

In Fig. 2.1 (a) a schematic representation of the photosynthetic unit from purple bacteria is depicted, illustrating the so-called light reactions of bacterial photosynthesis. Photons from the sun are first absorbed by peripheral or light-harvesting 2 (LH2) pigment-protein complexes (This step is indicated with ① in the figure). The excitation energy is then rapidly and efficiently transferred within and between several LH2 complexes, ②, via another type of pigment-protein complex, named light-harvesting 1 (LH1) complex, ③, towards the RC, ④, which is enclosed by LH1. In the RC a charge separation occurs, ⑤, which build up a proton gradient across the cytoplasmic membrane in which the whole photosynthetic unit is embedded. Leaving details aside, this gradient finally drives an ATPase complex - an elaborate molecular machinery located next to the RC in the membrane - which synthesizes ADP to ATP, the universal chemical energy unit used for keeping the metabolism of the bacteria running [32].

The supramolecular structure of the photosynthetic unit is well reflected in the absorption spectrum of native membrane fragments, also called chromatophores. Chromatophores are produced by the fragmentation of the intracytoplasmic membrane of purple bacteria and contain LH complexes as well as the RC [33]. Fig. 2.1 (b) shows the fluorescence-detected absorption spectrum of chromatophores from the species *Rhodospseudomonas (Rps.) acidophila* in a buffer solution recorded at 1.2 K. The two intense bands around 800 and 870 nm can be assigned to the absorption of the B800-850 or LH2 complexes, whereas the less intense band at around

900 nm represents absorption of LH1 complexes.

It is worth to note that depending on the growth conditions the ratio between peripheral and core complexes, i.e. LH2 and RC-LH1 complexes, in the membrane may be altered by the bacterium [34]. Furthermore some species are even able to synthesize other types of peripheral complexes under "stressed" growth conditions, e.g. low-light conditions, giving rise to absorption bands at different wavelength positions. From *Rps. acidophila* (strain 7050), for example, the peripheral B800-820 or LH3 complex is known, which reveals an absorption band shifted to the blue wavelength region with respect to that of the LH2 complex [35].

Solubilization of the photosynthetic membrane with a suitable detergent enabled the isolation and purification of the LH2 and RC-LH1 pigment-protein complexes [8, 36]. Furthermore, successful crystallization of the purple bacteria antenna complexes opened the door for X-ray crystallographic studies [37]. The determination of the X-ray crystal structure of the RC in 1984 [38], was followed by highly-resolved structures of LH2 [10, 11] and yet less-resolved ones of the LH1 complex [12], set the basis for a deeper understanding of photosynthesis in purple bacteria.

X-ray crystallography revealed that the LH complexes feature highly symmetric structures having an important influence on their spectral characteristics and function. In the following, the structure and the function, as well as their interdependence, will be discussed in detail for the LH2 complex from the purple non-sulfur photosynthetic bacterium *Rps. acidophila* (strain 10050), since in this thesis only studies on this specific type of pigment-protein complex have been performed. However, it is worth to note that some of the discussed phenomena might be relevant for other types of pigment-protein complexes from this species like LH1 and LH3, as well as for the LH complexes from other species of purple bacteria, due to their high structural similarity. At the same time, most of the results obtained from studies on LH complexes of other species can be applied in turn to the LH2 complex from *Rps. acidophila*.

### 2.3 Light-harvesting 2 complexes

LH complexes from purple bacteria consist of pigments and so-called transmembrane proteins. While the two types of pigments, carotenoids (Car) and bacteriochlorophyll (Bchl) *a*, are responsible for the light absorption, the proteins act as a scaffold for the pigments within the photosynthetic membrane. X-ray studies have proved that the construction of LH complexes is based on a modularized principle.

In Fig. 2.2 (a) this modular principle is illustrated for the LH2 complex from *Rps. acidophila*. One Car pigment of *rhodopin glucoside* together with three Bchl<sub>a</sub> molecules (left hand side) are combined with two different low-molecular weight  $\alpha$ -helical shaped apoproteins called  $\alpha$  and  $\beta$  polypeptides. The three Bchl pigments are non-covalently liganded via their central Mg atoms to amino acid residues of the two apoproteins, while the Car pigment is spanned across this structure in close

van der Waals contact to the Bchl pigments for "bolting" together with the neighbouring  $\alpha\beta$ -apoprotein pairs (middle). Starting from this basic building block, also called protomer, a circular arrangement from nine of those units forms the ring-like structure of the LH2 pigment-protein complex with a nonameric symmetry (right hand side). In total, 27 Bchl and nine Car pigments are embedded between an inner and outer wall formed by the two rings of 9  $\alpha$ - and  $\beta$ -apoproteins, respectively. The diameter of this cylindrical aggregate, comprising about 21000 atoms with a total molecular weight of  $\sim 140000$  g/mol, is about 65 Å [7].

On left hand side of Fig. 2.2 (b) the room-temperature absorption spectrum of LH2 from *Rps. acidophila* in buffer-detergent solution is depicted. The absorption bands can be assigned to the different pigments within the LH2 complex. In the visible region around 500 nm the absorption band is due to the Car pigments, which is also responsible for the brown/purple color of isolated LH complexes from purple bacteria. The carotenoid *rhodopin glucoside* is a linear molecule with conjugated double bonds (blue structure in (a)). The characteristic absorption band in the blue-green spectral region is the result of an electronic transition from the ground state,  $S_0$ , to the higher singlet state,  $S_2$  [39], which is, in contrast to the  $S_0 \rightarrow S_1$  transition, optically allowed for one-photon absorption [40]. Besides the light-harvesting function in the visible region and structural stabilization effects, the main function of Car pigments is the protection of bacterial photosynthesis from the harmful effects of singlet oxygen. Carotenoids act as photoprotective agents by either direct non-photochemical quenching of singlet oxygen, or preventing its production by quenching the excited triplet states of Bchl molecules which may otherwise form singlet oxygen by reacting with molecular oxygen [41].

The Bchl *a* molecule consists of a porphyrin ring with a central Mg atom and a phytol chain (see grey structure in (a)). The delocalisation of the electronic wavefunction within the porphyrin macrocycle determines the photophysical properties of this pigment. Transitions into higher excited singlet states ( $S_0 \rightarrow S_3/S_4$  transition), named  $B_x/B_y$  or Soret band, give rise to an absorption band in the UV spectral region below  $\sim 400$  nm, as can be seen in (b).

While the less intense absorption band at  $\sim 590$  nm can be assigned to transitions into the second lowest excited singlet state ( $S_0 \rightarrow S_2$  transition) of the Bchl pigments, the two more intense bands in the near infrared region at 800 nm and around 850 nm are due to transitions into the lowest excited singlet state ( $S_0 \rightarrow S_1$  transition). The transition dipole moments of these two transitions are indicated by the orthogonal arrows in the porphyrin structure in (a) and named  $Q_x$  and  $Q_y$ , respectively.

Usually, the  $Q_y$  transition of monomeric Bchl *a* in organic solvent absorbs at 772 nm [8]. However, in the LH2 complex, because of the highly ordered arrangement of the Bchl pigments within the protein walls into two concentric rings, the  $Q_y$  transition give rise to two absorption bands instead of only one, although the Bchls are chemically identical. On the right hand side of Fig. 2.2 (b) the two Bchl rings

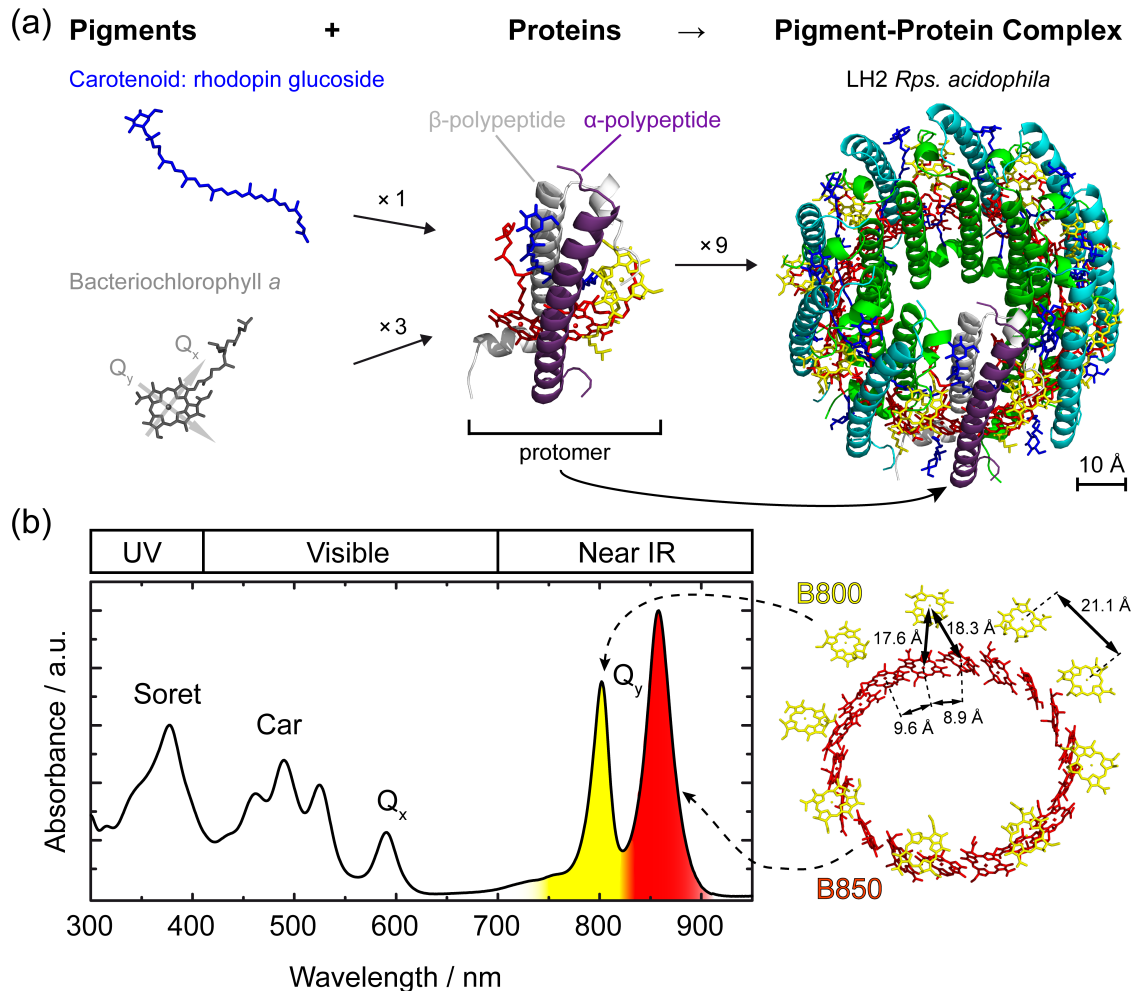


**Figure 2.2:** Building principle and room-temperature absorption spectrum of LH2 from *Rps. acidophila* in buffer-detergent solution. (a) Left-hand side: Structure of the Car and Bchl a pigments. Middle: Combination of pigments with an  $\alpha/\beta$ -polypeptide pair forming the protomer of a LH2 complex. Right-hand side: LH2 complex consisting of a circular arrangement of nine protomers. The scale bar is only valid for this figure. (b) Left-hand side: Room-temperature absorption spectrum of LH2 in detergent solution with assignment of different bands. Right-hand side: Spatial arrangement of the two concentric Bchl pigment rings being responsible for the two intense absorption bands in the NIR region. The numbers give the center-to-center distances between the Bchl pigments as determined by X-ray crystallography. The phytol chains of the pigments have been removed for clarity.

inside the LH2 complex are displayed without the protein backbone, Car pigments and phytol chains. 9 of the 27 Bchl pigments (yellow color) are circularly oriented with their bacteriochlorin rings parallel to the photosynthetic membrane at its cytoplasmic side (i.e. towards the N-termini of the polypeptide helices) having a mutual distance of about 21 Å. According to the spectral peak position at around 800 nm, this ring is named B800 ring and the tuning of the absorption wavelength with respect to monomeric Bchl is mainly caused by the non-covalent H-bonding of the pigments with the surrounding proteins [8].

The remaining 18 Bchl molecules (red color), which are oriented in a turbine-wheel manner with their bacteriochlorin rings vertical to the photosynthetic membrane towards its periplasmic side (i.e. near the C-termini of the polypeptides). The center-to-center distances between adjacent molecules is less than 10 Å. Because of their binding to either an  $\alpha$ - or a  $\beta$ -apoprotein (see above), the distances between nearest neighbored Bchls in this ring are slightly smaller for every second pigment, resulting in an overall dimeric structure of this ring with  $C_9$  symmetry [42–44]. This Bchl ring is responsible for the absorption at 858 nm and thus called the B850 ring. Due to the small inter-pigment distances and the fact that the individual  $Q_y$  transition-dipole moments are oriented parallel to each other along the ring, the pigments in the B850 ring can strongly interact with each other. The extensive strong pigment-pigment interactions lead to excitonic effects with which the red-shifted absorption relative to the monomer absorption can be explained [45]. In Fig. 2.2 (b) the assignment of the rings with their corresponding absorption bands is indicated by the dashed arrows.

Due to their great importance in the light-harvesting and excitation energy-transfer function of the LH2 complex, the structure-function relationship of these two rings, as well as their theoretical description, will be discussed in more detail in the following chapter of this thesis.

## 3 Spectroscopy on LH2 complexes

A great deal of information about the structure-function relationship in LH2 complexes can be obtained by means of optical spectroscopy. The electronic structure and dynamics of these complexes are mainly determined by the pigment-pigment interaction strength, spectral broadening and electron-phonon coupling. In the following, these parameters and related quantities will be shortly explained including some general aspects and a brief introduction to the Frenkel exciton formalism, which is commonly used for a theoretical description of the absorption properties of LH complexes. With this at hand steady-state ensemble and single complex absorption characteristics, as well as shortcomings of the formalism for the description of the emission properties, will be discussed and an alternative explanation dealing with the self-trapping of excitons is presented. Furthermore, in the context of ensemble and single-molecule studies addressing the absorption and emission characteristics of LH2 complexes that are available in literature, the aim of this work is outlined.

### 3.1 Interaction strengths and excitation energy transfer

#### Interaction strengths

For neighboring Bchls in the B800 ring interaction strengths in the order of 20 - 30  $\text{cm}^{-1}$  have been reported [8, 46] while between the B800 and B850 Bchls a slightly larger coupling strength of  $\sim 50 \text{ cm}^{-1}$  was found [25, 47]. In the B850 ring, owing to the smaller mutual distances, the interaction strength between the pigments is about  $\sim 300 \text{ cm}^{-1}$ , ten times larger than in the B800 ring. It is important to note that for the latter value various numbers exist in the literature, ranging from  $\sim 200$  to more than  $800 \text{ cm}^{-1}$ , depending on the experimental methods and theoretical calculations used for determination [8]. As temperature is thought to influence the nearest neighbor couplings in the B850 ring also (a 35 % increase for low temperature structures with respect to room temperature is reported in [48]), care has to be taken when absolute values from different studies are compared with each other.

### Excitation energy transfer between and within LH complexes

Depending on the different distances and interaction strengths, the times for excitation energy transfer (EET) between the pigments/rings within the LH2 complex differ. At room temperature the energy from one B800 Bchl to another is transferred within  $\sim 0.5$  ps. The next step of EET, between the B800 and B850 rings, occurs within  $\sim 1.2$  ps and between the closely spaced B850 Bchls the energy is transferred within about 100 - 200 fs. Further transfer steps, i.e. LH2  $\rightarrow$  LH2, LH2  $\rightarrow$  LH1, LH1-Bchl  $\rightarrow$  LH1-Bchl and LH1  $\rightarrow$  RC, happen in 10 ps, 3 - 5 ps, 80 fs and 35 ps, respectively. Hence, it is the last step (LH1  $\rightarrow$  RC) which mainly determines the  $\sim 50$  ps overall energy transfer time between a LH2 complex and the RC [45, 49–52]. Typically, at low temperature the observed times for energy transfer are slightly increased with respect to the room temperature values.

While the EET in the B800 ring can be best characterized by a so-called incoherent (hopping) process, in the B850 ring coherent (wavelike) EET is assumed (see below for a further description of the two processes). Interestingly, none of the EET steps relevant in the photosynthesis of purple bacteria can be satisfactorily described by the traditional theory of EET, the Förster resonance energy transfer [53–57], although this theory has been widely used, due to its simplicity for the EET description in these systems, with success in many aspects [30, 51].

The dynamics of the multichromophoric excitations in LH complexes are theoretically better described by the generalized Förster theory [47, 58–60] or by so-called Redfield theories, which in contrast to the traditional Förster theory are not only based on the pigment-pigment interactions, but take also intramolecular vibrations of the molecules and intermolecular interaction with the protein backbone, i.e. electron-phonon couplings, into account [56, 61–63].

### 3.2 Theory of excitons

For the description of the optically excited states in the LH2 complexes a quantum mechanical framework is useful, which is provided by the model of molecular excitons developed by Frenkel and Davydov [64–67]. A ringlike aggregate, consisting of  $N$  two-level molecules whose transition energies do slightly deviate by  $\Delta E_n$  and which are coupled to each other, can be described by the following Hamiltonian [8, 68, 69]:

$$H = \sum_{n=1}^N (E_0 + \Delta E_n) |n\rangle \langle n| + \sum_{n=1}^N \sum_{m \neq n} (V_{nm} + \Delta V_{nm}) |n\rangle \langle m| \quad (3.1)$$

Here,  $|n\rangle$  represents a molecule  $n$  in the electronically excited state and all other molecules  $1, 2, \dots, n-1, n+1, \dots, N$  in the ground state. Each molecule can be assumed as a two-level system consisting of a ground state and a single electronically excited state and  $E_0$  denotes the excitation or site energy which separates the

two states.  $V_{nm}$  is the interaction strength between the molecules in the excited states located on molecule  $n$  and  $m$  and is mainly determined by the electrostatic interactions between electrons and nuclei from neighboring pigments. If the pigments are not permanently charged and if their relative distances are considered to be large compared to their size, i.e. if the exchange interactions can be neglected with respect to the Coulomb interaction, one can approximate  $V_{nm}$  with the dipole term in the multipole expansion of the Coulomb interaction, which is inversely proportional to the cubic relative distance between the two transition dipole moment vectors of the neighboring pigments. For details the reader is referred to [8, 27].

If the Hamiltonian is written in matrix form, the first term in Eq.(3.1) refers to the diagonal elements of the matrix, whereas the second term represents the off-diagonal ones. The diagonal disorder  $\Delta E_n$  accounts for local differences in the protein environment nearby the pigments, which leads to variations in the site energies  $E_0$ . Deviations from perfect symmetry, which will result in variations of the pigment-pigment interactions or dielectric fluctuations, are considered by  $\Delta V_{nm}$  in the second term of Eq.(3.1) and therefore denoted as off-diagonal disorder [8, 70]. It depends on the ratio between the interaction strength  $V$  and the site energy difference  $\Delta E$ , whether the site representation  $|n\rangle$  or the exciton representation, i.e. linear combinations of the localized wavefunctions, so-called Frenkel excitons,

$$|k\rangle = \frac{1}{\sqrt{N}} \sum_{n=1}^N e^{i2\pi k \frac{n}{N}} |n\rangle \quad (k = 0, \dots, N-1) \quad (3.2)$$

is more appropriate for the description of the electronically excited states in the circular array of  $N$  pigments [8].

If  $|V/\Delta E| \ll 1$  (weak coupling limit) the interaction between the transition dipole moments of the pigments is much smaller than the difference in site energies and the excitations are localized on single pigments. For this case the wavefunctions of the individual pigments can be regarded as proper eigenfunctions of the Hamiltonian in Eq.(3.1) and the description in terms of localized states  $|n\rangle$  is a good approximation. The transfer of energy between these pigments then takes place as a diffusive hopping process, which is also termed incoherent energy transfer [8].

In case of  $|V/\Delta E| \gg 1$  (strong coupling limit), where the interaction strength is much larger than the energetic disorder, the description of the excited states with the Frenkel excitons  $|k\rangle$  is more appropriate. Here, the transfer of excitation occurs in a wavelike manner which is also denoted as coherent energy transfer [8].

Although the requirements are not fulfilled completely, these limiting cases can be used to describe the characteristics of the B800 and B850 rings in the LH2 complexes. In the B800 ring, where the interaction  $V$  is about  $20 \text{ cm}^{-1}$  [51] and the disorder is about  $180 \text{ cm}^{-1}$  (estimated from the inhomogeneously broadened ensemble spectrum at room temperature) one gets for  $|V/\Delta E|$  a value in the order of  $\approx 0.1$  [8]. The absorption band of LH2 observable at around  $800 \text{ nm}$  (see Fig. 2.2

(b)) can thus be attributed to the optical excitations of weakly coupled B800 Bchl pigments which are mainly localized on individual pigments [46, 51]. In contrast, for the B850 ring, for which an interaction strength of  $\sim 300 \text{ cm}^{-1}$  and a disorder of about  $200 \text{ cm}^{-1}$  can be assumed,  $|V/\Delta E|$  proposes a delocalization of the excitation at least over a part of the ring [71–73].

If the disorders are assumed to be zero ( $\Delta E, \Delta V = 0$ ), the interaction term  $V_{nm}$  in Eq.(3.1) leads to a splitting of the initially degenerated localized excited states of the 18 pigments in the B850 ring and results in a manifold of energy levels called exciton band. Neglecting the slight dimerization of the B850 Bchl molecules, this exciton band consists of two nondegenerate (denoted as  $k = 0$  and  $k = 9$ ) and eight pairwise degenerate ( $k = \pm 1, \pm 2, \dots, \pm 8$ ) exciton levels [74] and is distributed over a width of about four times the typical intermolecular interaction strength,  $\delta E \approx 4V$  [51, 67, 75]. Calculated and experimentally determined values for the B850 exciton bandwidth of the LH2 complex range from  $1100 - 2500 \text{ cm}^{-1}$  [28, 46, 48, 50, 54, 68, 76–79].

The absorption of the B850 band is caused by the optical transitions between the ground state and any given exciton state in the manifold. A calculation of the transition dipole moments reveals that, due to the circular arrangement of the pigments in the LH2, only the exciton states  $k = 0, \pm 1$  at the low-energy, and  $k = \pm 8, 9$  at the high-energy side of the exciton band have a non vanishing dipole moment [8]. However, by virtue of the head-to-tail arrangement of the transition dipole moments within the individual Bchl dimers in the B850 ring, most of the oscillator strength is concentrated in the lower exciton states  $k = 0, \pm 1$ , whereby the contribution from the  $k = 0$  state turns out to be only small. Thus, the characteristic B850 absorption band of LH2, which is observable at  $850 - 860 \text{ nm}$  in the NIR spectral region (see Fig. 2.2 (b)), can be mainly assigned to the  $k = \pm 1$  states [80]. The minor amount of the oscillator strength ( $< 3 \%$ ) which is distributed to the upper exciton states  $k = \pm 8, 9$ , gives rise to a very weak absorption peak only. Due to its overlap with the B800 band, it is very difficult to observe it in steady-state experiments [26, 46].

### 3.3 Disorder, homogeneous and inhomogeneous broadening

Energetic and structural heterogeneities in the B850 ring, however, do affect the unperturbed exciton manifold and result in a mixing of the different exciton levels, a modification of the energy separation between the exciton levels, a lifting of their pair-wise degeneracy, and a redistribution of the oscillator strength to adjacent states, which makes these states also visible in optical spectroscopy. This is described by the so-called disordered Frenkel exciton model [8, 15, 69].

Energetic  $\Delta E$  and structural  $\Delta V$  disorder can be considered also as slow fluctuations of the transition energies or inter-pigment couplings and are therefore called static disorder. Static disorder leads to an inhomogeneously broadening of the ab-

sorption bands in the ensemble spectra of LH2.

In contrast, the high-frequency fluctuations of the interactions of the pigments with their surrounding can cause the energy gap between the excited and the ground states to fluctuate on a much faster timescale - thus named dynamic disorder - leading to homogeneous broadening of the absorption band. Another contribution to the homogeneous broadening comes, for example, from the life-time broadening due to the finite lifetime of the excited state and the time-energy uncertainty relation [81].

Within this context, the terms (i) homogeneous and (ii) inhomogeneous mean that for (i), the broadening is regarded the same for each and every chemically identical molecule in the ensemble and for (ii), that the pigment in a disordered host (e.g. glass, polymer and protein) is able to adopt a very large number of energetically inequivalent sites, i.e. different microenvironments [82]. As a consequence the spectroscopically observed width of an absorption band reflects always the influence of both types of disorders, and has a homogeneous and inhomogeneous component.

### 3.4 Homogeneous linewidth of ZPL

The homogeneous linewidth  $\Gamma_{\text{hom}}$  (full width at half maximum, FWHM) of the absorption line of an electronic transition can be described by [27, 82]

$$\Gamma_{\text{hom}}(T) = \frac{1}{\pi\tau_2} = \frac{1}{2\pi\tau_1} + \frac{1}{\pi\tau_2^*(T)}, \quad (3.3)$$

where  $\tau_2$  refers to the total dephasing (phase relaxation) time which is determined by the excited state (energy relaxation) lifetime  $\tau_1$  and the pure dephasing (coherence) time  $\tau_2^*$  that depends on temperature.

At room temperature, typical excited state lifetimes  $\tau_1$  of molecules lie in the range of ns, whereas pure dephasing times  $\tau_2^*$  are in the order of ps or even smaller [83].  $\tau_2^*$  represents the time it takes for the coherence of the electronic transition to get lost due to the interactions of the pigment with its surrounding, i.e. pigment-protein interactions. At low temperatures  $\tau_2^*$  increases and the homogeneous linewidth is determined by the excited state lifetime  $\tau_1$  only.

### 3.5 Linear electron-phonon coupling, PSB and S-factor

In the absorption (emission) spectrum of a single pigment at low temperature (see Fig. 3.1) a sharp line of Lorentzian shape with a width  $\Gamma_{\text{hom}}$  will be observed, accompanied by an asymmetric band at higher (lower) frequency. The sharp band is called zero-phonon line (ZPL) and reflects the purely electronic transition, whereas the asymmetric band is denoted as the phonon sideband (PSB) and corresponds to the excitations of low-frequency vibrations, also called phonons, which are simultaneously excited with the electronic transition [84]. In general, for molecular

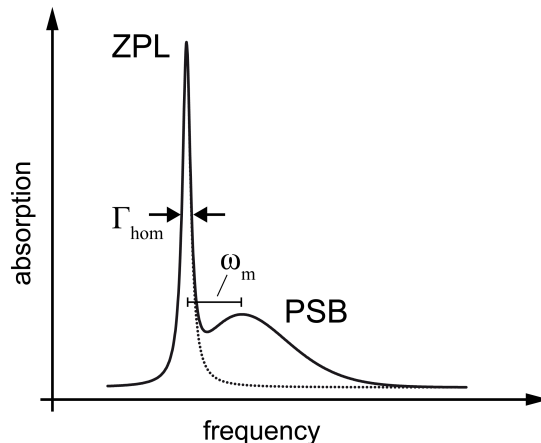


**Figure 3.1:** Schematic view of a narrow zero-phonon line (ZPL) and a broad phonon sideband (PSB) seen in the absorption spectrum of a single molecule at low temperature.  $\Gamma_{\text{hom}}$  denotes the homogeneous linewidth of the ZPL and  $\omega_m$  the mean phonon frequency.

crystals and aggregates the term phonon denote the vibrations of the lattice surrounding a pigment, while in the case of pigment-protein complexes this term is typically referred to the protein vibrations [27]. The PSB is displaced from the ZPL towards higher (lower in the case of emission) energies by the so-called mean phonon frequency  $\omega_m$ , which is in the order of 20 - 30  $\text{cm}^{-1}$  for organic molecules [82].

It is the electron-phonon interaction (also called vibronic interaction) that determines the shape of the absorption spectrum displayed in Fig. 3.1. The quantity with which this coupling in the linear regime is commonly described in spectroscopy, is the so-called dimensionless Huang-Rhys factor or electron-phonon coupling constant  $S$ . In the low-temperature limit ( $T \sim 0$ )  $S$  can be related to the (also dimensionless) Debye-Waller factor  $\alpha_{DW}$  via

$$\alpha_{DW} = \frac{I_{ZPL}}{I_{ZPL} + I_{PSB}} = \exp(-S), \quad (3.4)$$

with  $I_{ZPL}$  and  $I_{PSB}$  being the relative, spectrally integrated intensities (i.e. areas) of the ZPL and the PSB in the spectrum, respectively.

In Fig. 3.2 the relation between electron-phonon coupling and the resulting emission spectrum for an electronic transition in a hypothetical molecule is schematically illustrated.

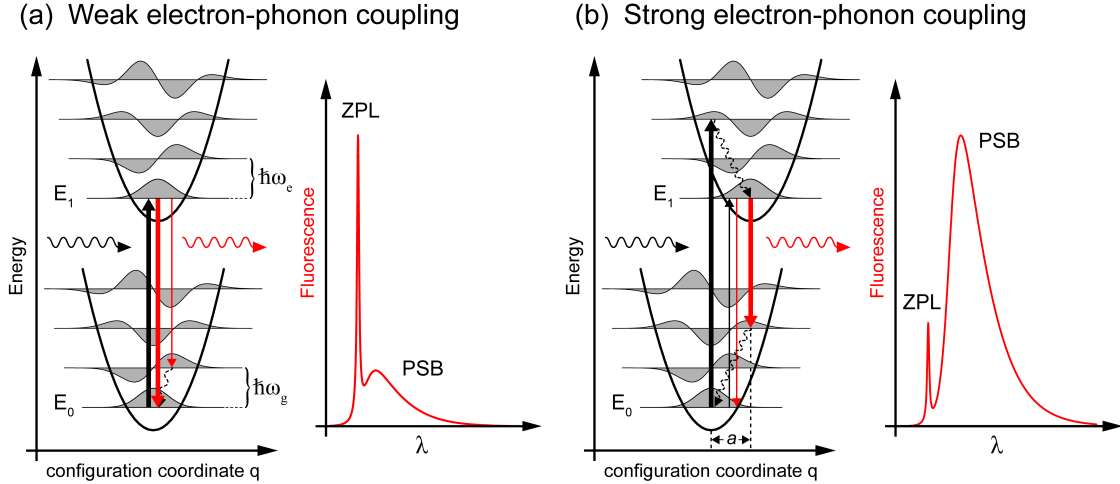


**Figure 3.2:** Configuration coordinate diagram of the electronic ground ( $E_0$ ) and excited ( $E_1$ ) state potentials (black parabolas) of a single molecule at low temperature in the linear electron-phonon coupling regime ( $\hbar\omega_e = \hbar\omega_g$ ). The two cases of weak (a) and strong coupling (b) are depicted. The horizontal lines refer to the vibrational levels and the vertical arrows display the optical transitions (absorption - black, fluorescence - red) according to the Franck-Condon principle. Next to the parabolas the corresponding fluorescence spectrum is schematically drawn (red curve). Figure redrawn with modifications from [82].

It shows the configuration coordinate diagram of the ground and excited state for the case of weak and strong electron-phonon coupling strength. In the case of linear electron-phonon coupling  $\hbar\omega_g = \hbar\omega_e = \hbar\omega$ , that is the frequency of the phonon mode in the ground and excited state is the same, only the equilibrium positions, i.e. the centers of the two parabolas, are shifted horizontally with respect to each other [82]. This horizontal displacement between the minimum energy positions of the harmonic vibrational potentials, denoted as  $a$  in Fig. 3.2 (b), can be related to the Huang-Rhys factor by the expression

$$S = a^2/2. \quad (3.5)$$

The relative intensities of the transitions can be explained according to the Franck-Condon principle, which states that transitions between two electronic states do most likely occur for those vibrational levels, for which the vibrational wavefunctions have the biggest overlap [85]. Hence, a change in the equilibrium positions of the ground and excited state potentials results in a poor Franck-Condon overlap, as the optical transition is redistributed between transitions into the vibronic sub-states of the electronic ground (excited) state [27].

It is the displacement of the equilibrium position  $a$ , and therefore the value of  $S$ , that determines the shape of the spectrum and if the electron-phonon coupling of

a transition is regarded as weak or strong. Typically, for  $S \ll 1$  a prominent ZPL, accompanied by a weak PSB, reflects a small electron-phonon coupling, Fig. 3.2 (a), whereas for  $S \gg 1$  the PSB is increased with respect to the ZPL signal, which corresponds to a strong electron-phonon coupling, Fig. 3.2 (b), [82]. However, the exact definition of weak and strong electron-phonon coupling depends largely on the system which is investigated.

Physically, one can explain the meaning of  $S$  as being the average number of phonons (or vibrational quanta) that accompany a particular electronic transition, i.e. the number of phonons absorbed/emitted upon electronic transition. This is expressed in the equation

$$S = \lambda / \hbar\omega_m, \quad (3.6)$$

with  $\lambda = \frac{a^2}{2} \hbar\omega_m$  being the Franck-Condon-, (optical) reorganization or lattice relaxation energy and  $\hbar\omega_m$  the mean quantum energy of a vibration.

In the case of a molecular aggregate, like the LH complex,  $S$  is sometimes defined as  $S = E_{LR} / \hbar\omega_m$ . Here,  $E_{LR}$  is the so-called gap or site reorganization (deformation) energy, which is the product of the lattice relaxation energy  $\lambda$  and the localization length  $L$ , describing the delocalization of the excitation among the molecules of the aggregate [86].

Moreover, if the quadratic electron-phonon coupling is taken into account the curvature of the parabola, representing the excited state, will change, which in turns results in a different spacing between the vibrational levels with respect to those from the ground state, i.e.  $\hbar\omega_e \neq \hbar\omega_g$ . This would lead to a temperature dependent line-broadening of the ZPL, in contrast to the case of linear electron-phonon coupling, for which the width of the ZPL is independent of temperature [82, 87]. However, here we restrict ourselves to the linear approximation, with the Huang-Rhys factor  $S$  being the proper parameter for a description of the observed effects.

### 3.6 Stokes shift

If the corresponding spectra of the electronic transitions in absorption and emission are compared to each other, one will discover that the maxima of the spectra are shifted with respect to each other. The spectral distance between the absorption and emission band belonging to the same electronic transition, i.e. the difference in energy, is called Stokes shift [87] and it is related to the Huang-Rhys factor  $S$  via

$$\text{Stokes shift (SS)} = 2S\hbar\omega. \quad (3.7)$$

Disregarding big vibrational quantum energies, large Stokes shifts can generally be attributed to strong electron-phonon coupling, as the two parabolas are widely displaced and thus the peak of the emission band is spectrally shifted more to the red with respect to that from the absorption. In contrast, small Stokes shifts are typically observed in systems with weak electron-phonon coupling [87].

### 3.7 Ensemble spectroscopy

As pointed out above, the influence of disorder in a molecular aggregate of identical pigments, like the LH2 complex, is spectroscopically reflected in the inhomogeneous linewidth of the steady-state absorption/emission spectrum of an ensemble of complexes. Experimental methods to disentangle the different contributions of homogeneous and inhomogeneous broadening effects in spectra from pigment-protein complexes are, for example, spectral hole burning (SHB) and fluorescence line narrowing (FLN) methods. Whereas SHB probes the transitions from the (lowest) ground state to the excited state, i.e. the absorption, FLN does the same for transitions from the (lowest) excited state to the ground state, i.e. the emission properties. Besides information about the electronic structure, EET and electron-transfer dynamics, these so-called site-selective spectroscopy methods enable also an accurate determination of electron-phonon coupling strengths in terms of the Huang-Rhys factor  $S$  [27, 82]. Prerequisites for these methods are basically very low temperatures (typically  $\leq 5$  K) and narrow-bandwidth lasers.

#### Absorption

Within the framework presented above, the ensemble absorption spectrum of LH2 complexes dissolved in glycerol-buffer solution at cryogenic temperature (schematically illustrated in Fig. 3.3 (a), black dashed line, left-hand side) can be described as follows. The linewidth of the B800 absorption band is denoted as inhomogeneously broadened ( $\Gamma_{\text{inhom}}^{\text{B800}} = 120 - 150 \text{ cm}^{-1}$ ), due to the fact that it consists of many sharp absorption lines from single, weakly coupled Bchl pigments in the B800 ring, which absorb at different wavelengths [49, 83, 88–90]. The homogeneous linewidths experimentally observed by SHB in the B800 band, which are in the order of some wavenumbers ( $\Gamma_{\text{hom}}^{\text{B800}} \leq 5 \text{ cm}^{-1}$ ), however, do not reflect the actual homogeneous linewidth. They rather represent a superposition between the excited state lifetime of a single Bchl transition, including the fast energy transfer from the B800 Bchl to higher lying exciton states of the B850 exciton manifold, and spectral diffusion effects (see below) [82, 90]. From SHB experiments, the electron-phonon coupling strength in the B800 band was classified to be weak.

In contrast, from SHB and absorption spectroscopy the linewidth of the B850 band was found to be dominated by homogeneous broadening with  $\Gamma_{\text{hom}}^{\text{B850}} = 200 - 250 \text{ cm}^{-1}$  (Fig. 3.3 (a), black dashed line, middle part) [49, 89, 91, 92]. The homogeneity arises from the broad absorption lines attributed to the B850 exciton states, which lie in the range of  $50 - 200 \text{ cm}^{-1}$ , and reflects the ultrafast ( $\sim 100$  fs) interexciton relaxation processes in the B850 manifold [49, 93].

Interestingly, by zero-phonon hole (ZPH) action spectroscopy experiments, a weak but distinct shoulder (Fig. 3.3 (a), purple shaded area in the inset, right-hand side, enhanced with respect to the B850 absorption) was found in the red edge of the

B850 band, located about  $200 \text{ cm}^{-1}$  below the B850 absorption maximum. This shoulder comprises a distribution of sharp absorption lines (marked in the inset of Fig. 3.3 (a) in white color), featuring an inhomogeneous width of  $\Gamma_{\text{inhom}}^{\text{B870}} = 120 - 150 \text{ cm}^{-1}$  [48, 93, 94].

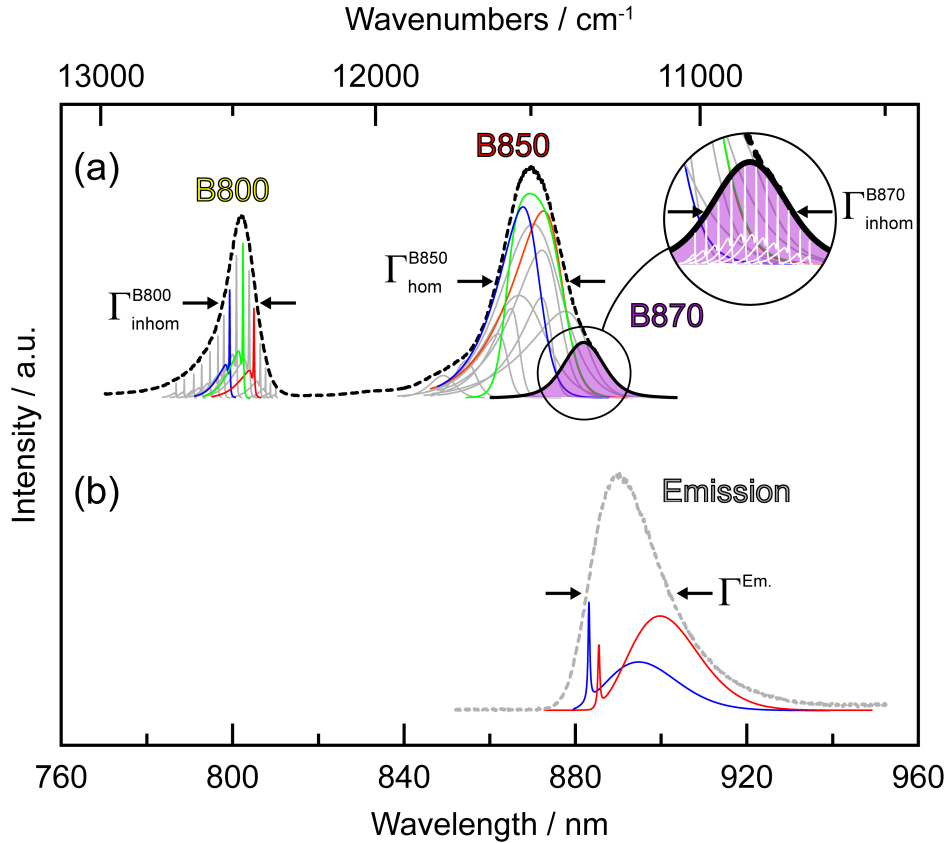


**Figure 3.3:** Schematic representation of the line broadening types in the (fluorescence-detected) absorption (a) and emission (b) spectrum of an ensemble of LH2 complexes in solution, recorded at low temperature. For details see text.

This band, either denoted as inhomogeneous distribution function (IDF), inhomogeneous distribution of the exciton origin states (ISDF)[86, 95] or simply as B870 band, has been assigned to the lowest energy exciton level ( $k = 0$  state) of the B850 manifold and is not visible in usual absorption or fluorescence-excitation spectroscopy experiments [80, 91, 93, 96]. The homogeneous widths of ZPLs obtained from the holes that could be burned into the B870 band, were determined to be no smaller than  $0.3 \text{ cm}^{-1}$ , which correspond to excited state lifetimes in the range of ps [91, 93, 96]. However, these values did not represent the excited lifetime of the B870 state which from time resolved experiments is known to be  $\sim 1 \text{ ns}$

[92, 94, 97, 98], but are rather due to the limited resolution of the experimental setups. Moreover, the electron-phonon coupling strength, determined from these ZPH action experiments, has been found to be weak ( $S \approx 0.3$ ) [95].

Mostly all of the experimental findings from absorption spectroscopy can be very well described by the disordered Frenkel exciton model. This, however, does not hold true for the corresponding emission spectrum, which lacks a satisfying explanation with this approach, as shown in the following.

## Emission

In contrast to the inhomogeneously broadened absorption band of the lowest energy exciton level (B870), the emission band of the LH2 ensemble (Fig. 3.3 (b), grey dashed line) is mostly dominated by homogeneous broadening. FLN spectroscopy methods revealed that instead of a resonant, well-structured fluorescence with a narrow bandwidth, the observed LH2 emission displayed a broad ( $\Gamma^{\text{Em.}} = 250 - 300 \text{ cm}^{-1}$ ) considerably red shifted and almost structureless shape under both, resonant and non-resonant excitation [95, 99]. Furthermore, the overall shape and width of the emission spectrum did only change little upon selective excitation in the B870 band, thereby, suggesting a strong electron-phonon coupling [99]. Obviously, this finding is inconsistent with the above described characteristics of the B870 absorption band, revealing a two-times narrower bandwidth.

### 3.7.1 Discrepancies of the Frenkel exciton model

Besides the discrepancies from steady state absorption and emission spectroscopy outlined above, time-resolved spectroscopy studies, at room and low temperature, revealed that the collective coherent excitation, i.e. the exciton, which is supposed to be almost delocalized over the whole B850 ring at the moment of excitation [100], as proposed by the Frenkel exciton model, contracts significantly with time and gets localized [97, 101–103]. Suffering from different definitions and/or from the differences of the applied theoretical and experimental studies (method, temperature, etc.), the number of pigments that share the excitation, usually denoted as exciton delocalization length, range from a few pigments to the whole ring [8, 72]. Despite this, an important common result from these studies was that the loss of coherence in the B850 ring and thus the degree of delocalization or the localization of the excitation is mainly determined by both, static and dynamic disorder [27, 103, 104]. As a consequence, the lowest exciton state  $k = 0$ , from which emission occurs, will gain considerable oscillator strength at the expense of the  $k = \pm 1$  states [102]. This is supported by temperature dependent measurements of the fluorescence lifetime of LH2, which reveal only a small change of about 20 % between cryogenic and ambient temperatures, although a significant reduction is expected due to the thermal population of the strongly allowed  $k = \pm 1$  exciton states [97].

On the basis of the Frenkel exciton model, this can only be explained by assuming static disorder in the Bchl pigments site energies, being much too large to be consistent with the absorption spectrum [105].

Furthermore, the localization process after the initial delocalization of the excitation occurs on a time scale of a few hundred fs and thus being three orders of magnitude faster than the fluorescence lifetime of the exciton. This strongly suggests again that the dynamic type of disorder should be taken into consideration for these systems [50, 75, 103, 106, 107]. Some of the above described discrepancies, therefore, led to the conclusion that the excitons might be strongly coupled to their dynamic environment, i.e. the electron-phonon coupling strength in the B850 assembly cannot be any longer regarded as weak.

### 3.7.2 Polaron formation, self-trapping of excitons

In the case of strong electron-phonon coupling, which in general leads to a further localization of the excitation, it is also possible that a polaron formation takes place. Whereas in the solid-state picture a polaron is defined as a charge together with its deformation in a crystal lattice, in the field of molecular crystals, one can think about a polaron as an excitation accompanied by a lattice distortion [108–112]. At sufficiently large electron-phonon coupling strengths, i.e. if the interaction of the exciton with the phonon field becomes strong, the exciton induces a structural reorganization of its environment, which lowers its energy to an extent such that the excitation energy can get trapped on a limited region of the molecular assembly. Theoretical [113] and experimental studies [94, 99, 114] revealed that this phenomenon, which is commonly referred to as exciton self-trapping [27], is of relevance for LH complexes from purple bacteria. For one-dimensional systems it has been shown theoretically that self-trapping inherently takes place for any nonvanishing electron-phonon coupling [109]. Within certain reservations the B850 ring, consisting of the strongly electronically coupled Bchl *a* molecules, can be considered as an one-dimensional system.

In Fig. 3.4 a configuration coordinate diagram for excitations in the B850 assembly of LH2 complexes is displayed, illustrating the effect of self-trapping. Due to the strong electron-phonon coupling, the energy parabola of the excited state (red color) is shifted along the configuration coordinate  $q$  and lowered in energy by the self-trapping binding energy  $E_{ST}$  with respect to the ordinary excited state. As a result, the emission band, corresponding to the transition to the ground state, is red shifted and according to the Franck-Condon principle (see above) it gets broadened and unstructured. The site reorganization energy  $E_{LR}$  denotes hereby the energy that is released to the lattice upon light emission. Sometimes, this energy is also regarded as the difference between the Stokes shift and  $E_{ST}$ , which then however is based on another definition of the Stokes shift, being the difference in energy between the absorption in the B870 band and the emission band maximum [94, 99].

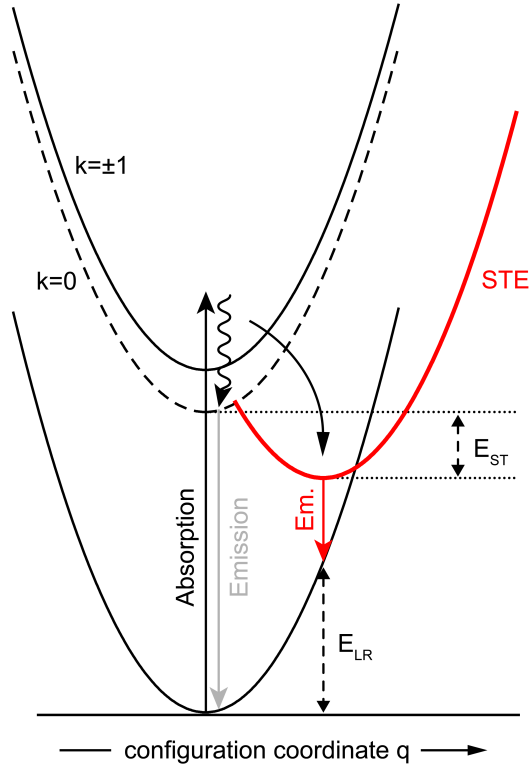


**Figure 3.4:** Configuration coordinate diagram illustrating self-trapping of excitons in the LH2 complex. The straight and curved arrows represent optical and relaxational transitions, respectively. The red parabola represents the self-trapped exciton state, which is shifted along the configuration coordinate axis with respect to the parabolas representing the lowest exciton states  $k = 0$  (black dashed) and  $k = \pm 1$  (black continuous) of the B850 assembly. Dashed vertical arrows denote the self-trapping binding energy  $E_{ST}$  and the lattice relaxation energy  $E_{LR}$ , respectively.

Both, resonant and non-resonant excitation, revealed that the LH2 emission is broad and considerably red shifted with respect to the B870 band [99]. As the emission from a self-trapped state, due to its relaxation in energy, has a significant red shift compared to the emission from the ordinary lowest exciton state, the concept of exciton self-trapping would not only explain the unusually large Stokes shift observed in the low temperature steady-state fluorescence of LH2 [115]. At the same time, it could also explain the above discussed apparent mismatch and poor mirror symmetry between the spectral shape of the B870 absorption and the emission spectrum, which is interpreted as a loss of direct correspondence between exciton absorption and emission [99, 116]. This qualitative difference between the absorbing and emitting state is also supported by pressure dependent studies, which showed that emission spectra do reveal a larger pressure sensitivity compared to that of the absorption spectra [117].

From spectrally selective excitation within the B870 band only a minor narrowing of the fluorescence band was found, thereby, suggesting that the electron-phonon coupling must be strong. This, however, is in contrast to results from ZPH action spectroscopy of the B870 band, indicating a weak electron-phonon coupling strength [48, 80]. Indeed, from  $\Delta$ FLN experiments, a double spectral selection technique simultaneously utilizing SHB and FLN spectroscopy, a larger electron-phonon coupling was determined as previously assumed [95]. Moreover, in these studies evidence was found that the emission profile most probably consists of two overlapping contributions, having different electron-phonon coupling strengths which was further supported by fluorescence lifetime measurements [94]. One contribution is representing the resonant B870 fluorescence, characterized with a Huang-Rhys factor of  $S = 0.8 - 1.1$ , whereas the other accounts for the red-shifted self-trapped exciton states with considerably larger electron-phonon coupling strength, thus suggesting a dual nature of the emission band [95, 118, 119]. From subsequent studies, however, it follows that the  $S$ -factors are slightly higher and that a rather continuous changeover between the two distributions is more likely. Furthermore, it was found that the coupling generally increases with burn fluence [86, 118].

Quantitatively, the exciton self-trapping, which depends on the times scales for the transfer of the excitation energy within the B850 assembly and the time that the nuclei need to react upon a change in the electronically excited state manifold [112], can be characterized by the dimensionless coupling constant

$$g = \frac{E_{LR}}{2V}. \quad (3.8)$$

Therein, the enumerator  $E_{LR}$  denotes the already introduced site reorganization energy, i.e. the energy that is absorbed by the surrounding lattice after optical excitation, and the denominator expresses half the exciton bandwidth, with  $V$  being the interaction strength between the pigments [86]. For  $g \rightarrow 0$  the exciton states are delocalized, whereas towards larger values, starting at a critical value  $g > g_c$ , the self-trapping of the exciton states increases. Depending on the influence of disorder, the critical value for LH2 is theoretically expected to be  $g \approx 0.3 - 0.6$  and, furthermore, it was found that the onset of self-trapping does depend on the excitation conditions [120].

As the time constants for the polaron formation in the LH2 antenna complexes were found to be on a time scale of a few hundred fs [50, 75, 94, 99, 103, 107, 121, 122], which is due to the coupling of the excitation with the phonon modes, i.e. the lattice vibrations of the protein environment, this phenomenon is regarded as a dynamic exciton localization effect. Besides in LH2 complexes, the effect of polaron formation was also found to play a role in the LH1 complexes from purple bacteria, though not as dominant as in LH2 [118].

Recent experiments suggesting the survival of excitons over the whole temperature range in isolated LH2 complexes as well as in intact cells of photosynthetic bacte-

ria [26, 78] corroborate the finding that exciton self-trapping persists not only at cryogenic but also at physiological temperatures [94]. If an excitonic polaron formation in a full photosynthetic unit occurs in the proximity of the regions connecting LH2 and LH1 complexes, this effect may improve, by broadening of the emission spectra and by maximizing the emission rate, the energy resonance between these complexes as well as between the complexes and the RC. From this, it follows that exciton self-trapping might be one of the key factors that is responsible for the high energy-transfer efficiency (nearly 100 %) within the photosynthetic apparatus and thus be a part of nature's strategy increasing the speed and efficiency of energy transfer in photosynthesis [86, 94, 99, 114].

### 3.8 Spectroscopy on single LH2 complexes

Besides the described site selective methods, another possibility to circumvent the inhomogeneous broadening of ensemble spectra and to obtain specific information about spectral characteristics of LH2 complexes is the method of single-molecule spectroscopy (SMS). By this technique an in detail investigation of the whole distribution of parameters (e.g. spectral position, linewidth, polarization, etc.), which determine the electronic structure of LH complexes, is possible, rather than it is from ensemble averaged values. Furthermore, it enables to follow the temporal development of these parameters and thus provides valuable information about the dynamics of the electronic structure, which is not accessible by ensemble spectroscopy methods. For this technique, cryogenic temperatures are advantageous with respect to ambient conditions, due to the reduction of photobleaching and line-broadening effects [8]. Usually, spectral information about either the absorbing or the emitting states of an individual LH complex is obtained by recording the fluorescence-detected absorption, i.e. fluorescence-excitation, or the emission spectrum of that complex, respectively.

In Fig. 3.5 the main differences between ensemble spectroscopy and SMS on LH2 complexes are illustrated. The black vertical trace (highlighted with yellow and red colors), on the left-hand side of (a), represents the fluorescence-excitation spectrum of an ensemble of LH2 complexes, embedded in a polymer film. This spectrum exhibits the already discussed broad absorption bands at around 800 and 860 nm. The black vertical trace on the right-hand side of (a), displays an time-averaged fluorescence-excitation spectrum of a single LH2 complex, featuring significant differences from the ensemble spectrum pictured on the left-hand side. In contrast to the ensemble spectrum, sharp lines around 800 nm are visible and in the spectral region between 850 - 870 nm, yet broad, but structured bands are resolved.

In the middle of Fig. 3.5 (a) black horizontal lines schematically illustrate the electronic level structure of a LH2 complex, with which the single complex spectrum can be very well understood. The fine structure in the 800 nm region can be related to optical excitations of individual, weakly coupled Bchl pigments that are orga-

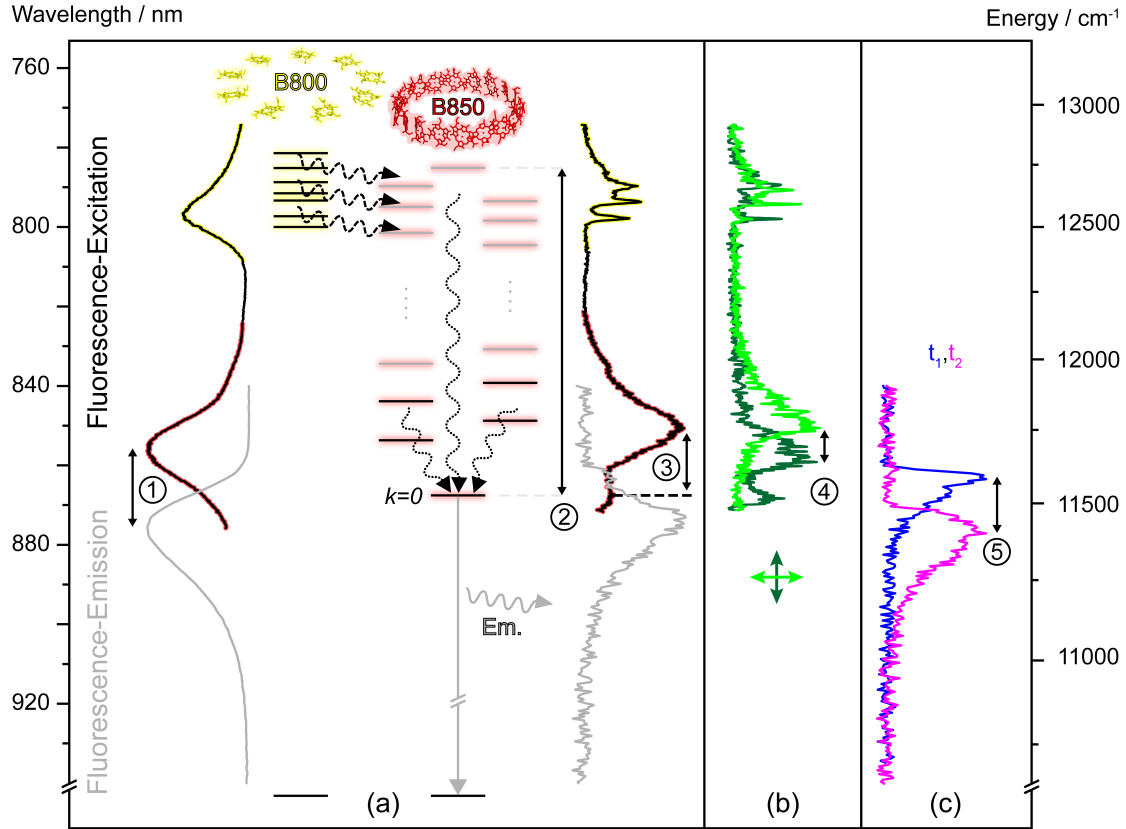


**Figure 3.5:** (a) Black/grey vertical traces on the left- and right-hand side represent fluorescence-excitation/emission spectra of an ensemble of LH2 complexes and a single LH2 complex, respectively. Horizontal black lines in the middle part schematically illustrate the electronic level structure of a single LH2 complex. Yellow/red colors are used to highlight the correspondence between the B800/B850 ring structures and electronic levels with the absorption regions in the two spectra. (b) Dark/light green vertical traces that correspond to two individual fluorescence-excitation scans recorded with mutually orthogonal polarization of the excitation light from the same complex as shown in right-hand side of part (a). (c) Blue/magenta vertical traces that represent two individual emission spectra recorded at different times from the same complex as shown in the right-hand side of part (a).

The black vertical arrows in (a-c) correspond to five spectral parameters, which are discussed in the course of this work: ① Stokes shift, ② exciton bandwidth  $\delta E$ , ③ mean energetic separation,  $\Delta E_{01}$ , between the  $k = 0$  and averaged  $k = \pm 1$  exciton states, ④ energetic separation,  $\Delta E_{\pm 1}$ , between the  $k = \pm 1$  exciton states, ⑤ spectral separation between the two most spectrally separated emission spectra. For details see text.

nized in the B800 ring (yellow ring structure). Whereas the broad absorption bands around 860 nm stem from optically allowed exciton states of the exciton manifold that is formed by the strongly coupled Bchls in the B850 ring (red ring structure). However, the observed linewidths in the single complex spectrum in Fig. 3.5 (a) do not represent the actual homogeneous linewidths due to the lifetimes of the B800 and B850 Bchls, but reflect rather the kinetics (dephasing times) of the excitations in a single LH2 complex. Excitations into the B800 band (black horizontal lines underlined with yellow color) are radiationless transferred on a  $\sim$  ps timescale (black dashed curved arrows) towards the upper exciton state manifold of the B850 ring (upper part of black horizontal lines underlined with red color), from which a very fast downward relaxation of  $\sim$  100 fs (black dotted curved arrows) towards the lowest lying exciton state ( $k = 0$  state) follows, thus giving rise to the sharp absorption lines, corresponding the dephasing time within some ps. The broad absorption bands around 860 nm in the single complex spectrum, however, reflect direct excitations into the optically allowed lower exciton states of the B850 ring with subsequent ultrafast relaxation towards the  $k = 0$  state. Regardless of the excitation process, the emission (grey straight and curved arrows) occurs within  $\sim$  1 ns always from the  $k = 0$  state. The grey vertical traces on the left- and right-hand side of Fig. 3.5 (a) represent the emission spectrum from a LH2 ensemble and a single LH2 complex, respectively.

A further advantage of SMS is illustrated in Fig. 3.5 (b). Here the dark/light green vertical traces correspond to two individual fluorescence-excitation scans that are recorded with mutually orthogonal polarization of the excitation light from the same complex as shown in right-hand side of part (a). By doing so, the absorption bands of the lower exciton states that carry most of the oscillator strength in an individual complex, can be recorded. Such detailed information cannot be obtained by ensemble spectroscopy.

In Fig. 3.5 (c) two individual emission spectra are displayed, which have been recorded at different times from the same complex as shown in (a), revealing significant differences with respect to shape and spectral position. The observation of such spectral changes in the emission spectra of single LH2 complexes, varying with time, is another information that is not accessible in ensemble spectroscopy.

### Spectral diffusion

These (gradual) spectral drifts or abrupt jumps with time, observable in both, emission and fluorescence-excitation spectra of single complexes, are generally denoted as spectral diffusion [123]. This phenomenon can be explained by the temporal fluctuating interaction between a pigment and its surrounding local environment. More precisely, as the interaction depends strongly on distance through different terms varying as  $R^{-n}$ , including dipole-dipole ( $n = 3$ ), dispersion ( $n = 6$ ), repulsion ( $n = 12$ ), etc., fluctuations in the local environment will correspond to distance

changes between the pigment and its environment and, thus, result in fluctuations of the absorption frequency of the pigment [124, 125]. In the configuration coordinate diagram, where the two energy parabolas are representing the ground and the excited state of a molecule (see Fig. 3.2 and 3.4), this fluctuation can be interpreted as a temporally varying vertical distance between the two parabolas.

In the case of individual LH2 complexes, the experimentally observed spectral diffusion at 1.2 K is mainly a light-induced effect. Due to the low fluorescence quantum yield of about 10 % [97], the optical excitation by the laser leads to an increase of the local temperature in the protein environment of the LH2 complex, as the excess energy will be radiationless dissipated to the surrounding. As a consequence, nuclear motions of the protein (phonons) are excited, which result in modulations of the local interactions of the pigments. However, monitoring the light-driven changes of the spectral positions of the pigment absorptions as a function of time, can provide valuable information about the energy landscape and the diffusion kernel of a single protein [126–128].

It is important to note that selective techniques in the ensemble domain do suffer from spectral diffusion as well. E.g. in SHB experiments, temporal fluctuations of the absorption frequency show up as waiting time dependent line broadening phenomena [129, 130]. In SMS experiments, however, the spectral diffusion trajectories can be directly observed in the time domain and lead to the inhomogeneous broadening of the absorption lines. As the information gained from SMS do crucially depend on the mutual relationship between the timescales of the experiment and that of the spectral fluctuations, the observed widths cannot always be related to the actual lifetime of the states (see above) [129].

#### Results from single-molecule experiments

By the SMS experiments, conducted at low temperature, a large variability in the absorption characteristics of LH2 antenna spectra could be confirmed [131, 132]. Furthermore, together with the high resolution crystal structure of LH2 [10, 11] and theoretical studies [68, 133, 134], the results obtained from fluorescence-excitation spectra of single LH2 complexes [69, 132, 135, 136] helped to refine and establish the concept of the disordered Frenkel exciton model for the B850 ring, which had been previously proposed by theory [46, 74, 137, 138] and SHB experiments [48, 80, 89, 91, 96] (see above).

The analysis of the B800 spectra from single LH2 complexes further showed that the results about the electron-phonon coupling, at least for the B800 ring, are in agreement with those obtained from SHB studies [130, 139]. Interestingly, it was found that the excitations in the B800 band are not completely localized, but to some extent can also be delocalized among more pigments [140].

First emission experiments on single LH2 complexes from *Rps. acidophila* performed at cryogenic temperatures, confirmed that the line broadening of the spectra could

be reduced and proved, thereby, the heterogeneity of the sample [141]. The spectra, peaking on average at 874.9 nm, featured a distribution in center of gravity of about  $300 \text{ cm}^{-1}$  with linewidths (FWHM) being no smaller than  $120 \text{ cm}^{-1}$  at 7 K. However, as the asymmetric spectral shape appeared still broad, without any indication of a ZPL structure, the electron-phonon coupling was considered to be strong in this system and the possibility of exciton trapping was discussed. Moreover, the distribution in spectral shape and position, which has been found among different complexes, was related to differences in the electronic structure of the complex rather than to differences of the vibrational modes. Despite the long integration times of 1 - 5 minutes, which were necessary for a sufficient signal-to-noise ratio, the influence of spectral diffusion on the shape of the emission spectra has not been discussed in this study.

Later on, several studies on the emission behavior of single LH2 complexes at ambient temperatures were performed [61, 142–147]. In these studies a high temporal resolution (0.5 - 2 seconds) allowed to observe huge spectral jumps of the emission spectra to the blue as well to the red spectral region, both accompanied by a broadening of the spectral lineshape. While the blueshift broadening was related to exciton relaxation (relaxation-induced broadening) and interpreted as a sign for delocalization, the redshift broadening was assigned to the large splitting of the  $k = 0, \pm 1$  states and a localization of the  $k = 0$  state [142]. Moreover, frequency and size of the spectral jumps were associated with different structural flexibilities of the pigment-protein complexes and a variation of the strength of the factors determining the electronic transition (site) energies of the pigments, i.e. the electron-phonon coupling [143]. Simulations employing modified Redfield theory, suggested that the changes of time-averaged spectral envelopes can be related to distinct conformations of the protein environment which, in turn, induce different site energies for each individual pigment within the B850 assembly. In accordance with the assumption of a strong electron-phonon coupling, the possibility for the existence of self-trapped exciton states was suggested [148, 149].

In the second emission experiment performed on single LH2 complexes from *Rps. acidophila* at low temperature (1.2 K), spectra peaking on average at 874 nm with linewidths (FWHM) of about  $25 - 300 \text{ cm}^{-1}$  (average value  $\sim 72 \text{ cm}^{-1}$ ) were reported [150]. The majority of spectra in this study exhibited a single band with a steep rise on the blue edge and a shoulder on the red side. In this work the influence of spectral diffusion on the shape of the recorded spectra was considered and the observed spectral dynamics were assigned to be strictly light-induced. Though, the shape of the spectra have been obviously governed by a superposition of a ZPL and a broad PSB, no conclusions about the fine-structure of the spectra and thus about the electron-phonon coupling could be made, owing to the poor spectral ( $\sim 2 \text{ nm}$ ) and temporal (10 minutes) resolution of the experiment. Additionally, numerical simulations were employed for examining the apparent discrepancy between the sum of emission spectra from many single complexes and the emission spectrum

from an ensemble of LH2 complexes, dissolved in a glycerol-buffer solution (peaking at around 890 nm), in terms of the static and dynamic disorder of the  $k = 0$  energy level distribution. From that it was reasoned that disorder might be reduced in the thin polymer film matrix with respect to a glycerol-buffer solution environment, together with pointing out that the solvent matrix may have a significant effect on the spectroscopic and dynamic properties of the chromophores in pigment-protein complexes.

#### 3.9 Aim of this work

With regard to the above described discrepancies between the absorption and emission spectra obtained from ensemble experiments and between separate fluorescence-excitation and emission spectroscopy studies on single LH2 complexes, the idea of performing fluorescence-excitation and emission spectroscopy on the same individual LH2 complex arises. By doing so, one not only avoids the ensemble averaging, but gains direct information about the absorbing and emitting B850 exciton states on the level of single LH2 complexes. For individual LH1 complexes and self-assembled aggregates of LH2 and LH1-RC complexes (serving as the simplest model of a single PSU), combined studies of fluorescence-excitation and emission spectroscopy at cryogenic temperatures have been reported [151, 152]. However, no equivalent experiment for single LH2 complexes has been performed hitherto. Therefore, in this work the fluorescence-excitation and emission spectra on the same individual LH2 complexes have been recorded at 1.2 K for the first time. Prior to that, a study was conducted dealing with the optical spectra of LH2 ensembles as a function of the sample preparation conditions and temperature for providing comparability between the results from ensemble and single-molecule studies given in the literature. Materials and methods, used for the experiments, are described in chapter 4 of this thesis. The results, including analysis and discussion, were published in four articles which can be found in part II of this work.

#### Spectral parameters obtained by experiments

For the reason of comprehension, five spectral parameters, which have been determined and analyzed in the course of this thesis, are indicated in Fig. 3.5 as vertical black arrows, numbered from ① to ⑤. Parameters ① and ② are obtained from ensemble spectroscopy, whereas the parameters ③, ④ and ⑤ are solely accessible in SMS experiments.

- Arrow ① denotes the Stokes shift (see definition above), which can be regarded as the spectral distance, i.e. the energetic separation, between the absorption maximum of the B850 band and the emission band maximum. Values for the Stokes shift have been determined in this work to be  $\sim 120 \text{ cm}^{-1}$  at room and

$\sim 260 \text{ cm}^{-1}$  at low temperatures, independent from sample preparation (see publication **P1**).

Here it is worth to note that the definition of the Stokes shift with respect to the excitonic nature of the absorption band is not straightforward and can therefore differ. For example, some studies do not consider the energetic difference between the B850 band peak and the emission band maximum as Stokes shift, but use instead the spectral difference between the absorption in the B870 band ( $k = 0$  state) and the emission band maximum [94].

- Arrow ② denotes the previously introduced B850 exciton bandwidth  $\delta E$ , which can be estimated by means of fluorescence-anisotropy excitation spectroscopy on LH2 ensembles (see chapter 4.2.5). This quantity was analyzed in **P1** and values ranging from  $1300 - 1500 \text{ cm}^{-1}$ , dependent on sample preparation, have been found.
- Arrow ③ indicates the mean energetic separation,  $\Delta E_{01}$ , between the spectral position of the  $k = 0$  state and the average spectral position of the  $k = \pm 1$  states of an individual complex. The analysis of this parameter resulted in values around  $200 \text{ cm}^{-1}$ , which supports the assumption that it can be directly related to the energetic distance between the B850 and B870 band obtained by SHB ensemble experiments (see above). This parameter is being discussed in publication **P4** of the thesis.
- Arrow ④ displays the energetic separation,  $\Delta E_{\pm 1}$ , between the  $k = \pm 1$  exciton states, which can be extracted from single-molecule studies by recording fluorescence-excitation spectra with different polarizations of the excitation light. This value, which is of crucial importance for modeling the energetic and geometric structure of LH2 complexes [69, 135], amounts to about  $100-130 \text{ cm}^{-1}$  and is covered in publication **P4** of this work.
- Arrow ⑤ marks the spectral separation between the two spectrally most separated emission spectra recorded from the same individual complex at different times. This quantity, analyzed in **P3**, shows a broad distribution from some  $10 \text{ cm}^{-1}$  to  $350 \text{ cm}^{-1}$ . Concomitantly with such spectral jumps, changes of spectral shape and width are very often observed, suggesting fluctuations in the electron-phonon coupling (analyzed in terms of Huang-Rhys factor  $S$ ) which probably reflect light-induced conformational changes of the complex (see **P2** and **P3**).



## 4 Materials and methods

In the following chapter the materials and methods which have been used for this work are described. Information about sample preparation, experimental setups and the software for analysis of the data are given. Tables at the end of the chapter provide detailed information about chemicals, optical filters and detectors that were used.

### 4.1 Sample preparation

The single molecule experiments performed for this thesis deal exclusively with the peripheral light-harvesting complex LH2 from the species *Rhodopseudomonas (Rps.) acidophila* (strain 10050). Cultivation, isolation and purification of this sample were carried out by a cooperation partner (Prof. R.J. Cogdell, University of Glasgow, UK) and are described in [153]. Until use a stock solution of the sample is stored in buffer solution (20 mM Tris/HCl, pH 8.0, 0.1 % LDAO) in small aliquots at -80 °C.

For single-molecule studies the stock solution was diluted in several steps with the detergent buffer to a concentration of about  $10^{-11}$  M. The buffer solution used for dilution in the last dilution step contained 1.8 % (w/w) polyvinyl alcohol (PVA). A drop ( $\sim 20$   $\mu$ l) from the final solution was spin-coated onto a cleaned quartz (SiO<sub>2</sub>) substrate ( $\varnothing$  10 mm) for 10 s at 500 rpm and 60 s at 2500 rpm, which resulted in amorphous polymer films with thicknesses of about 100 nm. The samples were immediately mounted in a liquid-helium cryostat (see below) and cooled down to 1.2 K.

For ensemble studies of LH2 complexes two different sample preparation methods have been used, as described in **P1**. Briefly, an ensemble of LH2 complexes was embedded either in a PVA film ("thin film sample") for which the stock solution was diluted to a concentration of about  $10^{-6}$  M in a buffer-PVA solution followed by spin-coating on a cleaned quartz substrate as described above. Or the stock solution of LH2 complexes was further diluted in a buffer solution (with and without glycerol) and were taken in quartz cuvettes with optical path lengths of 1.5 or 10 mm ("bulk-buffer sample"). For the preparation with glycerol, which serves as a cryoprotectant for biological samples at low temperature, the stock solution was diluted

with a buffer-glycerol mixture (1:2 volume ratio), whereas the concentration of LDAO was increased to 1 % to maintain well-isolated complexes [94]. For ensemble experiments, additionally native membranes, i.e. chromatophores including LH2, LH1-RC and membrane fragments, from *Rps. acidophila* (strain 10050), have been used. They have been stored at -20 °C and for use diluted in a 20 mM Tris/HCl buffer (pH 8.0) without detergent (see **P1**). In all these experiments care was taken so that the optical density at the peak of the B850 absorption band did not exceed 0.1 to avoid fluorescence reabsorption effects.

### 4.2 Experimental setup

Single LH2 complexes were detected by means of the so-called fluorescence-excitation spectroscopy. In this method the absorption signal of a single molecule is detected by tuning the frequency of the excitation laser across the molecular absorption lines and recording the Stokes-shifted fluorescence as a function of the excitation wavelength [154]. If the energy transfer efficiency between absorbing and emitting band in a single molecule is close to 100 % (or if the radiationless processes for absorption and fluorescence-excitation are equal), fluorescence-excitation spectroscopy allows to monitor the excited state structure ( $S_0 \rightarrow S_1$  transition) of the molecule and the resulting fluorescence-excitation spectrum then represents an image of the absorption spectrum [7]. Thereby, inhomogeneous broadening effects, inherent in ensemble spectroscopy, are circumvented and dynamical processes, usually hidden in ensemble measurements, can be observed [124].

All single-molecule experiments in this work are performed at liquid helium temperature (1.2 K), because low temperature not only reduces photobleaching processes and the linewidths of the optical transitions, but also slows down the dynamics of structural fluctuations within and around the single molecules and, thereby, enables one to follow the changes in the electronic structure at observable time scales.

In the following the experimental setup and the different configurations (wide-field imaging, fluorescence-excitation and fluorescence-emission) are described. The main focus will be on the application of single-molecule spectroscopy at low temperature, although ensemble samples (at room and low temperature) have been measured with this setup as well. Additionally, the setup for fluorescence-anisotropy excitation spectroscopy (situated in the laboratory of another cooperation partner, Prof. A. Freiberg, University of Tartu, Estonia), which has been used for ensemble spectroscopy studies presented in **P1**, will be briefly described.

The single-molecule setup is a home-built fluorescence microscope that can be operated either in wide-field imaging or confocal mode [155]. As a light source for all experiments a continuous-wave, tunable titanium-sapphire (Ti:Sa) laser (3900S, Spectra Physics) pumped by a frequency doubled, continuous-wave neodymium-yttrium-vanadate (Nd:YVO<sub>4</sub>) laser (Millennia Vs, Spectra Physics) was used. The wavelength of the Ti:Sa laser could be tuned in well-defined steps between 770 - 920

nm by rotating an intracavity birefringent filter with a motorized micrometer screw (Newport, MM4005). For calibration of the laser frequency a wavemeter (WaveMaster, Coherent) has been used and the accuracy as well as the reproducibility was verified to be about  $1 \text{ cm}^{-1}$ . With a 5 W output power of the pump laser an output power of the Ti:Sa laser between 400 - 800 mW, depending on the wavelength, was reached.

#### 4.2.1 Wide-field imaging

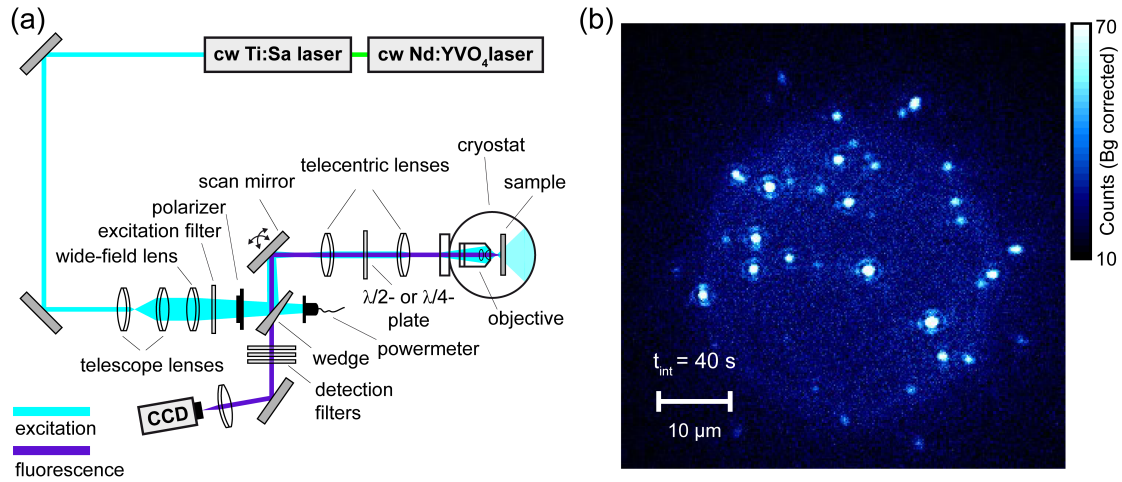


**Figure 4.1:** (a) Schematic illustration of the excitation (cyan) and detection light path (purple) when the setup is operated in the wide-field imaging mode. (b) 2D representation of a wide-field image with spatially well-isolated bright spots each corresponding to a diffraction limited Airy pattern of an individual LH2 complex recorded at 1.2 K.

For wide-field imaging the sample was aligned in the focal plane of a microscope objective ( $f = 2.9 \text{ mm}$ ,  $\text{NA} = 0.85$ ; Microthek) which was mounted together with the sample inside the bath cryostat and immersed in liquid helium. A  $40 \times 40 \mu\text{m}^2$  region of the sample was excited around 855 nm with an excitation intensity of  $\sim 100 \text{ W/cm}^2$  through a bandpass (BP) excitation filter (either BP 858/30; Dr. Hugo Anders or BP850/30; AHF Analysetechnik) and a biconvex lens with large focal length ( $f = 300 \text{ mm}$ ) for defocusing the excitation beam, see Fig. 4.1 (a). The emission from the sample was collected by the same microscope objective and the signal was focused by an achromatic lens ( $f = 200 \text{ mm}$ ) onto a back-illuminated CCD camera (TE/CCD-512-TKB; Roper Scientific or iKon-M 934-BR-DD; Andor Technology) after passing a set of bandpass filters (BP 900/50; AHF Analysetechnik) which blocked the residual laser light. An example of a wide-field image with an integration time  $t_{\text{int}} = 40 \text{ s}$  is depicted in Fig. 4.1 (b). In this 2D

representation each bright spot represents a diffraction limited Airy pattern of an individual LH2 complex. From this image spatially well-isolated complexes were selected for further investigation.

#### 4.2.2 Fluorescence-excitation spectroscopy

For fluorescence-excitation spectroscopy on individual LH2 complexes identified in the wide-field image the microscope was used in the confocal mode. The setup used for fluorescence-excitation spectroscopy is displayed in Fig. 4.2 (a).

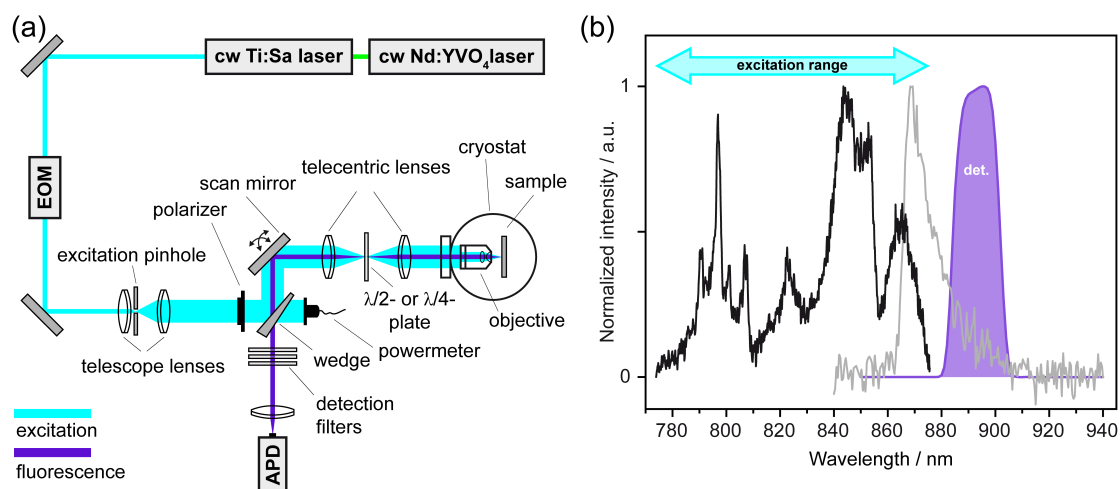


**Figure 4.2:** (a) Schematic illustration of the excitation (cyan) and detection light path (purple) when the setup is operated in the fluorescence-excitation mode. (b) A typical example of a fluorescence-excitation spectrum of a single LH2 complex recorded at 1.2 K, averaged over all polarizations of the excitation light (black line). For comparison the corresponding emission spectrum from the same complex is displayed by the grey line. The spectral range for excitation and the transmission characteristics of the detection filter used in the fluorescence-excitation mode are indicated by the cyan arrow/purple area, respectively. The fluorescence-excitation/emission spectra are peak normalized.

In this mode the laser light (cyan color) is focused onto a pinhole and the image of the pinhole in turn is focused onto the sample by a high numerical aperture objective creating a diffraction-limited focal volume of less than  $1 \mu\text{m}^3$  (1 femtolitre). By directing the excitation beam by means of a gimbal mounted scan mirror, this volume was made to coincide with one in the wide-field imaging mode previously selected single LH2 complexes. A pair of telecentric lenses ( $f = 100 \text{ mm}$ ) was further used, ensuring that the confocal volume is displaced in a controlled manner on the sample plane and at the same time keeping the focal distance to the objective. The fluorescence (purple color) was collected by the same objective and after passing a set of

bandpass filters (BP 893/21; Dr. Hugo Anders, BP890/20, BP900/50; AHF Analysetechnik) focused through an achromatic lens ( $f = 50$  mm) onto a single-photon counting avalanche photodiode (APD) (SPCM-AQR-16, Perkin-Elmer). The finite size of the diode ( $\varnothing \sim 170$   $\mu\text{m}$ ) assumed hereby the role of the detection pinhole in the confocal setup. Therefore background light, which did not come from the conjugated focal plane on the sample, was efficiently suppressed and the signal-to-noise ratio is significantly enhanced with respect to conventional microscopy [156]. A fluorescence-excitation spectrum has been recorded by continuously scanning the excitation wavelength with a rate of 3 nm/s ( $\sim 50$   $\text{cm}^{-1}/\text{s}$ ) and an acquisition time of 10 ms per data point. This yielded a nominal spectral resolution of  $\sim 0.5$   $\text{cm}^{-1}$  and ensured that the spectral resolution of the experiment is limited by the spectral bandwidth of the laser ( $\sim 1$   $\text{cm}^{-1}$ ). By recording many spectra of the same complex consecutively and a separate storing, on the one hand the signal-to-noise ratio, which is proportional to  $\sqrt{N}$  (with  $N =$  number of scans), was improved, and on the other hand, information about the spectral evolution of the absorption lines in time could be gained.

Depending on the filter set used in the detection path, the laser wavelength was scanned in a range from 770 nm to 872 nm or 875 nm (see **P4**) with an excitation intensity of about 100 - 150  $\text{W}/\text{cm}^2$ . As the output power of the Ti:Sa laser was not constant over the broad scanning range, a feedback loop controlled electro-optical modulator (EOM) was used to ensure the stability of the excitation intensity, which is a prerequisite for single-molecule experiments. For examination of the polarization dependence of the absorption lines from single complexes the linear polarization of the excitation light was rotated in steps of  $6.2^\circ$  between two successive scans by means of a half-waveplate placed between the pair of the telecentric lenses.

An example of a fluorescence-excitation spectrum (black line) of a single LH2 complex is displayed together with the transmission characteristics of the filter set used in the detection path (purple colored area) in Fig. 4.2 (b). For comparison the corresponding emission spectrum of the same complex is depicted (grey line) as well, which has been recorded in a subsequent measurement as described in the next section.

### 4.2.3 Fluorescence-emission spectroscopy

The above described experimental setup was originally constructed for widefield-imaging and fluorescence-excitation spectroscopy use only. However, for this thesis it was required to extend the existing setup in such a way that the emission spectrum of a single LH2 complex could be recorded as well. For this purpose a spectrometer together with a CCD camera had to be implemented. The experimental setup for fluorescence-emission spectroscopy mode is depicted Fig. 4.3 (a).

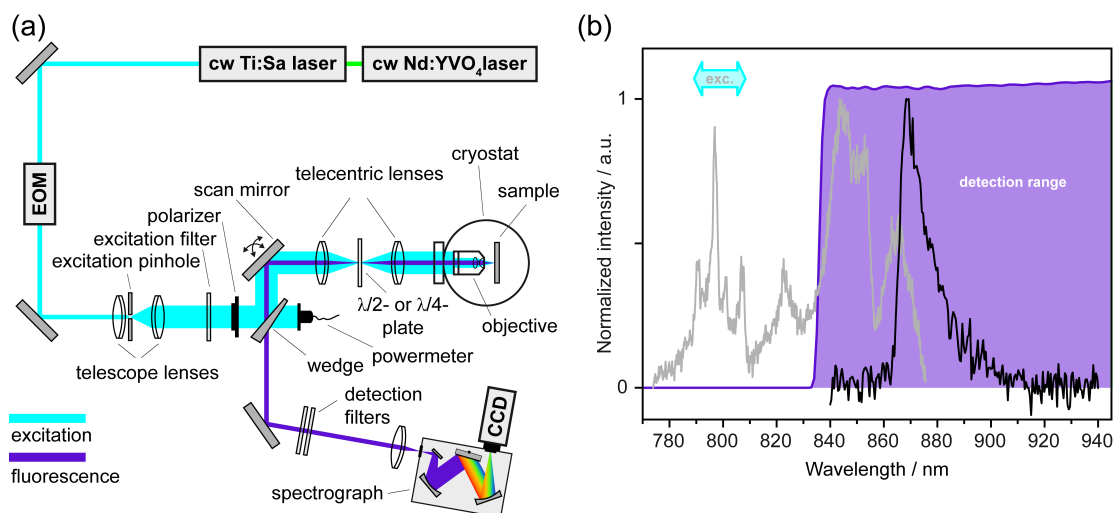


**Figure 4.3:** (a) Schematic illustration of the excitation (cyan) and detection light path (purple) when the setup is operated in the fluorescence-emission mode. (b) A typical example of a fluorescence-emission spectrum from a single LH2 complex recorded at 1.2 K (black line). For comparison the corresponding fluorescence-excitation spectrum from the same complex is displayed by the grey line. The spectral range for excitation and the transmission characteristics of the detection filter used in the fluorescence-emission mode are indicated by the cyan arrow/purple area, respectively. The fluorescence-excitation/emission spectra are peak normalized.

For emission spectroscopy the complexes were excited around 800 nm with linearly polarized light through an excitation filter (BP805/30, AHF Analysetechnik) which was inserted in the excitation beam path. In order not to miss the narrow B800 absorptions, which have been determined in the previous fluorescence-excitation measurement, the laser wavelength was wobbled over a range of 2 - 6 nm with a rate of 3 nm/s during data acquisition. The excitation intensity was about 1 kW/cm<sup>2</sup>.

The fluorescence signal from the confocal volume was directed through a set of longpass filters (LP830, AHF Analysetechnik) and focused into the spectrometer by an achromatic lens ( $f = 100$  mm). This allowed to record the fluorescence signal from a single complex spectrally resolved with the CCD camera which was attached to the spectrometer. The fluorescence was not recorded as a function of polarization.

In Fig. 4.3 (b) an example of an emission spectrum (black line) from a single LH2 complex is displayed together with the transmission characteristics of the filter set (purple area) used in the detection path. For comparison the corresponding fluorescence-excitation spectrum of the same complex, which has been recorded in a previous step (see above), is depicted in grey color.

### Temporal resolution

The temporal resolution which could be achieved in emission spectroscopy, depended strongly on the CCD camera used for detection. During the course of this thesis three different CCD cameras (Luca-R 604M-OM / iDus DV420A-OE / iKon-M 934 BR-DD, all Andor Technology, see Table 4.3) were used, and depending on the type of camera the integration times for a single spectrum have been 600 s / 60 s / 3 - 15 s, respectively. In order to follow the spectral evolution of the fluorescence signal in time, 10 (iDus) or 100 - 2000 (iKon) emission spectra from an individual complex were recorded successively.

### Spectral resolution

As a spectrometer for the emission measurements the SpectraPro-150 (Acton Research Corporation) dual grating imaging monochromator/spectrograph with a focal length of 150 mm was used. This spectrometer is mounted with one turret holding a mirror and a grating. In this work, two different turrets, holding either a grating with 300 or 600 lines/mm, have been used as dispersing element, both with a blaze wavelength at 1  $\mu\text{m}$ , ensuring high diffraction efficiency in the NIR spectral region. The calibration of the detection system, i.e. spectrograph and attached CCD, has been done with the excitation laser and a wavemeter (WaveMaster, Coherent). The spectral resolution depended on the specific grating and detector used for the experiments and could be improved in the course of the thesis from 1.5 nm ( $\sim 20 \text{ cm}^{-1}$ ) in the case of the 300 lines/mm grating with the Luca/iDus CCD, to 0.5 nm ( $\sim 7 \text{ cm}^{-1}$ ) for the 600 lines/mm grating with the iKon CCD.

### Sensitivity correction

The wavelength sensitivity of the detection system in case of the 300 lines/mm grating with the Luca/iDus CCD was sufficiently constant over the detected spectral range and no further correction was needed.

Out of consideration for the spectral sensitivity of the detection system consisting of the 600 lines/mm grating in combination with the iKon CCD, the measured spectra have been corrected by the spectral instrument response function. To obtain this function, the spectrum of a tungsten halogen lamp (Osram 64623 HLX, color temperature  $T = 3300 \text{ K}$ ) was recorded with the setup and for taking into account its differences with respect to a real black-body spectrum, divided by the theoretical black-body spectrum, which has been calculated with Planck's law [157].

#### 4.2.4 Ensemble spectroscopy

While the fluorescence-excitation and emission spectra of an ensemble of LH2 complexes embedded in a PVA film have been recorded similarly as described for the

single-molecule samples (see above), the collection of spectra from an ensemble of LH2 complexes dissolved in a bulk-buffer solution with/without glycerol and the native membrane sample in pure buffer-solution required a slight modification of the setup.

Instead of the sample holder including the microscope objective and the sample, a modified holder was used in the cryostat, which did not hold the objective anymore, but a cuvette instead. Furthermore, in this configuration no telecentric lenses have been used and an achromatic lens ( $f = 200$  mm) in front of the cryostat served as objective. Thereby, recording of fluorescence-excitation and emission spectra for ensemble samples in solution, either under vacuum conditions (at room temperature) or in an inert liquid helium environment (at low temperature), with the existing setup was possible (see **P1**).

#### 4.2.5 Fluorescence-anisotropy excitation spectroscopy

The fluorescence-anisotropy excitation measurements presented in this thesis (see **P1**) have been conducted in the optical laboratory of a cooperation partner (Prof. A. Freiberg, University of Tartu, Estonia).

In general, the fluorescence-anisotropy as a function of the excitation wavelength  $r(\lambda)$  is defined as

$$r(\lambda) = \frac{I_{vv}(\lambda) - I_{vh}(\lambda)}{I_{vv}(\lambda) + 2I_{vh}(\lambda)}, \quad (4.1)$$

where  $I_{vv}$  and  $I_{vh}$  are the emission intensities that are polarized parallel ( $vv$ ) and perpendicular ( $vh$ ) with respect to the orientation of the electric field vector of the linearly polarized excitation light, respectively [85].

Via  $r(\lambda) = \langle (3 \cos(\alpha) - 1) / 5 \rangle$ , where the chevrons denote ensemble averaging, the macroscopic quantity  $r(\lambda)$ , i.e. the fluorescence-anisotropy excitation spectrum, is connected to the microscopic angles  $\alpha$  between the absorbing and emitting states within the sample [78]. The setup used for this experiment is depicted in Fig. 4.4 (a). The sample was mounted in a liquid helium cryostat (Cryosystem Utreks-LSO) and excited by a continuous-wave, tunable titanium-sapphire (Ti:Sa) laser (3900S, Spectra Physics) which was pumped by an Ar<sup>+</sup>-ion laser (model 171, Spectra Physics). The emission signal was recorded in a 90° geometry with respect to the excitation light beam by a 0.3 m spectrograph (Shamrock SR-303i, Andor Technology) which was equipped with an electrically cooled CCD camera (iDus DV420A-OE, Andor Technology). For fluorescence-anisotropy measurements two high-contrast polarizers were placed in front of the entrance slit of the spectrograph. The first polarizer was set parallel or perpendicular to the vertically polarized excitation light and served as an analyzer. The second one, which was set to an angle of 45° with respect to the polarization axis of the excitation light, served to minimize the deformation of the polarization due to the spectrograph. Emission spectra could also be recorded with this setup. For that purpose the polarizers in

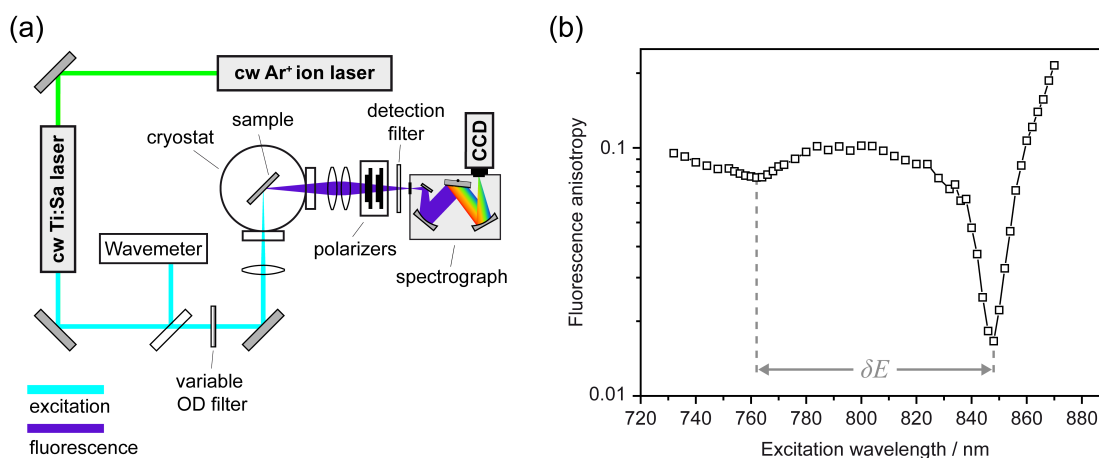


**Figure 4.4:** (a) Schematic illustration of the excitation (cyan) and detection light path (purple) of the fluorescence-anisotropy excitation setup used in **P1**. (b) A typical example of a fluorescence-anisotropy excitation spectrum from an ensemble of LH2 complexes embedded in a PVA film recorded at 5K. The horizontal arrow indicates the exciton bandwidth  $\delta E$ .

the detection beam were removed.

In Fig. 4.4 (b) a typical fluorescence-anisotropy excitation spectrum from an ensemble of LH2 complexes, embedded in a PVA film, is displayed. It yields two low-anisotropy dips, which can be mainly related to the  $k = \pm 1$  (at low energy) and  $k = \pm 8$  (at high energy) exciton states, respectively, and thus the spectral distance between the two dips (indicated by the horizontal arrow) provides a measure for the exciton bandwidth  $\delta E$  (see chapter 3.2). For further details of this method, including experimental setup and theory, the reader is referred to [26, 92, 158] and references therein.

The fluorescence-anisotropy excitation spectroscopy method is solely applicable on ensemble samples. Hence, with this method only ensembles of either LH2 complexes (embedded in PVA film or dissolved in bulk-buffer solution with/without glycerol) or native membranes (in solution) have been investigated (see **P1**).

### 4.3 Data analysis

Analysis of the data presented in this thesis has been performed by programmed LabVIEW 7.1 and MATLAB 7 software, as well as by Origin 7.0 / OriginPro8 standard software.

The consecutively recorded fluorescence-excitation spectra of the same complex are typically displayed in a two-dimensional representation, where the horizontal axis corresponds to wavelength, the vertical axis to time, and the color to the signal

intensity. This representation is commonly referred to as spectral diffusion plot and allows one to follow the spectral evolution of absorption bands from a single complex in time and/or as a function of the polarization of the excitation light.

In the case when the iKon CCD was used as a detector in the emission setup (see above), an analogous representation for the emission spectra, though, not as a function of the polarization, was possible, because of the high number of recorded spectra. This allows to follow the temporal evolution of the fluorescence from a single LH2 complex for the first time (see **P3**). Furthermore, it opens the possibility for a direct comparison between the diffusion plots derived by both methods for the same individual complex. Thereby, temporal and spectral averaging effects could be surpassed and corresponding bands have been unambiguously identified (see **P4**).

In addition, the consecutively recorded emission spectra that have been recorded with short integration times by the iKon CCD, were analyzed by means of a multivariate statistical pattern recognition algorithm (MSA; IMAGIC-5, ImageScience) to surpass the strong spectral diffusion. This algorithm was originally developed for reconstructing the three-dimensional structure of large biomolecules from two-dimensional projections that have been obtained by cryo-electron microscopy [159–164]. It has been previously successfully applied in spectroscopy for analysis of the B800 lineshapes of LH2 complexes [139, 165] and the emission spectra from conjugated polymers in disordered hosts [166, 167]. Briefly, the algorithm groups spectra which are sufficiently similar into a predetermined number of classes by pattern recognition techniques. This is achieved by maximizing the interclass variance and minimizing the intraclass variance (in a mathematical, least squares sense). Spectra, which are assigned to the same class, were averaged and resulted in so-called class-averaged spectra (CAS). By this approach the line broadening caused by spectral diffusion slower than the exposure time was eliminated and spectra with a reasonable signal-to-noise ratio could be extracted. These spectra allowed then a further analysis of the electron-phonon coupling strengths in terms of the Huang-Rhys factor  $S$ , according to the analysis of those spectra, which have been recorded with longer integration times by the two other detectors (see **P2**). The results of the above described MSA approach, which for the first time was applied on the emission spectra of single LH2 complexes, have been published in **P3**.

## 4.4 Tables of chemicals, optical filters and detectors

Trade Name	Chemical Name	Company
LDAO	lauryldimethylamine <i>N</i> -oxide	Sigma-Aldrich
Tris	Tris-(hydroxymethyl)-aminomethane	Sigma-Aldrich
PVA	polyvinyl alcohol ( $M_W = 30000-70000$ g/mol)	Sigma-Aldrich
Glycerol	Glycerin 1,2,3-Propanetriol	Sigma-Aldrich

**Table 4.1:** Table of chemicals, listing trade name, chemical name and producing company.

Filter Name	Filter Type	Transmission Width (nm)	Company
BP 805	Bandpass	60	AHF Analysetechnik
BP 850	Bandpass	30	AHF Analysetechnik
BP 858	Bandpass	30	Dr. Hugo Anders
BP 890	Bandpass	20	AHF Analysetechnik
BP 893	Bandpass	21	Dr. Hugo Anders
BP 900	Bandpass	50	AHF Analysetechnik
BP 935	Bandpass	40	AHF Analysetechnik
LP 830	Longpass	$> 840$ nm <sup>a</sup>	AHF Analysetechnik
LP 885	Longpass	$> 895$ nm <sup>a</sup>	AHF Analysetechnik

**Table 4.2:** Table of optical filters, listing filter type, transmission width and distributing company. Numbers in the filter name column give the central wavelength for the bandpass or the edge wavelength (for 50 % transmission) in case of the longpass filters. Numbers with <sup>a</sup> denote the edge wavelength for 90 % transmission.

#### 4 Materials and methods

---

Name of detector	Type	Pixel number (size)	Company	Application
NTE/CCD-512-TKB	CCD	512×512 (24 $\mu\text{m}$ )	Roper Scientific	Imaging
Luca-R 604M-OM	CCD	1004×1002 (8 $\mu\text{m}$ )	Andor Technology	Spectroscopy
iDus DV420A-OE	CCD	1024×255 (26 $\mu\text{m}$ )	Andor Technology	Spectroscopy
iKon-M 934-BR-DD	CCD	1024×1024 (13 $\mu\text{m}$ )	Andor Technology	Imaging, spectr.
SPCM-AQR-16	APD	1×1 ( $\sim$ 170 $\mu\text{m}$ )	Perkin-Elmer	Fl.-exc. spectr.

---

**Table 4.3:** Table of detectors listing pixel number (size), manufacturing company and application.

## 5 Supplementary information

In the following chapter some noteworthy issues, which have not been published in any of the articles, will be shortly discussed. In general, this chapter is meant as a supplementary information for the reader but might also be helpful if the outcome of this thesis should be considered as a starting point for future studies. It contains a section dealing with the shortcomings and comparability of the described experimental spectroscopy techniques on isolated LH complexes of purple bacteria. In another section some additional information about experimental findings and discrepancies with former studies on single LH2 complexes is given.

### 5.1 Shortcomings and comparability of ensemble and single-molecule studies

Ensemble and single-molecule spectroscopy methods typically not only require different sample preparation conditions and experimental equipment, they might suffer from inherent shortcomings as well, which in turn might question the general comparability of the results.

#### 5.1.1 Site selective ensemble spectroscopy

On the one hand, site selective ensemble spectroscopy (see section 3.7) exploits spectral selectivity for reducing ensemble averaging, but on the other hand this selectivity involves a risk for probing only a certain subgroup of complexes within the ensemble. For example, while SHB is sensitive only to those complexes which are in resonance with the narrow excitation laser, i.e. which display a sharp ZPL and thus having a weak electron phonon coupling, FLN spectroscopy mainly monitors complexes which are less sensitive to SHB (which "survive" the SHB process) and thus correspond to complexes having a stronger electron-phonon coupling. However, the  $\Delta$ FLN spectroscopy method reveals the contribution of the signal that has been lost due to the SHB method, corresponding to those sites/states that were burnt out during irradiation and giving therefore a complementary information to the SHB method. Furthermore, as the spectra obtained from  $\Delta$ FLN are virtually free from scattering artifacts influencing the FLN spectra (e.g. the ZPL cannot be

measured in FLN due to its resonance with the laser excitation frequency) and systematic errors of SHB (e.g. a fraction of complexes will always be excited via their PSB, leading to artificial line shapes), less corrections are required with respect to those obtained from FLN and SHB spectroscopy [95, 118, 168].

Nevertheless, the selectivity issue has also to be taken into account, when estimates of the electron-phonon coupling strength, resulting from SHB or  $\Delta$ FLN experiments, are directly compared to each other, as these methods might lead to an under- or overestimation of the Huang-Rhys factors [86, 169]. Furthermore, it is important to note that the analysis of the electron-phonon coupling from the spectra obtained by site-selective methods in general is not straightforward, as the electron-phonon coupling in LH complexes in principal cannot be considered as a one-phonon process per se, but is rather determined by multi-phonon processes.

The influences of spectral diffusion (see section 3.8) and too high burn fluences might be of relevance in ensemble studies. Also artificial features like pseudo-PSB holes and/or antiholes require careful consideration [86, 118, 168, 170]. In summary, the above described difficulties can lead to strong distortions of the obtained spectra and care has to be taken that this does not result in wrong estimates of the Huang-Rhys factor [95, 120, 169].

### 5.1.2 Single-molecule spectroscopy

#### Filter-dependent preselection

SMS in general is not completely free from preselection effects due to experimental imitations and limited statistics. In the following two situations are considered. First, the selection of single complexes/particles/molecules for further investigation, which is made in the wide-field imaging step, is done by an experimentalist. Typically he/she is biased to bright ones and the selection is therefore subjective. Particularly this issue, being not just a problem of SMS on LH2 complexes, has been discussed in the case of conjugated polymers, where it resulted even in non-representative statistics [171]. Second, the optical detection filters that are used in the experiment might suppress signal from some of the complexes, which are therefore disregarded or even not noticed at all.

As this second point was quantitatively investigated in the course of the thesis, the results from this investigation are presented in the following, due to their great importance for future studies in this field. A part of this work can also be found in the Supplementary Information (SI) of publication **P4**.

The choice of excitation wavelength and detection filter set used in the wide-field imaging mode (see section 4.2.1) might influence the selection of the single complexes that are observable in the wide-field image. This is because the overlap of the emission spectrum from a single LH2 complex with the transmission range of the bandpass filter in the detection path, which determines the signal strength in

the wide-field image, is not the same for all complexes, due to the heterogeneity of the sample. While for some complexes just a small part of the emission spectrum falls into the transmission range of the detection filter set, for others a much bigger overlap is found. This problem is displayed in Fig. 5.1.

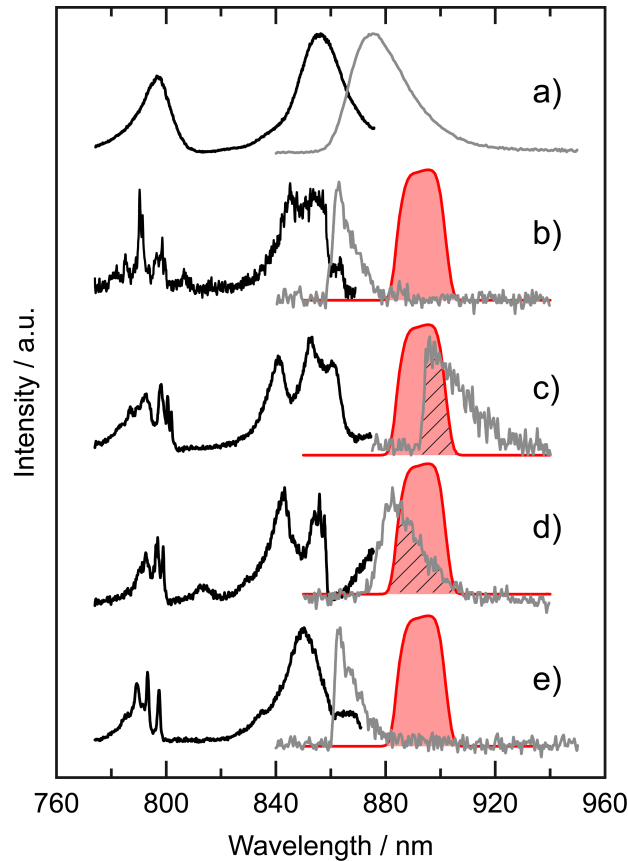


**Figure 5.1:** Fluorescence-excitation (black line) and emission spectra (grey line) of an ensemble of LH2 complexes from *Rps. acidophila* in PVA film (a) and four different single LH2 complexes (b-e). The red shaded area displays the transmission characteristics of a specific bandpass filter set which was used amongst others throughout the thesis. All spectra are peak-normalized and those in a)-d) have been off-set for clarity. The data have been recorded at 1.2 K. For details see text.

The black/grey lines correspond to fluorescence-excitation/emission spectra of an ensemble of LH2 complexes embedded in a PVA film (a) and four different single LH2 complexes (b-e), respectively. The fluorescence-excitation spectra of the single complexes show clear differences not only in the number of spectral absorption bands and their structure, but also in the spectral positions of the individual bands. The corresponding emission spectra that were excited in the B800 band and recorded with an integration time of 60 seconds deviate, as well, by their shapes,

widths (FWHM), and spectral peak positions. If in the wide-field imaging mode a bandpass filter set with a transmission characteristics as illustrated in the figure (red shaded area) would have been used, probably, one could have only observed complexes c) and d), due to the significant overlap of their emission spectra with the transmission characteristics of the filter set (black diagonal pattern). Complexes b) and e), however, might have appeared too dim or even not seen at all with this filter set. Furthermore, as shown in **P3**, the emission spectra of single LH2 complexes are not stationary in time but subjected to spectral diffusion. Thus, a fixed excitation wavelength and the usage of only one detection filter set in the wide-field imaging mode might, together with the heterogeneity of the sample, lead to preselection effects.

For a systematic investigation of this issue, wide-field images of the same sample area with different excitation wavelengths and detection filters were recorded. In Fig. 5.2 a,b (this figure resembles Fig. S1 a,b in the SI of **P4**) the experimental scheme is illustrated on the ensemble fluorescence-excitation spectrum (full black line) and the emission spectrum (full grey line) of LH2 from *Rps. acidophila*. The magenta shaded area represents the spectral region along which the circularly polarized laser light was wobbled (855 - 865 nm). The black dashed line shows the transmission profile of the excitation filter which has been used for suppression of unwanted light from the Ti:Sa laser in the infrared spectral region. In red/blue color the transmission curves of different detection filter sets (BP1/BP2) are displayed (see Tab. 4.2 and **P4** for details of the filters). The excitation intensity was about  $100 \text{ W/cm}^2$  and the integration time of the image was 40 seconds.

Fig. 5.2 c,d show the same cutout of a wide-field image from a sample that has been registered with the two different detection filter sets. At the bottom of the wide-field images (Fig. 5.2 e) the observable LH2 complexes are shown schematically by colored open/filled circles, where the color refers to a LH2 complex that has been identified with the corresponding detection filter. From this it is obvious that, owing to the better spectral overlap of the (ensemble) LH2 emission spectrum and the transmission characteristics of the detection filter BP2, a larger fraction of single LH2 complexes can be identified in the wide-field image for this configuration.

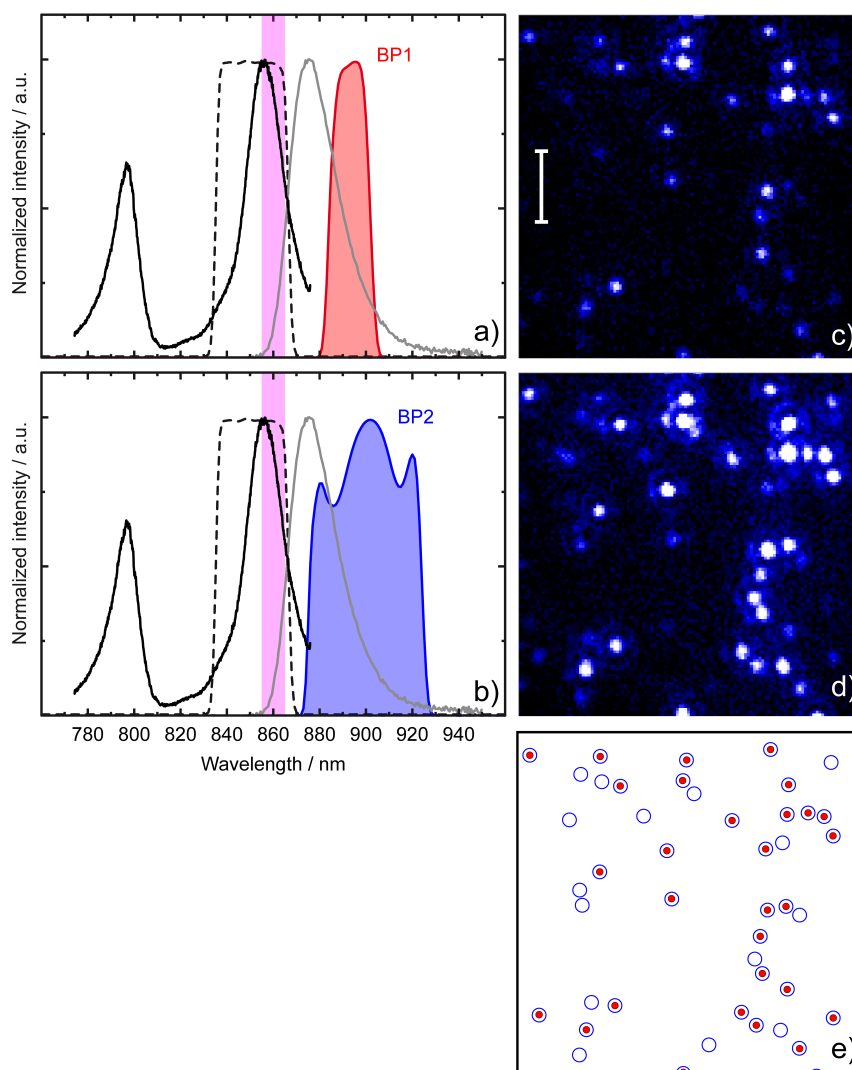


**Figure 5.2:** Left: Illustration of the influence of the spectral characteristics of the optical filters on the wide-field imaging. Transmission curves of the detection filters with respect to the spectral positions of the absorption (solid black lines) and emission (solid grey line) of LH2 for two different detection filters. a) BP1: center wavelength 893 nm, bandwidth 18 nm; b) BP2: 900 nm, 48 nm. The dashed line corresponds to the transmission characteristics of a bandpass filter (850 nm, 30 nm) that is used in the excitation path to suppress background from the laser. All transmission curves of the optical filters are shown on a normalized scale. The sample is excited with circularly polarized light, the wavelength is wobbled between 855 nm and 865 nm (magenta shaded area), and the excitation intensity is about  $100 \text{ W/cm}^2$ . Right: Wide-field images from the same sample area: c) detected with filter BP1, d) detected with filter BP2. The scale bar in c) corresponds to  $10 \mu\text{m}$ . e) Schematic representation of individual complexes that are identified in the two images. Red filled circles refer to part c) of the figure (BP1), and blue open circles refer to part d) of the figure (BP2).

However, it is also possible to excite the single LH2 complexes in the B800 region. This approach is illustrated in Fig. 5.3. The scheme of Fig. 5.3 is similar to that used for Fig. 5.2. Fig. 5.3 a,b shows the B800 excitation with the same detection filters, BP1/BP2, that are used for B850 excitation (Fig. 5.2 a,b). The only difference is here the excitation wavelength range (wobbled between 795 - 805 nm), which is displayed by the cyan shaded area, and the filter (BP805/60) used in the excitation path (black dashed line) for blocking residual light from the Ti:Sa laser. Yet, due to the excitation at around 800 nm, a longpass (LP) filter set (LP830) could be used in the detection path. The transmission characteristics of this filter set is displayed in Fig. 5.3 c in green color. For details of this filter see Tab. 4.2 and **P4**. In this configuration the excitation filter has to be tilted not to overlap with the detection filter (black dashed line in Fig. 5.3 c). The resulting wide-field images of the same sample area for the three configurations are shown in Fig. 5.3 d,e,f. Likewise Fig. 5.2 e, Fig. 5.3 g represents a schematic illustration of those LH2 complexes which can be identified in each of the wide-field images above. The color of each circle refers to a LH2 complex that has been identified with the corresponding detection filter.

As the complexes that are identified from the wide-field images, Fig. 5.2 e and Fig. 5.3 g, do certainly depend on the individual person's eye-sight as well as on the actual settings of the CCD contrast, this phenomenon was quantitatively analyzed by collecting the signal strength from the single complexes for each of the different excitation/detection schemes on the total CCD wide-field image. For this, first, the coordinates of all complexes which could be seen in any of the applied excitation/detection schemes (here one has to consider possible pixel shifts due to the usage of different filters) were determined. Second, an algorithm has been applied which extracts from all these pixel-coordinates the intensity of each pixel plus one or two neighboring pixels, surrounding the coordinate pixel, owing to the size of each of individual complex on the CCD image. Then the resulting intensities have been divided by the number of pixels contributing to the signal. For comparability reasons the values from B850 and B800 excitations have been normalized with a factor that takes into account the slightly different excitation intensities due to the different wavelength regions of the laser. Note, that the different absorption cross sections for the B850 and B800 band are not taken into account here. This was due to the fact, that not the absolute count rates of the complexes between B850 and B800 excitation have been of interest, but the relative number of visible complexes for the different filter sets used in the detection path.

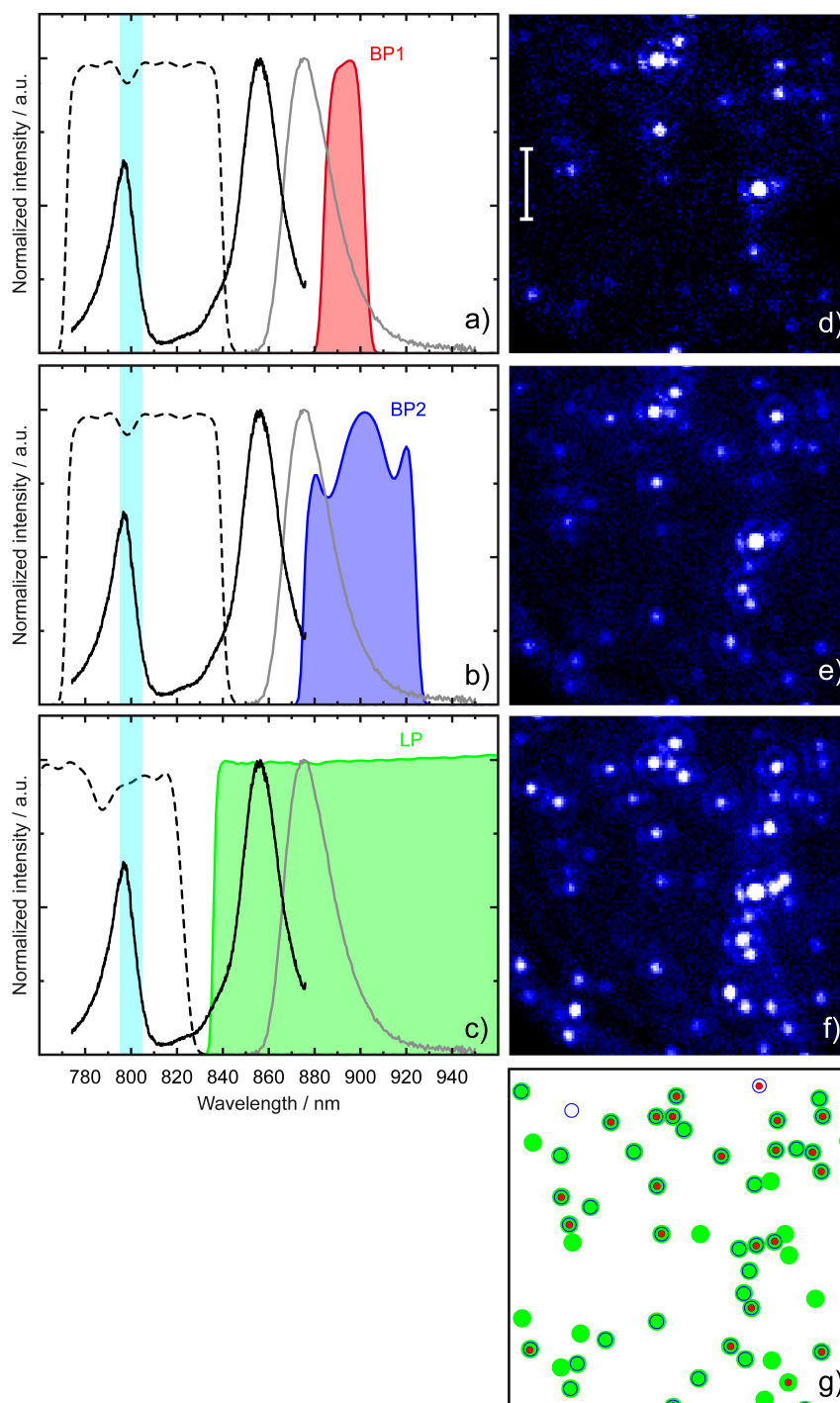
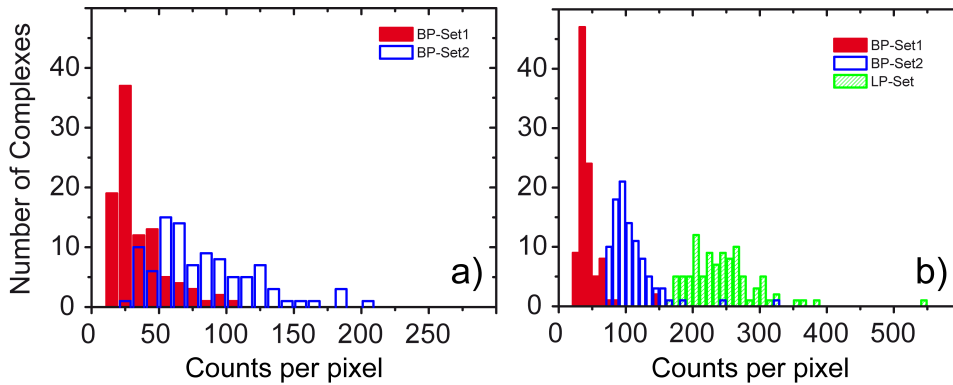


Figure 5.3: For caption see next page.

**Figure 5.3:** *Left: Illustration of the influence of the spectral characteristics of the optical filters on the wide-field imaging. Transmission curves of the detection filters with respect to the spectral positions of the absorption (solid black lines) and emission (solid grey line) of a LH2 ensemble for three different detection filters. a) BP1: center wavelength 893 nm, bandwidth 18 nm; b) BP2: 900 nm, 48 nm; c) LP: > 840 nm. The dashed line corresponds to the transmission characteristics of a bandpass filter (805 nm, 60 nm) that is used in the excitation path to suppress background from the laser. In c) this filter has been tilted. All transmission curves of the optical filters are shown on a normalized scale. The sample is excited with circularly polarized light, the wavelength is wobbled between 795 nm and 805 nm (cyan shaded area), and the excitation intensity is  $\sim 100 \text{ W/cm}^2$ . Right: Wide-field images from the same sample area: d) detected with filter BP1, e) detected with filter BP2, f) detected with filter LP. The scale bar in d) corresponds to 10  $\mu\text{m}$ . g) Schematic representation of individual complexes that are identified in the three images. Red filled circles refer to part d) (BP1), blue open circles refer to part e) (BP2), and green filled circles to part f) (LP) of the corresponding figures.*

In Fig. 5.4 the results for 97 positions of single complexes is shown. In histogram a) the distribution of intensity counts per pixel is shown for excitation in the B850 band when filter sets BP1 and BP2 are used in the detection path. The intensity distribution for the BP1 filter set (red full bars) with respect to that from BP2 (blue open bars) is located at (about a factor of two) smaller values. This holds true also for excitation in the B800 band (see Fig. 5.4 b) and can be explained by a smaller overlap of the emission spectra from single complexes with the transmission window of the respective filter set. However, histogram b) shows that the signal count rate for individual complexes excited in the B800 region is highest for the use of the LP filter set in the detection path (green patterned bars). About a factor of three with respect to that from BP1 (red full bars) and about a factor of two and a half with respect to that from BP2 (blue open bars). This is not surprising, as this detection filter set probably does not cut away any signal of the emission spectra from the single complexes and thus allows the recording of maximum fluorescence photons which are spectrally located  $> 840 \text{ nm}$ .

From the histograms in Fig. 5.4 it becomes clear that the choice of the detection filter and/or excitation wavelength plays a crucial role for the selection of a single complex for spectroscopy. This is because some of the complexes might be difficult to detect for different bandpass filters in the detection path or may even not be detectable at all. Hence, if it is an experimental aim to collect as many photons as possible from a single complex, as for example for recording an emission spectrum or for studying blinking processes, the best approach is to excite the complexes around 800 nm and to use a longpass filter in the detection path. However, in fluorescence-excitation spectroscopy not just the number of the emitted photons (spectrally resolved or not) is counted, but the frequency of an absorbed photon



**Figure 5.4:** Distributions of the intensity counts per pixel for 97 positions on the total wide-field image for the different excitation and detection conditions that have been used in Fig. 5.2 and Fig. 5.3. a) Excitation in the B850 band, b) Excitation in the B800 band. Different colors of the bars correspond to the different detection filters used: BP1 (red full bars), BP2 (blue open bars), LP (green patterned bars). For comparability reasons the intensity counts from B850 (a) and B800 excitation (b) have been normalized to an equal excitation intensity which takes into account the slightly different excitation intensities due to the different wavelength regions of the laser that have been used for the two excitation modes. Note: The different absorption cross sections for the B850 and B800 band are not taken into account here. For details see text.

is also of interest. Therefore the use of a detection filter which has a transmission characteristics too far in the blue spectral region is not recommendable for this spectroscopy method, because this might lead to cutting off absorption bands in the red edge of the spectrum.

In fact, the best way to find out which filter is most suitable for a specific single LH2 complex is to perform both, fluorescence-excitation and emission spectroscopy on the same complex (see **P4**). Additionally, preselection effects resulting from the wide-field imaging mode, can be best surpassed when different detection filters and/or excitation wavelengths regions are used, as presented here.

### Influence of preselection

From the discussion above, it gets clear that the preselection of certain complexes might influence the results obtained from the experiments. In the worst case scenario this could mean that the complexes, which have been selected for SMS, may represent only a subgroup of all the complexes in the ensemble. This can be checked by comparing the summed fluorescence-excitation and emission spectra from the recorded individual LH2 complexes with the fluorescence-excitation and emission spectra recorded from an ensemble of LH2 complexes prepared under similar conditions, i.e. in a PVA film (see **P4**, Fig. 5 a,b, black and grey traces, respectively).

While the summed fluorescence-excitation spectrum from 74 individual LH2 complexes practically overlaps with the fluorescence-excitation spectrum of the LH2 ensemble, peaking at 855.6 nm ( $11688\text{ cm}^{-1}$ ), one, indeed, will recognize that the peak of the summed emission spectrum from the same LH2 complexes is about 4.8 nm red shifted with respect to that from the ensemble peaking at 875.6 nm ( $11421\text{ cm}^{-1}$ ). Additionally, the comparison with the two previous emission studies performed on single LH2 complexes from *Rps. acidophila* at cryogenic temperatures, for which the averaged spectral peak position was found to be at 874.9 nm ( $11430\text{ cm}^{-1}$ ) [141] and 874.0 nm ( $11442\text{ cm}^{-1}$ ) [150], respectively, confirms this red-shift. However, in these two studies only emission measurements have been performed which allowed to use optical filters for spectroscopy with transmission ranges more to the blue spectral region (850 nm edge filter in [141] and a bandpass filter ranging from 820 - 915 nm in [150]). In contrast, for the complexes that have been investigated in this thesis also fluorescence-excitation spectra had to be recorded and thus the selection of complexes in the wide-field imaging step was made according to the above discussed criterion.

Moreover, the summed fluorescence-excitation and emission spectra from those LH2 complexes for which an entire fluorescence-excitation spectrum has been recorded (see **P4**, Fig. 5 c, black/grey traces) do not deviate much from those of the LH2 ensemble. Therefore, it is most likely that the difference in emission spectra can be solely related to the filter characteristics in the wide-field imaging step and that the conclusions made in this thesis can be considered to be valid for all LH2 complexes and not only for a subgroup of complexes.

### **Analysis of electron-phonon coupling**

Another issue concerns the analysis of the electron-phonon coupling from emission spectra of single complexes in terms of the  $S$  factor. Here, the analysis is per se limited to those spectra which allow an unambiguous distinction between the ZPL and the PSB (see **P2** and supporting information of **P3**) and thus might be related to a subgroup only. This has to be kept in mind when the results related to the electron-phonon coupling determined by SMS are compared with those from ensemble spectroscopy techniques.

### **Sample environment**

Apart from the influence of preselection and the analysis of electron-phonon coupling, a more general issue concerns the observations of spectral diffusion in the spectra of single LH complexes (see section 3.8). Here it might be questioned whether the typical low temperature behavior, which is observed in SMS, can be exclusively related to the pure LH2 pigment-protein complex, or if some of the observations do rather reflect the dynamics of the surrounding environment, i.e.

the amorphous host, or host-protein interface, instead [82]. For example, the effect of glycerol and PVA on the conformation of single photosystem I (PSI) complexes from cyanobacteria was studied in [172] and revealed a higher spectral heterogeneity for complexes embedded in PVA with respect to those that were prepared in glycerol/buffer mixtures. From this finding a more compact protein conformation with less structural variability for PSI complexes embedded in glycerol/buffer was concluded, whereas the spectra of the PSI complexes embedded in the PVA matrix reflect a much higher heterogeneity due to structural distortions induced by the PVA. However, with respect to LH2 complexes, this issue is rather difficult to evaluate here as hitherto most of SMS studies on single LH2 complexes, that have been conducted at low temperatures, are dealing with LH2 complexes that are prepared in PVA.

Although the influence of the sample preparation conditions and temperature on ensembles of isolated LH2 complexes, either dissolved in a buffer-detergent solution (with/without glycerol) or embedded in a spin-coated PVA film, has been comprehensively studied related to static spectral parameters such as peak position, width (FWHM) of the absorption/emission band, Stokes shift, excitonic bandwidth, etc. (see **P1**), no investigation were made regarding the dynamics of the spectra for single complexes that have been prepared in the PVA matrix and/or a comparison between single LH2 complexes embedded in different environments. Thus, a thorough study comparing different environments for single LH2 complexes is recommended here that allows a detailed discussion.

### Excitation intensity

Another issue that is worth to mention is related to the excitation intensities which were used for SMS of LH2 complexes in this study. While for fluorescence-excitation spectroscopy laser intensities of about 100 - 150 W/cm<sup>2</sup> were applied (see section 4.2.2), for emission spectroscopy the excitation intensity has been increased to about 1 kW/cm<sup>2</sup> (see section 4.2.3) in order to obtain a reasonable signal.

In general the absorption rate of a single molecule is defined as

$$k = \sigma \cdot \frac{I}{h\nu}, \quad (5.1)$$

where  $\sigma$  is the absorption cross section,  $I$  the intensity, and  $h\nu$  the energy of the excitation light. The absorption cross section  $\sigma$  itself can be calculated via

$$\sigma = \frac{2.303 \cdot \varepsilon(\lambda)}{N_A}, \quad (5.2)$$

with  $\varepsilon(\lambda)$  being the extinction coefficient and  $N_A$  the Avogadro constant. An extinction coefficient  $\varepsilon$  of about  $3.8 \cdot 10^6 \frac{1}{\text{M cm}}$  for the B800 band of LH2 from *Rps. acidophila* at low temperatures (123 K) [74] gives an absorption cross section of

$$\sigma = 14.5 \cdot 10^{-15} \text{ cm}^2.$$

Together with the excitation intensity of  $1 \text{ kW/cm}^2$  at a wavelength of  $800 \text{ nm}$  this results in a value of about  $6 \cdot 10^7 \frac{1}{\text{s}}$  for the absorption rate. Thus, within  $5 \text{ s}$  of integration time, a single LH2 complex will be excited  $\sim 3 \cdot 10^8$  times. However, due to the  $1 \text{ ns}$  lifetime [97], it will stay only around  $0.3 \text{ s}$  in the electronically excited state [173]. Moreover, because of the low emission efficiency of LH2 ( $\sim 10 \%$  [97]) and singlet-triplet annihilation processes related to the carotenoids, only a fraction of the absorbed photons will be emitted as fluorescence [142, 174]. Instead, most of the absorbed excitation energy will be dissipated non-radiatively as heat and lead to an increase of the local temperature in the immediate environment of the pigments. Therefore, it is most likely that the fluctuations of the electron-phonon coupling strength, as reported in **P3**, reflect light-induced conformational changes of the complex. Because the spectral jumps and corresponding spectral profiles are reversible, a deterioration of the complexes can be excluded. Furthermore, the robustness of the LH2 complexes was checked by recording fluorescence-excitation spectra of several LH2 complexes before and after the emission spectroscopy experiments (see **P2**). In experimental SHB studies it was shown that the ZPL feature within the B870 band practically vanishes above temperatures of  $35 \text{ K}$  [96]. As the emission spectra of single LH2 complexes still display a clear ZPL feature after an illumination of more than  $1 \text{ hour}$  (see **P3**), a tremendous increase of the macroscopic equilibrium temperature is very unlikely to occur. However, this does not exclude temperature changes on the microscopic scale that could induce reversible conformational changes.

### Ergodicity

The ensemble emission spectrum of LH2 complexes in a polymer film recorded at  $1.2 \text{ K}$  shows a width (FWHM) of  $\sim 300 \text{ cm}^{-1}$  (see **P1**). Moreover, the spectral separations between the two extreme CAS, which were obtained from the series of emission spectra recorded from individual LH2 complexes at  $1.2 \text{ K}$ , have been determined to be within the range of  $10 - 350 \text{ cm}^{-1}$  with an average value of  $\sim 150 \text{ cm}^{-1}$  (see **P3**). By comparing these numbers, one could think about the possibility, that the emission of an individual complex may sample the whole spectral positions of the ensemble spectrum, if only observed over long enough periods of time. Hence, this behavior could be regarded as an ergodic process. The term ergodicity was originally introduced by Boltzmann to deduce the equality of time means and phase means in the field of thermodynamics. In simple words, it describes the phenomenon that a single dynamical system (e.g. a diffusing particle) has the same behavior averaged over time as an ensemble (of particles) averaged over the space of all the states of the system, meaning that the ensemble average is equal to the time average (of a single particle) [175].

If the ergodic hypothesis is assumed to be true for the emission spectra of LH2

complexes, it raises the question why the emission behavior of the single complexes is highly variant, i.e. containing both, complexes that are spectrally very stable and others showing high spectral diffusion characteristics (see **P3**).

For an investigation in terms of ergodicity one has to consider the experimental conditions of the emission experiment, i.e. the number of spectra recorded in the series and the integration time for one spectrum on the one hand, and, the photo-physical properties of the LH2 complex on the other hand. If it is assumed that within the integration duration of for example 5 s no spectral diffusion occurs, nevertheless, it cannot be a priori stated if series of 100, 1000, 10000 or more emission spectra are sufficient for a comprehensive ergodic picture from an individual complex. Moreover, if an absorption rate of  $k \approx 3 \cdot 10^8 \frac{1}{s}$  is assumed during the integration time of 5 s (see above), a fluorescence quantum yield of  $\sim 10\%$  [97] results in  $3 \cdot 10^7$  emission events of an individual complex. Therefore, registration of any deviation from ergodicity would require to detect for each individual photon the emission wavelength, which is hardly possible due to experimental limitations. Thus, it is difficult to draw any conclusions with respect to the ergodicity of the emission characteristics of single LH2 complexes at low temperature on the basis of the experiments reported in this thesis.

### 5.1.3 Comparability of ensemble and single-molecule studies

Being far from complete, the specified shortcomings have to be taken into account when results from both ensemble and single-molecule studies on LH complexes are compared with each other. However, the results presented in this work (see publications **P1**, **P2**, **P3** and **P4**) provide a basis for further comparison between ensemble and single-molecule experiments in the field of LH complexes.

The rest of this chapter deals with two more findings that are related to the SMS experiments on LH2 complexes. As these findings have not been adequately discussed in the publications but might have an importance for further studies, they will be shortly presented here.

## 5.2 Polarization dependence of the B850 ring exciton states

In previous studies of single LH2 complexes from *Rps. acidophila* the fluorescence-excitation spectra recorded at low temperature revealed always a nearly mutual orthogonal polarization difference of the transition dipole moments from the most intense absorption bands in the B850 band, i.e. the  $k = +1$  and  $k = -1$  exciton states [132, 135, 136, 176]. However, the statistical analysis of the mutual angle of orientation of the transition dipole moments of the  $k = \pm 1$  exciton states for the complexes investigated in this study showed a much broader distribution. With a mean value of  $65^\circ$  and a width of  $92^\circ$ , the distribution clearly deviates from the sharp distributions peaking at  $90^\circ$  with widths of  $\sim 20^\circ$ , which were reported in

previous works [176]. Additionally, some complexes showed spectra with broad bands without any polarization dependencies, which prohibited further analysis in terms of their polarization characteristics. Such phenomena have also not been reported in earlier studies. However, similar results were discussed in a diploma thesis performed with the same setup [177] and proved thereby that the described findings do not depend on the experimenter.

Differences in sample preparation conditions (e.g. different molecular weight of PVA and different spin-coating velocities) have been ruled out to be responsible for the above described deviation. Despite the improvement in angular resolution - the change of polarization of the excitation light between two successive scans was reduced from  $30^\circ$  in [135], to  $18^\circ$  and  $14.4^\circ$  in [136] and [176], respectively, to a value of  $6.2^\circ$  in this study - and a further improvement of optical elements in the setup (usage of NIR broadband wave plates and NIR antireflection coated optical lenses) it was not possible to get similar results as in previous works.

One possible reason for the above described deviations with respect to former studies might be that the orientation of the  $C_9$  symmetry axis of the investigated single LH2 complexes has not been perpendicular to the plane of the substrate but tilted instead. This argument, which has been recently proposed in other single-molecule studies on LH2 complexes as well [174, 178, 179], however, requires a further investigation. Furthermore, influences of the optics (changes of the glue of the microscope objective, influence of light polarization by the cryostat windows, etc.) and/or changes in the preparation conditions still remain possible sources of errors.

### 5.3 Interaction strength calculation

As pointed out above, the combination of fluorescence-excitation and emission spectroscopy on the same single LH2 complexes at low temperature, allows the identification of those complexes for which the recorded fluorescence-excitation can be considered as complete (see **P4**). By that, an unambiguous assignment of the lowest lying exciton state in the fluorescence-excitation spectra was possible. In previous studies this state has been seen either rarely [132] or only after elaborate processing of the spectral data [135].

The assignment of the exciton states for 28 complexes, for which the spectra have been completely recorded (see **P4**), is displayed in Fig. 5.5. Squares filled with different colors represent the spectral peak positions of different exciton states from the 28 individual complexes. The mean values of these exciton states are given by the horizontal lines and the numbers with standard deviations next to the lines. From those numbers the energetic separations between the exciton states in the B850 manifold can be calculated. The energetic separation  $\Delta E_{\pm 1} \approx 110 \text{ cm}^{-1}$  between the  $k=\pm 1$  states resembles the values reported in [135, 136, 176, 177]. Also the energetic separation  $\Delta E_{higher} \approx 300 \text{ cm}^{-1}$  between the average spectral position of the  $k = \pm 1$  states of an individual complex and the next higher exciton state of

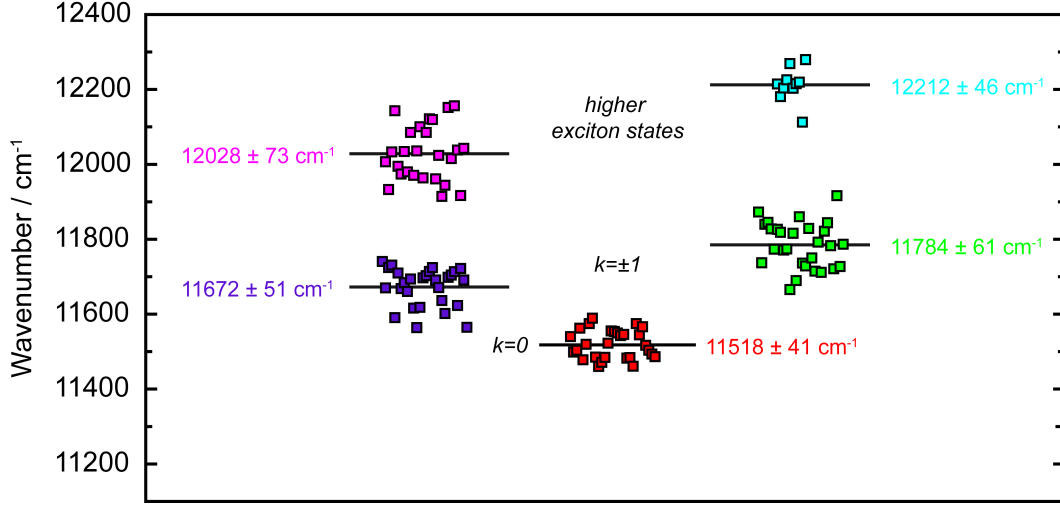


**Figure 5.5:** Spectral peak positions (squares) of the bands observed in the fully recorded fluorescence-excitation spectra from 28 individual LH2 complexes. The horizontal lines correspond to the mean values which are given next to the lines. The different colors correspond to different exciton states.

the same complex is similar to the values reported in [135, 177].

The energetic separation  $\Delta E_{01} \approx 210 \text{ cm}^{-1}$ , which denotes the mean energetic separation between spectral position of the  $k = 0$  state and the average spectral position of the  $k = \pm 1$  state, is not comparable with the corresponding value ( $84 \text{ cm}^{-1}$ ) given in [135]. However, it is in reasonable agreement to the value of  $200 \text{ cm}^{-1}$  obtained from SHB spectroscopy on LH2 from *Rps. acidophila* in bulk-buffer solution with glycerol [93] (see **P4**).

The values of the energetic separations can be used for a calculation of the nearest-neighbor interaction strength between the Bchl pigments within the B850 ring. Neglecting diagonal and off-diagonal disorder, the excited states of the unperturbed B850 ring aggregate can be deduced from [135]

$$E_k^\pm = E_0 + 2 W_0 \cos(k\delta) \pm \sqrt{[E_{\alpha\beta}/2 + W_{\alpha\beta} \cos(k\delta)]^2 + V_i^2 + V_e^2 + 2 V_i V_e \cos(k\delta)} \quad (5.3)$$

with

$$\begin{aligned} E_0 &= (E_\alpha + E_\beta) / 2, \quad E_{\alpha\beta} = (E_\alpha - E_\beta) \\ W_0 &= (W_\alpha + W_\beta) / 2, \quad W_{\alpha\beta} = (W_\alpha - W_\beta), \end{aligned} \quad (5.4)$$

where  $E_\alpha$  and  $E_\beta$  denote the excitation energies of the  $\alpha$ - and  $\beta$ -bound pigments,  $V_i$  and  $V_e$  the intra- and interdimer nearest-neighbor interactions and  $W_\alpha$  and  $W_\beta$  the next-nearest-neighbor interactions between the  $\alpha$ - and  $\beta$ -bound pigments, respectively.

As a dimer the  $\alpha\beta$  unit is taken here, the quantum number  $k$  is ranging from  $0, \pm 1, \dots, \pm 4$ , and  $\delta = 2\pi/9$  [135].

If the excitation energies of the  $\alpha$ - and  $\beta$ -bound pigments are assumed to be all equal ( $E_\alpha = E_\beta = E_0$ ) as well as the second-neighbor interactions ( $W_\alpha = W_\beta = W_0$ ), Eq. 5.3 can be written in a simplified form:

$$E_k^\pm = E_0 + 2 W_0 \cos(k\delta) \pm 2 V_0 \cos(k\delta/2) \quad (5.5)$$

As the distance between the second-neighbor pigments is about twice the nearest-neighbor distance one can assume that  $W_0 = -V_0/8$  [69]. Furthermore, if only the lower exciton branch is regarded one gets

$$E_k^- = E_0 - V_0 \left[ \frac{1}{4} \cos(k\delta) + 2 \cos\left(\frac{k\delta}{2}\right) \right]. \quad (5.6)$$

Taking the energetic separation  $\Delta E_{higher} \approx 300 \text{ cm}^{-1}$  (see above) between the average spectral position of the  $k = \pm 1$  states and the next higher exciton state (regarded as the  $k = \pm 3$  states) one can calculate, by using Eq. 5.6, an interaction strength of  $V_0 = 250 \pm 62 \text{ cm}^{-1}$ . This value is very close to the  $240 \pm 35 \text{ cm}^{-1}$  reported in [135].

If one assumes the higher exciton state being the  $k = \pm 2$  states instead of the  $k = \pm 3$  states, one ends up with an interaction strength of  $V_0 = 603 \pm 149 \text{ cm}^{-1}$ . This value is still comparable with a value of  $585 \pm 35 \text{ cm}^{-1}$  which has been calculated in the same way in [135].

However, when the energetic separation  $\Delta E_{01} \approx 210 \text{ cm}^{-1}$  is taken for a calculation the interaction strength results in  $V_0 = 1221 \pm 243 \text{ cm}^{-1}$ . This is an obviously inconsistent result and indicates that Eq. 5.3 with the assumptions made in [135] and herein is probably too much simplified for a description of the real situation.

Values that have been calculated for the interaction strength in the B850 ring in other studies vary between  $200 - 800 \text{ cm}^{-1}$  and depend strongly on the experiment and the different theoretical model used for the calculation [8].

For example, in [48] it was pointed out that calculations of the nearest neighbor coupling in LH2 give a  $\sim 35 \%$  larger value for the low temperature structure with respect to that calculated for the room temperature structure. Thus, a value of about  $500 \text{ cm}^{-1}$  was postulated to be reasonable for the nearest-neighbor Bchl-Bchl interaction strength in the B850 ring of *Rps. acidophila* at low temperature by these authors [180].

However, from the exciton bandwidth ( $\delta E = 1332 \text{ cm}^{-1}$ ) investigated by fluorescence-anisotropy excitation spectroscopy of an ensemble of LH2 complexes embedded in a PVA film at low temperature (see **P1**), one can estimate an interaction strength via  $V \approx \delta E/4$  of about  $330 \text{ cm}^{-1}$ . Here, it is worth to note that this method probably underestimates the exciton bandwidth, as only the  $k = \pm 1$  and  $\pm 8$  states and not the actual borders of the exciton manifold, i.e. the  $k = 0$  and

$k = 9$  states, are registered. One might get a better estimate by simply adding the observed energetic separation between the spectral position of the  $k = 0$  state and the average spectral position of the  $k = \pm 1$  state, either deduced from SMS (see **P4**) or SHB experiments [93] ( $\Delta E_{01} \approx 200 \text{ cm}^{-1}$ ) to the determined bandwidth. This results in a value of  $V \approx 380 \text{ cm}^{-1}$ , which is considerably higher than it was postulated in previous studies [135] but rather similar to a value of  $374 \text{ cm}^{-1}$ , that was recently determined for the nearest-neighbor exciton coupling strength in LH2 rings at 5 K [78].

Yet, as already pointed out above, here one has to keep in mind that the spectral characteristics and, thus, possible influences on the interaction strength might crucially depend on the environment in which the LH complexes are embedded. In a theoretical study, that was shortly published after the first SMS fluorescence-excitation experiments on LH2 complexes [70], the comparability between SHB and SMS experiments was claimed as an urgent need for a better structural model of the LH2 complex. In this context, also alternatives to the model of elliptical deformation [69, 132, 135, 136] have been presented. However, checking the validity of these alternative models would require that SHB and SMS experiments on the LH complexes have to be conducted under the same condition. The present study and especially publication **P1** have made a first attempt for providing a better comparability between ensemble and SMS experiments.

In conclusion, the above presented discrepancies between theory and experimental results with respect to the interaction strength, are calling not only for further SMS experiments, but also for a more thorough investigation from theoreticians.



## Bibliography

- [1] A. CHO, “Energy’s Tricky Tradeoffs”, *Science* **329**, 786-787 (2010).
- [2] J. BARBER, “Photosynthetic Energy Conversion: Natural and Artificial”, *Chem. Soc. Rev.* **38**, 185–196 (2009).
- [3] A. RUBAN, “The Photosynthetic Membrane”, *Wiley*, 2013.
- [4] R.E. BLANKENSHIP, D.M. TIEDE, J. BARBER, G.W. BRUDVIG, G. FLEMING, M. GHIRARDI, M.R. GUNNER, W. JUNGE, D.M. KRAMER, A. MELIS, T.A. MOORE, C.C. MOSER, D.G. NOCERA, A.J. NOZIK, D.R. ORT ET AL., “Comparing Photosynthetic and Photovoltaic Efficiencies and Recognizing the Potential for Improvement”, *Science* **332**, 805–809 (2011).
- [5] D. GUST, T.A. MOORE AND A.L. MOORE, “Realizing Artificial Photosynthesis”, *Faraday Discuss.* **155**, 9–26 (2012).
- [6] “Anoxygenic Photosynthetic Bacteria”, ed. R.E. BLANKENSHIP, M.T. MADIGAN AND C.E. BAUER, *Kluwer Academic Publishers*, 1995.
- [7] R.E. BLANKENSHIP, “Molecular Mechanisms of Photosynthesis”, *Blackwell Science*, 2002.
- [8] R.J. COGDELL, A. GALL AND J. KÖHLER, “The Architecture and Function of Purple Bacteria: from Single Molecules to in Vivo Membranes”, *Q. Rev. Biophys.* **39**, 227–324 (2006).
- [9] H. SCHEER, “Light-Harvesting in Photosynthesis”, *Acta Phys. Pol., A* **122**, 247–251 (2012).
- [10] G. MCDERMOTT, S.M. PRINCE, A.A. FREER, A.M. HAWTHORNTHWAITELAWLESS, M.Z. PAPIZ, R.J. COGDELL AND N.W. ISAACS, “Crystal Structure of an Integral Membrane Light-Harvesting Complex from Photosynthetic Bacteria”, *Nature* **374**, 517–521 (1995).
- [11] J. KOEPKE, X. HU, C. MUENKE, K. SCHULTEN AND H. MICHEL, “The Crystal Structure of the Light Harvesting Complex II (B800 - B850) from *Rhodospirillum rubrum*”, *Structure* **4**, 581–597 (1996).
- [12] A.W. ROSZAK, T.D. HOWARD, J. SOUTHALL, A.T. GARDINER, C.J. LAW, N.W. ISAACS AND R.J. COGDELL, “Crystal Structure of the RC-LH1 Core Complex from *Rhodospseudomonas palustris*”, *Science* **302**, 1969–1971 (2003).

- [13] T. PULLERITS AND V. SUNDSTRÖM, “Photosynthetic Light-Harvesting Pigment-Protein Complexes: Toward Understanding How and Why”, *Acc. Chem. Res.* **29**, 381–389 (1996).
- [14] T. RITZ, X. HU, A. DAMJANOVIĆ AND K. SCHULTEN, “Excitons and Excitation Transfer in the Photosynthetic Unit of Purple Bacteria”, *J. Lumin.* **76 & 77**, 310–321 (1998).
- [15] X. HU, T. RITZ, A. DAMJANOVIĆ, F. AUTENRIETH AND K. SCHULTEN, “Photosynthetic Apparatus of Purple Bacteria”, *Q. Rev. Biophys.* **35**, 1–62 (2002).
- [16] N.P. REYNOLDS, S. JANUSZ, M. ESCALANTE-MARUN, J. TIMNEY, R.E. DUCKER, J.D. OLSEN, C. OTTO, V. SUBRAMANIAM, G.J. LEGGETT AND C.N. HUNTER, “Directed Formation of Micro- and Nanoscale Patterns of Functional Light-Harvesting LH2 Complexes”, *J. Am. Chem. Soc.* **129**, 14625–14631 (2007).
- [17] M. ESCALANTE, A. LENFERINK, Y. ZHAO, N. TAS, J. HUSKENS, C.N. HUNTER, V. SUBRAMANIAM AND C. OTTO, “Long-Range Energy Propagation in Nanometer Arrays of Light Harvesting Antenna Complexes”, *Nano Lett.* **10**, 1450–1457 (2010).
- [18] J. YANG, M.C. YOON, H. YOO, P. KIM AND D. KIM, “Excitation Energy Transfer in Multiporphyrin Arrays with Cyclic Architectures: Towards Artificial Light-Harvesting Antenna Complexes”, *Chem. Soc. Rev.* **41**, 4808–4826 (2012).
- [19] J.E. LEE, V. STEPANENKO, J. YANG, H. YOO, F. SCHLOSSER, D. BELLINGER, B. ENGELS, I. SCHEBLYKIN, F. WÜRTHNER AND D. KIM, “Structure-Property Relationship of Perylene Bisimide Macrocycles Probed by Atomic Force Microscopy and Single-Molecule Fluorescence Spectroscopy”, *ACS Nano* **7**, 5064–5076 (2013).
- [20] A. FREIBERG, “Coupling of Antennas to Reaction Centers” in *Anoxygenic Photosynthetic Bacteria*, ed. R.E. BLANKENSHIP, M.T. MADIGAN AND C.E. BAUER, *Kluwer Academic Publishers*, 1995, Vol. 2, pp. 385.
- [21] E. HAREL AND G.S. ENGEL, “Quantum Coherence Spectroscopy Reveals Complex Dynamics in Bacterial Light-Harvesting Complex 2 (LH2)”, *Proc. Natl. Acad. Sci. U. S. A.* **109**, 706–711 (2012).
- [22] J. STRÜMPFER, M. ŞENER AND K. SCHULTEN, “How Quantum Coherence Assists Photosynthetic Light-Harvesting”, *J. Phys. Chem. Lett.* **3**, 536–542 (2012).

- 
- [23] E. HAREL, “Long Range Excitonic Transport in a Biomimetic System Inspired by the Bacterial Light-Harvesting Apparatus”, *J. Chem. Phys.* **136**, 174104 (2012).
- [24] F. FASSIOLI, A. OLAYA-CASTRO AND G.D. SCHOLES, “Coherent Energy Transfer under Incoherent Light Conditions”, *J. Phys. Chem. Lett.* **3**, 3136–3142 (2012).
- [25] R. HILDNER, D. BRINKS, J.B. NIEDER, R.J. COGDELL AND N.F. VAN HULST, “Quantum Coherent Energy Transfer over Varying Pathways in Single Light-Harvesting Complexes”, *Science* **340**, 1448–1451 (2013).
- [26] A. FREIBERG, M. PAJUSALU AND M. RÄTSEP, “Excitons in Intact Cells of Photosynthetic Bacteria”, *J. Phys. Chem. B* **117**, 11007–11014 (2013).
- [27] H. VAN AMERONGEN, L. VALKUNAS AND R. VAN GRONDELLE, “Photosynthetic Excitons”, *World Scientific*, 2000.
- [28] A. FREIBERG, K. TIMPMANN AND G. TRINKUNAS, “Spectral Fine-Tuning in Excitonically Coupled Cyclic Photosynthetic Antennas”, *Chem. Phys. Lett.* **500**, 111–115 (2010).
- [29] R.J. COGDELL AND J. KÖHLER, “Sunlight, Purple Bacteria and Quantum Mechanics: How Purple Bacteria Harness Quantum Mechanics for Efficient Light Harvesting” in *Quantum Efficiency in Complex Systems, Part I: Biomolecular systems*, ed. E. WEBER, M. THORWART AND U. WÜRFEL, *Academic Press*, 2010, pp. 77–94.
- [30] M. ŞENER, J. STRÜMPFER, J. HSIN, D. CHANDLER, S. SCHEURING, C.N. HUNTER AND K. SCHULTEN, “Förster Energy Transfer Theory as Reflected in the Structures of Photosynthetic Light-Harvesting Systems”, *ChemPhysChem* **12**, 518–531 (2011).
- [31] N. PFENNIG, “Photosynthetic Bacteria”, *Annu. Rev. Microbiol.* **21**, 285–324 (1967).
- [32] S. SCHEURING, “AFM Studies of the Supramolecular Assembly of Bacterial Photosynthetic Core-Complexes”, *Curr. Opin. Chem. Biol.* **10**, 387–393 (2006).
- [33] S.C. HOLT AND A. MARR, “Isolation and Purification of the Intracytoplasmic Membranes of *Rhodospirillum rubrum*”, *J. Bacteriol.* **89(5)**, 1413–1420 (1965).
- [34] S. SCHEURING AND J.N. STURGIS, “Chromatic Adaption of Photosynthetic Membranes”, *Science* **309**, 484–487 (2005).

- [35] K. McLUSKEY, S.M. PRINCE, R.J. COGDELL AND N.W. ISAACS, “The Crystallographic Structure of the B800-820 LH3 Light-Harvesting Complex from the Purple Bacteria *Rhodospseudomonas acidophila* Strain 7050”, *Biochemistry* **40**, 8783–8789 (2001).
- [36] R.J. COGDELL, I. DURANT, J. VALENTINE, J.G. LINDSAY AND K. SCHMIDT, “The Isolation and Partial Characterisation of the Light-Harvesting Pigment-Protein Complement of *Rhodospseudomonas acidophila*”, *Biochim. Biophys. Acta* **722**, 427–435 (1983).
- [37] R. COGDELL AND A.M. HAWTHORNTHWAITTE, “Preparation, Purification, and Crystallization of Purple Bacteria Antenna Complexes” in *The Photosynthetic Reaction Center*, ed. J. DEISENHOFER AND J.R. NORRIS, *Academic Press*, 1993, Vol. 1, pp. 23–42.
- [38] J. DEISENHOFER, O. EPP, K. MIKI, R. HUBER AND H. MICHEL, “Structure of the Protein Subunits in the Photosynthetic Reaction Centre of *Rhodospseudomonas viridis* at 3 Angström Resolution”, *Nature* **318**, 618 (1985).
- [39] R.J. COGDELL AND H.A. FRANK, “How Carotenoids Function in Photosynthetic Bacteria”, *Biochim. Biophys. Acta* **895**, 63–79 (1987).
- [40] I. STEPANENKO, V. KOMPANETZ, Z. MAKHNEVA, S. CHEKALIN, A. MOSKALENKO AND A. RAZJIVIN, “Two-Photon Excitation Spectroscopy of Carotenoid-Containing and Carotenoid-Depleted LH2 Complexes from Purple Bacteria”, *J. Phys. Chem. B* **113**, 11720–11723 (2009).
- [41] R.J. COGDELL, T.D. HOWARD, R. BITTL, E. SCHLODDER, I. GEISENHEIMER AND W. LUBITZ, “How Carotenoids Protect Bacterial Photosynthesis”, *Philos. Trans. R. Soc., B* **355**, 1345–1349 (2000).
- [42] R.A. BRUNISHOLZ AND H. ZUBER, “Structure, Function and Organization of Antenna Polypeptides and Antenna Complexes from the Three Families of *Rhodospirillaneae*”, *J. Photochem. Photobiol., B* **15**, 113–140 (1992).
- [43] R.J. COGDELL, N.W. ISAACS, A.A. FREER, T.D. HOWARD, A.T. GARDINER, S.M. PRINCE AND M.Z. PAPIZ, “The Structural Basis of Light-Harvesting in Purple Bacteria”, *FEBS Lett.* **555**, 35–39 (2003).
- [44] J. KÖHLER AND T.J. AARTSMA, “Single Molecule Spectroscopy of Pigment Protein Complexes from Purple Bacteria” in *Chlorophylls and Bacteriochlorophylls: Biochemistry, Biophysics, Functions and Applications*, ed. B. GRIMM, R.J. PORRA, W. RÜDIGER AND H.E. SCHEER, *Springer*, 2004, pp. 309–321.

- [45] B. ROBERT, R. COGDELL AND R. GRONDELLE VAN, “The Light-Harvesting System of Purple Bacteria” in *Light-Harvesting Antennas in Photosynthesis*, ed. B.R. GREEN AND W.W. PARSON, *Kluwer Academic Publishers*, 2003, Vol. 13, pp. 169-194.
- [46] K. SAUER, R.J. COGDELL, S.M. PRINCE, A.A. FREER, N.W. ISAACS AND H. SCHEER, “Structure Based Calculations of the Optical Spectra of the LH2 Bacteriochlorophyll-Protein Complex from *Rhodopseudomonas acidophila*”, *Photochem. Photobiol.* **64**, 564–576 (1996).
- [47] G.D. SCHOLES AND G.R. FLEMING, “On the Mechanism of Light Harvesting in Photosynthetic Purple Bacteria: B800 to B850 Energy Transfer”, *J. Phys. Chem. B* **104**, 1854–1868 (2000).
- [48] H.M. WU, M. RÄTSEP, R. JANKOWIAK, R.J. COGDELL AND G.J. SMALL, “Comparison of the LH2 Antenna Complex of *Rhodopseudomonas acidophila* (strain 10050) and *Rhodobacter sphaeroides* by High Pressure Absorption, High Pressure Hole Burning, and Temperature Dependent Absorption Spectroscopies”, *J. Phys. Chem. B* **101**, 7641–7653 (1997).
- [49] H.M. WU, S. SAVIKHIN, N.R.S. REDDY, R. JANKOWIAK, R.J. COGDELL, W.S. STRUVE AND G.J. SMALL, “Femtosecond and Hole-Burning Studies of B800’s Excitation Energy Relaxation Dynamics in the LH2 Antenna Complex of *Rhodopseudomonas acidophila* (strain 10050)”, *J. Phys. Chem. B* **100**, 12022–12033 (1996).
- [50] Y.Z. MA, R.J. COGDELL AND T. GILLBRO, “Energy Transfer and Exciton Annihilation in the B800-850 Antenna Complex of the Photosynthetic Purple Bacterium *Rhodopseudomonas acidophila* (strain 10050). A Femtosecond Transient Absorption Study”, *J. Phys. Chem. B* **101**, 1087–1095 (1997).
- [51] V. SUNDSTRÖM, T. PULLERITS AND R. VAN GRONDELLE, “Photosynthetic Light-Harvesting: Reconciling Dynamics and Structure of Purple Bacterial LH2 Reveals Function of Photosynthetic Unit”, *J. Phys. Chem. B* **103**, 2327–2346 (1999).
- [52] C. SMYTH, F. FASSIOLI AND G.D. SCHOLES, “Measures and Implications of Electronic Coherence in Photosynthetic Light-Harvesting”, *Philos. Trans. R. Soc., A* **370**, 3728–3749 (2012).
- [53] T. FÖRSTER, “10th Spiers Memorial Lecture: Transfer Mechanisms of Electronic Excitation”, *Discuss. Faraday Soc.* **27**, 7–17 (1959).
- [54] H. SUMI, “Bacterial Photosynthesis Begins with Quantum-Mechanical Coherence”, *Chem. Rec.* **1**, 480–493 (2001).

- [55] S.E. BRASLAVSKY, E. FRON, H.B. RODRÍGUEZ, E. SAN ROMÁN, G.D. SHOLES, G. SCHWEITZER, B. VALEUR AND J. WIRZ, “Pitfalls and Limitations in the Practical Use of Förster’s Theory of Resonance Energy Transfer”, *Photochem. Photobiol. Sci.* **7**, 1444–1448 (2008).
- [56] A. OLAYA-CASTRO AND G.D. SHOLES, “Energy Transfer from Förster-Dexter Theory to Quantum Coherent Light-Harvesting”, *Int. Rev. Phys. Chem.* **30**, 49–77 (2011).
- [57] J. KÖHLER, “Tutorial: Light-Harvesting Processes”, *Lecture given at the University of Bayreuth* (2013).
- [58] X. HU AND K. SCHULTEN, “Model for the Light Harvesting Complex I (B875) of *Rhodobacter sphaeroides*”, *Biophys. J.* **75**, 683–694 (1998).
- [59] S.J. JANG, M.D. NEWTON AND R.J. SILBEY, “Multichromophoric Förster Resonance Energy Transfer”, *Phys. Rev. Lett.* **92**, 218301 (2004).
- [60] S. JANG, M.D. NEWTON AND R.J. SILBEY, “Multichromophoric Förster Resonance Energy Transfer From B800 to B850 in the Light Harvesting Complex 2: Evidence for Subtle Energetic Optimization by Purple Bacteria”, *J. Phys. Chem. B* **111**, 6807–6814 (2007).
- [61] L. VALKUNAS, J. JANUSONIS, D. RUTKAUSKAS AND R. VAN GRONDELLE, “Protein Dynamics Revealed in the Excitonic Spectra of Single LH2 Complexes”, *J. Lumin.* **127**, 269–275 (2007).
- [62] R. VAN GRONDELLE AND V.I. NOVODEREZHKIN, “Spectroscopy and Dynamics of Excitation Transfer and Trapping in Purple Bacteria” in *The Purple Phototrophic Bacteria, Advances in Photosynthesis and Respiration*, ed. C.N. HUNTER, F. DALDAL, M.C. THURNAUER AND J.T. BEATTY, *Springer*, 2008, Vol. 28, pp. 231–252.
- [63] D. BELJONNE, C. CURUTCHET, G.D. SHOLES AND R.J. SILBEY, “Beyond Förster Resonance Energy Transfer in Biological and Nanoscale Systems”, *J. Phys. Chem. B* **113**, 6583–6599 (2009).
- [64] J. FRENKEL, “On the Transformation of Light into Heat in Solids. I”, *Phys. Rev.* **37**, 17–44 (1931).
- [65] J. FRENKEL, “On the Transformation of Light into Heat in Solids. II”, *Phys. Rev.* **37**, 1276–1294 (1931).
- [66] R.S. KNOX, “The Electronic Structure”, ed. H. EHRENREICH, F. SEITZ AND D. TURNBULL, *Academic Press*, 1963.

- [67] A.S. DAVYDOV, “Theory of Molecular Excitons”, *Plenum Press*, 1971.
- [68] M.V. MOSTOVOY AND J. KNOESTER, “Statistics of Optical Spectra from Single Ring Aggregates and its Application to LH2”, *J. Phys. Chem. B* **104**, 12355–12364 (2000).
- [69] M. MATSUSHITA, M. KETELAARS, A.M. VAN OIJEN, J. KÖHLER, T.J. AARTSMA AND J. SCHMIDT, “Spectroscopy on the B850 Band of Individual Light-Harvesting 2 Complexes of *Rhodospseudomonas acidophila* II. Exciton States of an Elliptically Deformed Ring Aggregate”, *Biophys. J.* **80**, 1604–1614 (2001).
- [70] S. JANG, S.E. DEMPSTER AND R.J. SILBEY, “Characterization of the Static Disorder in the B850 Band of LH2”, *J. Phys. Chem. B* **105**, 6655–6665 (2001).
- [71] M. CHACHISVILIS, O. KUEHN, T. PULLERITS AND V. SUNDSTRÖM, “Excitons in Photosynthetic Purple Bacteria: Wavelike Motion or Incoherent Hopping?”, *J. Phys. Chem. B* **101**, 7275–7283 (1997).
- [72] M. DAHLBOM, T. PULLERITS, S. MUKAMEL AND V. SUNDSTRÖM, “Exciton Delocalization in the B850 Light-Harvesting Complex: Comparison of Different Measures”, *J. Phys. Chem. B* **105**, 5515–5524 (2001).
- [73] A. DAMJANOVIĆ, I. KOSZTIN, U. KLEINEKATHÖFER AND K. SCHULTEN, “Excitons in a Photosynthetic Light-Harvesting System: A Combined Molecular Dynamics, Quantum Chemistry, and Polaron Model Study”, *Physical Review E* **65**, 031919 (2002).
- [74] R.G. ALDEN, E. JOHNSON, V. NAGARAJAN, W.W. PARSON, C.J. LAW AND R.J. COGDELL, “Calculations of Spectroscopic Properties of the LH2 Bacteriochlorophyll-Protein Antenna Complex from *Rhodospseudomonas acidophila*”, *J. Phys. Chem. B* **101**, 4667–4680 (1997).
- [75] A. FREIBERG, J.A. JACKSON, S. LIN AND N.W. WOODBURY, “Subpicosecond Pump-Supercontinuum Probe Spectroscopy of LH2 Photosynthetic Antenna Proteins at Low Temperature”, *J. Phys. Chem. A* **102**, 4372–4380 (1998).
- [76] J. LINNANTO, J.E.I. KORPPI-TOMMOLA AND V.M. HELENIUS, “Electronic States, Absorption Spectrum and Circular Dichroism Spectrum of the Photosynthetic Bacterial LH2 Antenna of *Rhodospseudomonas acidophila* as Predicted by Exciton Theory and Semiempirical Calculations”, *J. Phys. Chem. B* **103**, 8739–8750 (1999).
- [77] H. SUMI AND K. MUKAI, “Detection of the Upper Edge of Exciton Multiplets in the Antenna Complexes LH1 and LH2 of Bacterial Photosynthesis, by Optical Reflection”, *Chem. Phys. Lett.* **368**, 547–554 (2003).

- [78] M. PAJUSALU, M. RÄTSEP, G. TRINKUNAS AND A. FREIBERG, “Davydov Splitting of Excitons in Cyclic Bacteriochlorophyll *a* Nanoaggregates of Bacterial Light-Harvesting Complexes between 4.5 and 263 K”, *ChemPhysChem* **12**, 634–644 (2011).
- [79] G. TRINKUNAS, O. ZERLAUSKIENE, V. URBONIENÈ, J. CHMELIOV, A. GALL, B. ROBERT AND L. VALKUNAS, “Exciton Band Structure in Bacterial Peripheral Light-Harvesting Complexes”, *J. Phys. Chem. B* **116**, 5192–5198 (2012).
- [80] N.R. REDDY, R. PICOREL AND G.J. SMALL, “B896 and B870 Components of the *Rhodobacter sphaeroides* Antenna: a Hole Burning Study”, *J. Phys. Chem.* **96**, 6458–6464 (1992).
- [81] “Light Harvesting Antennas in Photosynthesis”, ed. B.R. GREEN AND W. PARSON, *Kluwer Academic Publishers*, 2003.
- [82] R. JANKOWIAK, M. REPERT, V. ZAZUBOVICH, J. PIEPER AND R. T., “Site Selective and Single Complex Laser-Based Spectroscopies: A Window on Excited State Electronic Structure, Excitation Energy Transfer, and Electron-Phonon Coupling of Selected Photosynthetic Complexes”, *Chemical Review* **111**, 4546–4598 (2011).
- [83] R. PURCHASE AND S. VÖLKER, “Spectral Hole Burning: Examples from Photosynthesis”, *Photosynth. Res.* **101**, 245–266 (2009).
- [84] K.K. REBANE, “Zero Phonon Lines as the Foundation Stone of High-Resolution Matrix Spectroscopy, Persistent Spectral Hole Burning, Single Impurity Molecule Spectroscopy”, *Chem. Phys.* **189**, 139–148 (1994).
- [85] B. VALEUR, “Molecular Fluorescence: Principles and Applications”, *Wiley-VCH*, 2001.
- [86] A. FREIBERG, M. RÄTSEP, K. TIMPMANN AND G. TRINKUNAS, “Excitonic Polarons in Quasi-One-Dimensional LH1 and LH2 Bacteriochlorophyll *a* Antenna Aggregates from Photosynthetic Bacteria: A Wavelength-Dependent Selective Spectroscopy Study”, *Chem. Phys.* **357**, 102–112 (2009).
- [87] J. FRIEDRICH AND D. HAARER, “Photochemical Hole Burning: A Spectroscopic Study of Relaxation Processes in Polymers and Glasses.”, *Angew. Chem. Int. Ed.* **23**, 113–140 (1984).
- [88] H. VAN DER LAAN, T. SCHMIDT, R.W. VISSCHERS, K. VISSCHER, R. VAN GRONDELLE AND S. VÖLKER, “Energy Transfer in the B800-850 Antenna Complex of Purple Bacteria *Rhodobacter Sphaeroides*: a Study by Spectral Hole-Burning”, *Chem. Phys. Lett.* **170**, 231–238 (1990).

- 
- [89] N.R.S. REDDY, G.J. SMALL, M. SEIBERT AND R. PICOREL, “Energy Transfer Dynamics of the B800-B850 Antenna Complex of *Rhodobacter sphaeroides*: a Hole Burning Study”, *Chem. Phys. Lett.* **181**, 391–399 (1991).
- [90] C. DE CARO, R.W. VISSCHERS, R. VAN GRONDELLE AND S. VÖLKER, “Spectral Hole Burning in Pigment Protein Complexes of Photosynthetic Bacteria”, *J. Lumin.* **58**, 149–153 (1994).
- [91] N.R. REDDY, R. COGDELL, L. ZHAO AND G.J. SMALL, “Nonphotochemical Hole Burning of the B800-B850 Antenna Complex of *Rhodospseudomonas Acidophila*”, *Photochem. Photobiol.* **57**, 33–39 (1993).
- [92] A. FREIBERG, M. RÄTSEP AND K. TIMPMANN, “A Comparative Spectroscopic and Kinetic Study of Photoexcitations in Detergent-Isolated and Membrane-Embedded LH2 Light-Harvesting Complexes”, *Biochim. Biophys. Acta, Bioenerg.* **1817**, 1471–1482 (2012).
- [93] H.M. WU, N.R.S. REDDY AND G.J. SMALL, “Direct Observation and Hole Burning of the Lowest Exciton Level (B870) of the LH2 Antenna Complex of *Rhodospseudomonas acidophila* (strain 10050)”, *J. Phys. Chem. B* **101**, 651–656 (1997).
- [94] A. FREIBERG, M. RÄTSEP, K. TIMPMANN, G. TRINKUNAS AND W.N. WOODBURY, “Self-Trapped Excitons in LH2 Antenna Complexes between 5 K and Ambient Temperature”, *J. Phys. Chem. B.* **107**, 11510–11519 (2003).
- [95] M. RÄTSEP AND A. FREIBERG, “Resonant Emission From the B870 Exciton State and Electron-Phonon Coupling in the LH2 Antenna Chromoprotein”, *Chem. Phys. Lett.* **377**, 371–376 (2003).
- [96] H.M. WU, M. RÄTSEP, I.J. LEE, R.J. COGDELL AND G.J. SMALL, “Exciton Level Structure and Energy Disorder of the B850 Ring of the LH2 Antenna Complex”, *J. Phys. Chem. B* **101**, 7654–7663 (1997).
- [97] R. MONSHOUWER, M. ABRAHAMSON, F. VAN MOURIK AND R. VAN GRONDELLE, “Superradiance and Exciton Delocalization in Bacterial Photosynthetic Light-Harvesting Systems”, *J. Phys. Chem. B* **101**, 7241–7248 (1997).
- [98] T.J. PFLOCK, S. OELLERICH, J. SOUTHALL, R.J. COGDELL, G.M. ULLMANN AND J. KÖHLER, “The Electronically Excited States of LH2 Complexes from *Rhodospseudomonas acidophila* Strain 10050 Studied by Time-Resolved Spectroscopy and Dynamic Monte Carlo Simulations. I. Isolated, Non-Interacting LH2 Complexes”, *J. Phys. Chem. B* **115**, 8813–8820 (2011).

- [99] K. TIMPMANN, Z. KATILIENE, N.W. WOODBURY AND A. FREIBERG, “Exciton Self Trapping in One-Dimensional Photosynthetic Antennas”, *J. Phys. Chem. B* **105**, 12223–12225 (2001).
- [100] L.D. BOOK, A.E. OSTAFIN, N. PONOMARENKO, J.R. NORRIS AND N.F. SCHERER, “Exciton Delocalization and Initial Dephasing Dynamics of Purple Bacterial LH2”, *J. Phys. Chem. B* **104**, 8295–8307 (2000).
- [101] T. PULLERITS, M. CHACHISVILLIS AND V. SUNDSTRÖM, “Exciton Delocalization Length in the B850 Antenna of *Rhodobacter sphaeroides*”, *J. Phys. Chem.* **100**, 10787–10792 (1996).
- [102] J.T.M. KENNIS, A.M. STRELTSOV, H. PERMENTIER, T.J. AARTSMA AND J. AMESZ, “Exciton Coherence and Energy Transfer in the LH2 Antenna Complex of *Rhodopseudomonas acidophila* at Low Temperature”, *J. Phys. Chem. B* **101**, 8369–8374 (1997).
- [103] S.I.E. VULTO, J.T.M. KENNIS, A.M. STRELTSOV, J. AMESZ AND T.J. AARTSMA, “Energy Relaxation within the B850 Absorption Band of the Isolated Light-Harvesting Complex LH2 from *Rhodopseudomonas acidophila* at Low Temperature”, *J. Phys. Chem. B* **103**, 878–883 (1999).
- [104] H. FIDDER, J. KNOESTER AND D.A. WIERSMA, “Optical Properties of Disordered Molecular Aggregates: A Numerical Study”, *J. Chem. Phys.* **95**, 7880–7890 (1991).
- [105] A. FREIBERG, K. TIMPMANN, R. RUUS AND N.W. WOODBURY, “Disordered Exciton Analysis of Linear and Nonlinear Absorption Spectra of Antenna Bacteriochlorophyll Aggregates: LH2-Only Mutant Chromatophores of *Rhodobacter sphaeroides* at 8 K under Spectrally Selective Excitation”, *J. Phys. Chem. B* **103**, 10032–10041 (1999).
- [106] R. JIMENEZ, S.N. DIKSHIT, S.E. BRADFORD AND G.R. FLEMING, “Electronic Excitation Transfer in the LH2 Complex of *Rhodobacter sphaeroides*”, *J. Phys. Chem.* **100**, 6825–6834 (1996).
- [107] J.T.M. KENNIS, A.M. STRELTSOV, S.I.E. VULTO, T.J. AARTSMA, T. NOZAWA AND J. AMESZ, “Femtosecond Dynamics in Isolated LH2 Complexes of Various Species of Purple Bacteria”, *J. Phys. Chem. B* **101**, 7827–7834 (1997).
- [108] Y. TOYOZAWA, “Theory of Lineshapes of the Exciton Absorption Bands”, *Prog. Theor. Phys.* **20**, 53–81 (1958).
- [109] E.I. RASHBA, “Self-Trapping of Excitons”, ed. E.I. RASHBA AND M.D. STURGE, *North-Holland Publishing Company*, 1982.

- 
- [110] H. SUMI AND A. SUMI, “Dimensionality Dependence in Self-Trapping of Excitons”, *J. Phys. Soc. Jpn.* **63**, 637–657 (1994).
- [111] Y. TOYOZAWA, “Polaron and the Self-Trapped State”, ed. Y. TOYOZAWA, *Cambridge University Press*, 2003.
- [112] J. KNOESTER AND V.M. AGRANOVICH, “Frenkel and Charge-Transfer Excitations in Organic Solids”, *Elsevier*, 2003.
- [113] T. MEIER, Y. ZHAO, V. CHERNYAK AND S. MUKAMEL, “Polarons, Localization, and Excitonic Coherence in Superradiance of Biological Antenna Complexes”, *J. Chem. Phys.* **107**, 3976–3893 (1997).
- [114] T. POLIVKA, T. PULLERITS, J.L. HEREK AND V. SUNDSTRÖM, “Exciton Relaxation and Polaron Formation in LH2 at Low Temperature”, *J. Phys. Chem. B* **104**, 1088–1096 (2000).
- [115] R.J. VAN DORSSSEN, C.N. HUNTER, R. VAN GRONDELLE, A.H. KORENHOF AND J. AMESZ, “Spectroscopic Properties of Antenna Complexes of *Rhodobacter sphaeroides* in Vivo”, *Biochim. Biophys. Acta, Bioenerg.* **932**, 179–188 (1988).
- [116] A. FREIBERG, M. RÄTSEP, K. TIMPMANN AND G. TRINKUNAS, “Self-Trapped Excitons in Circular Bacteriochlorophyll Antenna Complexes”, *J. Lumin.* **102-103**, 363–368 (2003).
- [117] K. TIMPMANN, A. ELLERVEE, A. KUZNETSOV, A. LAISAAR, G. TRINKUNAS AND A. FREIBERG, “Self-Trapped Excitons in LH2 Bacteriochlorophyll-Protein Complexes under High Pressure”, *J. Lumin.* **102**, 220–225 (2003).
- [118] K. TIMPMANN, M. RÄTSEP, C.N. HUNTER AND A. FREIBERG, “Emitting Excitonic Polaron States in Core LH1 and Peripheral LH2 Bacterial Light-Harvesting Complexes”, *J. Phys. Chem. B* **108**, 10581–10588 (2004).
- [119] A. FREIBERG, M. RÄTSEP, K. TIMPMANN AND G. TRINKUNAS, “Dual Fluorescence of Single LH2 Antenna Nanorings”, *J. Lumin.* **108**, 107–110 (2004).
- [120] A. FREIBERG AND G. TRINKUNAS, “Unravelling the Hidden Nature of Antenna Excitations” in *Photosynthesis in silico: Understanding Complexity from Molecules to Ecosystems*, ed. A. LAISK, L. NEDBAL AND GOVINDJEE, *Springer*, 2009, Vol. 29, pp. 55–82.
- [121] A. FREIBERG, K. TIMPMANN, S. LIN AND N.W. WOODBURY, “Exciton Relaxation and Transfer in the LH2 Antenna Network of Photosynthetic Bacteria”, *J. Phys. Chem. B* **102**, 10974–10982 (1998).

- [122] K. TIMPMANN, N.W. WOODBURY AND A. FREIBERG, “Unraveling Exciton Relaxation and Energy Transfer in LH2 Photosynthetic Antennas”, *J. Phys. Chem. B* **104**, 9769–9771 (2000).
- [123] W.P. AMBROSE AND W.E. MOERNER, “Fluorescence Spectroscopy and Spectral Diffusion of Single Impurity Molecules in a Crystal”, *Nature* **349**, 225–227 (1991).
- [124] “Single Molecule Optical Detection, Imaging and Spectroscopy”, ed. T. BASCHÉ, W.E. MOERNER, M. ORRIT AND U.P. WILD, *Wiley-VCH*, 1997.
- [125] C. HOFMANN, F. KULZER, R. ZONDERVAN, J. KÖHLER AND M. ORRIT, “Single Biomolecules at Cryogenic Temperatures: From Structure to Dynamics” in *Single Molecules and Nanotechnology*, ed. R. RIGLER AND H. VOGEL, *Springer*, 2008, pp. 1–27.
- [126] C. HOFMANN, T.J. AARTSMA, H. MICHEL AND J. KÖHLER, “Direct Observation of Tiers in the Energy Landscape of a Chromoprotein: A Single-Molecule Study”, *Proc. Natl. Acad. Sci. U. S. A.* **100**, 15534–15538 (2003).
- [127] J. BAIER, M.F. RICHTER, R.J. COGDELL, S. OELLERICH AND J. KÖHLER, “Determination of the Spectral Diffusion Kernel of a Protein by Single Molecule Spectroscopy”, *Phys. Rev. Lett.* **100**, 018108 (2008).
- [128] H. OIKAWA, S. FUJIYOSHI, T. DEWA, M. NANGO AND M. MATSUSHITA, “How Deep Is the Potential Well Confining a Protein in a Specific Conformation? A Single-Molecule Study on Temperature Dependence of Conformational Change between 5 and 18 K”, *J. Am. Chem. Soc.* **130**, 4580–4581 (2008).
- [129] Y. BERLIN, A. BURIN, J. FRIEDRICH AND J. KÖHLER, “Low Temperature Spectroscopy of Proteins. Part II: Experiments with Single Protein Complexes”, *Phys. Life Rev.* **4**, 64–89 (2007).
- [130] D. GROZDANOV, N. HERASCU, T. REINOT, R. JANKOWIAK AND V. ZAZUBOVICH, “Low-Temperature Protein Dynamics of the B800 Molecules in the LH2 Light-Harvesting Complex: Spectral Hole Burning Study and Comparison with Single Photosynthetic Complex Spectroscopy”, *J. Phys. Chem. B* **114**, 3426–3438 (2010).
- [131] A.M. VAN OIJEN, M. KETELAARS, J. KÖHLER, T.J. AARTSMA AND J. SCHMIDT, “Spectroscopy of Single Light-Harvesting Complexes from Purple Photosynthetic Bacteria at 1.2 K”, *J. Phys. Chem. B* **102**, 9363–9366 (1998).
- [132] A.M. VAN OIJEN, M. KETELAARS, J. KÖHLER, T.J. AARTSMA AND J. SCHMIDT, “Unraveling the Electronic Structure of Individual Photosynthetic Pigment-Pigment Complexes”, *Science* **285**, 400–402 (1999).

- 
- [133] S. JANG AND R.J. SILBEY, “Single Complex Line Shapes of the B850 Band of LH2”, *J. Chem. Phys.* **118**, 9324–9336 (2003).
- [134] S. JANG, R.J. SILBEY, R. KUNZ, C. HOFMANN AND J. KÖHLER, “Is There Elliptic Distortion in the Light Harvesting Complex 2 of Purple Bacteria?”, *J. Phys. Chem. B* **115**, 12947–12953 (2011).
- [135] M. KETELAARS, A.M. VAN OIJEN, M. MATSUSHITA, J. KÖHLER, J. SCHMIDT AND T.J. AARTSMA, “Spectroscopy on the B850 Band of Individual Light-Harvesting 2 Complexes of *Rhodopseudomonas acidophila* I. Experiments and Monte-Carlo Simulations”, *Biophys. J.* **80**, 1591–1603 (2001).
- [136] C. HOFMANN, T.J. AARTSMA AND J. KÖHLER, “Energetic Disorder and the B850-Exciton States of Individual Light-Harvesting 2 Complexes from *Rhodopseudomonas acidophila*”, *Chem. Phys. Lett.* **395**, 373–378 (2004).
- [137] V.I. NOVODEREZHKIN AND A.P. RAZJIVIN, “Excitonic Interactions in the Light-Harvesting Antenna of Photosynthetic Purple Bacteria and Their Influence on Picosecond Absorbance Difference Spectra”, *FEBS Lett.* **330**, 5–7 (1993).
- [138] T.V. DRACHEVA, V.I. NOVODEREZHKIN AND A.P. RAZJIVIN, “Exciton Delocalization in the Antenna of Purple Bacteria: Exciton Spectrum Calculations Using X-Ray Data and Experimental Site Inhomogeneity”, *FEBS Lett.* **387**, 81–84 (1996).
- [139] C. HOFMANN, H. MICHEL, M. VAN HEEL AND J. KÖHLER, “Multivariate Analysis of Single-Molecule Spectra: Surpassing Spectral Diffusion”, *Phys. Rev. Lett.* **94**, 195501 (2005).
- [140] C. HOFMANN, T.J. AARTSMA, H. MICHEL AND J. KÖHLER, “Spectral Dynamics in the B800 Band of LH2 from *Rhodospirillum molischianum*: A Single-Molecule Study”, *New J. Phys.* **6**, 1–15 (2004).
- [141] C. TIETZ, O. CHEKLOV, A. DRÄBENSTEDT, J. SCHUSTER AND J. WRACHTRUP, “Spectroscopy on Single Light-Harvesting Complexes at Low Temperature”, *J. Phys. Chem. B* **103**, 6328–6333 (1999).
- [142] D. RUTKAUSKAS, R. NOVODEREZHKIN, R.J. COGDELL AND R. VAN GRONDELLE, “Fluorescence Spectral Fluctuations of Single LH2 complexes from *Rhodopseudomonas acidophila* strain 10050”, *Biochemistry* **43**, 4431–4438 (2004).
- [143] D. RUTKAUSKAS, J. OLSEN, A. GALL, R.J. COGDELL, C.N. HUNTER AND R. VAN GRONDELLE, “Comparative Study of Spectral Flexibilities of Bacterial Light-Harvesting Complexes: Structural Implications”, *Biophys. J.* **90**, 2463–2474 (2006).

- [144] D. RUTKAUSKAS, V. NOVODEREZHKIN, A. GALL, J. OLSEN, R.J. COGDELL, C.N. HUNTER AND R. VAN GRONDELLE, “Spectral Trends in the Fluorescence of Single Bacterial Light-Harvesting Complexes: Experiments and Modified Redfield Simulations”, *Biophys. J.* **90**, 2475–2485 (2006).
- [145] D. RUTKAUSKAS, R.J. COGDELL AND R. VAN GRONDELLE, “Conformational Relaxation of Single Bacterial Light-Harvesting Complexes”, *Biochemistry* **45**, 1082–1086 (2006).
- [146] V.I. NOVODEREZHKIN, D. RUTKAUSKAS AND R. VAN GRONDELLE, “Multistate Conformational Model of a Single LH2 Complex: Quantitative Picture of Time-Dependent Spectral Fluctuations”, *Chem. Phys.* **341**, 45–56 (2007).
- [147] J. JANUSONIS, L. VALKUNAS, D. RUTKAUSKAS AND R. VAN GRONDELLE, “Spectral Dynamics of Individual Bacterial Light-Harvesting Complexes: Alternative Disorder Model”, *Biophys. J.* **94**, 1348–1358 (2008).
- [148] R. VAN GRONDELLE AND V.I. NOVODEREZHKIN, “Energy transfer in photosynthesis: Experimental Insights and Quantitative Models”, *Phys. Chem. Chem. Phys.* **8**, 793–807 (2006).
- [149] V.I. NOVODEREZHKIN, D. RUTKAUSKAS AND R. VAN GRONDELLE, “Dynamics of the Emission Spectrum of a Single LH2 Complex: Interplay of Slow and Fast Nuclear Motions”, *Biophys. J.* **90**, 2890–2902 (2006).
- [150] W.P.F. DE RUIJTER, J.M. SEGURA, R.J. COGDELL, A.T. GARDINER, S. OELLERICH AND T.J. AARTSMA, “Fluorescence-Emission Spectroscopy of Individual LH2 and LH3 Complexes”, *Chem. Phys.* **341**, 320–325 (2007).
- [151] U. GERKEN, F. JELEZKO, B. GÖTZE, M. BRANSCHÄDEL, C. TIETZ, R. GHOSH AND J. WRACHTRUP, “Membrane Environment Reduces the Accessible Conformational Space Available to an Integral Membrane Protein”, *J. Phys. Chem. B* **107**, 338–343 (2003).
- [152] D. UCHIYAMA, H. OIKAWA, K. OTOMO, M. NANGO, T. DEWA, S. FUJIYOSHI AND M. MATSUSHITA, “Reconstitution of Bacterial Photosynthetic Unit in a Lipid Bilayer Studied by Single-Molecule Spectroscopy at 5 K”, *Phys. Chem. Chem. Phys.* **13**, 11615–11619 (2011).
- [153] R. COGDELL AND A.M. HAWTHORNTHWAITTE, “Preparation, Purification, and Crystallization of Purple Bacteria Antenna Complexes” in *The Photosynthetic Reaction Center*, ed. J. DEISENHOFER AND J. NORRIS, *Academic Press*, 1993, Vol. 1, pp. 23–42.

- 
- [154] M. ORRIT AND J. BERNARD, “Single Pentacene Molecules Detected by Fluorescence Excitation in a p-Terphenyl Crystal”, *Phys. Rev. Lett.* **65**, 2716–2719 (1990).
- [155] J.E. PAWLEY, “Handbook of Biological Confocal Microscopy”, *Plenum Press*, 1989.
- [156] E. LANG, J. BAIER AND J. KÖHLER, “Epifluorescence, Confocal and Total Internal Reflection Microscopy for Single-Molecule Experiments: A Quantitative Comparison”, *J. Microsc.* **222**, 118–123 (2006).
- [157] M. PLANCK, “The Theory of Radiation”, *P. Blakiston’s Son & Co.*, 1914.
- [158] K. TIMPMANN, G. TRINKUNAS, J.D. OLSEN, C.N. HUNTER AND A. FREIBERG, “Bandwidth of Excitons in LH2 Bacterial Antenna Chromoproteins”, *Chem. Phys. Lett.* **398**, 384–388 (2004).
- [159] L. BORLAND AND M. VAN HEEL, “Classification of Data in Conjugate Representation Spaces”, *J. Opt. Soc. Am. A* **7**, 601–610 (1990).
- [160] M. VAN HEEL, “A New Family of Power Multivariate Statistical Sequence Analysis Techniques”, *J. Mol. Biol.* **220**, 87–7-887 (1991).
- [161] M. VAN HEEL, G. HARAUZ AND E.V. ORLOVA, “A New Generation of the IMAGIC Image Processing System”, *J. Struct. Biol.* **116**, 17–24 (1996).
- [162] M. VAN HEEL, B. GOWEN, R. MATADEEN, E.V. ORLOVA, R. FINN, T. PAPE, D. COHEN, H. STARK, R. SCHMIDT, M. SCHATZ AND A. PATWARDHAN, “Single-Particle Electron Cryo-Microscopy: Towards Atomic Resolution”, *Q. Rev. Biophys.* **33**, 307–369 (2000).
- [163] P. DUBE, J.B. HARRIS, E.V. ORLOVA, F. ZEMLIN, M. VAN HEEL AND J. MARKL, “Three-Dimensional Structure of Keyhole Limpet Hemocyanin by Cryoelectron Microscopy and Angular Resolution”, *J. Struct. Biol.* **115**, (1999).
- [164] P. DUBE, M. WIESKE, H. STARK, M. SCHATZ, J. STAHL, F. ZEMLIN, G. LUTSCH AND M. VAN HEEL, “The 80S Rat Liver Ribosome at 25 Å Resolution by Electron Cryomicroscopy and Angular Reconstitution”, *Structure* **6**, 389–399 (1998).
- [165] J. BAIER, M. GABRIELSEN, S. OELLERICH, H. MICHEL, M. VAN HEEL, R.J. COGDELL AND J. KÖHLER, “Spectral Diffusion and Electron-Phonon Coupling of the B800 BChl *a* Molecules in LH2 Complexes from Three Different Species of Purple Bacteria”, *Biophys. J.* **97**, 2604–2612 (2009).

- [166] R. HILDNER, U. LEMMER, U. SCHERF, M. VAN HEEL AND J. KÖHLER, “Revealing the Electron-Phonon Coupling in a Conjugated Polymer by Single-Molecule Spectroscopy”, *Advanced Materials* **19**, 1978–1982 (2007).
- [167] R. HILDNER, L. WINTERLING, U. LEMMER, U. SCHERF AND J. KÖHLER, “Single-Molecule Spectroscopy on a Ladder-Type Conjugated Polymer: Electron-Phonon Coupling and Spectral Diffusion”, *ChemPhysChem* **10**, 2524–2534 (2009).
- [168] M. RÄTSEP AND A. FREIBERG, “Electron-Phonon and Vibronic Couplings in the FMO Bacteriochlorophyll *a* Antenna Complex Studied by Difference Fluorescence Line Narrowing”, *J. Lumin.* **127**, 251–259 (2007).
- [169] M. RÄTSEP, C.N. HUNTER, J.D. OLSEN AND A. FREIBERG, “Band Structure and Local Dynamics of Excitons in Bacterial Light-Harvesting Complexes Revealed by Spectrally Selective Spectroscopy”, *Photosynth. Res.* **86**, 37–48 (2005).
- [170] V. LUBCHENKO AND R.J. SILBEY, “Spectral Diffusion and Drift: Single Chromophore and *En Masse*”, *J. Chem. Phys.* **126**, 064701 (2007).
- [171] O. MIRZOV AND I.G. SCHEBLYKIN, “Photoluminescence Spectra of a Conjugated Polymer: From Films and Solutions to Single Molecules”, *Phys. Chem. Chem. Phys.* **8**, 5569–5576 (2006).
- [172] M. HUSSELS AND M. BRECHT, “Effect of Glycerol and PVA on the Conformation of Photosystem I”, *Biochemistry* **50**, 3628–3637 (2011).
- [173] M.A. BOPP, A. SYTNIK, T.D. HOWARD, R.J. COGDELL AND R.M. HOCHSTRASSER, “The Dynamics of Structural Deformations of Immobilized Single Light-Harvesting Complexes”, *Proc. Natl. Acad. Sci. U. S. A.* **96**, 11271–11276 (1999).
- [174] S. TUBASUM, R.J. COGDELL, I.G. SCHEBLYKIN AND T. PULLERITS, “Excitation-Emission Polarization Spectroscopy of Single Light Harvesting Complexes”, *J. Phys. Chem. B* **115**, 4963–4970 (2011).
- [175] P. WALTERS, “An Introduction to Ergodic Theory”, *Springer*, 1982.
- [176] M.F. RICHTER, J. BAIER, R.J. COGDELL, J. KÖHLER AND S. OELERICH, “Single-Molecule Spectroscopic Characterization of Light-Harvesting 2 Complexes Reconstituted into Model Membranes”, *Biophys. J.* **93**, 183–191 (2007).

- [177] P. REICHL, “Spektroskopische Untersuchungen der Exzitonen-Zustände in der B850-Bande von LH-Komplexen”, *Diplomarbeit, Lehrstuhl Experimentalphysik IV, Universität Bayreuth*, 2005.
- [178] S. TUBASUM, S. SAKAI, T. DEWA, V. SUNDSTRÖM, I. SCHEBLYKIN, M. NANGO AND T. PULLERITS, “Anchored LH2 Complexes in 2D Polarization Imaging”, *J. Phys. Chem. B* **117**, 11391-11396 (2013).
- [179] S. TUBASUM, R. CAMACHO, M. MEYER, D. YADAV, R.J. COGDELL, T. PULLERITS AND I.G. SCHEBLYKIN, “Evidence of Excited State Localization and Static Disorder in LH2 Investigated by 2D-Polarization Single-Molecule Imaging at Room Temperature”, *Phys. Chem. Chem. Phys.* **15**, 19862–19869 (2013).
- [180] H.M. WU, M. RÄTSEP, R. JANKOWIAK, R.J. COGDELL AND G.J. SMALL, “Hole Burning and Absorption Studies of the LH1 Antenna Complex of Purple Bacteria: Effects of Pressure and Temperature”, *J. Phys. Chem. B* **102**, 4023–4034 (1998).



## List of publications

### Author

1. R. KUNZ, K. TIMPMANN, J. SOUTHALL, R.J. COGDELL, J. KÖHLER AND A. FREIBERG, “Fluorescence-Excitation and Emission Spectra from LH2 Antenna Complexes of *Rhodopseudomonas acidophila* as a Function of the Sample Preparation Conditions”, *J. Phys. Chem. B*, **117**, 12020-12029 (2013).
2. R. KUNZ, K. TIMPMANN, J. SOUTHALL, R.J. COGDELL, A. FREIBERG AND J. KÖHLER, “Exciton Self Trapping in Photosynthetic Pigment-Protein Complexes Studied by Single-Molecule Spectroscopy”, *J. Phys. Chem. B*, **116**, 11017-11023 (2012).
3. R. KUNZ, K. TIMPMANN, J. SOUTHALL, R.J. COGDELL, A. FREIBERG AND J. KÖHLER, “Fluctuations in the Electron-Phonon Coupling of a Single Chromoprotein”, *Ang. Chem. Int. Ed.*, **52**, 8726-8730 (2013).
4. R. KUNZ, K. TIMPMANN, J. SOUTHALL, R.J. COGDELL, A. FREIBERG AND J. KÖHLER, “Single-Molecule Spectroscopy Unmasks the Lowest Exciton State of the B850 Assembly in LH2 from *Rps. acidophila*”, *Biophys. J.*, **106**, 2008-2016 (2014).

### Co-Author (These publications are not covered in the underlying thesis.)

1. P.S. BÖHM, R. KUNZ, J. SOUTHALL, R.J. COGDELL, AND J. KÖHLER, “Does the Reconstitution of RC-LH1 Complexes from *Rhodopseudomonas acidophila* Strain 10050 into a Phospholipid Bilayer Yield the Optimum Environment for Optical Spectroscopy?”, *J. Phys. Chem. B*, DOI: 10.1021/jp409980k (2013).
2. S. JANG, R.J. SILBEY, R. KUNZ, C. HOFMANN AND J. KÖHLER, “Is There Elliptic Distortion in the Light Harvesting Complex 2 of Purple Bacteria?”, *J. Phys. Chem. B*, **115**, 12947-12953 (2011).
3. T.H.P. BRODOSUDARMO, R. KUNZ, P. BÖHM, A.T. GARDINER, V.MOULISOVÁ, R.J. COGDELL AND J. KÖHLER, “Single-Molecule Spectroscopy Reveals that Individual Low-Light LH2 Complexes from *Rhodopseudomonas palustris* 2.1.6. Have a Heterogeneous Polypeptide Composition”, *Biophys. J.*, **97**, 1491-1500 (2009).



## Danksagung

Am Ende möchte ich die Gelegenheit nutzen, mich bei einigen Personen, die zum Gelingen dieser Arbeit beigetragen haben, zu bedanken.

Erster Dank gilt meinem Doktorvater Prof. Dr. Jürgen Köhler für die interessante Themenstellung und die Möglichkeit an seinem Lehrstuhl zu promovieren. Vor allem die Kooperation in Estland und die damit verbundenen Reisen waren nicht nur fachlich, sondern auch menschlich eine tolle Erfahrung. Vielen Dank für diese Möglichkeit und die Betreuung meiner Promotion.

Prof. Dr. Anna Köhler danke ich für die Übernahme der Zweitkorrektur der Arbeit. Herzlichen Dank auch an Prof. Dr. Lothar Kador, dessen Tür immer offenstand und der mir mit großer Geduld auch Fragen außerhalb seines Arbeitsgebietes beantwortet hat.

Many thanks to Prof. Dr. Richard Cogdell for providing the samples and helpful discussions. Many thanks as well to Prof. Dr. Arvi Freiberg for the fruitful cooperation, his kind hospitality during my stay in his laboratories in Tartu and, of course, the nice conversations we had on the conferences in Banz and Tübingen.

One of the biggest gratitude I express to Dr. Kõu Timpmann from whom I learnt nearly everything what I know about emission and site-selective spectroscopy on LH samples. You have not only been a good teacher and advisor to me in all things that were related to spectroscopy, but became also a real friend during our intense cooperation in the last years. The hours we spent together in the lab and on many Skype conferences have been a great pleasure for me. Thank you very much, Kõu!

Bedanken möchte ich mich natürlich auch beim ganzen Lehrstuhl EP IV mit all seinen Arbeitsgruppen und Mitgliedern für die nette und angenehme Atmosphäre. Gesonderter Dank gilt hier vor allem dem Sekretariat mit Karin Baier, Evelyn Hülsmann und Claudia Masuch, die mich nicht nur in allen verwaltungstechnischen Fragen immer unterstützt haben, sondern auch sonst immer für mich da waren, wenn ich Hilfe, Unterstützung oder auch einfach nur ein offenes Ohr benötigt habe. Vielen Dank auch Dr. Wolfgang Richter und Dr. Uwe Gerken (u.a. aber nicht nur, für all die erheiternden Diskussionen in der Kaffeepause). Auch unseren Technikern Michael Heimler, Werner Reichstein und Stefan Schlicht sowie Waltraud Joy im Chemielabor danke ich ganz besonders. Ihr habt mir wirklich immer weitergeholfen!

Großer Dank geht auch an das Team von Frank Neumann in der Mechanikwerkstatt des NWII sowie an die Heliumwerkstatt im NWI, mit Piotr Sekowski, Harald Heindl und zuletzt auch Michael Heimler.

Zudem möchte ich mich bei meinen beiden Vorgängern an der Apparatur, Jürgen Baier und Martin Richter, bedanken, die mir nicht nur in der Anfangszeit mit wertvollen Tipps weiterhelfen konnten, sondern mich auch bei diversen Treffen

desöfteren mit Ihrem Humor erheitert haben.

Ein großes Dankeschön an meine Doktoranden-Kollegen am Lehrstuhl Hubert Aurdorff, Paul Böhm, Dominique Ernst, Christiane Hofmann, Marc Jendrny, Tobias Pflock und Florian Spreitler sowie die Postdocs Richard Hildner, Abey Issac und Martti Pärs, für die vielen schönen gemeinsamen Erlebnisse und die gegenseitige Unterstützung. Eine Doktorarbeit in der Experimentalphysik ist immer auch Teamwork und wir waren ein starkes Team! Der nachfolgendenen Doktoranden-Generation mit Sebastian Baderschneider, Sebastian Beyer, Alexander Löhner und Regina Schmidt wünsche ich einen ebenso starken Zusammenhalt, wie wir ihn hatten, und viel Erfolg für ihre Arbeit.

Gesonderter Dank gilt Richard Hildner für fachliche Diskussionen und gute Tipps, Dominique Ernst für seine Hilfsbereitschaft und das Fahrrad sowie Marc Jendrny für den Matlab-Support und auch einfach so. Extra-Dank auch an meinen Labor-kollegen Paul Böhm für den steten Gedankenaustausch, seine ruhige Art und das gute Miteinander am „Single-Molecule Setup for the Spectroscopy of Light Harvesting Complexes from Purple Bacteria at Low Temperature.“

Für das Korrekturlesen dieser Arbeit bedanke ich mich zudem ganz herzlich bei Richard Hildner, Abey Issac und Paul Böhm. Ihr habt die Qualität dieser Arbeit enorm gesteigert.

Herzlichen Dank auch an Martti Pärs, der mir für die letzte Zeit in Bayreuth einen unkomplizierten Schlaf- und Fahrradstellplatz in Uninähe ermöglicht hat.

Am Ende möchte ich mich noch bei meiner Familie und meinen Freunden außerhalb der Uni für Ihre Unterstützung während meiner Promotion bedanken.

Letzter und herzlichster Dank gilt meiner Partnerin Monique, für die gemeinsame Zeit und das Verständnis für all die Entbehrungen, die mit dieser Arbeit verbunden waren.

Bayreuth, im Dezember 2013

Ralf Kunz

## Erklärung

Hiermit versichere ich an Eides statt, dass ich die vorliegende Arbeit selbstständig verfasst und keine anderen als die von mir angegebenen Quellen und Hilfsmittel benutzt habe.

Ich erkläre, dass ich keine früheren Promotionsversuche unternommen habe. Die vorgelegte Abhandlung wurde weder in gleicher noch in ähnlicher Form einer anderen Prüfungsbehörde zur Erlangung eines akademischen Grades vorgelegt.

Desweiteren erkläre ich, dass ich Hilfe von gewerblichen Promotionsberatern bzw. -vermittlern oder ähnlichen Dienstleistern weder bisher in Anspruch genommen habe noch künftig in Anspruch nehmen werde.

Bayreuth, den 01.12.2013

---

Ralf Kunz



Part II

Publications



PUBLICATION P1

**Fluorescence-Excitation and Emission Spectra  
from LH2 Antenna Complexes of  
*Rhodopseudomonas acidophila* as a Function of  
the Sample Preparation Condition**

Ralf Kunz, Kōu Timpmann, June Southall, Richard J. Cogdell, Jürgen Köhler,  
and Arvi Freiberg

published in:

*The Journal of Physical Chemistry B* **117**, 12020-12029, (2013)

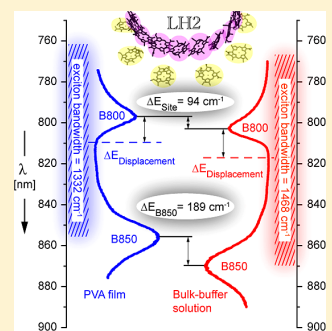
© 2013 American Chemical Society  
[DOI:10.1021/jp4073697](https://doi.org/10.1021/jp4073697)



# Fluorescence-Excitation and Emission Spectra from LH2 Antenna Complexes of *Rhodospseudomonas acidophila* as a Function of the Sample Preparation Conditions

Ralf Kunz,<sup>†</sup> Kōu Timpmann,<sup>‡</sup> June Southall,<sup>§</sup> Richard J. Cogdell,<sup>§</sup> Jürgen Köhler,<sup>†</sup> and Arvi Freiberg<sup>\*,‡,⊥</sup><sup>†</sup>Experimental Physics IV and Bayreuth Institute for Macromolecular Research (BIMF), University of Bayreuth, 95440 Bayreuth, Germany<sup>‡</sup>Institute of Physics, University of Tartu, Riia 142, Tartu EE-51014, Estonia<sup>§</sup>Institute of Molecular, Cell and Systems Biology, College of Medical, Veterinary and Life Sciences, University of Glasgow, Glasgow G12 8TA, United Kingdom<sup>⊥</sup>Institute of Molecular and Cell Biology, University of Tartu, Riia 23, Tartu EE-51010, Estonia

**ABSTRACT:** The high sensitivity of optical spectra of pigment–protein complexes to temperature and pressure is well known. In the present study, we have demonstrated the significant influence of the environments commonly used in bulk and single-molecule spectroscopic studies at low temperatures on the LH2 photosynthetic antenna complex from *Rhodospseudomonas acidophila*. A transfer of this LH2 complex from a bulk-buffer solution into a spin-coated polymer film results in a  $189\text{ cm}^{-1}$  blue shift of the B850 excitonic absorption band at 5 K. Within the molecular exciton model, the origin of this shift could be disentangled into three parts, namely to an increase of the local site energies, a contraction of the exciton band, and a decrease of the displacement energy.



## 1. INTRODUCTION

The light-harvesting (LH) systems of photosynthetic organisms, plants, algae, and bacteria, are highly optimized for efficient collection and delivery of solar energy to the photochemical reaction centers (RC).<sup>1,2</sup> The mechanisms of this optimization, as well as its regulation by variable environmental conditions, have been of considerable long-time interest. The spatial arrangement of the LH complexes within the photosynthetic membranes is very random, though sometimes this is not immediately obvious. In many cases, some order is followed so that the chromophores closer to the RC absorb progressively more red-shifted light and an energetic funnel toward the RC is formed.<sup>3,4</sup> Wonderful examples of this funneling principle are seen in purple photosynthetic bacteria, where two types of LH pigment–protein complexes, the core RC-LH1 and the peripheral LH2 complexes, are found working in unison.<sup>5–7</sup> The LH1 complex with its intense long-wavelength absorption band at about 875 nm, in close resonance with the respective RC band, directly encircles the RCs, whereas the usually more numerous LH2 complexes, featuring strong absorption bands around 800 and 850 nm, are located in the periphery.<sup>8,9</sup> Bacteriochlorophyll *a* (Bchl *a*) acts as the main LH molecule in both of these complexes.

The high-resolution crystal structure of the LH2 complex from *Rhodospseudomonas (Rps.) acidophila* reveals that it is a cyclic array of nine transmembrane  $\alpha,\beta$ -polypeptide pairs.<sup>10</sup> Each polypeptide pair binds 2 Bchl *a* molecules at the outer

membrane surface and one molecule on its intracytoplasmic side, forming two concentric pigment circles with  $C_9$ -symmetry. The inner ring consists of 18 strongly excitonically coupled Bchl *a* molecules that feature intermolecular distances of less than 1 nm. These slightly dimerized molecules give rise to the intense absorption band around 850–870 nm in the various species of purple bacteria, traditionally named the B850 band.<sup>11</sup> The 9 largely monomeric Bchl *a* molecules in the other ring, being separated by about 2 nm from each other, absorb light at around 800 nm (B800 band).

The B850 and B800 bands are related to the lowest-energy  $Q_y$  singlet electronic transitions in Bchl *a* molecules. The exact spectral position of these bands, however, depends in a complex manner on the binding of the Bchl *a* chromophores to the surrounding protein as well as on the distance and mutual orientation of the chromophores with respect to each other.<sup>11</sup> For simplicity, it is commonly assumed that the transition energies for the individual chromophores (site energies for short) are determined by the chromophore–protein interactions. The ability to flexibly change both the site energies and the exciton coupling energies is an ecological advantage that photosynthetic bacteria use to adapt to varying environmental conditions. For example, the light-harvesting apparatuses of

Received: July 24, 2013

Revised: September 9, 2013

Published: September 13, 2013

several species of purple bacteria feature additional peripheral LH complexes with the exciton absorbance at 820 nm when grown under low-light conditions.<sup>12–17</sup> Subtle changes in the surroundings of chromophores are thus sensitively probed by the exciton spectra of LH complexes.

Many of the spectroscopic investigations of photosynthetic LH complexes are carried out on the systems that are grown under artificial, laboratory-based illumination conditions involving solubilization of these complexes out of their native membranes and assembly into non-natural environments. The present study is motivated by the observation of significant variations in the published optical absorption, fluorescence-excitation, and fluorescence spectra of LH pigment–protein complexes in principle assumed to be similar.<sup>18–23</sup> This problem is far from being new, having been raised and studied in multiple contexts in the past (e.g., see refs 23–26 and references therein). In this work, rather than trying to solve the general problem, we specifically investigate possible influences of the surrounding medium on the low temperature fluorescence and fluorescence-excitation/absorption spectra of the LH2 complexes from *Rps. acidophila* (strain 10050), a paradigmatic photosynthetic light-harvesting complex. Experiments were designed in order to assess to what extent the single-molecule spectroscopy data<sup>14,19,20,27,28</sup> are comparable with the spectral data obtained by selective spectroscopy methods on bulk samples.<sup>18,23,26,29,30</sup> Because in the bulk studies the detergent solubilized complexes are usually embedded in a glassy buffer–detergent–glycerol matrix, whereas in single-molecule experiments they are immobilized in thin polymer films, this issue directly addresses the question of whether and how the spectral observations correlate with the preparation conditions of the samples. The optical spectra of LH2 antenna complexes from *Rps. acidophila* are compared when the samples are embedded in buffer–detergent and buffer–detergent–glycerol solutions, a thin polymer film, or in a native membrane.

## 2. EXPERIMENTAL SECTION

Isolation and purification of the LH2 complexes were carried out following a standard protocol.<sup>31</sup> The highly concentrated stock solution, stored at  $-80\text{ }^{\circ}\text{C}$ , was diluted with a 20 mM Tris–HCl buffer (pH 8.0) containing 0.1% of the detergent lauryldimethyl amine oxide (LDAO) to yield the desired optical density of the bulk-buffer sample. For the preparation with glycerol, the stock solution was diluted with a buffer–glycerol mixture (1:2 volume ratio) and the concentration of LDAO was increased to 1% to maintain well-isolated complexes.<sup>32</sup> For the thin film samples, 2% polyvinyl alcohol (PVA) was added to a buffer that was diluted to an LH2 concentration of  $10^{-6}\text{ M}$ . A small drop of this solution was spin-coated onto a quartz substrate with a 10 mm diameter, giving a polymer film sample of about 100 nm thickness.<sup>33</sup> Native membranes from *Rps. acidophila* (strain 10050), stored at  $-20\text{ }^{\circ}\text{C}$ , were diluted with a 20 mM Tris–HCl buffer (pH 8.0) without detergent.

In optical experiments, a continuous wave Ti:Sapphire laser (Model 3900S, Spectra Physics) with a spectral bandwidth of  $\sim 1\text{ cm}^{-1}$  served as an excitation source. For the fluorescence-excitation spectroscopy, the fluorescence of the sample was detected with an avalanche photodiode (SPCM-AQR-16, Perkin-Elmer) after passing through the set of band-pass (BP) and long-pass (LP) filters (BP 890/20, BP 900/50, BP 935/40 and LP 885, AHF Analysetechnik). Emission spectroscopy was carried out using a spectrometer and a CCD camera,

either SpectraPro 150 (Acton Research) combined with iKon-M DU934N-BR-DD (Andor Technology) or Shamrock SR-303i (Andor Technology) and iDus DV420A-OE (Andor Technology). For fluorescence-anisotropy measurements, two high-contrast polarizers placed in front of the entrance slit of the spectrograph have been used. The first one, which was set parallel or perpendicular to the vertically polarized excitation light, served as an analyzer; the second one, which was set at  $45^{\circ}$  with respect to the polarization axis of the excitation light, served to minimize the deformation of the polarization due to the spectrograph. The detected emission was restricted to different spectral windows; that is, 880 nm–915 nm for the bulk-buffer solution, 875 nm–910 nm for the thin film sample, and 890 nm–950 nm for the natural membrane sample. The low temperature measurements were performed at 5 K or at 1.2 K using a liquid helium cryostat. For bulk-buffer samples, the quartz cuvettes with optical path lengths of 1.5 or 10 mm were used in different measurements; the PVA film samples were measured either under vacuum conditions (at room temperature) or in an inert helium environment (at low temperature). In all cases, care was taken that the optical density of the sample at the peak of the B850 absorption band did not exceed 0.1 to avoid fluorescence reabsorption effects.

The measured spectra were evaluated with standard software (OriginPro8). In both modes, fluorescence-excitation and emission spectroscopy, the standard deviation from the mean value of the spectral position of the bands did not exceed more than 0.7 nm in any series of the measurements. Similarly, the variations of the spectral bandwidths from the mean value were smaller than  $\pm 18\text{ cm}^{-1}$ .

## 3. RESULTS AND DISCUSSION

**Fluorescence–Excitation and Emission Spectra.** The room temperature fluorescence-excitation and emission spectra of the LH2 complexes from *Rps. acidophila* that either dissolved in bulk-buffer solution or bulk-buffer–glycerol solution or embedded in a thin PVA film are compared in Figure 1 with the fluorescence-excitation and emission spectra of a membrane sample from *Rps. acidophila*. The spectra from the isolated LH2 complexes show small variations with respect to each other. Though the fluorescence-excitation spectra of the two bulk-buffer samples (with and without glycerol) practically coincide, the spectrum for the PVA film sample is slightly shifted to the higher energies. The B850 band shift is approximately 1 nm and the B800 band shift is circa 3 nm with respect to the two bulk-buffer samples. The full width at half-maximum (fwhm) of the B850 band shows similar values for the bulk-buffer and the PVA film samples, whereas the B800 bandwidth is approximately 10% broader for the PVA film sample. Broadening of the B800 bandwidth of the PVA film sample is also reflected in the ratio of the B850 to B800 peak intensities, which are 1.4 for the bulk-buffer samples and 1.5 for the PVA film samples. For precise band position and bandwidth values, refer to Figure 1 and Table 1.

For reference, Figure 1 also shows the fluorescence-excitation spectrum from native membranes, complete with both LH1 and LH2 light-harvesting complexes. The absorption bands from the LH2 complexes are located at 803.2 nm (B800) and 862.8 nm (B850) and feature a peak intensity ratio of 1.4. The widths of the bands amount to  $307\text{ cm}^{-1}$  (B800) and  $413\text{ cm}^{-1}$  (B850). The refined parameters of the B850 band are evaluated via the deconvolution of the spectrum of the native membranes with the LH2 and LH1 sub-spectra in the spectral region from

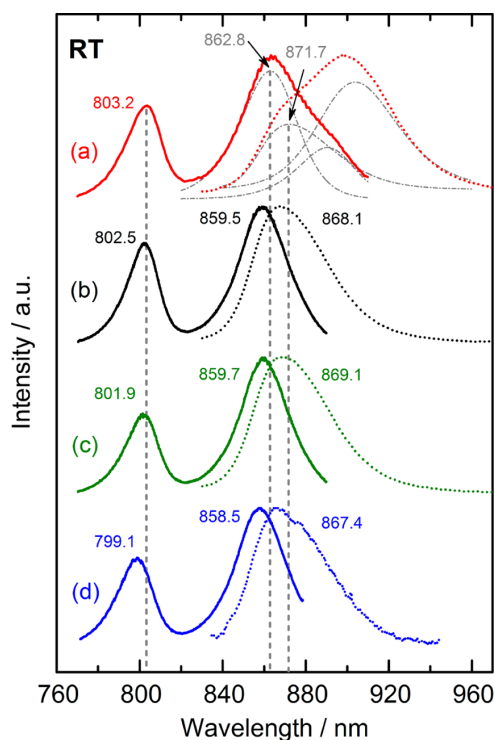


**Figure 1.** Comparison of the fluorescence-excitation (continuous line) and emission (dotted) spectra of the samples from *Rps. acidophila* taken at room temperature. (a) Fluorescence-excitation and emission spectra of native membranes in plain buffer solution, the gray dash-dotted spectra present deconvoluted LH2 and LH1 fluorescence-excitation and emission subpectra. (b) Fluorescence-excitation and emission spectra of LH2 complexes in bulk-buffer solution. (c) Fluorescence-excitation and emission spectra of LH2 complexes in bulk-buffer solution with glycerol. (d) Fluorescence-excitation and emission spectra of LH2 complexes in the PVA film. The spectra are normalized to the peak of the B850 band. The two gray vertical lines at 803.2 and 862.8 nm denote the peak positions of the fluorescence-excitation spectrum of the native membrane sample due to LH2 absorption; the third gray vertical line at 871.7 nm denotes the peak position of the evaluated LH2 emission in the native membrane sample.

820 to 910 nm. The bands of the isolated LH2 complexes are all blue-shifted (i.e., at higher energy) with respect to the spectra from the native membranes. Similar features have been observed for absorption spectra of the isolated LH2 complexes from *Rb. sphaeroides* in bulk-buffer solution in previous work.<sup>24,29,34</sup> The band shifts in the PVA film and bulk-buffer sample with (and without) glycerol relative to the native membranes are, 64  $\text{cm}^{-1}$  and 20  $\text{cm}^{-1}$  (11  $\text{cm}^{-1}$ ) for the B800 band and 58  $\text{cm}^{-1}$  and 42  $\text{cm}^{-1}$  (44  $\text{cm}^{-1}$ ) for the B850 band, respectively.

The emission spectra of isolated LH2 complexes at room temperature also show small variations as a function of the preparation method. The emission band positions deviate by less than 2 nm from each other, featuring the shortest wavelength value of 867.4 nm for the PVA film sample. The Stokes shift (i.e., the spectral interval between the peak of the B850 fluorescence-excitation band and the peak of the emission band) agrees within the experimental accuracy for all three LH2

samples and amounts to  $120 \pm 10 \text{ cm}^{-1}$ . The width of the emission band of the PVA film sample (576  $\text{cm}^{-1}$ ) is slightly broader with respect to the bulk-buffer samples (560  $\text{cm}^{-1}$  and 546  $\text{cm}^{-1}$  for the samples with and without glycerol, respectively). Comparison of the emission spectral parameters of isolated LH2 complexes with the corresponding parameters from the emission spectrum of the native membranes is more complex due to the dominant emission of the LH1 antenna. Still, a deconvolution with the LH2 and LH1 subpectra (see Figure 1) allows facilitating this comparison. The deconvoluted LH2 emission component from the native membranes appears a few nanometers toward the red compared to the isolated LH2 emission spectra, which is in accordance with the respective B850 fluorescence-excitation band red shift (see Table 1). As a consequence, the Stokes shift for the native membrane samples ( $118 \pm 16 \text{ cm}^{-1}$ ) practically coincides with the Stokes shift for the isolated LH2 samples in different environments.

The differences between the LH2 spectra as a function of the matrix material become more apparent upon cooling the samples to cryogenic temperatures. In Figure 2, the low temperature fluorescence-excitation and emission spectra of the LH2 complexes from *Rps. acidophila* dissolved in different matrixes and of native membranes are presented. The experiments were conducted at two different temperatures, 1.2 and 5 K, and yielded consistent results. Therefore, in the following, these data are commonly denoted as the low temperature data. Like at room temperature, the fluorescence-excitation spectra of LH2 complexes in the bulk-buffer sample with and without glycerol are rather similar to each other. They are also similar to the spectrum of the native membrane sample. In contrast to the band positions that vary only less than 1 nm with respect to each other, the fwhm of the bulk-buffer LH2 sample bands appear clearly narrower compared with the native membrane sample values (see Table 2). At the same time, the fluorescence-excitation spectrum of the PVA film sample differs from the spectra of the three other samples significantly. The positions (linewidths) of the B800 and the B850 bands in the spectrum of the PVA film sample are 796.9 nm (229  $\text{cm}^{-1}$ ) and 855.6 nm (276  $\text{cm}^{-1}$ ), respectively, equivalent to a blue shift of the B800 band by 94  $\text{cm}^{-1}$  and the B850 band by 189  $\text{cm}^{-1}$  with respect to the bands from the native membranes. The variations in the B850/B800 intensity ratio are also detectable depending on the sample environment. The peak intensity ratios are 1.3 for both bulk-buffer LH2 samples, 1.6 for the PVA film sample, and 1.5 for the native membrane sample.

The low temperature emission spectra of LH2 complexes in the different matrixes behave similarly to the fluorescence-excitation spectra. The emission band position of the bulk-buffer sample with glycerol is located at 889.8 nm, and for the bulk-buffer sample without glycerol, it lies at 889.0 nm. The bandwidths for both samples practically coincide at about 240  $\text{cm}^{-1}$ . In contrast, the emission spectrum of the PVA film sample is significantly shifted to higher energies and peaks at 875.6 nm. This corresponds to the spectral blue shift by 182  $\text{cm}^{-1}$  with respect to the bulk-buffer sample with glycerol. The fwhm of the PVA film sample emission band is 311  $\text{cm}^{-1}$ , showing an  $\sim 30\%$  broadening compared to the bulk-buffer sample values. Despite these shifts of the excitation and emission spectra of the samples in different matrixes, the Stokes shifts observed are similar and vary only from 261  $\text{cm}^{-1}$  for the bulk-buffer-glycerol sample to 267  $\text{cm}^{-1}$  for the PVA film sample. We note that the Stokes shifts in the low temperature

**Table 1. Spectral Positions, Linewidths, and Shifts (Mean Value  $\pm$  Standard Deviation) of the B800 Band, B850 Band, and the Emission of Native Membranes and Isolated LH2 from *Rps. acidophila* Embedded in Various Matrix Materials and Studied at Room Temperature<sup>a</sup>**

sample	native membranes	LH2:bulk-buffer solution	LH2:bulk-buffer solution with glycerol	LH2:PVA film	
fluorescence-excitation B800	spectral position (nm)	803.2 $\pm$ 0.2	802.5 $\pm$ 0.1	801.9 $\pm$ 0.1	799.1 $\pm$ 0.7
	relative spectral shift (cm <sup>-1</sup> )	0	11 $\pm$ 5	20 $\pm$ 5	64 $\pm$ 14
	width (cm <sup>-1</sup> )	307 $\pm$ 6	283 $\pm$ 5	306 $\pm$ 5	329 $\pm$ 10
fluorescence-excitation B850	spectral position (nm)	863.2 $\pm$ 0.5	859.5 $\pm$ 0.6	859.7 $\pm$ 0.1	858.5 $\pm$ 0.6
	relative spectral shift (cm <sup>-1</sup> )	0	44 $\pm$ 15	42 $\pm$ 8	58 $\pm$ 15
	width (cm <sup>-1</sup> )	535 $\pm$ 13	380 $\pm$ 5	380 $\pm$ 5	386 $\pm$ 13
	413 $\pm$ 18 <sup>b</sup>				
B800–B850 energy gap (cm <sup>-1</sup> )	860 $\pm$ 10	826 $\pm$ 10	838 $\pm$ 3	866 $\pm$ 19	
emission	spectral position (nm)	898.5 $\pm$ 0.3	868.1 $\pm$ 0.1	869.1 $\pm$ 0.3	867.4 $\pm$ 0.4
	relative spectral shift (cm <sup>-1</sup> )	0	48 $\pm$ 18	34 $\pm$ 13	57 $\pm$ 15
	width (cm <sup>-1</sup> )	554 $\pm$ 16 <sup>b</sup>	546 $\pm$ 7	560 $\pm$ 4	576 $\pm$ 9
	Stokes shift (cm <sup>-1</sup> )	118 $\pm$ 16	115 $\pm$ 9	126 $\pm$ 5	120 $\pm$ 13

<sup>a</sup>The spectral shifts of the bands are given relative to the spectral position of the respective band in the native membrane. In the lowest line, the Stokes shift is given. <sup>b</sup>Evaluated spectral parameters for LH2 antenna.

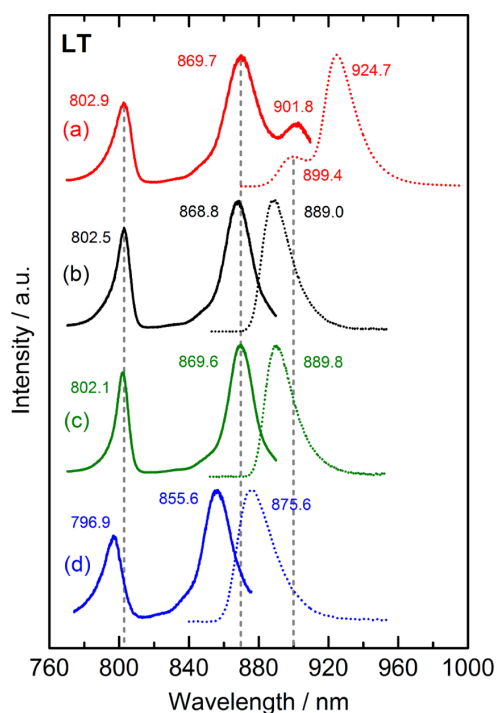


**Figure 2.** Comparison of the fluorescence-excitation (continuous line) and emission (dotted) spectra of the samples from *Rps. acidophila* taken at low temperature. (a) Fluorescence-excitation and emission spectra of native membranes in plain buffer solution. (b) Fluorescence-excitation and emission spectra of LH2 complexes in bulk-buffer solution. (c) Fluorescence-excitation and emission spectra of LH2 complexes in bulk-buffer solution with glycerol. (d) Fluorescence-excitation and emission spectra of LH2 complexes in PVA film. The spectra are normalized to the peak of the B850 band. The gray vertical lines denote the peak positions in the native membrane sample corresponding to the absorption in the B800 and B850 rings of LH2 (at 802.9 and 869.7 nm, respectively) and to the B850 fluorescence emission (899.4 nm).

spectra have increased by more than a factor of 2 with respect to the room temperature spectra.

At low temperatures, the comparison of the emission characteristics of isolated LH2 samples with those of the native membranes is not useful because, due to the energy transfer in the membranes, the fluorescence is mostly emitted from the lowest-energy LH1 antenna complexes, effectively shifting the emission band circa 30–35 nm to the longer wavelengths. The well-detected signal peaking at 899.4 nm in the emission spectrum of the native membranes (see Figure 2 as well as the inset of Figure 3b) is obviously related to the LH2 antenna pools that are energetically poorly contacted with the core antennas.<sup>29,35–39</sup>

The general findings of these measurements for the LH2 samples in different environments can be summarized as follows. At room temperature, the B850 band in the fluorescence-excitation spectrum from the bulk-buffer and PVA film samples feature about the same peak positions. Upon cooling to cryogenic temperatures, one observes a strong red shift of the B850 band for the bulk-buffer samples (for samples with glycerol, from 859.7 to 869.6 nm, corresponding to  $-132$  cm<sup>-1</sup>) and a slight blue shift of this band for PVA film sample (from 858.5 to 855.6 nm, corresponding to  $+39$  cm<sup>-1</sup>). Qualitatively similar behavior is found for the B800 band, yet the spectral red shift for the bulk-buffer samples is only a few wavenumbers, whereas the band for the PVA film sample blue shifts by 35 cm<sup>-1</sup>, similar to the spectral shift of the B850 band for the same sample. Peaks of the B850 and B800 bands in bulk-buffer samples almost coincide with those in native membranes at room and low temperatures. The spectral positions of the emission peaks of the LH2 samples in different matrices at room temperature have rather similar values. At low temperature, all the emission spectra feature an essential red shift; for the bulk-buffer samples, it amounts to  $-268$  cm<sup>-1</sup> (peaking at 889.8 nm), and for PVA samples, it is  $-108$  cm<sup>-1</sup> (peaking at 875.6 nm). Despite these different shifts of the emission spectra for the bulk-buffer and PVA samples, the Stokes shifts between their B850 excitation and emission spectra are similar, being 261 cm<sup>-1</sup> for the bulk-buffer sample and 267 cm<sup>-1</sup> for the PVA sample.

**Table 2.** Spectral positions, linewidths, and shifts (mean value  $\pm$  standard deviation) of the B800 band, B850 band and the emission of native membranes and isolated LH2 from *Rps. acidophila* embedded in various matrix materials and studied at low temperature.<sup>a</sup>

sample	native membranes	LH2:bulk-buffer solution	LH2:bulk-buffer solution with glycerol	LH2:PVA film	
fluorescence-excitation B800	spectral position (nm)	802.9 $\pm$ 0.4	802.5 $\pm$ 0.3	802.1 $\pm$ 0.1	796.9 $\pm$ 0.2
	relative spectral shift (cm <sup>-1</sup> )	0	6 $\pm$ 11	12 $\pm$ 8	94 $\pm$ 9
	width (cm <sup>-1</sup> )	197 $\pm$ 10	156 $\pm$ 10	134 $\pm$ 6	229 $\pm$ 13
fluorescence-excitation B850	spectral position (nm)	869.7 $\pm$ 0.5	868.8 $\pm$ 0.6	869.6 $\pm$ 0.1	855.6 $\pm$ 0.4
	relative spectral shift (cm <sup>-1</sup> )	0	12 $\pm$ 15	1 $\pm$ 8	189 $\pm$ 12
	width (cm <sup>-1</sup> )	310 $\pm$ 15 <sup>b</sup>	248 $\pm$ 4	226 $\pm$ 5	276 $\pm$ 9
B800–B850 energy gap (cm <sup>-1</sup> )	957 $\pm$ 13	936 $\pm$ 6	968 $\pm$ 3	861 $\pm$ 9	
emission	spectral position (nm)	924.7 $\pm$ 0.4	889.0 $\pm$ 0.4	889.8 $\pm$ 0.3	875.6 $\pm$ 0.7
		899.4 $\pm$ 0.4 <sup>c</sup>			
	relative spectral shift (cm <sup>-1</sup> )	0	130 $\pm$ 10	119 $\pm$ 9	302 $\pm$ 14
	width (cm <sup>-1</sup> )	250 $\pm$ 9	246 $\pm$ 8	242 $\pm$ 7	311 $\pm$ 11
Stokes shift (cm <sup>-1</sup> )	232 $\pm$ 18 <sup>c</sup>	380 $\pm$ 12	262 $\pm$ 13	261 $\pm$ 5	267 $\pm$ 15

<sup>a</sup>The spectral shifts of the bands are given relative to the spectral position of the respective band in the native membrane. In the lowest line, the Stokes shift is given. <sup>b</sup>Additionally broadened due to contribution from LH1 absorption. <sup>c</sup>Evaluated spectral parameters for LH2 antenna.

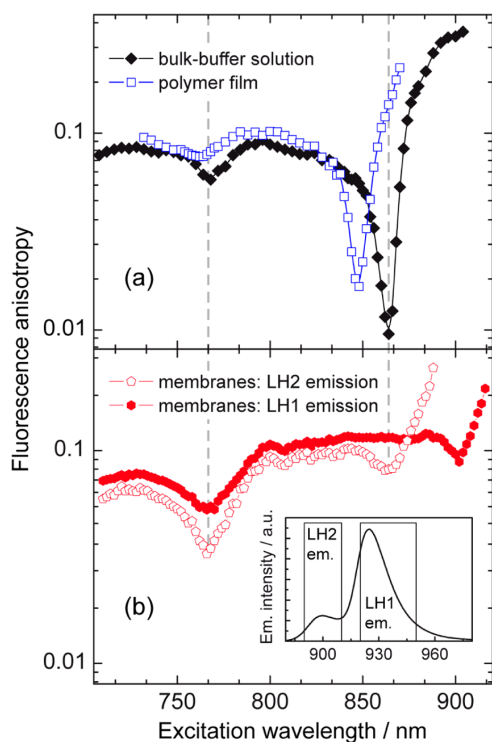


**Figure 3.** Fluorescence-anisotropy excitation spectra from *Rps. acidophila* recorded at 5 K. (a) Isolated LH2 complexes in bulk-buffer–glycerol solution (black filled diamonds) and isolated LH2 complexes in a PVA film (open blue squares). (b) Native membranes in bulk-buffer solution. Emission was recorded between 890 and 910 nm (the LH2 emission range, open red dots) or between 920 and 950 nm (the LH1 emission range, filled red dots), as shown in the inset. The gray vertical lines at 766.7 and 863.9 nm denote the minima found in the native membrane sample when recording in the LH2 emission range.

**Fluorescence-Anisotropy Excitation Spectra.** The main differences in the absorption band positions of the BChl *a*

molecules that are organized in the B800 ring and those organized in the B850 ring stem from the strong ( $\sim 300$ – $400$  cm<sup>-1</sup>) resonant coupling between the transition-dipole moments of the closely packed B850 BChl *a* molecules.<sup>5,18,40</sup> For the B800 molecules, the pigment–pigment interactions are in the order of 20–30 cm<sup>-1</sup>.<sup>5,27,40–42</sup> Disregarding these relatively weak interactions, the spectral position of the B800 band is mainly determined by the site energies of the pigments. In contrast, in the B850 assembly, the much stronger intermolecular interactions lead to the formation of exciton states.<sup>6,11,43–47</sup> In the simplest approximation, neglecting both the dimerization in the B850 ring and diagonal/off-diagonal disorder, the excited-state manifold for the C<sub>18</sub>-symmetric assembly of the pigments features two nondegenerate (denoted as  $k = 0$  and  $k = 9$ ) and eight pairwise degenerate ( $k = \pm 1, k = \pm 2, \dots, k = \pm 8$ ) exciton states. Due to the circular arrangement of the pigments, only the exciton states  $k = 0, k = \pm 1, k = \pm 8,$  and  $k = 9$  can be optically excited. Because the transition-dipole moments of the individual B850 pigments are oriented mainly in the plane of the ring, only a little of the total oscillator strength is associated with the nondegenerate exciton states  $k = 0$  and  $k = 9$ . Given the head-to-tail arrangement of the transition–dipole moments of adjacent B850 BChl *a* molecules, nearly all of the oscillator strength is concentrated in the  $k = \pm 1$  exciton states, which is reflected in a strong electronic transition seen as the main absorption band at about 850 nm. The upper exciton components,  $k = \pm 8$ , carry less than 3% of the total oscillator strength<sup>5,48</sup> and give rise to very weak absorptions in the spectral range around 750–780 nm,<sup>18,49,50</sup> depending on the bacterial species.

It is worth noting that in the systems with strong excitonic coupling, an additional contribution that determines the exact spectral position of an absorption band is given by the displacement energy. This accounts for the difference of the Coulomb interaction between neighboring pigments in the electronically excited state and in the ground state.<sup>51</sup> An ab initio estimation of the displacement energy for multi-chromophore systems is still a demanding theoretical task. From these considerations, it is clear that changes of the spectral position of the B800 band reflect, in the first approximation, only interactions that affect the chromophore

site energies, whereas the origin for changes of the spectral position of the B850 band is more complex and reflects contributions from interactions that affect both the site energies and their excitonic interactions.

In order to separate the various contributions to the spectral changes in the B850 band, it would be very helpful to have information about the B850 exciton bandwidth as a function of the sample. Generally, this could be obtained from the spectral signatures of the  $k = \pm 1$  and  $k = \pm 8$  exciton states, which can be considered as markers for the width of the exciton band. However, as pointed out above, the total oscillator strength of the  $k = \pm 8$  states is low and their weak absorption is buried under the much stronger absorption tail of the B800 molecules. As shown in ref 49, this obstruction can be overcome by exploiting polarization-resolved fluorescence-excitation spectroscopy. The fluorescence-anisotropy,  $r$ , is defined as  $r = (I_{\text{VV}} - I_{\text{Vh}})/(I_{\text{VV}} + 2I_{\text{Vh}})$ , where  $I_{\text{VV}}$  and  $I_{\text{Vh}}$  are the emission intensities that are polarized parallel (vv) and perpendicular (vh) with respect to the orientation of the electric field vector of the linearly polarized excitation light, respectively. Because the transition-dipole moments within the degenerate pairs  $k = \pm 1$  and  $k = \pm 8$  are mutually orthogonal, there exists an energy for each pair of states where the exciton states with mutually perpendicular oriented transition-dipole moments can be excited with equal probability. Hence, the fluorescence-anisotropy will feature a minimum at those energies, effectively designating the spectral position of the respective pair of exciton states.<sup>49,52</sup>

The fluorescence-anisotropy excitation spectra of the LH2 complexes from *Rps. acidophila* in PVA film and bulk-buffer environments with glycerol are compared in Figure 3a. The spectrum of the bulk-buffer sample without glycerol practically overlaps with the latter spectrum, and for clarity, it is not presented in the figure. For both PVA and bulk-buffer samples, the anisotropy is low, between 0.06 and 0.10, at short wavelengths, rising toward the theoretical limiting value of 0.4 across the B850 band. The most striking features of the anisotropy curves are the two distinct minima at low and high energies that are assigned to the edges of the B850 exciton state manifold.<sup>18,49,50</sup> The separations of the anisotropy minima are 1450  $\text{cm}^{-1}$  (1461  $\text{cm}^{-1}$ ) for the bulk-buffer sample with (and without) glycerol and 1332  $\text{cm}^{-1}$  for the PVA film sample (see Table 3). The data for the bulk-buffer samples coincide within

**Table 3. Bandwidths (Mean Value  $\pm$  Standard Deviation) in Wavenumbers of the B850 Excitons in the LH2 Complexes of *Rps. acidophila* Embedded into Various Matrix Materials and Studied at 5 K.<sup>a</sup>**

sample	native membranes	LH2:bulk-buffer solution	LH2:bulk-buffer-glycerol solution	LH2:PVA film
bandwidth ( $\text{cm}^{-1}$ )	1468 $\pm$ 18	1461 $\pm$ 24	1450 $\pm$ 24	1332 $\pm$ 24

<sup>a</sup>Evaluated as the energy gap between the two minima in the fluorescence-anisotropy excitation spectrum (see ref 55).

the experimental uncertainty with the respective values determined.<sup>18,50</sup> The exciton bandwidth in the PVA film sample is thus significantly narrowed (by 120–130  $\text{cm}^{-1}$ ) compared with the width in bulk-buffer samples. Moreover, the whole fluorescence-anisotropy excitation spectrum of the PVA film is shifted to the blue with respect to the bulk-buffer spectra.

The shift is asymmetric, being circa 16 nm ( $\sim 220 \text{ cm}^{-1}$ ) at low energies and circa 6 nm ( $\sim 98 \text{ cm}^{-1}$ ) at high energies.

In the one-dimensional molecular arrays, the width of the exciton band,  $\delta E$ , can be approximated by the nearest-neighbor interaction energy,  $V$ , as  $\delta E \approx 4V$ .<sup>51</sup> Hence, taking the separation of the minima in the anisotropy spectra as a measure of  $\delta E$ , average intermolecular coupling energies between the B850 BChl *a* molecules in the bulk-buffer sample and in the PVA film can be deduced as 365  $\text{cm}^{-1}$  and 333  $\text{cm}^{-1}$ , respectively. A more thorough modeling based on crystallographic structural data and taking into account both static and dynamic disorders in the bulk-buffer sample with added glycerol has resulted in values of  $V$  between 370  $\text{cm}^{-1}$  and 390  $\text{cm}^{-1}$ .<sup>18,50</sup>

Figure 3b displays the fluorescence-anisotropy excitation spectra for the native membrane samples. In order to distinguish the contributions from LH2 and LH1, the detection was restricted either to the spectral range from 890 to 910 nm or to the range from 920 to 950 nm. As indicated in the inset of Figure 3b, these ranges correspond to the spectral regions of predominant emission from the LH2 or LH1 complexes. The separation of the anisotropy minima recorded in the LH2 emission range is 1468  $\text{cm}^{-1}$ , which is consistent with the values measured for LH2 in bulk-buffer samples (see Table 3). In the LH1 emission range the separation of the anisotropy minima is much larger and amounts to 1951  $\text{cm}^{-1}$ , which is in close agreement with the value of 1969  $\text{cm}^{-1}$  obtained in ref 39. The exciton bandwidths of core complexes from different photosynthetic bacterial species appear to be similar. For example, the bandwidth 1978  $\text{cm}^{-1}$  has been found for the RC-LH1 complexes in bulk-buffer-glycerol solution of mutant membranes of *Rhodobacter (Rb.) sphaeroides*<sup>53</sup> that only contain core complexes. Also, in both *Rps. acidophila* and *Rb. sphaeroides* species, the high energy minima for the B850 and B875 exciton state manifolds overlap almost perfectly, meaning that the broader B875 exciton band totally embraces the narrower B850 one. Presumably, the good resonance between the electronically excited states is advantageous for efficient B850  $\rightarrow$  B875 energy transfer.<sup>39</sup>

**Stokes Shift between the Fluorescence-Excitation and Emission Spectra.** Above, it was shown that at low temperature, the exciton bandwidth of the LH2 complexes in PVA film is circa 9% narrower than in the bulk-buffer environment. It is reasonable to assume that energetic distances between different exciton levels are as well compressed in PVA sample compared to the bulk-buffer sample. The energy gap between the  $k = 0$  and  $k = \pm 1$  exciton states, which largely determines the Stokes shift of the spectra, is estimated to be 203  $\text{cm}^{-1}$  in the bulk-buffer sample of isolated LH2 complexes.<sup>23</sup> Accordingly, in the PVA environment this value should be  $\sim 185 \text{ cm}^{-1}$ . At the same time, the measured Stokes shift for the PVA sample (267  $\text{cm}^{-1}$ ) is a few  $\text{cm}^{-1}$  larger than that for the bulk-buffer sample (262  $\text{cm}^{-1}$ ). From the first glance, these data are inconsistent with each other, and one option to explain this discrepancy might be that the electron-phonon coupling strength in the PVA matrix is larger with respect to the bulk-buffer samples. In refs 29 and 30, the homogeneous lineshapes and the exciton-phonon coupling strengths as defined by the Huang-Rhys factors were determined for the isolated LH2 complexes from *Rb. sphaeroides* in bulk-buffer environment. It was shown that not only the homogeneous line shape and the exciton-phonon coupling strength but also the emission oscillator strength

depend on the spectral position.<sup>54</sup> Particularly, one of the important parameters of the homogeneous spectrum, the fwhm of the phonon sideband, changes from  $160\text{ cm}^{-1}$  at the center of the inhomogeneous distribution function (IDF) to the  $260\text{ cm}^{-1}$  at the red tail of the IDF. Hence, the Huang–Rhys factor increases from 2.0 to 3.1. For the LH2 complexes of *Rps. acidophila* in the PVA environment, comparable data are available from single molecule experiments.<sup>28</sup> In the single molecule spectra, the fwhm values range from  $160\text{ cm}^{-1}$  to  $280\text{ cm}^{-1}$  in the same IDF region. These numbers are close to the phonon sideband fwhm data from *Rb. sphaeroides* in bulk-buffer environment, practically excluding the option of a significantly larger electron–phonon coupling in the PVA samples.

In looking for another possibility to explain the above disagreement, it is instructive to note from Table 2 that at low temperatures, the B800 and B850 bands in the fluorescence-excitation spectra are much broader in the PVA matrix with respect to the spectra in bulk-buffer samples; the emission spectrum follows a similar trend. In Gaussian approximation for the band shapes, one can estimate an extra inhomogeneous broadening of the B800 absorption band in PVA relative to that in bulk-buffer solution as:  $(229^2 - 156^2)^{1/2}\text{ cm}^{-1} \approx 168\text{ cm}^{-1}$ . This is a considerable broadening, which, along with the rising oscillator strength toward the red edge of the IDF, readily explains the apparent increase of the Stokes shift between the fluorescence-excitation and emission spectra.

**Comparison of the B850 Excitons in the LH2 Complexes Embedded into Native Membrane or into Spin-Coated Polymer Film at Low Temperatures.** As we have shown, the fluorescence-excitation spectra of LH2 complexes in bulk-buffer solution and in native membranes are conserved within the experimental uncertainty. In contrast, the spectrum of the PVA film manifest significant blue shift, its B800 component shifting by  $94\text{ cm}^{-1}$  and the B850 component by  $189\text{ cm}^{-1}$ . The shifts are accompanied by narrowing of the B850 exciton state manifold as shown in Table 3. We have applied a simple model to evaluate the energetic parameters that are responsible for these spectral modifications.

As implied already above, the exciton Hamiltonian written down in matrix form includes diagonal and nondiagonal elements. The diagonal terms of the matrix correspond to the energies of uncoupled molecules, termed above as site energies. The site energies contains not only the electronic transition energy of the free molecule in vacuum but also the solvent shift caused by the interactions of the molecule with its local surroundings, which has a random component due to the static or dynamic fluctuations of the environment.<sup>45</sup> Ignoring for the moment differences in the exposure to the solvent and the different ligation of the B800 and B850 pigments, as well as the weak excitonic couplings between the B800 molecules, we use the peak position of the B800 fluorescence-excitation band in a specific solvent as the mean site energy for all the 27 pigment molecules in the LH2 protein dissolved in that solvent. Similarly, the width of the B800 band is a measure for the random fluctuations thereof. Under these approximations, the  $94\text{ cm}^{-1}$  relative shift found for the B800 absorption band between the native membranes and the PVA film samples is assigned to the relative shift between the site energies of the pigments in the B850 assembly. This implies that about half the overall  $189\text{ cm}^{-1}$  relative shift between the B850 fluorescence-excitation bands is attributed to interactions that affect site energies of all the pigments in LH2. Another component that contributes to the relative shift is the exciton bandwidth, which

is narrower in the PVA film. Once again, roughly half of the experimentally determined difference between the exciton bandwidths in native membranes and PVA matrix (i.e.,  $1/2 \times (1468 - 1332)\text{ cm}^{-1} = 68\text{ cm}^{-1}$ ) contributes into the relative shift of the B850 bands. The fraction is left over from the overall relative shift amounts  $(189 - 94 - 68)\text{ cm}^{-1} \approx 27\text{ cm}^{-1}$  and can be associated with the change in the displacement energy for the B850 molecules.

On the basis of the simplified model given above, it is possible to give an estimate for the absolute values of the displacement energies. The energy gap between the spectral positions of the B800 and B850 absorption bands can be regarded as the sum of two components: the half value of the B850 exciton bandwidth and the displacement energy value of the B850 excitons. An evaluation of the absolute values of the displacement energies results in  $\sim 223\text{ cm}^{-1}$  and  $\sim 195\text{ cm}^{-1}$  for the native membranes and the PVA samples, respectively. These numbers are fairly small, less than the exciton coupling energies.

A blue shift of the B850 excitonic absorption band that follows a transfer of the LH2 complex from a native membrane into a spin-coated polymer film at low temperatures can thus be disentangled into three parts: 50% due to an increase of the local site energies, 36% due to a contraction of the exciton band, and 14% due to a decrease of the displacement energy. The provided interpretation, although rather speculative in terms of specific numbers due to multiple assumptions involved, for the first time allows a hint toward the significance of various energetic components (and related physical mechanisms), including the displacement energy, in spectral tuning of the photosynthetic LH complexes with strong exciton coupling between the chromophores.

The systematic decrease observed for the nearest neighbor exciton coupling energy,  $V \approx \delta E/4$ , in the B850 system from  $\sim 367\text{ cm}^{-1}$  in the native membrane over  $\sim 363\text{ cm}^{-1}$  in the bulk-buffer–glycerol solution to  $\sim 333\text{ cm}^{-1}$  in the polymer film as calculated from the data in Table 3 (see also ref 18), points toward a looser packing (and thus weaker coupling) of the B850 BChl *a* molecules in the detergent-isolated LH2 complexes in comparison with the situation where the proteins are spontaneously assembled into the native membrane. It also appears that the specific bulk solvent where the detergent-isolated LH2 complexes are hosted plays some role in stabilizing the light-harvesting proteins, despite the detergent micelle tightly covering the hydrophobic parts of the membrane protein. From all the studied environments the LH2 spectra are most changed (in terms of the extent of the blue shift and broadening of the bands) in the PVA matrix.

An extra red shift of the exciton absorption bands (such as the B850 band in LH2 and the B875 band in LH1 complexes) relative to the absorption bands of localized excitations (B800/monomeric BChl *a*) upon application of hydrostatic external pressure due to increased exciton coupling has been observed.<sup>55–60</sup> Pressure-induced red shifts of the B850 band from *Rps. acidophila* (strain 10050) of about  $-760\text{ cm}^{-1}/\text{GPa}$  have been recorded at room temperature up to the pressures of  $0.6\text{ GPa}$ .<sup>58,59</sup> The corresponding shift rate at low temperature is approximately half the size:  $-398\text{ cm}^{-1}/\text{GPa}$ .<sup>56</sup> If we associate the blue shift observed in the PVA matrix with a decrease of the local pressure within the protein, a blue shift of  $189\text{ cm}^{-1}$  observed at low temperature corresponds to a pressure change of almost  $0.5\text{ GPa}$ . From the compressibility data as a function of temperature,<sup>57,61–64</sup> it can be estimated that pressures of  $0.5$

GPa may result in the B850 interpigment distance changes in the order of 0.1 Å. Changes on this length scale are small with respect to the overall structure of the assembly of the B850 molecules yet large enough to influence the molecular interactions to show up in the optical spectra. A negative thermal expansion observed in polymer films upon cooling below the glass transition temperature as reported in ref 65 supports the assumption made above, that the LH2 complexes embedded in the PVA film might sense a higher conformational freedom, which in turn points toward a looser packing of the B850 pigments. Furthermore, this might also explain the broadening of the spectral lineshapes of the LH2 complexes embedded in the PVA film compared to those observed in the bulk-buffer environment.

#### 4. SUMMARY

This work was set out to unify a body of conflicting data obtained by single-molecule spectroscopy and by more traditional spectroscopic methods. The data presented here show how (see Table 2) and why the details of the optical spectra of LH2 complexes (i.e., the exact spectral positions and widths of the absorption and emission bands) vary as a function of the environment in which the sample is housed. As an example, in the LH2 complexes from *Rps. acidophila* (strain 10050), changing the matrix from bulk-buffer solution to thin films of PVA leads to a 189 cm<sup>-1</sup> blue shift of the B850 exciton absorption band at low temperature. Taking into account a simultaneous increase of the B800 site energies by 94 cm<sup>-1</sup>, the blue shift of the B850 band could be disentangled into three parts: because of the increase of the B850 local site energies, the contraction of the B850 exciton band, and the decrease of the respective displacement energy. The differences of the LH2 exciton due to different sample preparations discovered in this study might help to ease the comparison of results stemming from the single-molecule research area with respect to those coming from the ensemble domain.

#### AUTHOR INFORMATION

##### Corresponding Author

\*A. Freiberg. Phone: +372 5645 3175. Fax: +372 7383 033. E-mail: arvi.freiberg@ut.ee.

##### Notes

The authors declare no competing financial interest.

#### ACKNOWLEDGMENTS

We gratefully acknowledge financial support from the Deutsche Forschungsgemeinschaft (KO 1359/16-1, GZ: 436 EST 113/4/0-1 and the GRK1640) and the BBSRC. K.T. and A.F. also acknowledge partial support from the Estonian Research Council (Grant IUT02-28).

#### ABBREVIATIONS

BChl: bacteriochlorophyll; LH1: light-harvesting 1 (complex); LH2: light-harvesting 2 (complex); IDF: inhomogeneous distribution function; fwhm: full width at half-maximum.

#### REFERENCES

- (1) Milo, R. What Governs the Reaction Center Excitation Wavelength of Photosystems I and II? *Photosynth. Res.* **2009**, *101*, 59–67.
- (2) Blankenship, R. E. *Anoxygenic Photosynthetic Bacteria*; Blankenship, R. E.; Madigan, M. T.; Bauer, C. E., Eds.; Kluwer Academic Publishers: Dordrecht, The Netherlands, 1995.

- (3) Duysens, L. N. M. *Transfer of Excitation Energy in Photosynthesis*; Utrecht: The Netherlands, 1952.
- (4) Freiberg, A. Coupling of Antennas to Reaction Centers. In *Anoxygenic Photosynthetic Bacteria*; Blankenship, R. E., Madigan, M. T., Bauer, C. E., Eds.; Kluwer Academic Publishers: Dordrecht, The Netherlands, 1995; Vol.2, pp 385–398.
- (5) Cogdell, R. J.; Gall, A.; Köhler, J. The Architecture and Function of Purple Bacteria: from Single Molecules to *in vivo* Membranes. *Q. Rev. Biophys.* **2006**, *39*, 227–324.
- (6) Hu, X.; Ritz, T.; Damjanovic, A.; Autenrieth, F.; Schulten, K. Photosynthetic Apparatus of Purple Bacteria. *Q. Rev. Biophys.* **2002**, *35*, 1–62.
- (7) Cogdell, R. J.; Köhler, J. Use of Single-Molecule Spectroscopy to Tackle Fundamental Problems in Biochemistry: Using Studies on Purple Bacterial Antenna Complexes as an Example. *Biochem. J.* **2009**, *422*, 193–205.
- (8) Scheuring, S. AFM Studies of the Supramolecular Assembly of Bacterial Photosynthetic Core-Complexes. *Curr. Opin. Chem. Biol.* **2006**, *10*, 387–393.
- (9) Bahatyrova, S.; Frese, R. N.; van der Werf, K. O.; Otto, C.; Hunter, C. N.; Olsen, J. D. Flexibility and Size Heterogeneity of the LH1 Light Harvesting Complex Revealed by Atomic Force Microscopy - Functional Significance for Bacterial Photosynthesis. *J. Biol. Chem.* **2004**, *279*, 21327–21333.
- (10) McDermott, G.; Prince, S. M.; Freer, A. A.; Hawthornthwaite-Lawless, A. M.; Papiz, M. Z.; Cogdell, R. J.; Isaacs, N. W. Crystal Structure of an Integral Membrane Light-Harvesting Complex from Photosynthetic Bacteria. *Nature* **1995**, *374*, 517–521.
- (11) van Amerongen, H.; Valkunas, L.; van Grondelle, R. *Photosynthetic Excitons*; World Scientific: Singapore, 2000.
- (12) McLuskey, K.; Prince, S. M.; Cogdell, R. J.; Isaacs, N. W. The Crystallographic Structure of the B800–820 LH3 Light-Harvesting Complex From the Purple Bacteria *Rhodospseudomonas acidophila* Strain 7050. *Biochemistry* **2001**, *40*, 8783–8789.
- (13) Ketelaars, M.; Segura, J. M.; Oellerich, S.; de Ruijter, W. P. F.; Magis, G.; Aartsma, T. J.; Matsushita, M.; Schmidt, J.; Cogdell, R. J.; Köhler, J. Probing the Electronic Structure and Conformational Flexibility of Individual Light-Harvesting 3 Complexes by Optical Single-Molecule Spectroscopy. *J. Phys. Chem. B* **2006**, *110*, 18710–18717.
- (14) de Ruijter, W. P. F.; Segura, J. M.; Cogdell, R. J.; Gardiner, A. T.; Oellerich, S.; Aartsma, T. J. Fluorescence-Emission Spectroscopy of Individual LH2 and LH3 Complexes. *Chem. Phys.* **2007**, *341*, 320–325.
- (15) Brotsudarmo, T. H. P.; Kunz, R.; Böhm, P.; Gardiner, A. T.; Moulisová, V.; Cogdell, R. J.; Köhler, J. Single-Molecule Spectroscopy Reveals that Individual Low-Light LH2 Complexes from *Rhodospseudomonas palustris* 2.1.6. Have a Heterogeneous Polypeptide Composition. *Biophys. J.* **2009**, *97*, 1491–1500.
- (16) Mascle-Allemand, C.; Duquesne, K.; Lebrun, R.; Scheuring, S.; Sturgis, J. N. Antenna Mixing in Photosynthetic Membranes from *Phaeospirillum molischianum*. *Proc. Natl. Acad. Sci. U. S. A.* **2010**, *107*, 5357–5362.
- (17) Ma, Y.-Z.; Cogdell, R. J.; Gillbro, T. Femtosecond Energy Transfer Dynamics between Bacteriochlorophylls in the B800–820 Antenna Complex of the Photosynthetic Purple Bacterium *Rhodospseudomonas acidophila* (Strain 7750). *J. Phys. Chem. B* **1998**, *102*, 881–887.
- (18) Freiberg, A.; Timpmann, K.; Trinkunas, G. Spectral Fine-Tuning in Excitonically Coupled Cyclic Photosynthetic Antennas. *Chem. Phys. Lett.* **2010**, *500*, 111–115.
- (19) van Oijen, A. M.; Ketelaars, M.; Köhler, J.; Aartsma, T. J.; Schmidt, J. Unraveling the Electronic Structure of Individual Photosynthetic Pigment-Protein Complexes. *Science* **1999**, *285*, 400–402.
- (20) Ketelaars, M.; van Oijen, A. M.; Matsushita, M.; Köhler, J.; Schmidt, J.; Aartsma, T. J. Spectroscopy of the B850 Band of Individual Light-Harvesting 2 Complexes of *Rhodospseudomonas*

- acidophila*: I. Experiments and Monte-Carlo Simulations. *Biophys. J.* **2001**, *80*, 1591–1603.
- (21) Gerken, U.; Redzko, F.; Götze, B.; Branschädel, M.; Tietz, C.; Ghosh, R.; Wrachtrup, J. Membrane Environment Reduces the Accessible Conformational Space Available to an Integral Membrane Protein. *J. Phys. Chem. B* **2003**, *107*, 338–343.
- (22) Ketelaars, M.; Hofmann, C.; Köhler, J.; Howard, T. D.; Cogdell, R. J.; Schmidt, J.; Aartsma, T. J. Spectroscopy on Individual Light-Harvesting 1 Complexes of *Rhodospseudomonas acidophila*. *Biophys. J.* **2002**, *83*, 1701–1715.
- (23) Wu, H.-M.; Reddy, N. R. S.; Small, G. J. Direct Observation and Hole Burning of the Lowest Exciton Level (B870) of the LH2 Antenna Complex of *Rhodospseudomonas acidophila* (Strain 10050). *J. Phys. Chem. B* **1997**, *101*, 651–656.
- (24) Hunter, C. N. Genetic Manipulations of the Antenna Complexes of Purple Bacteria. In *Anoxygenic Photosynthetic Bacteria*; Blankenship, R. E., Madigan, M. T., Bauer, C. E., Eds.; Kluwer Academic Publishers: Dordrecht, The Netherlands, 1995; Vol.2, pp 473–501.
- (25) Hussels, M.; Brecht, M. Effect of Glycerol and PVA on the Conformation of Photosystem I. *Biochemistry* **2011**, *50*, 3628–3637.
- (26) Zerlauskienė, O.; Trinkunas, G.; Gall, A.; Robert, B.; Urbonienė, V.; Valkunas, L. Static and Dynamic Protein Impact on Electronic Properties of Light-Harvesting Complex LH2. *J. Phys. Chem. B* **2008**, *112*, 15883–15892.
- (27) Hofmann, C.; Ketelaars, M.; Matsushita, M.; Michel, H.; Aartsma, T. J.; Köhler, J. Single-Molecule Study of the Electronic Couplings in a Circular Array of Molecules: Light-Harvesting-2 Complex from *Rhodospirillum molischianum*. *Phys. Rev. Lett.* **2003**, *90*, 013004.
- (28) Kunz, R.; Timpmann, K.; Southall, J.; Cogdell, R. J.; Freiberg, A.; Köhler, J. Exciton Self Trapping in Photosynthetic Pigment-Protein Complexes Studied by Single-Molecule Spectroscopy. *J. Phys. Chem. B* **2012**, *116*, 11017–11023.
- (29) Freiberg, A.; Rätsep, M.; Timpmann, K. A Comparative Spectroscopic and Kinetic Study of Photoexcitations in Detergent-Isolated and Membrane-Embedded LH2 Light-Harvesting Complexes. *Biochim. Biophys. Acta, Bioenerg.* **2012**, *1817*, 1471–1482.
- (30) Freiberg, A.; Rätsep, M.; Timpmann, K.; Trinkunas, G. Excitonic Polarons in Quasi-One-Dimensional LH1 and LH2 Bacteriochlorophyll *a* Antenna Aggregates from Photosynthetic Bacteria: A Wavelength-Dependent Selective Spectroscopy Study. *Chem. Phys.* **2009**, *357*, 102–112.
- (31) Cogdell, R.; Hawthornthwaite, A. M. Preparation, Purification, and Crystallization of Purple Bacteria Antenna Complexes. In *The Photosynthetic Reaction Center*; Deisenhofer, J., Norris, J. R., Eds.; Academic Press: San Diego, California, 1993; pp 23–42.
- (32) Freiberg, A.; Rätsep, M.; Timpmann, K.; Trinkunas, G.; Woodbury, W. N. Self-Trapped Excitons in LH2 Antenna Complexes between 5 K and Ambient Temperature. *J. Phys. Chem. B* **2003**, *107*, 11510–11519.
- (33) Hofmann, C.; Aartsma, T. J.; Michel, H.; Köhler, J. Spectral Dynamics in the B800 Band of LH2 from *Rhodospirillum molischianum*: A Single-Molecule Study. *New J. Phys.* **2004**, *6*, 1–15.
- (34) Urbonienė, V.; Vrublevska, O.; Trinkunas, G.; Gall, A.; Robert, B.; Valkunas, L. Solvation Effect of Bacteriochlorophyll Excitons in Light-Harvesting Complex LH2. *Biophys. J.* **2007**, *93*, 2188–2198.
- (35) Freiberg, A.; Godik, V. I.; Pullerits, T.; Timpmann, K. Directed Picosecond Excitation Transport in Purple Photosynthetic Bacteria. *Chem. Phys.* **1988**, *128*, 227–235.
- (36) Freiberg, A.; Godik, V. I.; Pullerits, T.; Timpman, K. Picosecond Dynamics of Directed Excitation Transfer in Spectrally Heterogeneous Light-Harvesting Antenna of Purple Bacteria. *Biochim. Biophys. Acta, Bioenerg.* **1989**, *973*, 93–104.
- (37) Scheuring, S.; Rigaud, J. L.; Sturgis, J. N. Variable LH2 Stoichiometry and Core Clustering in Native Membranes of *Rhodospirillum rubrum*. *EMBO J.* **2004**, *23*, 4127–4133.
- (38) Adams, P. G.; Hunter, C. N. Adaptation of Intracytoplasmic Membranes to Altered Light Intensity in *Rhodobacter sphaeroides*. *Biochim. Biophys. Acta, Bioenerg.* **2012**, *1817*, 1616–1627.
- (39) Freiberg, A.; Pajusalu, M.; Rätsep, M. Excitons in Intact Cells of Photosynthetic Bacteria. *J. Phys. Chem. B* **2013**, DOI: 10.1021/jp3098523.
- (40) Alden, R. G.; Johnson, E.; Nagarajan, V.; Parson, W. W.; Law, C. J.; Cogdell, R. J. Calculations of Spectroscopic Properties of the LH2 Bacteriochlorophyll-Protein Antenna complex from *Rhodospseudomonas acidophila*. *J. Phys. Chem. B* **1997**, *101*, 4667–4680.
- (41) Mukai, K.; Abe, S.; Sumi, H. Theory of Rapid Excitation Energy Transfer from B800 to Optically Forbidden Exciton States of B850 in the Antenna System LH2 of Photosynthetic purple bacteria. *J. Phys. Chem. B* **1999**, *103*, 6096–6102.
- (42) Cheng, Y. C.; Silbey, R. J. Coherence in the B800 Ring of Purple Bacteria LH2. *Phys. Rev. Lett.* **2006**, *96*, 028103.
- (43) Novoderezhkin, V. I.; Razjivin, A. P. Excitonic Interactions in the Light-Harvesting Antenna of Photosynthetic Purple Bacteria and Their Influence on Picosecond Absorbance Difference Spectra. *FEBS Lett.* **1993**, *330*, 5–7.
- (44) Reddy, N. R.; Picorel, R.; Small, G. J. B896 and B870 Components of the *Rhodobacter sphaeroides* Antenna: a Hole Burning Study. *J. Phys. Chem.* **1992**, *96*, 6458–6464.
- (45) Freiberg, A.; Timpmann, K.; Ruus, R.; Woodbury, N. W. Disordered Exciton Analysis of Linear and Nonlinear Absorption Spectra of Antenna Bacteriochlorophyll Aggregates: LH2-Only Mutant Chromatophores of *Rhodobacter sphaeroides* at 8 K under Spectrally Selective Excitation. *J. Phys. Chem. B* **1999**, *103*, 10032–10041.
- (46) Matsushita, M.; Ketelaars, M.; van Oijen, A. M.; Köhler, J.; Aartsma, T. J.; Schmidt, J. Spectroscopy on the B850 Band of Individual Light-Harvesting 2 Complexes of *Rhodospseudomonas acidophila*: II. Exciton States of an Elliptically Deformed Ring Aggregate. *Biophys. J.* **2001**, *80*, 1604–1614.
- (47) Didraga, C.; Knoester, J. Exchange Narrowing in Circular and Cylindrical Molecular Aggregates: Degenerate Versus Nondegenerate States. *Chem. Phys.* **2002**, *275*, 307–318.
- (48) Sauer, K.; Cogdell, R. J.; Prince, S. M.; Freer, A. A.; Isaacs, N. W.; Scheer, H. Structure Based Calculations of the Optical Spectra of the LH2 Bacteriochlorophyll-Protein Complex from *Rhodospseudomonas acidophila*. *Photochem. Photobiol.* **1996**, *64*, 564–576.
- (49) Timpmann, K.; Trinkunas, G.; Olsen, J. D.; Hunter, C. N.; Freiberg, A. Bandwidth of Excitons in LH2 Bacterial Antenna Chromoproteins. *Chem. Phys. Lett.* **2004**, *398*, 384–388.
- (50) Pajusalu, M.; Rätsep, M.; Trinkunas, G.; Freiberg, A. Davydov Splitting of Excitons in Cyclic Bacteriochlorophyll a Nanoaggregates of Bacterial Light-Harvesting Complexes between 4.5 and 263 K. *ChemPhysChem* **2011**, *12*, 634–644.
- (51) Davydov, A. S. *Theory of Molecular Excitons*; Plenum Press: New York, 1971.
- (52) Trinkunas, G.; Freiberg, A. A Disordered Polaron Model for Polarized Fluorescence Excitation Spectra of LH1 and LH2 Bacteriochlorophyll Antenna Aggregates. *J. Lumin.* **2006**, *119–120*, 105–110.
- (53) Timpmann, K.; Trinkunas, G.; Qian, P.; Hunter, C. N.; Freiberg, A. Excitons in Core LH1 Antenna Complexes of Photosynthetic Bacteria: Evidence for Strong Resonant Coupling and Off-Diagonal Disorder. *Chem. Phys. Lett.* **2005**, *414*, 359–363.
- (54) Freiberg, A.; Trinkunas, G. Unravelling the Hidden Nature of Antenna Excitations. In *Photosynthesis in silico: Understanding Complexity from Molecules to Ecosystems*; Laik, A., Nedbal, L., Govindjee, Eds.; Springer: Dordrecht, The Netherlands, 2009; Vol. 29, pp 55–82.
- (55) Freiberg, A.; Ellervee, A.; Kuk, P.; Laisaar, A.; Tars, M.; Timpmann, K. Pressure Effects on Spectra of Photosynthetic Light-Harvesting Pigment-Protein Complexes. *Chem. Phys. Lett.* **1993**, *214*, 10–16.
- (56) Wu, H.-M.; Rätsep, M.; Jankowiak, R.; Cogdell, R. J.; Small, G. J. Comparison of the LH2 Antenna Complex of *Rhodospseudomonas acidophila* (strain 10050) and *Rhodobacter sphaeroides* by High Pressure Absorption, High Pressure Hole Burning, and Temperature

Dependent Absorption Spectroscopies. *J. Phys. Chem. B* **1997**, *101*, 7641–7653.

(57) Timpmann, K.; Ellervee, A.; Pullerits, T.; Ruus, R.; Sundström, V.; Freiberg, A. Short-Range Exciton Couplings in LH2 Photosynthetic Antenna Proteins Studied by High Hydrostatic Pressure Absorption Spectroscopy. *J. Phys. Chem. B* **2001**, *105*, 8436–8444.

(58) Gall, A.; Ellervee, A.; Sturgis, J. N.; Fraser, N. J.; Cogdell, R. J.; Freiberg, A.; Robert, B. Membrane Protein Stability: High Pressure Effects on the Structure and Chromophore-Binding Properties of the Light-Harvesting Complex LH2. *Biochemistry* **2003**, *42*, 13019–13026.

(59) Kangur, L.; Timpmann, K.; Freiberg, A. Stability of Integral Membrane Proteins under High Hydrostatic Pressure: The LH2 and LH3 Antenna Pigment - Protein Complexes from Photosynthetic Bacteria. *J. Phys. Chem. B* **2008**, *112*, 7948–7955.

(60) Ellervee, A.; Freiberg, A. Formation of Bacteriochlorophyll *a* Coordination States Under External High-Pressure. *Chem. Phys. Lett.* **2008**, *450*, 386–390.

(61) Zollfrank, J.; Friedrich, J. Spectral Holes Under Pressure: Proteins and Glasses. *J. Opt. Soc. Am. B* **1992**, *9*, 956–961.

(62) Wu, H.-M.; Rätsep, M.; Jankowiak, R.; Cogdell, R. J.; Small, G. J. Hole Burning and Absorption Studies of the LH1 Antenna Complex of Purple Bacteria: Effects of Pressure and Temperature. *J. Phys. Chem. B* **1998**, *102*, 4023–4034.

(63) Timpmann, K.; Ellervee, A.; Kuznetsov, A.; Laisaar, A.; Trinkunas, G.; Freiberg, A. Self-Trapped Excitons in LH2 Bacteriochlorophyll–Protein Complexes Under High Pressure. *J. Lumin.* **2003**, *102*, 220–225.

(64) Baier, J.; Richter, M. F.; Cogdell, R. J.; Oellerich, S.; Köhler, J. Determination of the Spectral Diffusion Kernel of a Protein by Single Molecule Spectroscopy. *Phys. Rev. Lett.* **2008**, *100*, 018108.

(65) Mukherjee, M.; Bhattacharya, M.; Sanyal, M. K.; Geue, Th.; Grenzer, J.; Pietsch, U. Reversible Negative Thermal Expansion of Polymer Films. *Phys. Rev. E: Stat., Nonlinear, Soft Matter Phys.* **2002**, *66*, 061801.

PUBLICATION P2

**Exciton Self Trapping in Photosynthetic  
Pigment-Protein Complexes Studied by  
Single-Molecule Spectroscopy**

Ralf Kunz, Kōu Timpmann, June Southall, Richard J. Cogdell, Arvi Freiberg,  
and Jürgen Köhler

published in:

*The Journal of Physical Chemistry B* **116**, 11017-11023, (2012)

© 2012 American Chemical Society  
[DOI:10.1021/jp3040456](https://doi.org/10.1021/jp3040456)



# Exciton Self Trapping in Photosynthetic Pigment–Protein Complexes Studied by Single-Molecule Spectroscopy

Ralf Kunz,<sup>†</sup> Kõu Timpmann,<sup>‡</sup> June Southall,<sup>§</sup> Richard J. Cogdell,<sup>§</sup> Arvi Freiberg,<sup>‡,||</sup> and Jürgen Köhler<sup>\*,†</sup>

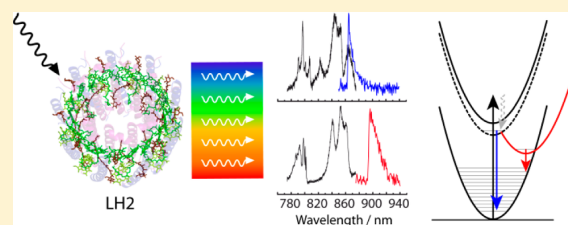
<sup>†</sup>Experimental Physics IV and Bayreuth Institute for Macromolecular Research (BIMF), University of Bayreuth, 95440 Bayreuth, Germany

<sup>‡</sup>Institute of Physics, University of Tartu, Riia 142, Tartu EE-51014, Estonia

<sup>§</sup>Institute of Molecular, Cell and Systems Biology, College of Medical Veterinary and Life Sciences, Biomedical Research Building, University of Glasgow, Glasgow G12 8QQ, Scotland, United Kingdom

<sup>||</sup>Institute of Molecular and Cell Biology, University of Tartu, Riia 23, Tartu EE-51010, Estonia

**ABSTRACT:** Evidence for the formation of self-trapped exciton states in photosynthetic antenna complexes is provided by comparing single-molecule fluorescence–excitation and emission spectra that have been recorded from the same individual LH2 complex from *Rhodospseudomonas acidophila*. While the excitation spectra showed the signatures for the B800 and B850 bands as observed previously, two distinctively different types of emission spectra were found. One group of antenna complexes shows spectra with a relatively narrow spectral profile with a clear signature of a zero-phonon line, whereas the other group of complexes displays spectra that consist only of a broad featureless band. Analysis of these data reveals clear correlations between the spectral position of the emission, the width of the spectral profile, and the associated electron–phonon coupling strength.



## INTRODUCTION

Purple photosynthetic bacteria have evolved an elegant system of modular units that make up their light-harvesting apparatus. These modules consist of pairs of hydrophobic, low molecular weight polypeptides, called  $\alpha$  and  $\beta$  (usually 50–60 amino acids long), that noncovalently bind a small number of bacteriochlorophyll (BChl  $a$ ) and carotenoid (Car) molecules. The modules then oligomerize to produce the functional light-harvesting complexes.<sup>1–6</sup> Light-harvesting complex 1 (LH1) encloses the reaction center (RC) and forms the core complex, whereas the peripheral light-harvesting complexes (LH2) are arranged around the perimeter of the RC-LH1 complex in a two-dimensional array.

Significant progress in our understanding of the light-harvesting reactions of photosynthesis was achieved when the structure of the LH2 pigment–protein complex from the purple bacterium *Rhodospseudomonas (Rps.) acidophila* was resolved.<sup>1</sup> This complex accommodates 27 BChl  $a$  molecules and 9 carotenoids. The BChl  $a$  molecules are organized in two concentric rings referred to as B800 and B850, according to the spectral position of their room temperature absorption bands. From the intermolecular distances determined by the X-ray structure, it can be concluded that the dipolar interaction between neighboring BChl  $a$  molecules in the B850 ring is significant and leads to delocalized excited states that are coherently distributed at least over a part of the ring. Hence a natural starting point to describe the lowest electronically excited states of this assembly is based on the Frenkel exciton

formalism.<sup>7–9</sup> Neglecting the slight dimerization of the B850 BChl  $a$  molecules, the proper eigenstates are exciton states and are characterized by a quantum number,  $k$ , which can take the values  $0, \pm 1, \pm 2, \dots, \pm 8$ , and  $9$ . Due to the circular symmetry, only the states  $k = \pm 1$  carry an appreciable transition-dipole moment that makes them accessible for optical spectroscopy. Structural and/or energetic heterogeneities are usually accounted for by random and/or correlated disorder in the site energies of and in the couplings between the BChl  $a$  molecules. The main effects of disorder on the exciton manifold are a mixing of the different exciton levels, a modification of the energy separation of the exciton levels and lifting their pairwise degeneracy, and a redistribution of oscillator strength to nearby states.<sup>10,11</sup> Overcoming the problem of sample heterogeneity and ensemble averaging by exploiting single-molecule techniques at low temperatures has helped to further refine the theoretical description of the B850 excitations.<sup>12–18</sup> The “disordered Frenkel exciton” model grasps the essential features observed in absorption and fluorescence–excitation spectroscopy for these systems.

However, comparison of ensemble-absorption and emission spectra from LH2 complexes has led to several discrepancies that are inconsistent with the disordered Frenkel exciton approach:<sup>19,20</sup> (i) Simulations based on the exciton model

Received: April 26, 2012

Revised: June 13, 2012

Published: August 21, 2012

distribute the lowest exciton state over a range of  $140\text{ cm}^{-1}$  (fwhm) on the low energy side of the ensemble absorption spectrum. This number is in agreement with results from hole-burning and single-molecule experiments.<sup>13,21–23</sup> Yet, the width of the respective ensemble emission spectrum exceeds this figure by more than a factor of 2.<sup>20,24</sup> (ii) Experimental evidence has been found that the emission spectrum is essentially homogeneously broadened suggesting that exciton–phonon coupling for the transition from the relaxed excited state must be strong.<sup>19</sup> This is in contrast to the quasiline absorption spectrum, which is mostly inhomogeneously broadened. Similar inconsistencies have been found for LH1 as well.<sup>25–28</sup> (iii) Raising the temperature should thermally populate the strongly allowed  $k = \pm 1$  exciton states and result in a significant reduction of the fluorescence lifetime. However, the fluorescence lifetime changes only by about 20% between cryogenic temperatures and room temperature.<sup>20</sup> On the basis of the exciton model this can only be explained by assuming static disorder in the site energies of the individual BChl *a* pigments that is much too large to be consistent with the absorption spectrum. (iv) While single-molecule fluorescence–excitation spectra are consistent with the disordered Frenkel exciton model, implying the observation of (fully) delocalized excitons,<sup>12,14,15,17,18,29,30</sup> time-resolved spectroscopy has led to the conclusion that the excitation energy is localized on about 2–7 pigments.<sup>20,31–34</sup>

In order trying to explain these conflicting observations, the Freiberg group has put forward a model that involves exciton self-trapping in the B850 assembly.<sup>19,20,28,35</sup> Self-trapping of excitons is a well-known phenomenon in solids.<sup>36–40</sup> It refers to the fact that, due to exciton–phonon interaction, the exciton induces a structural reorganization of its environment, which lowers its energy to an extent such that the excitation energy gets trapped on a limited region of the aggregate. This phenomenon is also referred to as polaron formation. It has been shown theoretically that in one-dimensional systems self-trapping inherently takes place for any nonvanishing electron–phonon coupling.<sup>37</sup> Within certain reservations, the B850 ring, consisting of strongly electronically coupled BChl *a* molecules, can be considered as a one-dimensional system. Freiberg and co-workers have developed a consistent description of the experimental findings based on ensemble studies on LH2 complexes.<sup>20,41–43</sup> However, the great difficulty encountered in these biological systems is the large heterogeneity of the samples that smears out the subtle details in the ensemble-averaged spectra. In order to avoid ensemble-averaging and to try to find direct evidence for self-trapping of excitons in the B850 manifold of LH2, it would be desirable to perform fluorescence–excitation and fluorescence emission spectroscopy on the same individual complex. Previous single-molecule studies that recorded emission spectra from these systems did not focus on possible self-trapping processes and/or were conducted at room temperatures where important spectral details are masked by thermal broadening.<sup>44–51</sup> The advantages of working at low temperatures are negligible photobleaching, which enables long observation times and concomitantly an improvement of the signal-to-noise ratio of the spectra, as well as a reduction in the linewidths of the spectral features due to the suppression of (thermal) motions of the nuclei. This allows us to resolve narrow spectral features which, even for a single molecule, would be hopelessly broadened at room temperature. Since electrons are very light particles, processes that involve their movements, i.e., transitions into electronically excited

states, are at low temperature as active as at room temperature. In other words cryogenic conditions are well suited to obtain a good approximation of the electronic structure of biomolecules. This should not be confused with dynamical properties of proteins, i.e., those that involve molecular rearrangements. The rates of such relaxations, of course, depend on temperature and do not agree with the corresponding rates under physiological conditions.<sup>52</sup> However, working at cryogenic temperatures shifts the time scale for these fluctuations into a range that is experimentally accessible.

Here we report on low-temperature fluorescence–excitation and emission spectroscopy carried out on the same individual LH2 complex that allows for a direct comparison of the absorbing and emitting electronic states. Analysis of the spectral profiles obtained leads us to conclude that for some of the LH2 complexes emitting at the red end of the spectrum exciton self-trapping does indeed occur.

## EXPERIMENTAL SECTION

**Sample Preparation.** The LH2 complexes from the species *Rps. acidophila* (strain 10050) were isolated and purified as described previously.<sup>53</sup> After purification, the LH2 complexes were transferred to a buffer solution (20 mM Tris HCl, pH 8.0, 0.1% LDAO) and stored in small aliquots at  $-80\text{ }^{\circ}\text{C}$  until used. This stock solution was diluted in detergent buffer solution in several steps to a concentration of about  $10^{-11}\text{ M}$ . In the last dilution step also 1.8% (w/w) polyvinyl alcohol (PVA;  $M_w = 125\,000\text{ g/mol}$ ) was present. A drop (20  $\mu\text{L}$ ) of this solution was spin-coated on a cleaned quartz ( $\text{SiO}_2$ ) substrate by spinning it for 10 s at 500 rpm and 60 s at 2500 rpm, producing high quality amorphous polymer films with a thickness of about 100 nm in which the pigment–protein complexes are embedded. The samples were immediately mounted in a liquid-helium cryostat and cooled to 1.2 K. For studying ensembles of LH2 complexes the stock solution was diluted to  $10^{-6}\text{ M}$ , and further the same protocol as described above was followed.

**Optical Setup.** For the optical experiments the samples were illuminated with a continuous-wave tunable titanium-sapphire (Ti:Sa) laser (3900S, Spectra Physics) pumped by a frequency doubled continuous-wave neodymium–yttrium–vanadate (Nd:YVO<sub>4</sub>) laser (Millennia Vs, Spectra Physics) using a home build microscope that can be operated either in widefield or confocal mode. To obtain a well-defined variation of the wavelength of the Ti:Sa laser the intracavity birefringent filter has been rotated with a motorized micrometer screw. For calibration purposes a wavemeter (WaveMaster, Coherent) has been used and an accuracy as well as a reproducibility of  $1\text{ cm}^{-1}$  for the laser frequency has been verified.

First a  $40 \times 40\ \mu\text{m}^2$  wide-field image of the sample was taken by exciting the sample around 855 nm through a band-pass (BP) excitation filter (BP 858/30; Dr. Hugo Anders). The emission from the sample was collected by a microscope objective (Mikrothek, NA = 0.85) that was mounted inside the cryostat and the signal was focused onto a back-illuminated CCD camera (512 SB, Princeton Instruments) after passing band-pass filters (BP 900/50; AHF Analysetechnik) that block residual laser light. Next, a spatially well-isolated complex was selected from the wide-field image, and the microscope was switched to the confocal mode. In this mode the excitation volume is in the order of  $0.1\ \mu\text{m}^3$ . A well-controlled adjustment of this volume with respect to the sample is achieved by a pair of telecentric lenses.

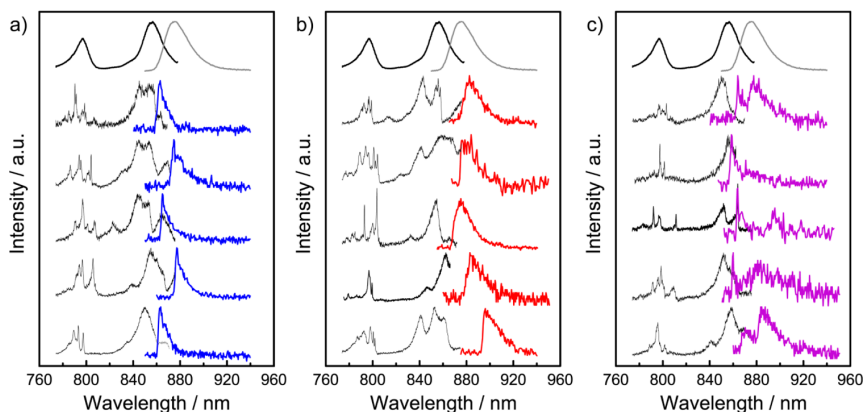


**Figure 1.** Fluorescence–excitation (black lines) and emission spectra (colored lines) from LH2 complexes of *Rps. acidophila*. In each panel the top traces show the ensemble spectra for comparison and five examples of excitation/emission spectra recorded from the same individual complex. The spectra are normalized to their peak intensity (of the B850 band for fluorescence–excitation) and offset for clarity. The fluorescence–excitation spectra correspond to averages over all polarizations of the excitation light, and the excitation power was  $100 \text{ W/cm}^2$ . The emission spectra were detected above  $830 \text{ nm}$  and the excitation power was  $1 \text{ kW/cm}^2$ . The exposure times were  $60 \text{ s}$ . All spectra were measured at  $1.2 \text{ K}$ . (a) Type I: Complexes with narrow, sharp edged emission spectrum. (b) Type II: Complexes with broad, featureless emission spectra. (c) Type III: Complexes for which the emission spectra show features from both previous categories.

**Fluorescence–Excitation Spectroscopy.** Fluorescence–excitation spectra have been recorded by scanning the linearly polarized excitation light either from  $774$  to  $872 \text{ nm}$  or from  $774$  to  $876 \text{ nm}$  with a scanning rate of  $3 \text{ nm/s}$  ( $\sim 50 \text{ cm}^{-1}/\text{s}$ ). The excitation intensity was about  $100 \text{ W/cm}^2$ . The polarization of the excitation light was rotated in steps of  $6.4^\circ$  between two successive scans by means of a waveplate. The emission passed through a set of bandpass filters (BP900/50, BP890/20; AHF Analysetechnik, BP893/21; Dr. Hugo Anders) and was focused onto a single-photon counting avalanche photodiode (APD) (SPCM-AQR-16, EG&G). The fluorescence–excitation spectra shown in this study correspond to the averages over all polarizations of the excitation light. All fluorescence–excitation spectra have been corrected for variations of the laser intensity as a function of the wavelength.

**Fluorescence-emission spectroscopy.** For the emission spectroscopy the individual complexes were excited around  $800 \text{ nm}$  through a band-pass filter (BP805/60; AHF Analysetechnik). Since the absorption bands in this spectral range are rather narrow the laser wavelength was wobbled with an amplitude of about  $5 \text{ nm}$  at a rate of  $3 \text{ nm/s}$  around the B800 absorptions of the complex under study. The polarization of the excitation light was rotated as described above. By changing the detection path of the setup using a flip mirror, the emitted light could be directed through a set of dielectric long-pass filters (LP830; AHF Analysetechnik) and was dispersed in a spectrometer (SpectraPro-150,  $300 \text{ lines/mm}$ , Acton Research Corporation) providing a spectral resolution of  $1.5 \text{ nm}$  ( $20 \text{ cm}^{-1}$ ). The signal was detected with a CCD camera (iDus DV420A-OE, Andor Technology or Luca-R 604M-OM, Andor Technology) using an exposure time of  $60 \text{ s}$  (iDus) or  $600 \text{ s}$  (Luca), respectively. The sensitivity of the combined spectrograph/camera system was sufficiently constant over the detected spectral range making a further correction unnecessary. Typically, ten emission spectra were recorded successively from one individual complex. In order to obtain a reasonable spectrally dispersed signal, we had to increase the excitation intensity to about  $1 \text{ kW/cm}^2$ . The integrity of the LH2 complexes was checked by recording the fluorescence–excitation spectra

before and after the emission spectroscopy experiments for several LH2 complexes. Significant changes between the excitation spectra were not observable.

## RESULTS AND DISCUSSION

In Figure 1 several examples of fluorescence–excitation (black lines) and emission spectra (colored lines) are shown that have been taken from the same individual LH2 complex. For comparison, the top traces show the respective ensemble spectra. As has been observed previously<sup>13,54–57</sup> the fluorescence–excitation spectra from individual complexes show remarkable differences which reflect the heterogeneity of the sample. Briefly, each complex and even each pigment within a complex experiences a slightly different local environment resulting in a slight change of the electrostatic interactions. This causes variations of the site energies of the BChl molecules as well as variations in the intermolecular interactions. In an ensemble of complexes this leads to an inhomogeneous broadening of the absorption line, which can be dismantled by studying the complexes individually. However, the excitation spectra have in common that they feature several narrow lines in the B800 spectral region and a few broad bands in the B850 region, reflecting the differences in lifetime/dephasing of the electronic states involved. Spectral variations are observed for the emission spectra as well. Yet to our surprise and in contrast to the excitation spectra the emission spectra can be grouped into three categories of qualitatively different spectra. In the first category (type I: 16 out of 44 complexes corresponding to 36%) the emission spectra show a relatively narrow spectral feature with a steep rise on the blue side and an asymmetric shoulder on the red side, Figure 1a. In the second category (type II: 22/44; 50%) the emission spectra show a broad featureless asymmetric band, Figure 1b. Finally in the third category (type III: 6/44; 14%) the emission spectra appear to be a superposition of the spectra found in the two other categories, Figure 1c.

Due to the low concentration of LH2 complexes the probability to find two LH2 complexes within the same excitation volume of  $0.1 \mu\text{m}^3$  is smaller than  $0.01\%$ , which

makes it highly unlikely that all type III spectra result from two or more spatially unresolved LH2 complexes. Given the exposure time of 60 s for recording the emission spectra, it is more likely that this group of spectra stems from LH2 complexes that underwent a change in their emission characteristics during data acquisition. Therefore, for the detailed analysis that follows, we focus on the spectra in the first two categories.

Figure 2a shows examples of type I and type II emission spectra on an expanded scale.

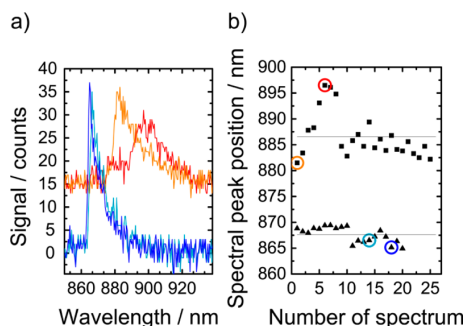


**Figure 2.** (a) Consecutively recorded type I (lower traces) and type II (upper traces) emission spectra. The time interval between the two examples selected for display was 240 s (type I) and 360 s (type II), respectively. The vertical axis is valid for the type I spectra, the type II spectra have been offset by 15 counts for clarity. (b) Spectral position of the peak of the emission spectrum as a function of exposures for type I (triangles) and type II (squares) spectra. The data have been recorded consecutively with an exposure time of 1 min per spectrum. The open circles correspond to the spectra shown in part a of the figure. The lines indicate the averaged peak positions.

Within each category the spectra have been recorded consecutively at a rate of one spectrum per minute from the same complex. Examples for the resulting spectra are shown in Figure 2a. The type I examples show only small changes between the two experiments. The spectral peaks occur at 866.5 and 865.0 nm, respectively, and the line width (fwhm) amounts to 133 and 125  $\text{cm}^{-1}$ , respectively. In contrast, a drastic change with respect to both peak position (881.8 nm/898.9 nm) and line width (209  $\text{cm}^{-1}$ /298  $\text{cm}^{-1}$ ) can be observed for the type II examples. Moreover, the shape of the spectrum changes from an asymmetric profile to a more symmetric one. For both complexes the changes in spectral peak position of the emission spectra as a function of the acquisitions are shown in Figure 2b. Although the type I spectrum shows only small peak shifts of less than  $\pm 3$  nm ( $\sim 40$   $\text{cm}^{-1}$ ), much larger spectral excursions exceeding 10 nm ( $\sim 130$   $\text{cm}^{-1}$ ) were found for the type II spectra. Generally we found that the spectral stability was higher for type I as compared to type II spectra.

Furthermore, we found a clear trend that most of the type I spectra are blue-shifted with respect to the type II spectra.

This is clearly seen in Figure 3a, which displays the observed linewidths of the spectra as a function of the spectral peak position averaged over the observation time for all complexes studied, and which reveals a clear correlation between spectral position and line width/type of spectra. This is quantified in panels b and c in Figure 3 that show the distributions of the averaged peak positions, Figure 3b, and observed linewidths,

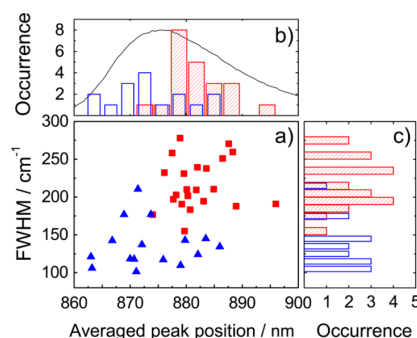


**Figure 3.** (a) Widths of the emission spectra as a function of the averaged peak position for type I (triangles) and type II (squares) spectra. (b) Distribution of the averaged peak positions for type I (blue) and type II (red) emission spectra. The overlaid black line corresponds to the emission spectrum from an ensemble of LH2 complexes. (c) Distribution of the widths for type I (blue) and type II (red) emission spectra.

Figure 3c, discriminated between type I (blue) and type II (red) spectra. The averaged peak positions of the emission spectra, Figure 3b, are distributed over the full spectral range that is covered by the ensemble emission spectrum (which has been overlaid (full line) for comparison). Yet the histogram for the type I spectra features a mean of 11 447  $\text{cm}^{-1}$  (873.6 nm), which is clearly blue-shifted with respect to the mean value of 11 337  $\text{cm}^{-1}$  (882.0 nm) that is found for the type II spectra. The mean of the line width distribution is 136  $\text{cm}^{-1}$  for the type I spectra and 217  $\text{cm}^{-1}$  for the type II spectra, see Figure 3c.

The striking differences in the spectral peak positions, spectral profiles, linewidths, and spectral diffusion behavior between the type I and type II emission spectra strongly suggests that there exist (at least temporarily) two pools of LH2 complexes that feature significant differences in their intra- and intermolecular interactions. For the type I emission spectra, we attribute the sharp spectral feature to the zero-phonon line (ZPL) and the asymmetric shoulder at higher wavelength to the phonon-sideband (PSB). The ZPL corresponds to the purely electronic transition, and the PSB corresponds to an electronic transition in combination with the simultaneous excitation of low-frequency vibrations. The distribution of the intensity between the ZPL and the PSB, is determined by the linear electron–phonon coupling strength. Information about this parameter can be obtained from the Debye–Waller factor,  $\alpha$ , or likewise from the Huang–Rhys (HR) factor,  $S$ , which are given as

$$\alpha = \frac{I_{\text{ZPL}}}{I_{\text{ZPL}} + I_{\text{PSB}}} = \exp(-S) \quad (1)$$

Here  $I_{\text{ZPL}}$  and  $I_{\text{PSB}}$  refer to the integrated intensities of the ZPL and the PSB, respectively. The HR factor is a measure of the average number of phonons that accompany a particular electronic transition and can be associated with the displacement of the equilibrium positions of the nuclei upon a photoexcitation of the chromophore. In order to analyze the spectral profiles in more detail, we fitted the high-energy wing of the ZPL by a Lorentzian or Gaussian that was subtracted from the data to uncover the PSB as illustrated in Figure 4a.

Unfortunately, for some (mainly type II) spectra an unambiguous distinction between the ZPL and the PSB was

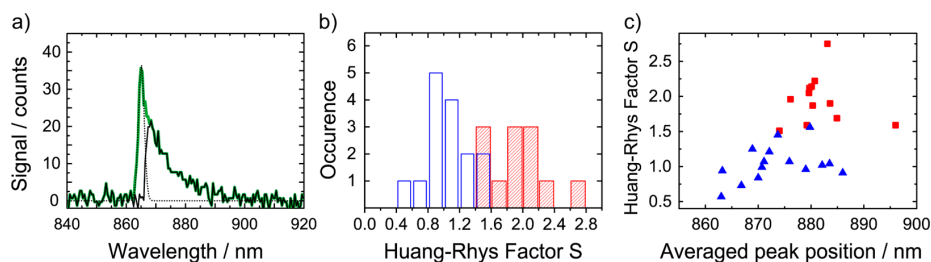


**Figure 4.** (a) Example of a type I emission spectrum (full green line). The low energy wing is fitted with a Gaussian (dotted line). The full black line corresponds to the difference spectrum between the signal and the fit function. (b) Histogram of the Huang–Rhys factors  $S$  for type I (blue) and type II (red) emission spectra. For the evaluation of the type II data, see text. (c) Huang–Rhys factors as a function of the averaged peak position of the emission spectrum for type I (triangles) and type II (squares) spectra.

impossible, and we therefore restrict the analysis to those spectra that allowed for a meaningful fitting of the ZPL (15 out of 16 for type I, and 12 out of 22 for type II). The resulting HR factors are shown in Figure 4b as a histogram, and in Figure 4c as a function of the averaged peak position of the emission spectrum. For type I spectra, Figure 4b blue bars, the HR factors covers the range from 0.6 - 1.6 peaking at 0.9. These numbers are slightly larger than those for the B800 BChl  $a$  molecules (0.2 - 0.9 peaking at 0.6)<sup>58–61</sup> and clearly larger than what has been found for BChl  $a$  in organic solvents (0.3 - 0.6).<sup>62</sup> For the type II spectra the HR factors cover the range from 1.5 - 2.8 with a mean around 2, Figure 4b red bars, which is in good agreement with the results obtained from fluorescence-line narrowing experiments by the Freiberg group.<sup>28,63,64</sup> From these data it can be stated that the type I spectra correlate with small HR factors; that is, there are no blue entries in the upper right corner of Figure 4c. However, we are not sensitive to type II complexes with a small HR factor which might be missed therefore.

Moreover the origin of the type II spectra is not as straightforward as suggested above. Next to reflecting a stronger exciton–phonon coupling, the broad and featureless profiles of the type II spectra could be the result of fast spectral diffusion processes, smearing out the typical ZPL/PSB profile. The two extremes are illustrated in Figure 5.

The top part of the figure displays schematically the configuration coordinate diagram for excitations in the B850 manifold. The potential curves of the electronic ground state and the lowest exciton states, denoted as  $k = 0$  and  $k = \pm 1$  are shown. For weak electron–phonon coupling, i.e., with no or only little horizontal displacement of the ground state and excited state potentials with respect to each other, the emission spectra feature a typical ZPL/PSB profile. Spectral diffusion (SD) corresponds to vertical displacements of the ground state and excited state potential energy curves with respect to each other. If these processes occur on time scales faster than the integration time of the CCD camera the typical ZPL/PSB profile is smeared out due to temporal averaging, see Figure 5 bottom left. This interpretation of the type II spectra is supported by the observation that such spectra in general show stronger spectral diffusion compared to type I spectra. Yet it does neither explain why the type I spectra are (predominantly) blue-shifted with respect to the type II spectra, nor does it explain the observed correlation between the spectral position and the HR factors for the type I spectra.

Alternatively, the type II spectra might reflect the formation of a self-trapped exciton state (STE). This is indicated in Figure 5 by the potential energy curve denoted STE. Emission from

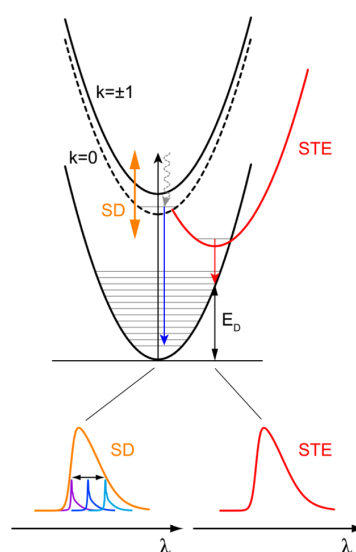


**Figure 5.** Configuration coordinate diagram of the electronic ground state (lowest potential energy curve) and the lowest exciton states ( $k = 0$ , dashed line,  $k = \pm 1$  full line). For clarity the splitting between the  $k = \pm 1$  states is neglected. Upon optical excitation (upward vertical arrow) the system relaxes to the lowest exciton state (wavy arrow). For weak electron phonon coupling the emission spectrum features a strong ZPL accompanied by a vibrational sideband (downward blue arrow, colored spectra bottom left). Spectral diffusion (SD) corresponds to vertical displacements of the potentials with respect to each other and is indicated by the double-headed arrow. If the spectral diffusion occurs on time scales faster than the data acquisition, temporal averaging smears out the spectral profile, and the measured spectrum corresponds to the envelope of the emission spectra, bottom left. For strong electron–phonon coupling the potential energy curves of the electronic ground state and the electronically excited states are horizontally shifted with respect to each other. This results in an emission spectrum with a strong vibrational sideband and only little or no intensity in the ZPL. Formation of a self-trapped exciton state (STE) lowers the potential energy with respect to the free exciton states ( $k = 0$  and  $\pm 1$ ) reflected as an additional red shift of the spectrum, bottom right.

this state is significantly red-shifted and shows a broad featureless profile due to stronger electron–phonon coupling, Figure 5, bottom right, in line with the experimental findings. Moreover, this interpretation is supported by computer simulations for the self-trapped exciton model,<sup>35,63</sup> which predict progressively growing HR factors for decreasing

emission energy that is in qualitative agreement with our experimental observations.

The formation of a self-trapped exciton is determined by the mutual time scales for the transfer of the excitation energy within the B850 assembly and the time that the nuclei need to react upon a change in the electronically excited state manifold.<sup>40</sup> This can be transformed into a coupling constant  $g = E_D/\Delta$ , where  $E_D$  corresponds to the lattice site deformation energy, and  $\Delta$  denotes half of the exciton bandwidth.<sup>38,41</sup> A measure for  $E_D$  can be obtained from the separation between the ZPL and the spectral peak position of the PSB in the emission spectra, which is on the order of 50–100  $\text{cm}^{-1}$ , and which differs from the energy  $E_D$  by the spatial extension of the self-trapped state; that is, the number of lattice sites over which the self-trapped exciton state is still delocalized. Hence, a typical lattice deformation energy  $E_D$  in the order of some 100  $\text{cm}^{-1}$  is reasonable. Via the approximation  $\Delta \approx 2V$  the half-width of the exciton band can be obtained from the intermolecular interaction strength,  $V$ , for which several estimates exist in the literature, covering the range between 250 and 400  $\text{cm}^{-1}$ .<sup>56,65</sup> From these figures we obtain  $g \approx E_D/2V$  that is on the order of 0.1–0.5 and is in quantitative agreement with the numerical values used for the simulations detailed in refs 35 and 63.

Although we cannot exclude spectral diffusion as the origin of some of the type II emission spectra, the current results together with the results from other experimental techniques<sup>20,41–43</sup> and from the simulations in refs 35 and 63 strongly suggest that for a part of the complexes that feature type II emission spectra exciton self-trapping does take place. This interpretation explains straightforwardly the discrepancies that have been found between the absorption and emission spectra as mentioned in the introduction. Due to self-trapping of the exciton, the absorbing state and the emitting state are not equivalent. Therefore, conclusions drawn from experiments that monitor properties of the absorbing state do not necessarily agree with conclusions drawn from experiments that monitor the properties of the emitting state. This is in line with the observation that the widths of the hole-burning action spectra of the lowest exciton state<sup>19–21,28,63</sup> and the ensemble emission spectra do not match and why in single-molecule spectroscopy the remarkable differences between type I and type II emission spectra are not reflected in the fluorescence–excitation spectra. Another discrepancy concerns the exciton delocalization length. Fluorescence–excitation spectroscopy monitors transitions from the electronic ground state to the electronically excited state; that is, it monitors the exciton state when it is “born”. In contrast, time-resolved spectroscopy monitors the reverse transition corresponding to the decay or “death” of the exciton. Therefore it refers to the delocalization of the exciton after relaxation (and STE formation) in the excited state manifold. According to<sup>38</sup> the number of units on which the STE is localized is given by  $N \approx 1/2g$ , which yields for the estimate given above  $N \approx 1–5$ . Interestingly, these numbers agree with what has been found by time-resolved spectroscopy.<sup>20,31–34</sup> Yet, it is reasonable to assume that for a distinct LH2 complex the coupling parameter  $g$ , which determines the formation of a self-trapped exciton state, has not a fixed value but rather fluctuates in time. In the illustration shown in Figure 5 this corresponds to a temporal variation of the position of the STE state (red parabola) along both the vertical and the horizontal direction. Whether this is of relevance for the biological function, for example for enhancing

the energy transfer between adjacent LH2 complexes, remains an open question at this point.

## CONCLUSIONS

Low temperature fluorescence–excitation and emission spectroscopy has been performed on individual LH2 complexes from *Rps. acidophila*. According to their shape the emission spectra can be grouped in two categories. One category features a narrow spectral profile containing a zero-phonon line, whereas the spectra of the other type display broad featureless bands. For each group of spectra, clear correlations between the spectral positions, the widths of the spectral profiles, and the electron–phonon coupling strength have been found. Interestingly the differences in the emission spectra between individual LH2 complexes are not reflected in their corresponding fluorescence–excitation spectra. Although fast unresolved spectral diffusion cannot be fully ruled out as being the origin for the broad spectra, the observed correlations lead us to conclude that at least for some of the LH2 complexes an exciton self-trapping process is effective.

## AUTHOR INFORMATION

### Corresponding Author

\*Telephone: +49 921 55 4000. Fax: +49 921 55 4002. E-mail: juergen.koehler@uni-bayreuth.de.

### Notes

The authors declare no competing financial interest.

## ACKNOWLEDGMENTS

We gratefully acknowledge financial support from the Deutsche Forschungsgemeinschaft (KO 1359/16-1, GZ: 436 EST 113/4/0-1 and GRK1640). A.F. and K.T. are also partially supported by the Estonian Science Foundation (Grant No. 8674) and the Ministry of Education and Science (Grant SF0180055s07).

## ABBREVIATIONS

BChl: bacteriochlorophyll; LH1: light harvesting 1 (complex); LH2: light harvesting 2 (complex); RC: reaction center

## REFERENCES

- (1) McDermott, G.; Prince, S. M.; Freer, A. A.; Hawthornthwaite-Lawless, A. M.; Papiz, M. Z.; Cogdell, R. J.; Isaacs, N. W. *Nature* **1995**, *374*, 517–521.
- (2) McLuskey, K.; Prince, S. M.; Cogdell, R. J.; Isaacs, N. W. *Biochemistry* **2001**, *40*, 8783–8789.
- (3) Koepke, J.; Hu, X.; Muenke, C.; Schulten, K.; Michel, H. *Structure* **1996**, *4*, 581–597.
- (4) Roszak, A. W.; Howard, T. D.; Southall, J.; Gardiner, A. T.; Law, C. J.; Isaacs, N. W.; Cogdell, R. J. *Science* **2003**, *302*, 1969–1971.
- (5) Qian, P.; Neil Hunter, C.; Bullough, P. A. *J. Mol. Biol.* **2005**, *349*, 948–960.
- (6) Cogdell, R. J.; Gardiner, A. T.; Roszak, A. W.; Law, C. J.; Southall, J.; Isaacs, N. W. *Photosynth. Res.* **2004**, *81*, 207–214.
- (7) Davydov, A. S. *Theory of Molecular Excitons*; Plenum Press: New York, 1971.
- (8) Knox, R. S. *Theory of Excitons*; Ehrenreich, H., Seitz, F., Turnbull, D., Eds.; Academic Press: New York, 1963; pp 7–37.
- (9) Robinson, C. W. *Annu. Rev. Phys. Chem.* **1970**, *21*, 429–474.
- (10) Wu, H.-M.; Rätsep, M.; Lee, I.-J.; Cogdell, R. J.; Small, G. J. *J. Phys. Chem. B* **1997**, *101*, 7654–7663.
- (11) Alden, R. G.; Johnson, E.; Nagarajan, V.; Parson, W. W.; Law, C. J.; Cogdell, R. J. *J. Phys. Chem. B* **1997**, *101*, 4667–4680.

- (12) van Oijen, A. M.; Ketelaars, M.; Köhler, J.; Aartsma, T. J.; Schmidt, J. *Science* **1999**, *285*, 400–402.
- (13) Ketelaars, M.; van Oijen, A. M.; Matsushita, M.; Köhler, J.; Schmidt, J.; Aartsma, T. J. *Biophys. J.* **2001**, *80*, 1591–1603.
- (14) Matsushita, M.; Ketelaars, M.; van Oijen, A. M.; Köhler, J.; Aartsma, T. J.; Schmidt, J. *Biophys. J.* **2001**, *80*, 1604–1614.
- (15) Mostovoy, M. V.; Knoester, J. *J. Phys. Chem. B* **2000**, *104*, 12355–12364.
- (16) Jang, S.; Silbey, R. J. *J. Chem. Phys.* **2003**, *118*, 9324–9336.
- (17) Jang, S.; Silbey, R. J.; Kunz, R.; Hofmann, C.; Köhler, J. *J. Phys. Chem. B* **2011**, *115*, 12355–12953.
- (18) Hofmann, C.; Aartsma, T. J.; Köhler, J. *Chem. Phys. Lett.* **2004**, *395*, 373–378.
- (19) Timpmann, K.; Katiliene, Z.; Woodbury, N. W.; Freiberg, A. *J. Phys. Chem. B* **2001**, *105*, 12223–12225.
- (20) Freiberg, A.; Rätsep, M.; Timpmann, K.; Trinkunas, G.; Woodbury, N. W. *J. Phys. Chem. B* **2003**, *107*, 11510–11519.
- (21) Wu, H.-M.; Reddy, N. R. S.; Small, G. J. *J. Phys. Chem. B* **1997**, *101*, 651–656.
- (22) Rätsep, M.; Hunter, C. N.; Olsen, J. D.; Freiberg, A. *Photosynth. Res.* **2005**, *86*, 37–48.
- (23) Richter, M. F.; Baier, J.; Prem, T.; Oellerich, S.; Francia, F.; Venturoli, G.; Oesterheld, D.; Southall, J.; Cogdell, R. J.; Köhler, J. *Proc. Natl. Acad. Sci. U.S.A.* **2007**, *104*, 6661–6665.
- (24) Creemers, T. M. H.; de Caro, C.; Visschers, R. W.; van Grondelle, R.; Völker, S. J. *J. Phys. Chem. B* **1999**, *103*, 9770–9776.
- (25) Reddy, N. R.; Picorel, R.; Small, G. J. *J. Phys. Chem.* **1992**, *96*, 6458–6464.
- (26) van Mourik, F.; Visschers, R. W.; van Grondelle, R. *Chem. Phys. Lett.* **1992**, *193*, 1–7.
- (27) Monshouwer, R.; Visschers, R. W.; van Mourik, F.; Freiberg, A.; van Grondelle, R. *Biochim. Biophys. Acta, Bioenerg.* **1995**, *1229*, 373–380.
- (28) Timpmann, K.; Rätsep, M.; Hunter, C. N.; Freiberg, A. *J. Phys. Chem. B* **2004**, *108*, 10581–10588.
- (29) Ketelaars, M.; Hofmann, C.; Köhler, J.; Howard, T. D.; Cogdell, R. J.; Schmidt, J.; Aartsma, T. J. *Biophys. J.* **2002**, *83*, 1701–1715.
- (30) Richter, M. F.; Baier, J.; Southall, J.; Cogdell, R. J.; Oellerich, S.; Köhler, J. *Proc. Natl. Acad. Sci. U.S.A.* **2007**, *104*, 20280–20284.
- (31) Pullerits, T.; Chachisvili, M.; Sundström, V. *J. Phys. Chem.* **1996**, *100*, 10787–10792.
- (32) Novoderezhkin, V. I.; Monshouwer, R.; van Grondelle, R. *J. Phys. Chem. B* **1999**, *103*, 10540–10548.
- (33) Freiberg, A.; Timpmann, K.; Lin, S.; Woodbury, N. W. *J. Phys. Chem. B* **1998**, *102*, 10974–10982.
- (34) Trinkunas, G.; Freiberg, A. *J. Lumin.* **2006**, *119–120*, 105–110.
- (35) Freiberg, A.; Trinkunas, G. *Photosynthesis in Silico: Understanding Complexity From Molecules to Ecosystems*; Laisk, A., Nedbal, L., Govindjee, Eds.; Springer: Netherlands, 2009; Vol. 29, pp 55–82.
- (36) Toyozawa, Y. *Prog. Theor. Phys.* **1958**, *20*, 53–81.
- (37) Rashba, E. I. *Excitons*; Rashba, E. I., Sturge, M. D., Eds.; North-Holland Publishing Company: North-Holland, 1982; Vol. 2, pp 544–602.
- (38) Sumi, H.; Sumi, A. *J. Phys. Soc. Jpn.* **1994**, *63*, 637–657.
- (39) Toyozawa, Y. *Optical Processes in Solids*; Toyozawa, Y., Ed.; Cambridge University Press: Cambridge, 2003; pp 149–191.
- (40) Knoester, J.; Agranovich, V. M. *Thin Films and Nanostructures*; Elsevier: Amsterdam, 2003; Vol. 31, pp 1–96.
- (41) Freiberg, A.; Rätsep, M.; Timpmann, K.; Trinkunas, G. *J. Lumin.* **2003**, *102–103*, 363–368.
- (42) Trinkunas, G.; Freiberg, A. *J. Lumin.* **2005**, *112*, 420–423.
- (43) Pajusalu, M.; Rätsep, M.; Trinkunas, G.; Freiberg, A. *ChemPhysChem* **2011**, *12*, 634–644.
- (44) Bopp, M. A.; Sytnik, A.; Howard, T. D.; Cogdell, R. J.; Hochstrasser, R. M. *Proc. Natl. Acad. Sci. U.S.A.* **1999**, *96*, 11271–11276.
- (45) Tietz, C.; Cheklov, O.; Dräbenstedt, A.; Schuster, J.; Wrachtrup, J. *J. Phys. Chem. B* **1999**, *103*, 6328–6333.
- (46) Gerken, U.; Jelezko, F.; Götze, B.; Branschädel, M.; Tietz, C.; Ghosh, R.; Wrachtrup, J. *J. Phys. Chem. B* **2003**, *107*, 338–343.
- (47) Gerken, U.; Lupo, D.; Tietz, C.; Wrachtrup, J.; Ghosh, R. *Biochemistry* **2003**, *42*, 10354–10360.
- (48) de Ruijter, W. P. F.; Segura, J. M.; Cogdell, R. J.; Gardiner, A. T.; Oellerich, S.; Aartsma, T. J. *Chem. Phys.* **2007**, *341*, 320–325.
- (49) Novoderezhkin, V. I.; Rutkauskas, D.; van Grondelle, R. *Chem. Phys.* **2007**, *341*, 45–56.
- (50) Uchiyama, D.; Oikawa, H.; Otomo, K.; Nango, M.; Dewa, T.; Fujiyoshi, S.; Matsushita, M. *Phys. Chem. Chem. Phys.* **2011**, *13*, 11615–11619.
- (51) Tubasum, S.; Thomsson, D.; Cogdell, R.; Scheblykin, I.; Pullerits, T. *Photosynth. Res.* **2011**, *111*, 41–45.
- (52) Hofmann, C.; Kulzer, F.; Zondervan, R.; Köhler, J.; Orrit, M. *Single Molecules and Nanotechnology*; Rigler, R., Vogel, H., Eds.; Springer: Heidelberg, 2008; Vol. 12, pp 25–51.
- (53) Cogdell, R.; Hawthornthwaite, A. M. *The Photosynthetic Reaction Center*; Deisenhofer, J., Norris, J. R., Eds.; Academic Press: San Diego, CA, 1993; Vol. 1, pp 23–42.
- (54) Hofmann, C.; Francia, F.; Venturoli, G.; Oesterheld, D.; Köhler, J. *FEBS Lett.* **2003**, *546*, 345–348.
- (55) Brotosudarmo, T. H. P.; Kunz, R.; Böhm, P.; Gardiner, A. T.; Moulisová, V.; Cogdell, R. J.; Köhler, J. *Biophys. J.* **2009**, *97*, 1491–1500.
- (56) Cogdell, R. J.; Gall, A.; Köhler, J. *Q. Rev. Biophys.* **2006**, *39*, 227–324.
- (57) Berlin, Y.; Burin, A.; Friedrich, J.; Köhler, J. *Phys. Life Rev.* **2007**, *4*, 64–89.
- (58) Wu, H.-M.; Savikhin, S.; Reddy, N. R. S.; Jankowiak, R.; Cogdell, R. J.; Struve, W. S.; Small, G. J. *J. Phys. Chem.* **1996**, *100*, 12022–12033.
- (59) Small, G. J. *Chem. Phys.* **1995**, *197*, 239–257.
- (60) Hofmann, C.; Michel, H.; van Heel, M.; Köhler, J. *Phys. Rev. Lett.* **2005**, *94*, 195501.
- (61) Baier, J.; Gabrielsen, M.; Oellerich, S.; Michel, H.; van Heel, M.; Cogdell, R. J.; Köhler, J. *Biophys. J.* **2009**, *97*, 2604–2612.
- (62) Rätsep, M.; Cai, Z.-L.; Reimers, J. R.; Freiberg, A. *J. Chem. Phys.* **2011**, *134* (024506), 1–15.
- (63) Freiberg, A.; Rätsep, M.; Timpmann, K.; Trinkunas, G. *Chem. Phys.* **2009**, *357*, 102–112.
- (64) Rätsep, M.; Freiberg, A. *Chem. Phys. Lett.* **2003**, *377*, 371–376.
- (65) Freiberg, A.; Timpmann, K.; Trinkunas, G. *Chem. Phys. Lett.* **2010**, *500*, 111–115.



PUBLICATION P3

## Fluctuations in the Electron-Phonon Coupling of a Single Chromoprotein

Ralf Kunz, Kōu Timpmann, June Southall, Richard J. Cogdell, Arvi Freiberg,  
and Jürgen Köhler

published in:

*Angewandte Chemie International Edition* **52**, 8726-8730, (2013)

© 2013 Wiley-VCH Verlag GmbH & Co. KGaA, Weinheim  
[DOI:10.1002/anie.201303231](https://doi.org/10.1002/anie.201303231)

This publication has been chosen as a "Hot Paper" by the Editors of  
*Angewandte Chemie International Edition*  
for its importance in a rapidly evolving  
field of high current interest.



A Journal of the Gesellschaft Deutscher Chemiker

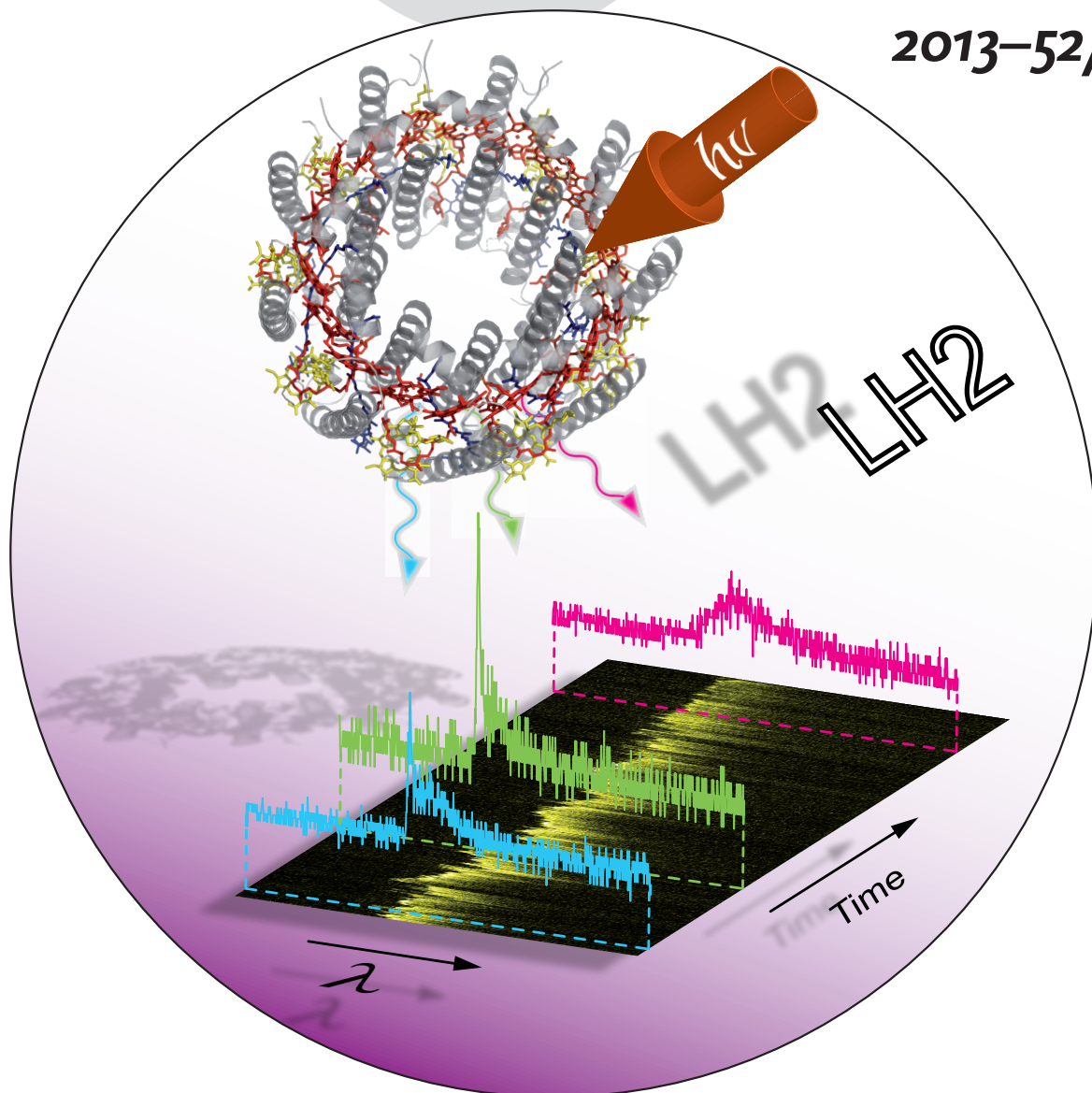
# Angewandte Chemie

GDCh

International Edition

www.angewandte.org

2013–52/33



## Sequences of high resolution ...

... low-temperature emission spectra from individual light-harvesting 2 (LH2) complexes from *Rhodospseudomonas acidophila*. In their communication on page 8726 ff. J. Köhler et al. show that these spectra reveal a much larger variety of the emission profiles than previously observed. The results provide direct evidence for substantial variations in electron–phonon coupling and concomitantly of exciton (de)localization within single pigment–protein complexes.

125 YEARS **Angewandte** Chemie

WILEY-VCH

115

## Fluctuations in the Electron–Phonon Coupling of a Single Chromoprotein\*\*

Ralf Kunz, Kõu Timpmann, June Southall, Richard J. Cogdell, Arvi Freiberg, and Jürgen Köhler\*

Since the determination of the X-ray structure of the peripheral light-harvesting complex, LH2, from the purple bacterium *Rhodospseudomonas (Rps.) acidophila*,<sup>[1,2]</sup> this pigment–protein complex has served as a cornerstone with which to elucidate the structure–function relationships that lie at the heart of the high efficiency of bacterial photosynthesis. This antenna complex accommodates 27 Bacteriochlorophyll (BChl) *a* molecules that are organized in two concentric rings, referred to as B800 and B850, according to the spectral positions of their absorption bands. Its structure has inspired many researchers, and convincing evidence was found that collective effects play an important role in the electronically excited states of the B850 manifold.<sup>[3–10]</sup> Yet, due to the heterogeneity in these systems, direct experimental confirmation of delocalized exciton states is difficult to obtain in conventional ensemble-averaged experiments, but was accomplished by single-molecule spectroscopy.<sup>[11]</sup> Apart from details that are still a matter of hot debate, it is now generally accepted that an exciton model that takes the heterogeneity in the site energies of the individual BChl *a* molecules into account grasps the essential features observed in absorption and fluorescence–excitation spectroscopy of LH2.<sup>[10,12,13]</sup>

There are several observations in the emission spectra that are inconsistent with this model, and this suggested a model that considers exciton self-trapping in the B850 assembly.<sup>[14–16]</sup> However, thus far, most of the single-molecule work performed on pigment–protein complexes from purple bacteria has focused on fluorescence–excitation spectroscopy, and the

few studies that dealt with single-complex emission spectroscopy did not consider self-trapping processes<sup>[17–21]</sup> and/or were conducted at room temperature, where all decisive spectral details are completely masked by thermal broadening.<sup>[22–30]</sup> Recently, we addressed this issue by performing fluorescence–excitation and fluorescence spectroscopy on the same individual complex.<sup>[31]</sup> We found that, in contrast to the excitation spectra, the emission spectra could be grouped into three categories. Those that consist of a narrow zero-phonon line (ZPL), accompanied by a broader phonon side band (PSB) at lower energy, those that showed a broad structureless asymmetric band, and those that looked like a superposition of spectra from the former two categories. Moreover, we observed a clear correlation between the spectral peak position of the emission and the widths of the emission spectra. In agreement with selective spectroscopy data obtained from ensembles of LH2,<sup>[32,33]</sup> the complexes with emission spectra that featured a clear ZPL/PSB profile occurred preferentially on the blue side of the ensemble-averaged emission peak, and complexes with rather red-shifted spectra typically featured structureless broad bands. This observation clearly indicates that the electron–phonon coupling strength strongly varies from complex to complex, as well as being a function of the spectral position. Therefore, we came to the conclusion that exciton self-trapping might indeed be effective for some of the LH2 complexes emitting at the red end of the spectrum. At that time, the minimum exposure time for recording an individual emission spectrum from a single complex was 60 s and we could not fully rule out that some of the broader spectra were the result of fast spectral diffusion processes smearing out the underlying ZPL/PSB profile.

Herein, we describe our investigations of single LH2 complexes with a significantly improved spectral resolution and, more importantly, a reduction of the exposure time for recording an emission spectrum by using improved CCD technology. We find that spectral diffusion does indeed play a role, but, more interestingly, we also observed that the electron–phonon coupling strengths within an individual complex vary strongly as a function of time. The spectral features and correlations for a single complex are similar to those we found before for the variations between different individual complexes. As the electron–phonon coupling strength can be associated with the displacement of the equilibrium positions of the nuclei upon photoexcitation of the chromophore assembly, these findings are of direct relevance for the degree of exciton delocalization within the B850 states.

In Figure 1 a we present a stack of 1000 consecutively recorded emission spectra from a single LH2 complex in

[\*] R. Kunz, Prof. Dr. J. Köhler  
Experimental Physics IV and Bayreuth Institute for Macromolecular Research (BIMF), University of Bayreuth  
95440 Bayreuth (Germany)  
E-mail: juergen.koehler@uni-bayreuth.de  
Homepage: <http://www.ep4.phy.uni-bayreuth.de>

Dr. K. Timpmann, Prof. Dr. A. Freiberg  
Institute of Physics, University of Tartu  
Tartu EE-51014 (Estonia)

J. Southall, Prof. Dr. R. J. Cogdell  
College of Medical, Veterinary and Life Sciences, University of Glasgow, Glasgow G12 8QQ (Scotland, UK)

[\*\*] R.K. and J.K. gratefully acknowledge financial support from the Deutsche Forschungsgemeinschaft (KO 1359/16-1, GZ: 436 EST 113/4/0-1 and GRK1640) and the State of Bavaria within the initiative “Solar Technologies go Hybrid”. K.T. and A.F. have been partially supported by the Estonian Research Council (IUT02-28). R.J.C. thanks the BBSRC for financial support. We thank Prof. M. van Heel (Imperial College London, UK) for providing us with the MSA algorithm.

Supporting information for this article is available on the WWW under <http://dx.doi.org/10.1002/anie.201303231>.

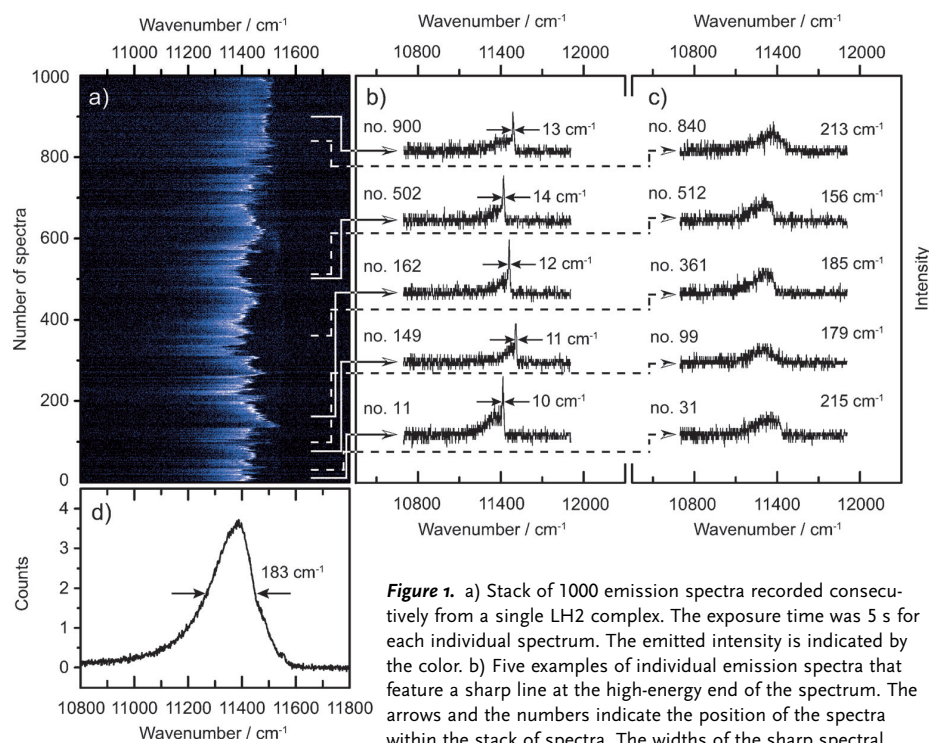


**Figure 1.** a) Stack of 1000 emission spectra recorded consecutively from a single LH2 complex. The exposure time was 5 s for each individual spectrum. The emitted intensity is indicated by the color. b) Five examples of individual emission spectra that feature a sharp line at the high-energy end of the spectrum. The arrows and the numbers indicate the position of the spectra within the stack of spectra. The widths of the sharp spectral features are given by the numbers next to the spectra and have

been determined to within ( $\pm 1 \text{ cm}^{-1}$ ). c) Five examples of individual emission spectra with a broad structureless profile. The arrows and the numbers indicate the position of the spectra within the stack of spectra. The widths of the bands are given by the numbers next to the spectra. For clarity, all spectra in (b) and (c) are offset with respect to each other. d) Sum of all 1000 emission spectra. Note the different scales for the abscissae in (a) and (d) with respect to (b) and (c).

a two-dimensional representation (see also the movie in the Supporting Information). The horizontal axis corresponds to the emission energy and the vertical axis indicates the number of individual spectra, each one recorded with an exposure time of 5 s. From the spectral trail displayed in Figure 1 a, we extracted ten examples of individual spectra, which are shown in Figure 1 b,c. The spectra are grouped according to their spectral profiles. On the left hand side (Figure 1 b), the individual spectra feature a sharp zero-phonon line (ZPL) at the high-energy end of the spectrum, and a spectrally broad phonon side band (PSB) at lower energies. The full width at half maximum (FWHM) of the ZPLs varies from  $10 \text{ cm}^{-1}$  to  $15 \text{ cm}^{-1}$ . Although these linewidths are the smallest ever observed in the emission of LH2, this is still far broader than the homogeneous linewidth of about  $0.005 \text{ cm}^{-1}$  (150 MHz) that one would expect from the lifetime of the first excited singlet state.<sup>[16,34,35]</sup> The contributions to the linewidths that exceed the finite spectral resolution of about  $7 \text{ cm}^{-1}$  probably reflect unresolved spectral diffusion. In contrast, the spectra on the right side (Figure 1 c) appear as asymmetric broad bands with a width in the order of  $150\text{--}200 \text{ cm}^{-1}$ . We cannot rule out that these profiles are still influenced by spectral fluctuations on time scales faster than 5 s. In both cases, the arrows that connect the spectra with the pattern in Figure 1 a indicate the position of the example spectrum within the stack of spectra. Apparently, both types of spectral profiles appear

randomly in time from the same single complex. These subtle details that are present in the individual spectra are completely masked in the time-averaged sum spectrum that is shown in Figure 1 d. It features an asymmetric profile with a width of  $183 \text{ cm}^{-1}$  (FWHM) and peaks at  $11386 \text{ cm}^{-1}$ . Given the spectral trail displayed in Figure 1 a, it is clear that both the shape and the width of the sum spectrum are heavily affected by spectral diffusion.

This example shows that a more quantitative analysis of the spectral profile of the time-averaged sum spectrum of many consecutively recorded emission spectra is prevented by the strong spectral diffusion. To extract emission spectra with a reasonable signal-to-noise ratio from the data, we applied a multivariate pattern recognition algorithm.<sup>[36,37]</sup> These algorithms are used to reconstruct the three dimensional structure of

large biomolecules from two-dimensional projections that have been obtained by cryo-electron microscopy.<sup>[38,39]</sup> We have previously demonstrated that such algorithms can be successfully exploited for spectroscopy to retrieve the optical spectra from individual objects in disordered hosts.<sup>[40-43]</sup> Briefly, the spectra are grouped into a predetermined number of classes by pattern recognition techniques. This is achieved by maximizing the interclass variance and minimizing the intraclass variance (in a mathematical, least squares sense). Subsequently, the spectra assigned to the same class are averaged, which yields the class-averaged spectra (CAS). In other words, only spectra that are sufficiently similar are averaged.<sup>[36]</sup> This method eliminates all contributions to line broadening from spectral diffusion that are slower than the exposure time of 5 s.

The bar graph in Figure 2 shows the number of individual spectra that contributed to a distinct CAS as a function of the spectral peak position of the CAS for the example presented in Figure 1. The distribution is surrounded by examples of CAS that are arranged from left to right, according to their spectral peak position from red to blue. The CAS on the blue side allow for a clear distinction between the ZPL and the PSB. Moving across from the blue to the red side, the intensity distribution between the ZPL and the PSB gradually changes until the narrow feature becomes invisible and an asymmetric band is observed for the emission spectra.

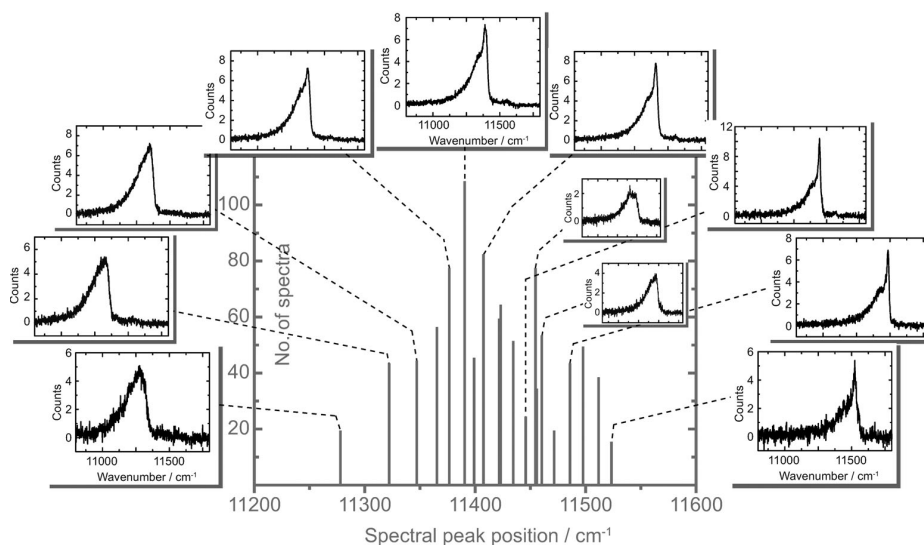


**Figure 2.** Distribution of the spectral peak position of the 20 class-averaged spectra (CAS). This analysis is based on a multivariate statistical pattern recognition algorithm (see text for details) and has been performed with the data shown in Figure 1a. The vertical axis corresponds to the number of individual spectra that have contributed to a distinct class. The bar graph is surrounded by examples of CAS.

The general trend is that spectra with distinctive ZPLs are predominantly blue shifted with respect to the averaged emission maximum, whereas spectra with a broad structureless band appear predominantly at the red end. This correlation is illustrated in Figure 3, which shows the widths of the CAS (taken as FWHM, regardless of the spectral profile), as a function of the spectral peak position. As can be seen, there are no entries in this graph in the lower left corner and only a few entries in the top right corner. Examples for CAS that qualify for the latter case are shown in the inset of the main figure, and it is argued that these spectral profiles might be the result of unresolved fast spectral diffusion.

Further examples of CAS from individual complexes are presented in Figure 4a. It shows the sum spectrum (black) together with the two CAS that feature the most blue- and red-shifted emission peaks for seven individual complexes. For an easier comparison, the most blue- and red-shifted CAS from the example shown in Figure 2, are reproduced as example 1. Extreme examples for complexes that feature only

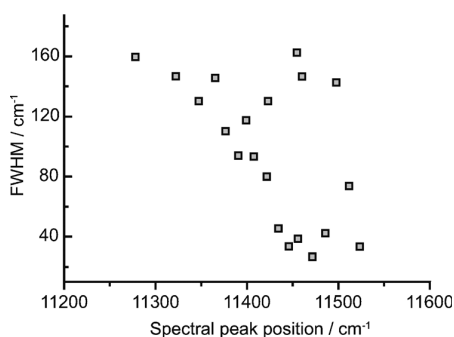


**Figure 3.** Spectral widths (FWHM) of the CAS presented in Figure 2 as a function of the spectral peak positions.

little variation of the spectral profile of their emission spectra are 2 and 3. For the spectra from example 2, both CAS feature a clear ZPL and a PSB, and the spectral separation between the two emission peaks amounts to  $94 \text{ cm}^{-1}$ . In contrast, for example 3, both the red-most and the blue-most CAS appear as structureless asymmetric bands. Here the spectral separation amounts to  $135 \text{ cm}^{-1}$ .

In total, we studied 26 LH2 complexes and, owing to the improved temporal and spectral resolution, the observed degree of heterogeneity (spectral profiles, fluctuations of the emitted intensity, spectral diffusion behavior, and magnitude of the spectral jumps) is far larger than previously observed by us.<sup>[31]</sup> Figure 4b displays the widths of the two most spectrally separated CAS (blue and red) as a function of their spectral peak position for all complexes studied. For better visibility, the CAS from the same individual complex are connected by a straight line. This reveals that for each individual complex the width of the red-most CAS is always larger than the width of the blue-most CAS, whatever the actual profile of the emission spectrum looked like. As shown in Figure 4c, the distribution of the spectral separations between the two extreme CAS is rather broad and covers the range from some  $10 \text{ cm}^{-1}$  to  $350 \text{ cm}^{-1}$ .

Such spectral jumps have been observed previously, either directly in room temperature experiments that allowed for recording sequences of spectra with short exposure times,<sup>[24]</sup> or as line broadening in experiments at cryogenic temperatures, where the signals were integrated over 1–10 min.<sup>[17,18]</sup> Given the low fluorescence quantum yield of LH2 (ca. 10%), the optical excitation of the complex leads to an increase of the local temperature in the protein environment due to radiationless dissipation of excitation energy. Therefore, it is likely that the fluctuations of the electron–phonon coupling strength reflect light-induced conformational changes of the complex. As the spectral jumps and the connected spectral

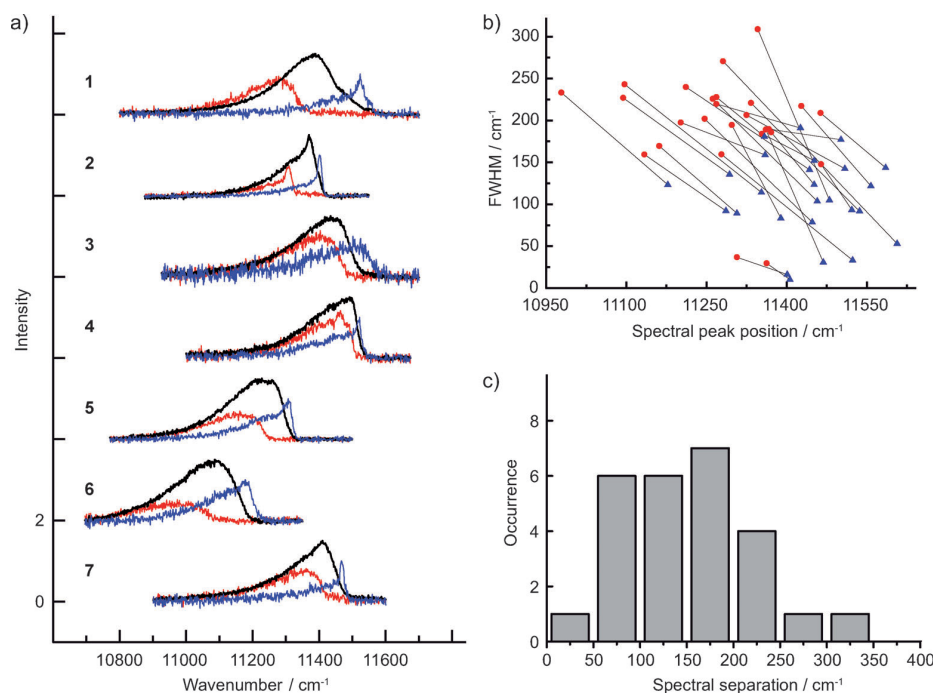


**Figure 4.** a) Examples of the most blue- and red-shifted CAS (blue and red, respectively) and the sum of all recorded emission spectra (black) for seven individual LH2 complexes. The blue CAS are peak normalized, and the red CAS are normalized such that the intensity ratio between the two CAS from the same complex is conserved. The sum spectra are peak normalized to 150% of the peak of the corresponding blue CAS for better visibility. Spectra that belong to different complexes have been offset with respect to each other for clarity. Example 1 was used for illustrations in Figures 1 and 2, and its spectra are reproduced here for comparison. b) Spectral widths (FWHM) of the most red-shifted (●) and the most blue-shifted CAS (▲) as a function of the spectral peak position. As a guide for the eye, CAS that belong to the same complex have been connected by a straight line. c) Distribution of the spectral separations between the most blue- and red-shifted CAS from the same complex.

profiles are reversible, we exclude deterioration of the complexes.

Given that the spectral separation between the most blue and most red emission spectra is on average around  $150\text{ cm}^{-1}$ , which roughly corresponds to the thermal energy at room temperature ( $200\text{ cm}^{-1}$ ), it can be expected that the lineshape fluctuations will be much faster at room temperature, which, together with thermal broadening effects, prevents the observation of distinctly different emission profiles. Although it was found that spectral jumps were well correlated with a broadening of the emission profile under ambient conditions. However, this correlation was both positive and negative; that is, broadening of the spectrum was observed for both spectral jumps to the blue and spectral jumps to the red.<sup>[24,27]</sup> To explain these time-averaged spectral envelopes, simulations using a modified Redfield theory were performed. There it was postulated that distinct conformations of the protein environment induce two different site energies for each individual pigment within the B850 assembly.<sup>[28,29]</sup> However, this model failed to explain the extreme spectral fluctuations and so it was later generalized to a four-state model, including two additional extremely blue- and red-shifted site energies for each pigment.<sup>[30]</sup> Thereby, the red-shifted realizations were associated with exciton self-trapping

and a concomitant degree of exciton localization. Our experiments directly visualize the fluctuations of the electron–phonon coupling strength within a single pigment–protein complex and demonstrate that the LH2 ensemble emission spectrum should not be regarded as static. For each individual complex that contributes to it, there is a continuous movement of the spectral peak position accompanied by a change of the spectral profile. Emissions at the red end of the spectrum are dominated by contributions of broad featureless individual spectra, whereas the blue end of the spectrum predominantly consists of a superposition of ZPL/PSB-type spectral profiles. This might explain the inconsistencies that have been observed in absorption and emission studies on ensembles of LH2 concerning the electron–phonon coupling strength.<sup>[15]</sup>

In summary, we have registered emission spectra from individual LH2 complexes from *Rps. acidophila* at low temperature. Even for an individual complex, drastic fluctuations of the spectral profile were found and the correlation between the shape and the peak position of the emission spectrum provides direct evidence for strong fluctuations of the electron–phonon coupling strength. This demonstrates that conclusions about the B850 electronic excitations based on fluorescence–excitation spectroscopy on the one hand, and emission spectroscopy on the other, should be compared only with great care.<sup>[27]</sup> Fluorescence–excitation spectroscopy monitors the exciton wavefunction when it is “born”. In contrast, emission spectroscopy provides information about the decay of the exciton, which might have undergone a temporal development, particularly if the electron–phonon coupling strength is fluctuating. This distinction is important for the correct interpretation of subsequent energy transfer reactions.

### Experimental Section

Sample preparation was carried out as described in [31]. Briefly, LH2 complexes from *Rps. acidophila* (strain 10050, stored at  $-80^\circ\text{C}$ ) were diluted in buffer solution (20 mM Tris/HCl, pH 8.0, 0.1% LDAO) to

concentrations of about  $10^{-11}$  M. In the last dilution step, 1.8% (wt/wt) polyvinyl alcohol (PVA;  $M_w = 30\,000\text{--}70\,000\text{ g mol}^{-1}$ ) was added and a small drop of the solution was spin-coated onto a quartz substrate. The samples were then mounted in a helium bath cryostat and cooled to 1.2 K. For the optical experiments, the samples were illuminated with a continuous-wave tuneable titanium-sapphire (Ti:Sa) laser (3900S, Spectra Physics) pumped by a frequency-doubled continuous-wave neodymium-yttrium-vanadate (Nd:YVO<sub>4</sub>) laser (Millennia Vs, Spectra Physics) using a home-built microscope. First, a wide-field image of the sample was taken by exciting the sample through a band-pass filter (BP 858/30; Dr. Hugo Anders) at ca. 855 nm. The emission was collected by a microscope objective (NA = 0.85, Mikrothek) that was mounted inside the cryostat. After passing a set of band-pass filters (BP 900/50, AHF-Analysetechnik) the signal was reflected by a mirror that was mounted on the turret inside a spectrometer (SpectraPro-150, Acton Research Corporation) and focused onto a back-illuminated CCD camera (iKon-M DU934N-BR-DD, Andor Technology). Next, spatially well-isolated complexes were selected from the wide-field image and the fluorescence–excitation spectra of these complexes were registered.<sup>[31]</sup> Finally, the complex under study was excited in the B800 spectral region. To do so, the laser light passed a band-pass filter (BP 805/60; AHF Analysetechnik) and the wavelength was wobbled across one (or more) of the sharp B800 absorptions determined before. The polarization was kept fixed and the excitation intensity was about  $1\text{ kW cm}^{-2}$ . The emitted light was directed through a set of long-pass filters (LP 830, AHF Analyse-technik), and, by rotating the turret in the aforementioned spectrometer, dispersed by a grating (600 lines/mm) to provide a spectral resolution of about  $7\text{ cm}^{-1}$ . For each complex, 100–2000 emission spectra were repetitively recorded by accumulating the emission for 3–15 s on the same CCD camera, as mentioned above. All spectra displayed have been corrected for the spectral instrument response.

Received: April 17, 2013

Revised: May 22, 2013

Published online: July 3, 2013

**Keywords:** excitons · light-harvesting complexes · photosynthesis · single-molecule studies

- [1] G. McDermott, S. M. Prince, A. A. Freer, A. M. Hawthornthwaite-Lawless, M. Z. Papiz, R. J. Cogdell, N. W. Isaacs, *Nature* **1995**, 374, 517–521.
- [2] M. Z. Papiz, S. M. Prince, T. Howard, R. J. Cogdell, N. W. Isaacs, *J. Mol. Biol.* **2003**, 326, 1523–1538.
- [3] T. V. Dracheva, V. I. Novoderezhkin, A. P. Razjivin, *FEBS Lett.* **1996**, 387, 81–84.
- [4] R. Monshouwer, R. van Grondelle, *Biochim. Biophys. Acta Bioenerg.* **1996**, 1275, 70–75.
- [5] K. Sauer, R. J. Cogdell, S. M. Prince, A. A. Freer, N. W. Isaacs, H. Scheer, *Photochem. Photobiol.* **1996**, 64, 564–576.
- [6] R. G. Alden, E. Johnson, V. Nagarajan, W. W. Parson, C. J. Law, R. J. Cogdell, *J. Phys. Chem. B* **1997**, 101, 4667–4680.
- [7] M. Chachisvilis, O. Kuehn, T. Pullerits, V. Sundström, *J. Phys. Chem. B* **1997**, 101, 7275–7283.
- [8] H.-M. Wu, M. Rätsep, I.-J. Lee, R. J. Cogdell, G. J. Small, *J. Phys. Chem. B* **1997**, 101, 7654–7663.
- [9] V. Sundström, T. Pullerits, R. van Grondelle, *J. Phys. Chem. B* **1999**, 103, 2327–2346.
- [10] X. Hu, T. Ritz, A. Damjanovic, F. Autenrieth, K. Schulten, *Q. Rev. Biophys.* **2002**, 35, 1–62.
- [11] A. M. van Oijen, M. Ketelaars, J. Köhler, T. J. Aartsma, J. Schmidt, *Science* **1999**, 285, 400–402.
- [12] H. van Amerongen, L. Valkunas, R. van Grondelle, *Photosynthetic Excitons*, World Scientific, Singapore, **2000**.
- [13] R. J. Cogdell, A. Gall, J. Köhler, *Q. Rev. Biophys.* **2006**, 39, 227–324.
- [14] T. Polívka, T. Pullerits, J. L. Herek, V. Sundström, *J. Phys. Chem. B* **2000**, 104, 1088–1096.
- [15] K. Timpmann, Z. Katiliene, N. W. Woodbury, A. Freiberg, *J. Phys. Chem. B* **2001**, 105, 12223–12225.
- [16] A. Freiberg, M. Rätsep, K. Timpmann, G. Trinkunas, W. N. Woodbury, *J. Phys. Chem. B* **2003**, 107, 11510–11519.
- [17] C. Tietz, O. Cheklov, A. Dräbenstedt, J. Schuster, J. Wrachtrup, *J. Phys. Chem. B* **1999**, 103, 6328–6333.
- [18] W. P. F. de Ruijter, J. M. Segura, R. J. Cogdell, A. T. Gardiner, S. Oellerich, T. J. Aartsma, *Chem. Phys.* **2007**, 341, 320–325.
- [19] U. Gerken, F. Jelezko, B. Götze, M. Branschädel, C. Tietz, R. Ghosh, J. Wrachtrup, *J. Phys. Chem. B* **2003**, 107, 338–343.
- [20] U. Gerken, D. Lupo, C. Tietz, J. Wrachtrup, R. Ghosh, *Biochemistry* **2003**, 42, 10354–10360.
- [21] D. Uchiyama, H. Oikawa, K. Otomo, M. Nango, T. Dewa, S. Fujiyoshi, M. Matsushita, *Phys. Chem. Chem. Phys.* **2011**, 13, 11615–11619.
- [22] M. A. Bopp, A. Sytnik, T. D. Howard, R. J. Cogdell, R. M. Hochstrasser, *Proc. Natl. Acad. Sci. USA* **1999**, 96, 11271–11276.
- [23] S. Tubasum, R. J. Cogdell, I. G. Scheblykin, T. Pullerits, *J. Phys. Chem. B* **2011**, 115, 4963–4970.
- [24] D. Rutkauskas, R. Novoderezhkin, R. J. Cogdell, R. van Grondelle, *Biochemistry* **2004**, 43, 4431–4438.
- [25] D. Rutkauskas, J. Olsen, A. Gall, R. J. Cogdell, C. N. Hunter, R. van Grondelle, *Biophys. J.* **2006**, 90, 2463–2474.
- [26] D. Rutkauskas, V. Novoderezhkin, A. Gall, J. Olsen, R. J. Cogdell, C. N. Hunter, R. van Grondelle, *Biophys. J.* **2006**, 90, 2475–2485.
- [27] V. I. Novoderezhkin, D. Rutkauskas, R. van Grondelle, *Biophys. J.* **2006**, 90, 2890–2902.
- [28] L. Valkunas, J. Janusonis, D. Rutkauskas, R. van Grondelle, *J. Lumin.* **2007**, 127, 269–275.
- [29] J. Janusonis, L. Valkunas, D. Rutkauskas, R. van Grondelle, *Biophys. J.* **2008**, 94, 1348–1358.
- [30] V. I. Novoderezhkin, D. Rutkauskas, R. van Grondelle, *Chem. Phys.* **2007**, 341, 45–56.
- [31] R. Kunz, K. Timpmann, J. Southall, R. J. Cogdell, A. Freiberg, J. Köhler, *J. Phys. Chem. B* **2012**, 116, 11017–11023.
- [32] K. Timpmann, M. Rätsep, C. N. Hunter, A. Freiberg, *J. Phys. Chem. B* **2004**, 108, 10581–10588.
- [33] A. Freiberg, M. Rätsep, K. Timpmann, G. Trinkunas, *Chem. Phys.* **2009**, 357, 102–112.
- [34] T. J. Pflöck, S. Oellerich, J. Southall, R. J. Cogdell, G. M. Ullmann, J. Köhler, *J. Phys. Chem. B* **2011**, 115, 8813–8820.
- [35] A. Freiberg, M. Rätsep, K. Timpmann, *Biochim. Biophys. Acta Bioenerg.* **2012**, 1817, 1471–1482.
- [36] L. Borland, M. van Heel, *J. Opt. Soc. Am. A* **1990**, 7, 601–610.
- [37] M. van Heel, B. Gowen, R. Matadeen, E. V. Orlova, R. Finn, T. Pape, D. Cohen, H. Stark, R. Schmidt, M. Schatz, A. Patwardhan, *Q. Rev. Biophys.* **2000**, 33, 307–369.
- [38] P. Dube, M. Wieske, H. Stark, M. Schatz, J. Stahl, F. Zemlin, G. Lutsch, M. van Heel, *Structure* **1998**, 6, 389–399.
- [39] P. Dube, E. V. Orlova, F. Zemlin, M. van Heel, J. R. Harris, J. Markl, *J. Struct. Biol.* **1995**, 115, 226–232.
- [40] C. Hofmann, H. Michel, M. van Heel, J. Köhler, *Phys. Rev. Lett.* **2005**, 94, 195501.
- [41] R. Hildner, U. Lemmer, U. Scherf, M. van Heel, J. Köhler, *Adv. Mater.* **2007**, 19, 1978–1982.
- [42] R. Hildner, L. Winterling, U. Lemmer, U. Scherf, J. Köhler, *ChemPhysChem* **2009**, 10, 2524–2534.
- [43] J. Baier, M. Gabrielsen, S. Oellerich, H. Michel, M. van Heel, R. J. Cogdell, J. Köhler, *Biophys. J.* **2009**, 97, 2604–2612.

Supporting Information

© Wiley-VCH 2013

69451 Weinheim, Germany

**Fluctuations in the Electron–Phonon Coupling of a Single Chromoprotein\*\***

*Ralf Kunz, Kōu Timpmann, June Southall, Richard J. Cogdell, Arvi Freiberg, and Jürgen Köhler\**

anie\_201303231\_sm\_miscellaneous\_information.pdf  
anie\_201303231\_sm\_si\_movie.avi

## Supporting Information

### Table of Contents

1. Multimedia File
2. Electron-Phonon Coupling Strength

#### 1. Multimedia file

A movie shows the sequence of 1000 consecutively recorded emission spectra from a single LH2 complex that is displayed in fig.1a of the paper in a two-dimensional representation. The horizontal axis corresponds to the emission energy in wavenumbers and the vertical axis to the emitted intensity in arbitrary units. The complex was excited in the B800 band with an intensity of  $\sim 1 \text{ kW/cm}^2$  and the exposure time for a single spectrum was 5 s.

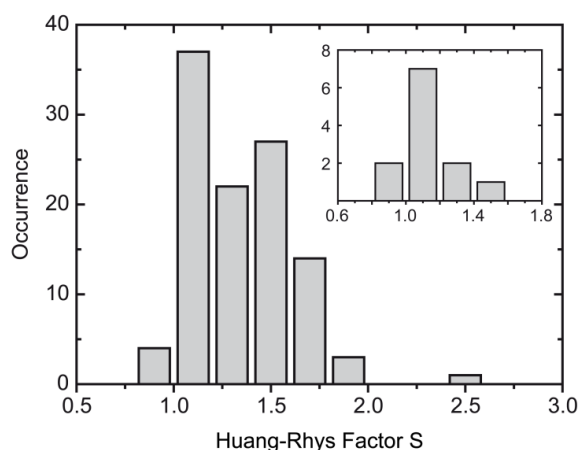
The movie can be downloaded from the following URL:

[https://dl.dropboxusercontent.com/u/102736174/SI\\_Movie.avi](https://dl.dropboxusercontent.com/u/102736174/SI_Movie.avi)

#### 2. Electron-Phonon Coupling Strength

The variations in the spectral profiles were ascribed to different realizations of the electron-phonon coupling strengths within the individual LH2 complexes. A measure for this parameter is the Huang-Rhys (HR) factor  $S$ , that can be determined from the relative intensity of the ZPL with respect to the total intensity of the emission band, i.e.  $I_{ZPL} / (I_{ZPL} + I_{PSB}) = \exp(-S)$ . For a quantitative analysis of the single-complex spectra the high energy wing of the ZPL of the CAS was fitted by a Lorentzian or Gaussian that was subtracted from the data to reveal the PSB. Yet, the analysis had to be restricted to those CAS that allowed for an unambiguous distinction between the ZPL and the PSB, i.e. 108 out of 265. The result is shown in Supporting Figure 1 that displays the distribution of the HR factors for this subgroup of 108

CAS from 26 different complexes. The histogram can be characterized by  $S = 1.3 \pm 0.3$  (mean  $\pm$  sdev). The inset in Supporting Figure 1 shows the corresponding distribution for the particular complex that served as example for figs.1 and 2 in the manuscript. Here the distribution yields  $S = 1.1 \pm 0.2$ . Within statistical accuracy both distributions, i.e. that for the group of 26 complexes and that for an individual complex are equivalent. These results testify that the electron-phonon coupling strength of an individual complex undergoes temporal fluctuations even at low temperature. Moreover, the absolute numbers found for  $S$  are considerably larger than those obtained for the absorptions within the B800 band.<sup>[1-3]</sup> We note that for CAS that did not allow for a quantitative analysis of the ZPL, larger values of the HR factor might be possible.



**Supporting Figure 1.** Distribution of the Huang-Rhys factors  $S$  from 108 CAS from 26 different LH2 complexes. The mean value of the distribution is 1.3 and the standard deviation is 0.3. Inset: Corresponding distribution obtained from 12 CAS of the individual complex that has been used for figs. 1 and 2 in the manuscript. The mean value is  $S = 1.1 \pm 0.2$ .

## Supporting References

- [1] H.-M. Wu , S. Savikhin, N. R. S. Reddy, R. Jankowiak, R. J. Cogdell, W. S. Struve, G. J. Small, *J. Phys. Chem.* **1996**, *100* 12022-12033.
- [2] C. Hofmann, H. Michel, M. van Heel, J. Köhler, *Phys. Rev. Lett.* **2005**, *94* 195501.
- [3] J. Baier , M. Gabrielsen, S. Oellerich, H. Michel , M. van Heel, R. J. Cogdell, J. Köhler, *Biophys. J.* **2009**, *97* 2604-2612.



PUBLICATION P4

**Single-Molecule Spectroscopy Unmasks the  
Lowest Exciton State of the B850 Assembly in  
LH2 from *Rps. acidophila***

Ralf Kunz, Kōu Timpmann, June Southall, Richard J. Cogdell, Arvi Freiberg,  
and Jürgen Köhler

published in:

*Biophysical Journal* **106**, 2008-2016, (2014)

© 2014 by the Biophysical Society

[DOI:10.1016/j.bpj.2014.03.023](https://doi.org/10.1016/j.bpj.2014.03.023)



## Single-Molecule Spectroscopy Unmasks the Lowest Exciton State of the B850 Assembly in LH2 from *Rps. acidophila*

Ralf Kunz,<sup>†</sup> Kōu Timpmann,<sup>‡</sup> June Southall,<sup>§</sup> Richard J. Cogdell,<sup>§</sup> Arvi Freiberg,<sup>†¶</sup> and Jürgen Köhler<sup>†\*</sup>

<sup>†</sup>Experimental Physics IV and Bayreuth Institute for Macromolecular Research (BIMF), University of Bayreuth, Bayreuth, Germany; <sup>‡</sup>Institute of Physics, University of Tartu, Tartu, Estonia; <sup>§</sup>Institute of Molecular, Cell and Systems Biology, College of Medical Veterinary and Life Sciences, Biomedical Research Building, University of Glasgow, Glasgow, Scotland, United Kingdom; and <sup>¶</sup>Institute of Molecular and Cell Biology, University of Tartu, Tartu, Estonia

**ABSTRACT** We have recorded fluorescence-excitation and emission spectra from single LH2 complexes from *Rhodospseudomonas (Rps.) acidophila*. Both types of spectra show strong temporal spectral fluctuations that can be visualized as spectral diffusion plots. Comparison of the excitation and emission spectra reveals that for most of the complexes the lowest exciton transition is not observable in the excitation spectra due to the cutoff of the detection filter characteristics. However, from the spectral diffusion plots we have the full spectral and temporal information at hand and can select those complexes for which the excitation spectra are complete. Correlating the red most spectral feature of the excitation spectrum with the blue most spectral feature of the emission spectrum allows an unambiguous assignment of the lowest exciton state. Hence, application of fluorescence-excitation and emission spectroscopy on the same individual LH2 complex allows us to decipher spectral subtleties that are usually hidden in traditional ensemble spectroscopy.

### INTRODUCTION

The initial event in bacterial photosynthesis is the absorption of a photon by a light-harvesting (LH) antenna system, which is followed by rapid and highly efficient transfer of the energy to the reaction center, where a charge separation takes place and the energy becomes available as chemical energy (1,2). In most purple bacteria, the photosynthetic membranes contain two types of LH complexes, the core RC-LH1 complex and the peripheral LH2 complex (3). The progress made in high-resolution structural studies of LH2 complexes of purple bacteria (4–6) has strongly stimulated theoretical (7–16) and experimental investigations on ensembles (17–25) as well as single molecules (26–36) to understand the efficient energy transfer in these antenna systems (3,23,37,38). The x-ray structure of the LH2 complex shows a remarkable symmetry in the arrangement of the light-absorbing pigments in their protein matrix. The basic building block of LH2 is a protein heterodimer ( $\alpha\beta$ ), which accommodates three bacteriochlorophyll *a* (BChl *a*) pigments and one carotenoid molecule. These modules then oligomerize to produce the native circular or elliptical LH complexes. For LH2 from *Rhodospseudomonas (Rps.) acidophila* the LH2 complex consists of nine such  $\alpha\beta$ -polypeptide heterodimers. A striking feature of the organization of the 27 BChl *a* molecules is their separation into two parallel rings. One ring consists of a group of 18 closely packed BChl *a* molecules, with their bacteriochlorin planes parallel to the symmetry axis, absorbing at 850 nm (B850), whereas the other ring comprises nine well-separated BChl

*a* molecules having their bacteriochlorin planes perpendicular to the symmetry axis of the complex, which absorb at 800 nm (B800) (4,6).

It has now been well established that the spatial arrangement of the pigments determines, to a large extent, the spectroscopic features of the complexes and that in these systems collective effects have to be considered to appropriately describe their electronically excited states (39). This leads to so-called Frenkel excitons, which arise from the interactions of the transition-dipole moments of the individual pigments corresponding to delocalized electronically excited states. Neglecting the slight dimerization of the B850 BChl *a* molecules, the proper eigenstates (exciton states) are characterized by a quantum number, *k*, which can take the values 0,  $\pm 1$ ,  $\pm 2$ , ...,  $\pm 8$ , 9. Because of the circular symmetry, only the states  $k = \pm 1$  carry an appreciable transition-dipole moment, which makes them accessible for optical spectroscopy. Structural- and/or energetic heterogeneities are usually accounted for by random and/or correlated disorder in the site energies of the BChl *a* molecules (14,40–43). The main effects of disorder on the exciton manifold are, a mixing of the different exciton levels, a modification of the energy separation of the exciton levels and lifting their pairwise degeneracy, and a redistribution of oscillator strength to nearby states (3,23). Recent studies suggested that, even at room temperature, quantum coherence could play an important role for the energy transfer properties in these systems (44–49).

Although the exciton model appropriately describes the essential features registered in fluorescence-excitation and absorption spectroscopy of the LH complexes, there are several observations in the emission spectra that are inconsistent with this model. For example, in hole burning

Submitted December 16, 2013, and accepted for publication March 19, 2014.

\*Correspondence: [juergen.koehler@uni-bayreuth.de](mailto:juergen.koehler@uni-bayreuth.de)

Editor: Antoine van Oijen.

© 2014 by the Biophysical Society  
0006-3495/14/05/2008/9 \$2.00

<http://dx.doi.org/10.1016/j.bpj.2014.03.023>



spectroscopy it was found that the lowest exciton state ( $k = 0$ ) was distributed over a range of 120–140  $\text{cm}^{-1}$  full width half-maximum (FWHM) (50–52) on the low energy side of the ensemble absorption spectrum, whereas the width of the respective ensemble emission spectrum exceeds this figure by more than a factor of two. Moreover, evidence has been found that the emission spectrum is essentially homogeneously broadened suggesting that exciton-phonon coupling for the transition from the relaxed excited state must be significant (52,53). This is in contrast to the quasiline absorption spectrum, which is mostly inhomogeneously broadened. To explain these conflicting observations a model has been put forward that involves exciton self-trapping in the B850 aggregate (52–54). Self-trapping of excitons is a well-known phenomenon in molecular crystals, and refers to the fact that due to exciton-phonon interaction, the exciton induces a structural reorganization of its environment, which lowers its energy to an extent that the excitation energy gets trapped on a limited region of the aggregate (55,56). In two previous works we have addressed this issue and found that the electron-phonon coupling strengths in the B850 excited state varies strongly as a function of time within an individual complex (57,58). A detailed analysis of the data yields that the fluctuating electron-phonon coupling strength in the B850 excited state manifold is one of the key mechanisms that cause the previously mentioned discrepancy between the excitation/absorption and emission spectra.

Another issue that has led to hot debates in the past was the discrepancy between hole burning and single-molecule experiments concerning the spectral position of the lowest exciton state,  $k = 0$ . If observable at all in single-molecule spectroscopy, the spectral position of the  $k = 0$  transition was always very close to the  $k = \pm 1$  bands (26,59), whereas the hole burning data suggested a spectral separation of  $\sim 200 \text{ cm}^{-1}$  from these bands (50,51). Yet, the igniting idea of how to address these conflicting results was obtained in the previous study (58), where we elucidated the fluctuation of the electron-phonon coupling strength within an individual complex. These fluctuations manifest themselves as fluctuations of the emission spectrum with respect to both spectral position and spectral profile, thereby causing an experimental problem. Usually the recording of an excitation spectrum requires the use of optical band-pass filters in the detection path to suppress unwanted scattered light from the sample. As a consequence of the spectral fluctuations of the emission spectrum the overlap with the transmission range of the band-pass filters changes as a function of time. Here, we address these temporal spectral fluctuations in more detail by recording sequences of fluorescence-excitation and fluorescence-emission spectra from the same individual LH2 complex. Our study reveals that for  $\sim 65\%$  of the LH2 complexes the  $k = 0$  transition in the excitation spectra appears to be red-shifted to such an extent that it prevents the recording of the full spectrum

due to spectral overlap with the transmission window of the detection filter. For the remaining LH2 complexes the comparison of the excitation and emission spectra allows for an unambiguous assignment of the lowest exciton state for which we find a spectral separation from the  $k = \pm 1$  states of  $209 \text{ cm}^{-1}$ .

## MATERIALS AND METHODS

### Sample preparation

The isolation/purification process of LH2 complexes from the species *Rps. acidophila* (strain 10050) has been performed as previously described (60). Until use, a stock solution of the sample is stored in buffer solution (20 mM Tris/HCl, pH 8.0, 0.1% LDAO) in small aliquots at  $-80^\circ\text{C}$ . For studying single complexes the concentration of the stock solution was diluted in several steps with the detergent buffer solution down to concentrations of  $\sim 10^{-11}$  M. The solution used for dilution in the last step contains 1.8% (w/w) polyvinyl alcohol (PVA;  $M_w = 30,000\text{--}70,000 \text{ g/mol}$ ; Sigma-Aldrich, St. Louis, MO). A drop of this solution was spin-coated onto a cleaned quartz ( $\text{SiO}_2$ ) substrate for 10 s at 500 rpm and 60 s at 2500 rpm, resulting in amorphous polymer films with thicknesses of  $\sim 100$  nm. The samples were immediately mounted in a liquid-helium cryostat and cooled to 1.2 K. For ensemble studies of LH2 complexes, the stock solution was diluted to concentrations of  $10^{-6}$  M, and the same protocol has been followed as described previously.

### Optical setup

All optical experiments have been performed using a homebuilt fluorescence microscope that can be operated in wide-field imaging mode or confocal mode. As light source, we used a continuous-wave tunable titanium-sapphire (Ti:Sa) laser (3900S, Spectra Physics, Santa Clara, CA) pumped by a frequency doubled continuous-wave neodymium-yttrium-vanadate ( $\text{Nd:YVO}_4$ ) laser (Millennia Vs, Spectra Physics). Tuning the laser wavelength of the Ti:Sa in well-defined steps was achieved by rotating the intracavity birefringent filter with a motorized micrometer screw. Calibration of the laser frequency has been verified by a wavemeter (WaveMaster, Coherent, Santa Clara, CA) and the accuracy as well as the reproducibility was verified to be  $\sim 1 \text{ cm}^{-1}$ .

### Wide-field imaging

For wide-field imaging a  $40 \times 40 \mu\text{m}^2$  region of the sample was excited around 855 nm through a band-pass (BP) excitation filter (either BP 858 nm/30 nm (center/width (FWHM)); Dr. Hugo Anders, Nabburg, Germany, or BP850/30; AHF Analysetechnik, AG, Tübingen, Germany). The emission from the sample was collected with a microscope objective (NA = 0.85; Mikrothek, Hamburg, Germany) that was mounted inside the cryostat, passed a set of band-pass filters (BP 900/50; AHF Analysetechnik), and was detected with a back-illuminated charge-coupled device (CCD) camera (TE/CCD-512-TKB; Roper Scientific or iKon-M 934 BR-DD; Andor Technology, Belfast, UK).

### Fluorescence-excitation spectroscopy

For fluorescence-excitation spectroscopy on the individual complexes identified in the wide-field image the microscope was used in confocal mode (61). The fluorescence-excitation spectra have been recorded by continuously scanning the excitation wavelength with a rate of 3 nm/s ( $\sim 50 \text{ cm}^{-1}/\text{s}$ ). To match the polarization of the incident radiation with the orientation of the transition-dipole moments of the absorption bands, the

linear polarization of the excitation light was changed by  $6.4^\circ$  by means of a half-waveplate between two successive laser scans. The signal passed a set of band-pass filters and was focused onto a single-photon counting avalanche photodiode (SPCM-AQR-16, Perkin-Elmer, Waltham, MA). As detection filters, two sets of band-pass filters have been used (BP1: 893/18; BP2: 900/48; Dr. Hugo Anders, AHF Analysetechnik). The excitation intensity was  $100\text{--}150\text{ W/cm}^2$ , and the spectral resolution of the experiment was  $\sim 1\text{ cm}^{-1}$ .

### Fluorescence-emission spectroscopy

For emission spectroscopy on individual complexes the sample was excited around  $800\text{ nm}$  through a band-pass filter (BP 805/60; AHF Analysetechnik) with linearly polarized light. In order not to miss the narrow B800 absorptions the laser wavelength was wobbled over a range of  $2\text{--}6\text{ nm}$  with a rate of  $3\text{ nm/s}$  during data acquisition. The emitted signal passed a set of dielectric long-pass filters (LP830; AHF Analysetechnik), was spectrally dispersed in a spectrometer (SpectraPro-150, 300 or 600 lines/mm, Acton Research Corporation, Roper Scientific, Martinsried, Germany), and registered with a CCD camera. During the project we used three different CCD cameras (Luca-R 604M-OM/iDus DV420A-OE / iKon-M 934 BR-DD; Andor Technology), and depending on the type of camera used, the exposure times were  $600\text{ s}/60\text{ s}/3\text{--}15\text{ s}$ , respectively. The spectral resolution varied as a function of the combination of grating and detector between  $1.5\text{ nm}$  ( $20\text{ cm}^{-1}$ ) and  $0.5\text{ nm}$  ( $7\text{ cm}^{-1}$ ). The excitation intensity was  $\sim 1\text{ kW/cm}^2$ .

## RESULTS AND DISCUSSION

### Fluorescence-excitation/emission spectroscopy on the same individual LH2 complex

The detection filters limit the possible scan range of the excitation laser from  $770\text{ nm}$  to  $876\text{ nm}$  for BP1 and from  $770\text{ nm}$  to  $872\text{ nm}$  for BP2. Because the peak position of the (ensemble) emission spectrum is at  $\sim 875\text{ nm}$ , and because the spectra from the individual LH2 complexes are heterogeneous, it is not clear a priori which scan range is sufficient (if at all) to obtain the entire excitation spectrum

of the complex under study, or whether the excitation spectrum will be cut off at the red end. The influence of the detection filter on the resulting fluorescence-excitation spectrum from an individual LH2 complex is illustrated in Fig. 1, which shows data that have been recorded from three different individual LH2 complexes.

The left side, Fig. 1 A, refers to fluorescence-excitation spectroscopy, and the right side, Fig. 1 B, refers to emission spectroscopy on the same LH2 complexes. In Fig. 1 A the black lines correspond to the fluorescence-excitation spectra, and for comparison the gray lines indicate the emission spectrum obtained from the same complex. This color code is reversed in Fig. 1 B. We note that excitation and emission spectra cannot be measured simultaneously but have to be recorded subsequently. The colored areas in Fig. 1 A visualize the transmission ranges of the band-pass filters used in the detection path. For emission spectroscopy we used a set of long-pass filters that are transparent for light above  $840\text{ nm}$ , as indicated by the green shaded area in Fig. 1 B, and excited the sample around  $800\text{ nm}$ , where the excitation wavelength has been wobbled from  $793\text{ nm}$  to  $796\text{ nm}$  for complex I ( $800\text{--}803\text{ nm}$  for complex II;  $791\text{--}797\text{ nm}$  for complex III), as shown by the blue shaded area in Fig. 1 B. We have verified that the exact spectral position of excitation in the B800 band had no influence on the emission spectrum. Because of the large spectral separation between excitation and detection, it is possible to record the full emission spectra from the individual LH2 complexes, as shown in Fig. 1 B by the black lines. Whether the fluorescence-excitation spectrum has been fully recorded or not can only be judged from comparison with the emission spectrum from the same complex. Only if the red edge of the excitation spectrum overlaps with the blue edge of the emission spectrum, the fluorescence-excitation spectrum

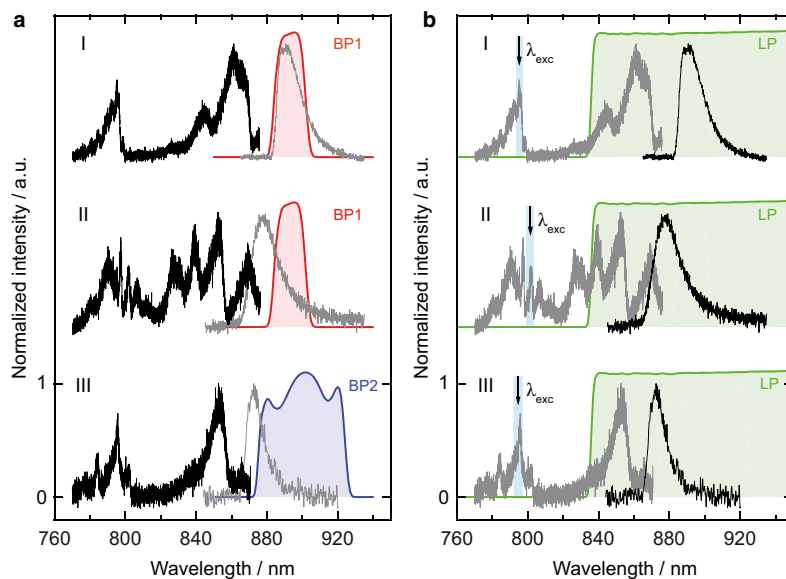


FIGURE 1 (A) Fluorescence-excitation spectra (black lines) from three individual LH2 complexes. The transmission characteristics of the detection filter used is shown by the colored areas. For comparison the corresponding emission spectra from the same complexes are indicated by the gray lines. (B) Emission spectra (black lines) from the same three individual LH2 complexes as in part (A). The transmission characteristics of the detection filter used is shown by the green area. The complexes are excited around  $800\text{ nm}$  (blue shaded area) and the respective fluorescence-excitation spectra are shown by the gray lines for the ease of comparison.

can be considered as complete. Apparently, in Fig. 1 A this criterion is fulfilled for complexes II and III but not for complex I. Moreover, Fig. 1 A illustrates a possible conflict of interest for the experimentalist. To properly record the fluorescence-excitation spectrum the detection filter should only cut out the Stokes-shifted red tail of the emission spectrum (see complexes II and III, Fig. 1 A), whereas for obtaining the strongest signal the overlap between the transmission of the detection filter and the emission spectrum should be maximized (see complex I, Fig. 1 A). In other words, if the complexes would be selected from the wide-field image only, according to their signal strength, most fluorescence-excitation spectra would be as incomplete as for complex I shown in Fig. 1 A (see the Supporting Material).

### The influence of spectral diffusion

Until now, we have treated all spectra as if they were stationary in time. However, the situation is much more complicated than this, because it is well known that both fluorescence-excitation and emission spectra show spectral diffusion. As an example, we show the fluorescence-excitation spectrum, Fig. 2 A, and the emission spectrum, Fig. 2 B, of complex II from Fig. 1 in a two-dimensional representation, which is commonly referred to as spectral diffusion plot.

For both patterns the horizontal axes correspond to wavelength, the vertical axes are equivalent to time, and the intensities are color coded. For the excitation spectra, Fig. 2 A, the vertical axis represents a stack of 65 (fluorescence-excitation) spectra recorded in rapid succession. The sum of these spectra is shown in Fig. 2 C by the black line (*top trace*). This is the same excitation spectrum as shown in Fig. 1 A, for complex II. For the emission spectra, Fig. 2 B, the vertical axis corresponds to 500 (*emission*) spectra that were consecutively recorded. The sum of the emission spectra is shown in Fig. 2 C by the gray line (*top trace*) and corresponds to the emission spectrum shown in Fig. 1 B for complex II. The spectral diffusion plot of the emission spectrum, Fig. 2 B, uncovers that for this complex the peak position of the emission spectrum can change by as much as 16 nm, which leads to a significant change of the spectral overlap between the emission spectrum and the transmission characteristics of the detection filter. Hence, during the recording of an excitation spectrum the emission might jump out of the detection window. This leads to periods of lower or even the absence of signal, as indicated by the arrow in Fig. 2 A, which might be misinterpreted as blinking, i.e., a reversible quenching of the fluorescence, although the fluorescence has not been quenched but has been spectrally shifted outside of the detection range.

Nevertheless, having the spectral diffusion plots at hand, we can search within the stacks of individual excitation/emission spectra for those where the reddest excitation and the most blue emission spectral bands coincide. For

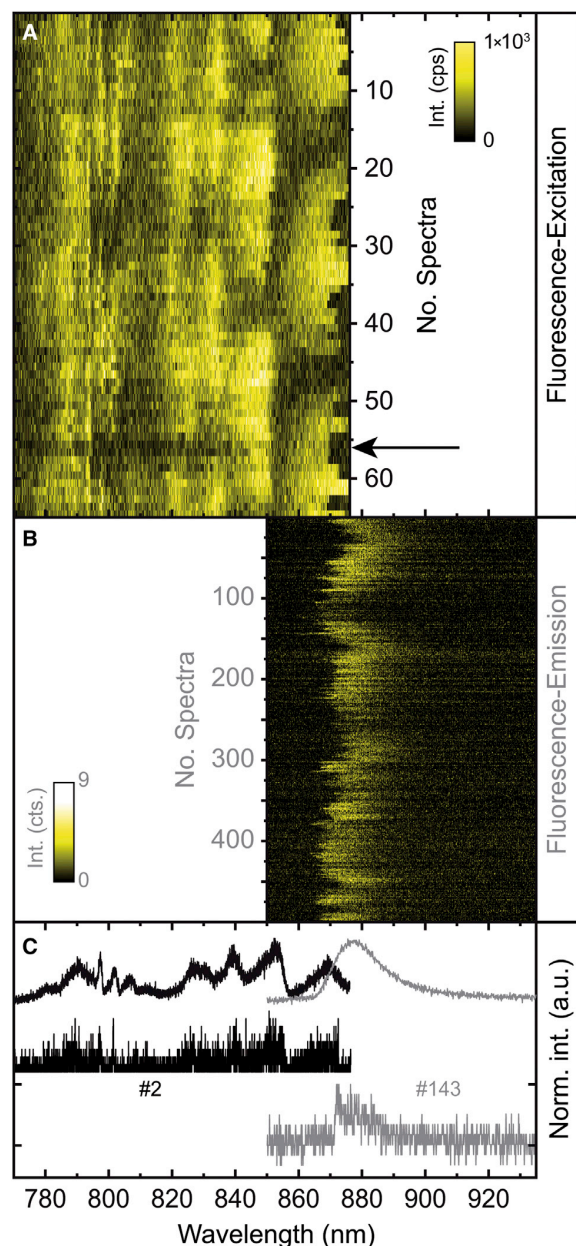


FIGURE 2 (A) Stack of 65 consecutively recorded fluorescence-excitation spectra from a single LH2 (complex II from Fig. 1). Between two successive scans the polarization of the incident radiation has been rotated by  $6.4^\circ$ . The duration for a single scan was 35 s, and the excitation intensity was  $125 \text{ W/cm}^2$ . The arrow denotes a time period with practically no signal as discussed in the text. (B) Stack of 500 consecutively recorded emission spectra from the same complex. The exposure time for an individual spectrum was 5 s. The excitation intensity was  $1 \text{ kW/cm}^2$ . (C) Top traces: Summed fluorescence-excitation spectrum (*black line*) and summed emission spectrum (*gray line*) from the corresponding stacks of spectra. Lower traces: Examples for a single fluorescence-excitation spectrum (*black line*) and a single emission spectrum (*gray line*) where the most red (*excitation*) and the most blue (*emission*) spectral bands overlap. All spectra have been peak normalized, and the individual spectra have been offset for clarity. To see this figure in color, go online.

the patterns displayed in Fig. 2, examples of such spectra are shown by the two lower traces in Fig. 2 C. Further examples from other individual LH2 complexes are shown in Fig. 3. For each part of this figure the top traces correspond to the summed excitation spectra (black) and to the summed emission spectra (gray) from a spectral diffusion plot (not shown), and the lower traces correspond to individual spectra that have been selected according to the previously mentioned coincidence requirement.

This selection procedure allowed us to extract complete fluorescence-excitation spectra from the spectral diffusion plots of 28 complexes (out of 74 complexes). From those spectra we determined the spectral peak positions of the absorption bands, and assigned these bands from red to blue to the  $k = 0$ , the  $k = \pm 1$ , and to higher exciton states, respectively. To check whether the restriction to those 28 complexes could lead to conclusions about the excitonic energy manifold that might not be representative for the ensemble of LH2 complexes, we compared the energetic separations between the spectral peak positions of the

exciton states with those obtained in previous work (30,59,62–64), see Table 1.

In Table 1,  $\Delta E_{01}$  denotes the mean energetic separation between the spectral position of the  $k = 0$  state and the average spectral position of the  $k = \pm 1$  states of an individual complex,  $\Delta E_{\pm 1}$  denotes the energetic separations between the  $k = \pm 1$  states of an individual complex, and for better comparison with previous work  $\Delta E_{\text{higher}}$  denotes the energetic separation between the average spectral position of the  $k = \pm 1$  states of an individual complex and the next higher exciton state of the same complex. The only significant discrepancy between the current study and previously obtained results concerns the energetic separation  $\Delta E_{01}$ . However, this mismatch is simple to understand. First of all, to reduce the influence of spectral diffusion, the individual scans of the spectral diffusion plots in (59) have been shifted with respect to each other such that the spectral positions of the  $k = 0$  transitions coincided. This step was crucial to make the  $k = 0$  transitions visible, yet it scrambled all other parts of the spectrum and affects the information about the spectral separations between the exciton bands. But notwithstanding this problem it was possible for 3 of 19 complexes to observe the  $k = 0$  transition and therefore to determine its spectral position. Based on our results here, we argue that the  $k = 0$  transition for the remaining LH2 complexes might have been red-shifted to an extent that it overlapped with the detection window. Hence, complexes that featured a larger spectral separation between the  $k = 0$  and  $k = \pm 1$  exciton states did not contribute to the data evaluation. Yet, the energetic separation between the  $k = \pm 1$  states, which is of crucial importance for modeling the energetic and geometric structure, is in close agreement for all studies and testifies that this parameter is not affected by having limited the LH2 complexes from which to select those with a full excitation spectrum.

To check whether the selection of the LH2 complexes according to the spectral position of the  $k = 0$  state leads to a bias in the  $\Delta E_{01}$  separation, we compared the spectral peak position of the red most band in the excitation spectra, and the peak position of the summed emission spectrum for the

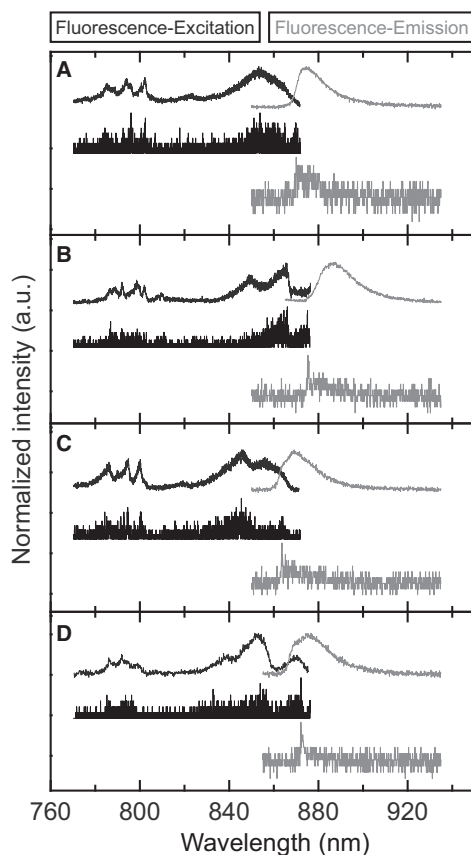


FIGURE 3 Examples of the summed (top) and individual (bottom) fluorescence-excitation spectra (black) and emission spectra (gray) from four individual LH2 complexes (A–D). The setup of each part of the figure is similar to the setup of Fig. 2 C.

TABLE 1 Energetic separation between the exciton states in the B850 manifold as obtained by single-molecule spectroscopy in different studies

Study	Number of complexes	$\Delta E_{01}$ ( $\text{cm}^{-1}$ )	$\Delta E_{\pm 1}$ ( $\text{cm}^{-1}$ )	$\Delta E_{\text{higher}}$ ( $\text{cm}^{-1}$ )
Ketelaars (59)	19	84 <sup>a</sup>	110	285
Hofmann (62)	144	–	126	–
Richter (30)	175	–	126 <sup>b</sup>	–
Reichl (63)	19	238	129	272
Uchiyama (64)	89 <sup>c</sup> /72 <sup>d</sup>	–	90 <sup>c</sup> /139 <sup>d</sup>	–
this work	28	209	111	299

<sup>a</sup>In (59)  $k = 0$  was detectable only for three of the 19 LH2 complexes.

<sup>b</sup>LH2 reconstituted into DOPC bilayer.

<sup>c</sup>LH2 reconstituted into DMPC bilayer.

<sup>d</sup>LH2 solubilized in OG micelle.

selected 28 individual complexes. The distribution of both parameters is shown in Fig. 4 A where we overlaid the ensemble fluorescence-excitation/emission spectra for comparison. The distribution of the spectral position of the most red band in fluorescence-excitation is centered at  $11518 \text{ cm}^{-1} \pm 41 \text{ cm}^{-1}$  (mean  $\pm$  sdev); i.e., it is spectrally separated by  $\sim 170 \text{ cm}^{-1}$  from the peak of the ensemble fluo-

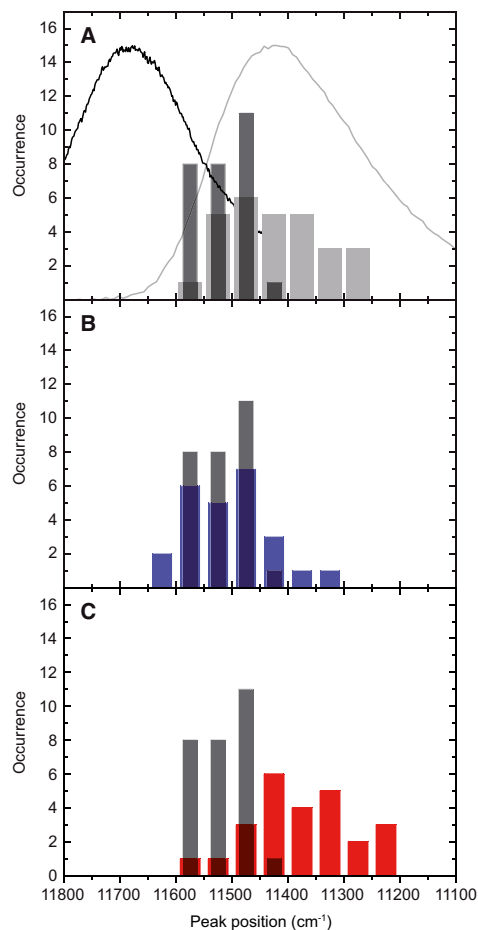


FIGURE 4 (A) Distribution of spectral peak positions of the most red excitation band in the excitation spectra (black) and distribution of the peak positions of the summed emission spectra (gray) for 28 LH2 complexes. For comparison the normalized fluorescence-excitation/emission spectrum (black/gray line) from a thin film of an ensemble of LH2 complexes has been overlaid. The distributions are characterized by  $11518 \text{ cm}^{-1} \pm 41 \text{ cm}^{-1}$  (mean  $\pm$  sdev), and  $11426 \text{ cm}^{-1} \pm 82 \text{ cm}^{-1}$ , respectively. (B) Comparison of the distributions of the spectral peak positions of the most red excitation band (black) and the spectral peak positions of the most blue emission spectra (blue). The distribution of the latter is characterized by  $11503 \text{ cm}^{-1} \pm 75 \text{ cm}^{-1}$ . (C) Comparison of the distributions of the spectral peak positions of the most red excitation band (black) and the spectral peak positions of the most red emission spectra (red). The distribution of the latter is characterized by  $11377 \text{ cm}^{-1} \pm 91 \text{ cm}^{-1}$ . The histograms differ in the number of entries for the emission spectra (A): 28; (B and C): 25, because for three complexes only the time-averaged spectrum has been measured.

rescence-excitation spectrum. The distribution for the peak positions of the emission spectra is characterized by  $11426 \text{ cm}^{-1} \pm 82 \text{ cm}^{-1}$ . The width of this distribution corresponds to a FWHM of  $194 \text{ cm}^{-1}$ , which is about a factor of two larger than the width of the distribution for the most red absorption peak. This factor is in close agreement with what has been found for LH2 from *Rhodobacter sphaeroides* in buffer/glycerol solutions (52,65).

The observed spectral separation of  $170 \text{ cm}^{-1}$  between the mean of the distribution of the reddest band in absorption and the peak of the ensemble fluorescence excitation spectrum is in good agreement with the results from hole burning spectroscopy on ensembles of LH2 in buffer/glycerol solution. For LH2 from *Rb. sphaeroides* this separation amounted to  $(176 \pm 10) \text{ cm}^{-1}$  (66), and for LH2 from *Rps. acidophila* to  $200 \text{ cm}^{-1}$  (50); the width of the distribution of the zero-phonon hole action spectra for LH2 from *Rps. acidophila* was  $120 \text{ cm}^{-1}$ , compared to  $97 \text{ cm}^{-1}$  found here when the standard deviation of  $41 \text{ cm}^{-1}$  is converted to FWHM. Recently, however, the possibility of a static deformation of LH2 complexes due to the PVA matrix has been discussed in (36). To verify whether embedding the LH2 complexes in a PVA matrix deforms the structure of these antenna complexes and, therefore, introduces, per se, significant changes in their spectroscopic behavior, we reconstituted LH2 and RC-LH1 into a lipid bilayer and compared the spectra with those from complexes that were embedded in PVA (30,67). These studies revealed that at least for the LH complexes from purple bacteria, PVA is a good choice as a matrix that does not influence the conclusions drawn about the excitonic states in those pigment-protein complexes. In general, as any solvent it has an influence on the absolute spectral positions of the exciton bands. For example, at cryogenic temperatures the peaks of the ensemble spectra from the samples prepared in buffer/glycerol solution and PVA are shifted by  $\sim 189 \text{ cm}^{-1}$  with respect to each other. More details about how the absolute spectral positions of the LH2 absorptions are influenced by the solvent and/or temperature can be found in (68,69).

As a matter of fact, both the fluorescence-excitation spectra and the emission spectra are affected by spectral diffusion, see for example Fig. 2. Although for each individual complex we dispose of the most blue/red emission spectra, and we can compare the spectral positions of those spectra with the distribution of the spectral positions that we assigned to the lowest exciton state ( $k = 0$ ) in fluorescence excitation. These comparisons are shown in Fig. 4, B and C, respectively. Given the limited statistics both histograms in Fig. 4 B are in good agreement, which testifies that those histograms correspond to the distributions of the spectral positions of the zero-phonon lines (0-0 transitions) of the individual complexes. This is in clear contrast to the ensemble emission spectrum that deviates significantly from the mirror image of the ensemble absorption spectrum.

The reason for this deviation becomes clear when looking at Fig. 4 C, where we compare the spectral positions of the  $k = 0$  state with the distribution of the most red emission spectra. Here, the mean of the distribution of the peak positions of the emission spectra is significantly red-shifted (by  $\sim 140 \text{ cm}^{-1}$ ) with respect to the mean of the distribution of the  $k = 0$  state.

These findings are in line with previous work where we found that both spectral position as well as spectral profile of the emission spectrum of an individual complex undergoes strong fluctuations (58). Thereby, emission spectra featuring a distinctive zero-phonon line occurred predominantly at the blue end of the emission spectrum, whereas broad and featureless emission bands occurred preferentially at the red end of the emission spectrum, being again in good qualitative agreement with the data obtained on an ensemble of LH2 from *Rb. sphaeroides* in a buffer/glycerol solution (70). These spectral variations were ascribed to fluctuations of the electron-phonon coupling strength of an individual LH2 complex and to the formation of self-trapped exciton states. Because all these fluctuations are inherent to an ensemble of complexes these subtle details are averaged out in an ensemble emission spectrum, giving rise to the discrepancies between absorption and emission spectra mentioned in the Introduction.

Finally, we show in Fig. 5 the ensemble fluorescence-excitation and emission spectra that were reconstructed from our single complex spectra for an increasing degree of selectivity. Traces A in Fig. 5 show the fluorescence-excitation and emission spectra from a thin film of an ensemble of LH2 complexes. The next traces correspond to the sum spectra from all 74 individual LH2 complexes that have been investigated in this study, Fig. 5 B, and to the sum spectra restricted to those 28 complexes for which the entire fluorescence-excitation spectrum was obtained, Fig. 5 C. The latter excitation spectrum (black line) features a substructure at the red end, which is masked in the previous spectra. However, as we find out from analysis of the individual spectral diffusion plots, this substructure reflects not only the presence of the lowest exciton state, but it also contains contributions from (spectrally diffusing) higher exciton states blurring this substructure due to temporal averaging. If we manually refine the spectral diffusion plots from all individual fluorescence-excitation spectra where higher exciton bands affect the spectrum of the most red absorption band, we obtain the trace shown in Fig. 5 D (black line), which clearly reveals the substructure at the red end of the excitation spectrum due to the lowest exciton state and nicely overlaps with the shoulder in the corresponding summed emission spectrum (gray line). It is worth noting that the relative oscillator strength of the  $k = 0$  transition cannot be obtained from Fig. 5 D by determining its relative contribution to the intensity of the whole B850 spectrum, because this spectrum has been constructed from selected data sets as explained in detail previously.

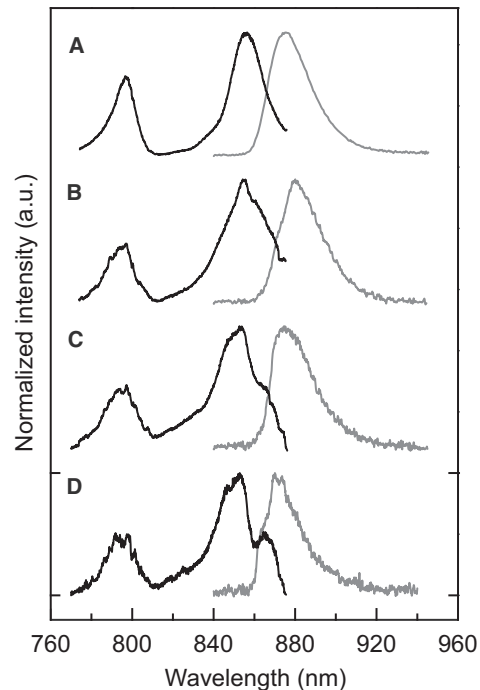


FIGURE 5 (A) Fluorescence-excitation (black) and emission (gray) spectra from an ensemble of LH2 complexes embedded in a PVA-film. (B) Summed fluorescence-excitation (black) and emission (gray) spectra from 74 LH2 complexes. For each complex the fluorescence-excitation/emission spectrum corresponds to the sum of all recorded individual scans/spectra for that complex as indicated in Fig. 2. (C) Summed fluorescence-excitation (black) and emission (gray) spectra from those 28 LH2 complexes for which an entire fluorescence-excitation spectrum has been recorded. For each complex the fluorescence-excitation/emission spectrum corresponds to the sum of all recorded individual scans/spectra for that complex as indicated in Fig. 2. (D) Summed fluorescence-excitation (black) and emission (gray) spectra from 21 (out of the previous 28) LH2 complexes. Here, for each complex only those individual fluorescence-excitation scans have been picked out from the spectral diffusion plots, for which no spectral overlap of the  $k = 0$  and the higher exciton states occurred during the observation time due to spectral diffusion. For the summed emission spectrum only those emission spectra have been used, which showed an overlap with the  $k = 0$  band in the corresponding fluorescence-excitation spectrum. Both types of spectra (fluorescence-excitation and emission) from each complex were first normalized and then summed up. All spectra are peak normalized and (A–C) have been offset for clarity. The data have been recorded at 1.2 K.

## CONCLUSIONS

Having both fluorescence-excitation and emission spectra from the same individual LH2 complexes from *Rps. acidophilus* at hand, shows that for  $\sim 2/3$  of the complexes the fluorescence-excitation spectra are cut off at the red end due to overlap with the detection filter. However, selection of those LH2 complexes for which the fluorescence-excitation spectra were complete, together with the reduction of the influence of the spectral diffusion on the spectra by the sequential acquisition protocol, enabled us to locate the

spectral position of the lowest exciton state ( $k = 0$ ) in their fluorescence-excitation spectra. The analysis of these data yields spectral separations between the  $k = 0$  state and the higher exciton states that are in good agreement with the data obtained from hole-burning spectroscopy, solving an old puzzle that has been discussed in the community for more than a decade. Furthermore, we could shed light on the origin of the disagreement between the width of the distribution of the spectral position of the  $k = 0$  state in absorption and the width of the ensemble emission spectrum.

## SUPPORTING MATERIAL

One figure and supporting data are available at [http://www.biophysj.org/biophysj/supplemental/S0006-3495\(14\)00323-3](http://www.biophysj.org/biophysj/supplemental/S0006-3495(14)00323-3).

This work was financially supported by the Deutsche Forschungsgemeinschaft (KO 1359/16-1, GZ: 436 EST 113/4/0-1 and GRK1640) and the State of Bavaria within the initiative “Solar Technologies go Hybrid”. K.T. and A.F. have been partially supported by the Estonian Research Council (IUT02-28). R.J.C. thanks the BBSRC for financial support.

## REFERENCES

- Blankenship, R. E., M. T. Madigan, and C. E. Bauer. 1995. *Anoxygenic Photosynthetic Bacteria*. Kluwer Academic Publishers, Dordrecht, The Netherlands.
- Blankenship, R. E. 2002. *Molecular Mechanisms of Photosynthesis*. Blackwell Science, Oxford, United Kingdom.
- Cogdell, R. J., A. Gall, and J. Köhler. 2006. The architecture and function of the light-harvesting apparatus of purple bacteria: from single molecules to in vivo membranes. *Q. Rev. Biophys.* 39:227–324.
- McDermott, G., S. M. Prince, ..., N. W. Isaacs. 1995. Crystal structure of an integral membrane light-harvesting complex from photosynthetic bacteria. *Nature*. 374:517–521.
- Koepke, J., X. Hu, ..., H. Michel. 1996. The crystal structure of the light-harvesting complex II (B800-850) from *Rhodospirillum rubrum*. *Structure*. 4:581–597.
- Papiz, M. Z., S. M. Prince, ..., N. W. Isaacs. 2003. The structure and thermal motion of the B800-850 LH2 complex from *Rps. acidophila* at 2.0 Å resolution and 100 K: new structural features and functionally relevant motions. *J. Mol. Biol.* 326:1523–1538.
- Sauer, K., R. J. Cogdell, ..., H. Scheer. 1996. Structure based calculations of the optical spectra of the LH2 bacteriochlorophyll-protein complex from *Rhodospseudomonas acidophila*. *Photochem. Photobiol.* 64:564–576.
- Alden, R. G., E. Johnson, ..., R. J. Cogdell. 1997. Calculations of spectroscopic properties of the LH2 bacteriochlorophyll-protein antenna complex from *Rhodospseudomonas acidophila*. *J. Phys. Chem. B*. 101:4667–4680.
- Krueger, B. P., G. D. Scholes, and G. R. Fleming. 1998. Calculation of couplings and energy-transfer pathways between the pigments of LH2 by the ab initio transition density cube method. *J. Phys. Chem. B*. 102:5378–5386.
- Mukai, K., S. Abe, and H. Sumi. 1999. Theory of rapid excitation energy transfer from B800 to optically forbidden exciton states of B850 in the antenna system LH2 of photosynthetic purple bacteria. *J. Phys. Chem. B*. 103:6096–6102.
- Scholes, G. D., I. R. Gould, ..., G. R. Fleming. 1999. Ab initio molecular orbital calculations of electronic couplings in the LH2 bacterial light-harvesting complex of *Rhodospseudomonas acidophila*. *J. Phys. Chem. B*. 103:2543–2553.
- Mostovoy, M. V., and J. Knoester. 2000. Statistics of optical spectra from single ring aggregates and its application to LH2. *J. Phys. Chem. B*. 104:12355–12364.
- Damjanović, A., I. Kosztin, ..., K. Schulten. 2002. Excitons in a photosynthetic light-harvesting system: a combined molecular dynamics, quantum chemistry, and polaron model study. *Phys. Rev. E Stat. Nonlin. Soft Matter Phys.* 65:031919.
- Jang, S., and R. J. Silbey. 2003. Single complex line shapes of the B850 band of LH2. *J. Chem. Phys.* 118:9324–9336.
- Zhao, Y., M.-F. Ng, and G. Chen. 2004. Low-lying excited states of light-harvesting system II in purple bacteria. *Phys. Rev. E Stat. Nonlin. Soft Matter Phys.* 69:032902.
- Ye, J., K. Sun, ..., J. Cao. 2012. Excitonic energy transfer in light-harvesting complexes in purple bacteria. *J. Chem. Phys.* 136:245104.
- Pullerits, T., and V. Sundström. 1996. Photosynthetic light-harvesting pigment-protein complexes: toward understanding how and why. *Acc. Chem. Res.* 29:381–389.
- Monshouwer, R., M. Abrahamson, ..., R. van Grondelle. 1997. Super-radiance and exciton delocalization in bacterial photosynthetic light-harvesting systems. *J. Phys. Chem. B*. 101:7241–7248.
- Freiberg, A., J. A. Jackson, ..., N. W. Woodbury. 1998. Subpicosecond pump-supercontinuum probe spectroscopy of LH2 photosynthetic antenna proteins at low temperature. *J. Phys. Chem. A*. 102:4372–4380.
- Freiberg, A., K. Timpmann, ..., N. W. Woodbury. 1998. Exciton relaxation and transfer in the LH2 antenna network of photosynthetic bacteria. *J. Phys. Chem. B*. 102:10974–10982.
- Sundström, V., T. Pullerits, and R. van Grondelle. 1999. Photosynthetic light-harvesting: reconciling dynamics and structure of purple bacterial LH2 reveals function of photosynthetic unit. *J. Phys. Chem. B*. 103:2327–2346.
- Timpmann, K., N. W. Woodbury, and A. Freiberg. 2000. Unravelling exciton relaxation and energy transfer in LH2 photosynthetic antennas. *J. Phys. Chem. B*. 104:9769–9771.
- Hu, X., T. Ritz, ..., K. Schulten. 2002. Photosynthetic apparatus of purple bacteria. *Q. Rev. Biophys.* 35:1–62.
- Timpmann, K., G. Trinkunas, ..., A. Freiberg. 2004. Bandwidth of excitons in LH2 bacterial antenna chromoproteins. *Chem. Phys. Lett.* 398:384–388.
- Timpmann, K., G. Trinkunas, ..., A. Freiberg. 2005. Excitons in core LH1 antenna complexes of photosynthetic bacteria: evidence for strong resonant coupling and off-diagonal disorder. *Chem. Phys. Lett.* 414:359–363.
- van Oijen, A. M., M. Ketelaars, ..., J. Schmidt. 1999. Unraveling the electronic structure of individual photosynthetic pigment-protein complexes. *Science*. 285:400–402.
- Bopp, M. A., A. Sytnik, ..., R. M. Hochstrasser. 1999. The dynamics of structural deformations of immobilized single light-harvesting complexes. *Proc. Natl. Acad. Sci. USA*. 96:11271–11276.
- Rutkauskas, D., J. Olsen, ..., R. van Grondelle. 2006. Comparative study of spectral flexibilities of bacterial light-harvesting complexes: structural implications. *Biophys. J.* 90:2463–2474.
- Berlin, Y., A. Burin, ..., J. Köhler. 2007. Low temperature spectroscopy of proteins. Part II: Experiments with single protein complexes. *Phys. Life Rev.* 4:64–89.
- Richter, M. F., J. Baier, ..., S. Oellerich. 2007. Single-molecule spectroscopic characterization of light-harvesting 2 complexes reconstituted into model membranes. *Biophys. J.* 93:183–191.
- Brotosudarmo, T. H. P., R. Kunz, ..., J. Köhler. 2009. Single-molecule spectroscopy reveals that individual low-light LH2 complexes from *Rhodospseudomonas palustris* 2.1.6. have a heterogeneous polypeptide composition. *Biophys. J.* 97:1491–1500.
- Oikawa, H., S. Fujiyoshi, ..., M. Matsushita. 2008. How deep is the potential well confining a protein in a specific conformation? A single-molecule study on temperature dependence of conformational change between 5 and 18 K. *J. Am. Chem. Soc.* 130:4580–4581.

33. Tubasum, S., R. J. Cogdell, ..., T. Pullerits. 2011. Excitation-emission polarization spectroscopy of single light harvesting complexes. *J. Phys. Chem. B.* 115:4963–4970.
34. Uchiyama, D., H. Oikawa, ..., M. Matsushita. 2011. Reconstitution of bacterial photosynthetic unit in a lipid bilayer studied by single-molecule spectroscopy at 5 K. *Phys. Chem. Chem. Phys.* 13:11615–11619.
35. Rajapaksha, S. P., Y. He, and H. P. Lu. 2013. Combined topographic, spectroscopic, and model analyses of inhomogeneous energetic coupling of linear light harvesting complex II aggregates in native photosynthetic membranes. *Phys. Chem. Chem. Phys.* 15:5636–5647.
36. Tubasum, S., R. Camacho, ..., I. G. Scheblykin. 2013. Evidence of excited state localization and static disorder in LH2 investigated by 2D-polarization single-molecule imaging at room temperature. *Phys. Chem. Chem. Phys.* 15:19862–19869.
37. Hu, X., A. Damjanović, ..., K. Schulten. 1998. Architecture and mechanism of the light-harvesting apparatus of purple bacteria. *Proc. Natl. Acad. Sci. USA.* 95:5935–5941.
38. Robert, B., R. J. Cogdell, and R. J. van Grondelle. 2003. The light-harvesting system of purple bacteria. In *Light-Harvesting Antennas in Photosynthesis*. B. R. Green and W. W. Parson, editors. Kluwer Academic Publishers, Dordrecht, The Netherlands, pp. 169–194.
39. van Amerongen, H., L. Valkunas, and R. van Grondelle. 2000. *Photosynthetic Excitons*. World Scientific, Singapore.
40. Wu, H.-M., M. Rätsep, ..., G. J. Small. 1997. Exciton level structure and energy disorder of the B850 ring of the LH2 antenna complex. *J. Phys. Chem. B.* 101:7654–7663.
41. Freiberg, A., K. Timpmann, ..., N. W. Woodbury. 1999. Disordered exciton analysis of linear and nonlinear absorption spectra of antenna bacteriochlorophyll aggregates: LH2-only mutant chromatophores of *Rhodobacter sphaeroides* at 8 K under spectrally selective excitation. *J. Phys. Chem. B.* 103:10032–10041.
42. Jang, S., S. E. Dempster, and R. J. Silbey. 2001. Characterization of the static disorder in the B850 band of LH2. *J. Phys. Chem. B.* 105:6655–6665.
43. Matsushita, M., M. Ketelaars, ..., J. Schmidt. 2001. Spectroscopy on the B850 band of individual light-harvesting 2 complexes of *Rhodospseudomonas acidophila*. II. Exciton states of an elliptically deformed ring aggregate. *Biophys. J.* 80:1604–1614.
44. Sumi, H. 2001. Bacterial photosynthesis begins with quantum-mechanical coherence. *Chem. Rec.* 1:480–493.
45. Harel, E., and G. S. Engel. 2012. Quantum coherence spectroscopy reveals complex dynamics in bacterial light-harvesting complex 2 (LH2). *Proc. Natl. Acad. Sci. USA.* 109:706–711.
46. Smyth, C., F. Fassioli, and G. D. Scholes. 2012. Measures and implications of electronic coherence in photosynthetic light-harvesting. *Philos. Trans. R. Soc. A.* 370:3728–3749.
47. Freiberg, A., M. Pajusalu, and M. Rätsep. 2013. Excitons in intact cells of photosynthetic bacteria. *J. Phys. Chem. B.* 117:11007–11014.
48. Strümpfer, J., M. Şener, and K. Schulten. 2012. How quantum coherence assists photosynthetic light-harvesting. *J. Phys. Chem. Lett.* 3:536–542.
49. Hildner, R., D. Brinks, ..., N. F. van Hulst. 2013. Quantum coherent energy transfer over varying pathways in single light-harvesting complexes. *Science.* 340:1448–1451.
50. Wu, H.-M., N. R. S. Reddy, and G. J. Small. 1997. Direct observation and hole burning of the lowest exciton level (B870) of the LH2 antenna complex of *Rhodospseudomonas acidophila* (strain 10050). *J. Phys. Chem. B.* 101:651–656.
51. Wu, H.-M., M. Rätsep, ..., G. J. Small. 1997. Comparison of the LH2 antenna complex of *Rhodospseudomonas acidophila* (strain 10050) and *Rhodobacter sphaeroides* by high pressure absorption, high pressure hole burning, and temperature dependent absorption spectroscopies. *J. Phys. Chem. B.* 101:7641–7653.
52. Timpmann, K., Z. Katiliene, ..., A. Freiberg. 2001. Exciton self trapping in one-dimensional photosynthetic antennas. *J. Phys. Chem. B.* 105:12223–12225.
53. Freiberg, A., M. Rätsep, ..., W. N. Woodbury. 2003. Self-trapped excitons in LH2 antenna complexes between 5 K and ambient temperature. *J. Phys. Chem. B.* 107:11510–11519.
54. Polivka, T., T. Pullerits, ..., V. Sundström. 2000. Exciton relaxation and polaron formation in LH2 at low temperature. *J. Phys. Chem. B.* 104:1088–1096.
55. Rashba, E. I. 1982. Self-trapping of excitons. In *Excitons*. E. I. Rashba and M. D. Sturge, editors. North-Holland Publishing, The Netherlands, pp. 544–602.
56. Freiberg, A., and G. Trinkunas. 2009. Unravelling the hidden nature of antenna excitations. In *Photosynthesis In Silico: Understanding Complexity from Molecules to Ecosystems*. A. Laisk, L. Nedbal, and Govindjee, editors. Springer, The Netherlands, pp. 55–82.
57. Kunz, R., K. Timpmann, ..., J. Köhler. 2012. Exciton self trapping in photosynthetic pigment-protein complexes studied by single-molecule spectroscopy. *J. Phys. Chem. B.* 116:11017–11023.
58. Kunz, R., K. Timpmann, ..., J. Köhler. 2013. Fluctuations in the electron-phonon coupling of a single chromoprotein. *Angew. Chem. Int. Ed. Engl.* 52:8726–8730.
59. Ketelaars, M., A. M. van Oijen, ..., T. J. Aartsma. 2001. Spectroscopy on the B850 band of individual light-harvesting 2 complexes of *Rhodospseudomonas acidophila*. I. Experiments and Monte Carlo simulations. *Biophys. J.* 80:1591–1603.
60. Cogdell, R., and A. M. Hawthornthwaite. 1993. Preparation, purification, and crystallization of purple bacteria antenna complexes. In *The Photosynthetic Reaction Center*. J. Deisenhofer and J. R. Norris, editors. Academic Press, San Diego, CA, pp. 23–42.
61. Lang, E., J. Baier, and J. Köhler. 2006. Epifluorescence, confocal and total internal reflection microscopy for single-molecule experiments: a quantitative comparison. *J. Microsc.* 222:118–123.
62. Hofmann, C., T. J. Aartsma, and J. Köhler. 2004. Energetic disorder and the B850-exciton states of individual light-harvesting 2 complexes from *Rhodospseudomonas acidophila*. *Chem. Phys. Lett.* 395:373–378.
63. Reichl, P. 2005. Spectroscopic investigation of the exciton states in the B850 band of LH complexes. Diploma Thesis, Universität Bayreuth, Bayreuth, Germany.
64. Uchiyama, D., H. Hoshino, ..., T. Dewa. 2011. Single-protein study of photoresistance of pigment-protein complex in lipid bilayer. *Chem. Phys. Lett.* 511:135–137.
65. Freiberg, A., M. Rätsep, and K. Timpmann. 2012. A comparative spectroscopic and kinetic study of photoexcitations in detergent-isolated and membrane-embedded LH2 light-harvesting complexes. *Biochim. Biophys. Acta.* 1817:1471–1482.
66. Purchase, R., and S. Völker. 2009. Spectral hole burning: examples from photosynthesis. *Photosynth. Res.* 101:245–266.
67. Böhm, P. S., R. Kunz, ..., J. Köhler. 2013. Does the reconstitution of RC-LH1 complexes from *Rhodospseudomonas acidophila* strain 10050 into a phospholipid bilayer yield the optimum environment for optical spectroscopy? *J. Phys. Chem. B.* 117:15004–15013.
68. Urboniene, V., O. Vrublevskaja, ..., L. Valkunas. 2007. Solvation effect of bacteriochlorophyll excitons in light-harvesting complex LH2. *Biophys. J.* 93:2188–2198.
69. Kunz, R., K. Timpmann, ..., A. Freiberg. 2013. Fluorescence-excitation and emission spectra from LH2 antenna complexes of *Rhodospseudomonas acidophila* as a function of the sample preparation conditions. *J. Phys. Chem. B.* 117:12020–12029.
70. Freiberg, A., M. Rätsep, ..., G. Trinkunas. 2009. Excitonic polarons in quasi-one-dimensional LH1 and LH2 bacteriochlorophyll *a* antenna aggregates from photosynthetic bacteria: a wavelength-dependent selective spectroscopy study. *Chem. Phys.* 357:102–112.

Supporting Material for manuscript

## **Single-Molecule Spectroscopy Unmasks the Lowest Exciton State of the B850 Assembly in LH2 from *Rps. acidophila***

Ralf Kunz,<sup>†</sup> Kõu Timpmann,<sup>‡</sup> June Southall,<sup>§</sup> Richard J. Cogdell,<sup>§</sup> Arvi Freiberg,<sup>‡,¶</sup> and Jürgen Köhler,<sup>†,\*</sup>

<sup>†</sup>*Experimental Physics IV and Bayreuth Institute for Macromolecular Research (BIMF), University of Bayreuth, 95440 Bayreuth, Germany*

<sup>‡</sup>*Institute of Physics, University of Tartu, Riia 142, Tartu EE-51014, Estonia*

<sup>§</sup>*Institute of Molecular, Cell and Systems Biology, College of Medical Veterinary and Life Sciences, Biomedical Research Building, University of Glasgow, Glasgow G12 8QQ, Scotland, UK*

<sup>¶</sup>*Institute of Molecular and Cell Biology, University of Tartu, Riia 23, Tartu EE-51010, Estonia*

\* Correspondence: [juergen.koehler@uni-bayreuth.de](mailto:juergen.koehler@uni-bayreuth.de)

## SUPPORTING MATERIAL

### 1. Selection of a single complex for spectroscopy

Usually the selection of a single LH complex for spectroscopy takes place in two steps. First a  $40 \times 40 \mu\text{m}^2$  region of the sample is excited around 855 nm with a laser and the red-shifted fluorescence from the individual complexes located in that area is registered with a CCD camera. Subsequently the optics is switched to the confocal mode such that the excitation volume coincides with one of the complexes observed with the CCD camera. The general problem that arises with this protocol is illustrated on the example of the ensemble fluorescence-excitation spectrum, Fig. S1 A, B black line, and the emission spectrum, Fig. S1 A, B grey line, of LH2 from *Rps. acidophila*. Emission from the Ti:Sa crystal in the infrared spectral region that propagates towards the detector is suppressed by an excitation filter, the transmission of which is shown by the black dashed line in Fig. S1 A, B. The fluorescence from the sample is detected through bandpass filter-sets, and the respective transmission curves are shown by the coloured areas in Fig. S1 A, B. The wide-field images from the same area of the sample that have been registered with the two different detection filters are shown in Fig. S1 C, D. At the bottom of the wide-field images the spotted LH2 complexes are shown schematically by the coloured dots, where the colour of each dot refers to a LH2 complex that has been identified with the corresponding detection filter. Owing to the better spectral coverage of the transmission characteristics of the blue detection filter with the emission spectrum from a LH2 ensemble, the number of complexes that can be identified is larger for this filter. Hence, the choice of the detection filter plays a crucial role for the selection of a single complex for spectroscopy, because some of the complexes might not be observable while others appear brighter/dimmer as a function of the detection filter.

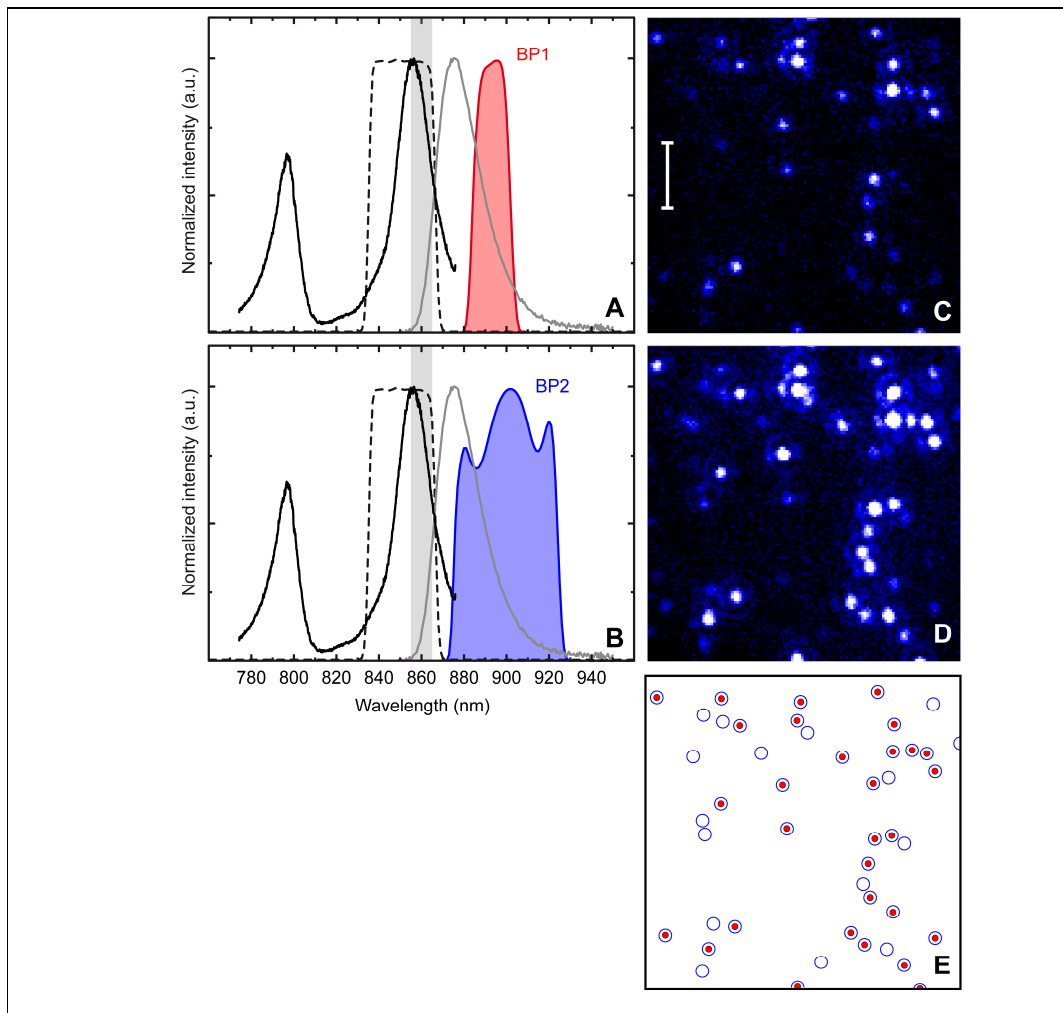


FIGURE S1 Left: Illustration of the influence of the spectral characteristics of the optical filters on the wide field imaging. Transmission curves of the detection filters with respect to the spectral positions of the absorption (*solid black lines*) and emission (*solid grey line*) of LH2 for two different detection filters. (A) BP1: center wavelength 893 nm, bandwidth 18 nm; (B) BP2: 900 nm, 48 nm. The *dashed line* corresponds to the transmission characteristics of a bandpass filter (850 nm, 30 nm) that is used in the excitation path to suppress background from the laser. All transmission curves of the optical filters are shown on a normalized scale. The sample is excited with circularly polarized light, the wavelength is wobbled between 855 nm and 865 nm (*grey shaded area*), and the excitation intensity is 100 W/cm<sup>2</sup>. Right: Wide field images from the same sample area: (C) detected with filter BP1, (D) detected with filter BP2. The scale bar in (C) corresponds to 10 μm. (E) Schematic representation of the individual complexes that are identified in the two images. *Red dots* refer to part (C) of the figure (BP1), and *blue circles* refer to part (D) of the figure (BP2).